Unravelling the molecular basis of subcuticular host-colonization by the apple scab fungus, *Venturia inaequalis*

Mercedes Rocafort Ferrer

A thesis presented in partial fulfillment of the requirements

for the degree of

Doctor of Philosophy (PhD)

in Plant Science

School of Agriculture and Environment

Massey University

2022

MASSEY UNIVERSITY
TE KUNENGA KI PŪREHUROA
UNIVERSITY OF NEW ZEALAND

GRADUATE RESEARCH SCHOOL

Note for Examiners
Explanation of COVID-19 Impacts

Thank you for taking the time to examine this thesis, which has been undertaken during the Covid-19 pandemic. The New Zealand Government's response to Covid-19 includes a system of Alert Levels which have impacted upon researchers. Our University's pandemic plan applied the Government's expectations to our research environment to ensure the health and safety of our researchers, however, research was impacted by restrictions and disruptions, as outlined below.

For a six-week period from March 26 to April 27 2020, New Zealand was placed under very strict lockdown conditions (Level 4 – Lockdown), with students and staff unable to physically access University facilities, unless they were involved in essential research related to Covid-19. All field work ceased and data collection with humans was restricted to online methods, if appropriate. The restrictions were partially lifted on April 27, but students and staff were not generally allowed back into University facilities until May 13.

Ongoing disruptions have also been encountered for some students due to uncertainties over the potential for future Covid-19-related restrictions on activities, and a Covid-19 cluster outbreak based in Auckland in New Zealand on 12 August 2020 led to the imposition of rolling Level 2 (Reduce) and Level 3 (Restrict) conditions until 23 September 2020. Auckland campus based students remained on Level 2 until 7 October 2020. This Alert Level system continues to be utilised throughout 2021.

These changing Alert Levels have meant that some research students had experimental, clinical, laboratory, field work, and/or data collection or analysis interrupted, and consequently may have had to adjust their research plans. For some students, the impacts of Covid-19 stretched far beyond the lockdown period in April/May 2020, as they may have had to significantly revise their research plans.

Overseas travel is not permitted by the University and restrictions have been placed on the New Zealand borders which are closed to non-New Zealand citizens and permanent residents. This meant that international students who were based offshore at the time of lockdown, were unable to return to New Zealand. A small number of offshore students were provided permission to return to New Zealand in early 2021. Many students have also suffered from anxiety and stress-related issues, and have had financial impacts, meaning their research progress has been significantly delayed.

This form, as completed by the supervisor and student, outlines the extent that the research has been affected by Covid-19 conditions.

Approved by DRC 10/Feb/2021
DRC 21/02/03

Please consider the factors listed below in your assessment of the work.

This statement has been prepared by the candidate's supervisor in consultation with the student and has been endorsed by the relevant Head of Academic Unit.

Student Name: Mercedes Rocafort Ferrer ID Number: 18041001

Supervisor Name: Carl Mesarich Date: 29-Sep-2022

Thesis title: Unravelling the molecular basis of subcuticular host-colonization by the apple scab fungus, Venturia inaequalis

Considerations to be taken into account. Note: This statement will remain in the final copy of the thesis which will be available from the Massey University Library following the examination process.
[*Enter key considerations here for the examiners. This can include but is not limited to change of scope, scale, topic, focus; limitations in relation to data collection, access to necessary literature or archival materials, laboratories, field sites; disruptions as a result of lockdown and various alert levels, medical or health considerations etc*]

Chapter 4 - reduction in scope: Originally, in addition to performing the glycosidic linkage analysis, the plan was to perform an assessment that allowed the alpha and beta linkages of Venturia inaequalis cell wall carbohydrates to be distinguished. Furthermore, the plan was to assess the presence of deacetylated chitin (chitosan) using a more detailed biochemical analysis. However, due to a delay in the processing of samples by external collaborators (as a result of the world-wide COVID-19 lock-down period), these analyses could not be performed.

Chapter 5 - reduction in scope: Originally, the plan was to disrupt a candidate effector gene of V. inaequalis (Cin1) using CRISPR-Cas9 technology. However, due to the first nation-wide lock-down, all transformants of this fungus, in which the Cin1 gene was targeted for disruption, could not be subcultured and therefore died. The loss of time and transformants meant that this part of the project had to be abandoned. Another plan in this chapter was to assess CRISPR-Cas9-generated THN mutants of V. inaequalis for reduced virulence or lack of pathogenicity on apple. However, due to lost time, this experiment could not be performed.

Chapters 3, 4 and 5 - complete cessation of work: During the first nation-wide lock-down, all laboratory work relating to Chapters 3, 4 and 5 had to be stopped. No bioinformatic work could be completed during this time, as these data were not yet available. Together, these issues significantly slowed the progress of the PhD project.

Approved by DRC 10/Feb/2021
DRC 21/02/03

Confidential for Examiners Only: [*Please enter any other considerations which are confidential for examiners only and should not be placed in the final thesis version submitted to Library following the examination process]*

Signed, confirming this is a fair reflection of the impact of Covid-19 on this research.

Student — Mercedes Rocafort Ferrer — Firmado digitalmente por Mercedes Rocafort Ferrer Fecha: 2022.09.29 11:08:19 +02'00'

Supervisor — Carl Mesarich — Digitally signed by Carl Mesarich Date: 2022.09.29 22:43:59 +13'00'

Head of Academic Unit (or nominee) — Peter Tozer — Digitally signed by Peter Tozer DN: cn=Peter Tozer, c=NZ, email=p.tozer@massey.ac.nz Date: 2022.09.30 08:28:27 +13'00'

Approved by DRC 10/Feb/2021
DRC 21/02/03

Abstract

Scab, caused by the fungal pathogen *V. inaequalis* (*Vi*), is the most economically important apple disease. During infection, *Vi* occupies the subcuticular environment, where it develops specialized infection structures, called stromata and runner hyphae. These structures are thought to be important for fungal nutrition and the delivery of proteins, with many of these anticipated to function as virulence factors (effectors) in promoting host infection or avirulence factors (Avr effectors) in triggering host resistance. To date, nothing is known about how these structures are differentiated and protected from recognition by the host immune system. Likewise, little is known about the identity and function of *Vi* effector proteins. To better control scab, a greater understanding of the molecular mechanisms underpinning infection structure differentiation and protection, as well as *Vi* virulence and avirulence, is first needed. In **Chapter 2**, a comprehensive review of apoplastic effector proteins from plant-associated fungi (and oomycetes) was provided. Given that *Vi* is an extracellular pathogen, this review provided insights into the potential types of effector proteins secreted by *Vi* into the subcuticular environment. Then, in **Chapter 3**, a multidisciplinary approach based on bioinformatics, transcriptomics, and structural biology was used to identify and characterize *Vi* effector candidates (ECs). This revealed that ECs were predominantly expressed in two temporal waves, and that many belonged to expanded protein families with predicted structural similarity to virulence and avirulence effectors from other plant-pathogenic fungi. This analysis helped to generate a list of ECs for further study and contributed to a better understanding of effector biology and evolution. Next, in **Chapter 4**, a multidisciplinary approach based on transcriptomics, proteomics, glycomics, and confocal microscopy was used to study *Vi* cell wall carbohydrate composition during the differentiation of infection structures. This

revealed that *Vi* down-regulates genes putatively associated with the biosynthesis of immunogenic carbohydrates, and deacetylates surface-exposed chitin to the less immunogenic carbohydrate, chitosan. Finally, in **Chapter 5**, CRISPR-Cas9 technology was applied to *Vi* for the first time, which will enable genes identified in this study to be functionally characterized. Altogether, this thesis has furthered our understanding of the *Vi* –apple pathosystem and has provided novel data that can be used to inform the development of new scab control strategies against *Vi*.

Acknowledgements

When I made the sudden decision to move all the way across the world from Spain to New Zealand, some people could have said it was a quite drastic and risky decision. Now, that my PhD has come to an end I can say that this decision was the greatest, and that I have enjoyed this PhD journey through all the highs and lows. The completion of this PhD thesis has been a very fulfilling, albeit challenging experience, and it would have never been the same without the support of everyone, form supervisors, friends to family.

First of all, I would like to thank my main PhD supervisor Dr. Carl Mesarich. Thank you for always being so approachable and supportive. At times, things got challenging and I really doubted myself, but you always managed to infect me with your optimism to stir me in the right directions.

I would also like to thank my co-supervisors, Dr Joana Bowen and Prof. Rossie Bradshaw. Dr Joana Bowen, thank you for going above and beyond as your role as co-supervisor, from hosting me in your house with your family during my stay in Plant and Food Research, to all the lively discussions and support. Prof. Rossie Bradshaw, thank you for your kindness and constructive feedback.

I would also like to express my gratitude to all the researchers that have helped me through the years with their advice. Prof. Murray Cox, thank you for all the support and help through the journey of learning bioinformatics. Prof. Kim Plummer, thank you for sharing your expertise in *Venturia inaequalis* and constructive criticism. To the MMIC team, Dr. Matthew Savoian and Raul Salomon, thank you for your help using the confocal microscope. Anja Schiemann thank you for all the technical guidance using different equipment through the years. Saadiah Arshed, thank you

for teaching me the *V. inaequalis* protoplast transformation method during my stay in Plant and Food Research.

To my collaborators, Dr. Vaibhav Srivastava thank you for performing the mass spectrometry and glycosidic analysis of the *V. inaequalis* cell wall samples. Prof. Vincent Bulone thank you for your feedback and discussions about the *V. inaequalis* cell wall.

I would also like to thank the researchers that have helped me and led me towards starting this PhD thesis. Dr. Nick Snelders, your teaching and supervision during my master thesis was crucial for my development as a scientist. I would also like to thank Prof. Bart Thomma, your advice and support during my master thesis was very helpful and inspired me to start this PhD thesis.

To my fantastic past and present co-workers at Massey University: Silvia de la Rosa, Ellie Bradley, Hannah McCarthy, Melissa Guo, Berit Hassing, Lukas Hunziker. I am so grateful to have shared this experience with such lively scientists, thank you for all your help and all the laughs during lunch breaks.

To all my friends in New Zealand, thank you for the great times during these years. Being so far away from home has been tough at times, but you have helped make me feel like home. Specially, I would like to thank my flatmates. Carlos Corella, I am very grateful for your friendship, but specially I am grateful for all the delicious Mexican food that you cooked me. Caio Kenup, thank you for all the great memories and your patience helping me with R. To my non-official flatmate, Rayen Leon, thank your being the greatest friend, all the coffee breaks, trips, and experiences with you have made this PhD journey memorable.

To my parents, gracias por todo, esta tesis no hubiera sido posible sin vuestro constante apoyo. Gracias por visitarme en Nueva Zelanda y por todas las experiencias que hemos vivido juntos. Sin duda, estar lejos de vosotros ha sido la parte más difícil de este doctorado.

To my friends back home, vuestro apoyo ha sido crucial durante todos estos años, gracias por continuar a mi lado y apoyarme siempre.

Joan, gràcies pel teu constant suport i mudar-te a l'altra punta del món per compartir aquesta aventura junts. Gràcies per escoltar-me sempre, gràcies per la paciència quan tornava del laboratori cansada, gràcies per estimar-me i fer-me riure cada dia. Moltes vegades no ha sigut fàcil, però tu has fet que cada moment sigui únic. T'estimo.

Table of Contents

List of Figures

List of Appendix Figures

List of Tables

List of Appendix Tables

List of Abbreviations

µl	Microlitre
µM	Micromolar
aa	Amino acid
AA	Auxiliary activity
ABC	Adenosine triphosphate binding cassette
AEP	Apoplastic effector protein
AGS	α-1,3-glucan synthase
AMP	Adenosine monophosphate
Avr	Avirulence
AvrRVi	*Avirulence to Rvi*
AWF	Apoplastic wash fluid
BCA	Biocontrol agent
BGS	β-1,3-glucan synthase
BH	Benjamini-Hochberg
BIC	Biotrophic interfacial complex
CAZyme	Carbohydrate-active enzyme
CBD	Chitin-binding domain
CBM	Carbohydrate-binding module
CC	Coiled-coil
ccdB	Control of cell death B
CDA	Chitin deacetylase
cDNA	Complementary DNA
CDS	Coding sequence
CE	Carbohydrate esterase
CFEM	Common fold in several fungal extracellular membrane protein
CHS	Chitin synthase
Cin	Cellophane-induced
CLSM	Confocal laser scanning microscopy
CM	Cellophane membrane

cm	Centimetre
CRISPR-Cas9	Clustered Regularly Interspaced Short Palindromic Repeats-Cas9
C-terminus	Carboxyl-terminus
CWDE	Cell wall degrading enzyme
DAB	3, 3'-diaminobenzidine
DAMP	Damaged associated molecular pattern
DEG	Differentially expressed gene
DMI	Demethylation inhibitors
DNA	Deoxyribonucleic acid
dpi	Days post-inoculation
DSB	Double strand break
EC	Effector candidate
EI-MS	Electron-impact mass spectrometer
EMC	Enzymatic mismatch cleavage
ER	Endoplasmic reticulum
EST	Expressed sequence tags
ETI	Effector-triggered immunity
ETS	Effector-triggered susceptibility
EWCA	Effectors with chitinase activity
FOLD	*Fusarium oxysporum* f. sp. *Lycopersici* dual-domain
Gal	Galactosyl
GC	Gas chromatography
gDNA	Genomic DNA
GFP	Green fluorescent protein
GH	Glycoside hydrolase
Glc	Glucosyl
GlcNAc	N-acetylglucosaminosyl
GMO	Genetically modified organism
GO	Gene ontology
GPI	Glycosylphosphatidylinositol
GT	Glycosyltransferase
HA	Hemagglutinin
HDR	Homology-directed repair

HMA	Heavy metal-associated
hpi	Hours post-inoculation
HR	Hypersensitive response
HRM	High-resolution melting
HRP	Horseradish peroxidase
HsbA	Hydrophobic surface-binding protein A
Hxp	Hexopyranose
IP	Invasion pattern
IPR	Invasion pattern receptor
Kb	Kilobase
kDa	Kilodalton
KP6	Killer protein 6
LARS	*Leptosphaeria* AviRulence-Suppressing
LC–ESI–MS/MS	Liquid chromatography electrospray ionization–tandem mass spectrometry
LRR	Leucine-rich repeat
LRR-RLP	Leucine-rich repeat–receptor-like protein
LysM	Lysin motif
MAMP	Microbe-associated molecular patterns
Man	Mannosyl
MATE	Multidrug and toxic compound extrusion
MAX	*Magnaporthe* Avrs and ToxB-like
MBC	Methyl benzimidazole carbamate
MFS	Major facilitator superfamily
ml	Millilitre
mm	Micrometre
mM	Micromolar
MS	Murashige and Skoog
MSA	Multiple sequence alignment
MTI	MAMP-triggered immunity
NB	Nucleotide-binding
NHEJ	Non-homologous end-joining mechanism
NLP	Necrosis- and ethylene-inducing-like protein
NLR	Nucleotide-binding domain and leucine-rich repeat receptor

nM	Nanomolar
N-terminus	Amino-terminus
OGA	Oligogalacturonate
OPT	Oligopeptide transporter
ORF	Open reading frame
PAGE	Polyacrylamide gel electrophoresis
PAM	Protospacer adjacent motif
PAMP	Pathogen-associated molecular pattern
PBS	phosphate buffer saline
PCA	Principal component analysis
PCR	Polymerase chain reaction
PCWDE	Plant cell wall degrading enzyme
PDA	Potato dextrose agar
PEG	Polyethylene glycol
PI	Propidium iodide
PL	Polysaccharide lyase
PMAA	Partially methylated alditol acetate
POT	Proton-dependent oligopeptide transporter
PP	Phosphopantetheine
PR	Pathogenesis-related
PRR	Pattern recognition receptor
PTI	PAMP-triggered immunity
QoI	Quinone outside inhibitors
QTL	Quantitative trait loci
R	Resistance
RALPH	RNAse-like proteins expressed in haustoria
RiPPs	Ribosomally synthesized and post-translationally modified cyclic peptides
RIPs	Repeat-induced mutations
RLK	Receptor-like kinases
RLP	Receptor-like proteins
RNA	Ribonucleic acid
RNAi	RNA interference
ROS	Reactive oxygen species

rpm	Revolution per minute
RT	Room temperature
RVi	Resistance to *Venturia inaequalis*
SDS	Sodium dodecyl sulfate
sgRNA	Single guide RNA
SHS	Subcuticular hyphal strands
SIX	Secreted in xylem
S-RLK	S–receptor-like kinase
TE	Transposable element
TFA	Trifluoroacetic acid
THN	Trihydroxynaphthalene reductase
TIR	Toll/Interleukin-1
TM	Transmembrane
TPM	Transcripts per million
TRI12	Trichothecene efflux pump
UV	Ultraviolet
VICE	*Venturia inaequalis* candidate effector
WAKL	Wall-associated receptor kinase-like
WB	Western blot
WGA	Wheat germ agglutinin
Wt	Wild type

Chapter 1:

Introduction

1. *Venturia inaequalis*: the apple scab pathogen

The *Venturia* Sacc. genus (anamorph *Fusicladium* Bonord [1]) taxonomically belongs to the kingdom Fungi, phylum Ascomycota, class Dothideomycetes, and order Venturiales [2,3]. Most species of the *Venturia* genus are plant pathogens that cause significant damage to horticulturally important crop trees [4-7]. For example, *V. asperata* infects apple [8], *V. pirina* infects European pear [9], *V. nashicola* infects Asian pear [10], *V. carpophila* infects peach and other *Prunus* spp. [11], *V. oleaginea* infects olive [12], *V. effusa* infects pecan [13], and *V. cerasi* infects cherry [14]. Other lesser-known species infect non-horticultural plants, such as *V. orbiculata* which infects mountain ash [15], and *V. paralias* which infects sea spurge [16]. In all cases, the host range of these individual *Venturia* species is restricted.

An additional species to those mentioned above is *V. inaequalis*, which is the most well-known and well-studied species of the *Venturia* genus [17]. *V. inaequalis* is the causal agent of the most economically important disease of apples worldwide, known as scab or black spot [5,18]. This pathogen mainly infects members of the genus *Malus*, such as species of cultivated apple (*Malus* x *domestica*), crab-apple (*M. sylvestris, M. floribunda*) and wild apple (*M. sieversii*), although other hosts such as firethorn (*Pyracantha* spp.) and loquat (*Eriobotrya japonica*) are also known [18]. Scab disease is geographically widespread in all countries where apples are grown. However, the disease is more severe in temperate countries with a cool and moist climate such as New Zealand [5,18,19].

1.1. *V. inaequalis* life cycle

During its life cycle, *V. inaequalis* has a pathogenic biotrophic asexual stage (*Spilocaea pomi* Fr. or *Fusicladium pomi* Fr.), when it feeds on living host tissue, and an overwintering sexual saprobic stage (*V. inaequalis* Cke.) when it feeds on dead host tissue (**Figure 1-1. A**) [18,20]. The biotrophic

stage starts in spring, when rainfall induces the release of ascospores from pseudothecia (sexual fruiting bodies) which are dispersed by wind to young, freshly unfurled leaves. Here, the ascospores adhere to the apple cuticle through the production of an extracellular mucilage, composed of proteins and carbohydrates, mostly β-galactose [21]. When conditions are suitable, with free water available and an optimal temperature from 15 to 25 ºC [17] ascospores germinate, develop a germ tube and, on some occasions, an appressorium (**Figure 1-2. A**). The appressorium is not essential to penetrate the host cuticle, as localized enzymatic degradation is the main process for cuticle penetration and mechanical pressure is not required [22,23].

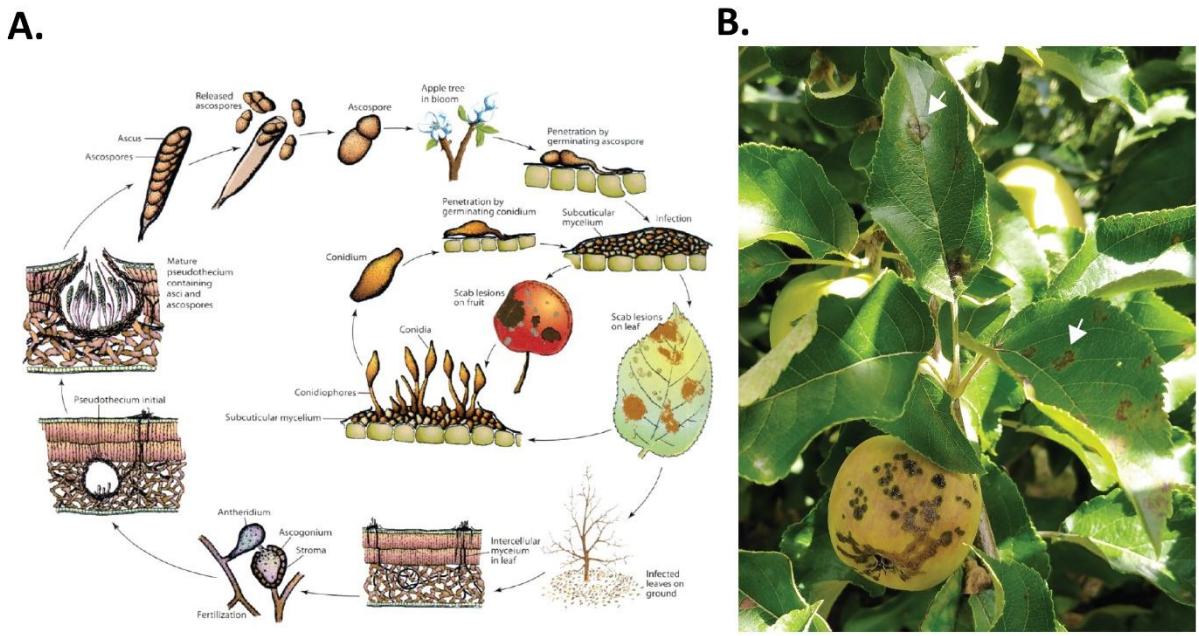

Figure 1-1. *Venturia inaequalis*, the causal agent of apple scab. A. Life cycle of *V. inaequalis*. This figure was published in Plant Pathology, Agrios (2005), p506, copyright Elsevier, reproduced with permission. **B.** Symptoms of infection by *V. inaequalis* on apple leaves and fruit. White arrows indicate scab lesions on infected leaves. Picture taken by C.H. Mesarich, Massey University, Palmerston North, New Zealand.

After penetration of a susceptible host, *V. inaequalis* grows biotrophically in the subcuticular environment, where it develops infection structures called runner hyphae (**Figure 1-2. B**) and stromata (**Figure 1-2. C, D**) [24-26]. Runner hyphae are much wider in diameter than regular tubular hyphae formed on the plant surface and are often fused lengthwise to form ‘hyphal

superhighways' (**Figure 1-2. B**). Stromata are made up of single or multiple layers of pseudoparenchyma, a cell type that results from a switch in the polarity of cell division (i.e. from polar tip extension to non-polar lateral division) (**Figure 1-2. C, D**) [25]. As hyphal superhighways, these runner hyphae enable the fungus to radiate out from the initial site of host penetration, acting as a base from which additional stromata can be differentiated. Stromata, on the other hand, give rise to asexual conidia, but are also likely required for nutrient acquisition and the secretion of proteins and other molecules that promote host-colonization, known as effectors (see section 4.3) [5,25,27].

Later during infection, conidiophores and conidia are produced from the surface of stromata that rupture through the cuticle (**Figure 1-2. D**), generating the characteristic velvety olive-brown scab lesions in buds, leaves and fruit that give the disease its name (**Figure 1-1. B)**. Over time, these lesions often coalesce and dry out, at which time they become corky in appearance and crack or tear. Under favourable conditions, conidia are dispersed from stromata by rain, which can initiate secondary infections on leaves and fruit throughout the growing season. However, disease incidence is reduced in older apple leaves, a phenomenon known as ontogenic resistance [18,28]. At sites of infection, the host cuticle appears to be thicker than at uninfected areas [25] (**Figure 1-2. E**). To date, it is unknown whether this increase in cuticle thickness is caused by the pathogen or is the result of a plant defence response. Additionally, reinforcement of the plant cell wall by callose deposition is often observed, even during compatible interactions (**Figure 1-2. F**). However, this deposition does not appear to restrict colonization of the subcuticular host environment [25].

At the end of the asexual biotrophic infection stage, the sexual saprobic stage is initiated (**Figure 1-1. A**). During autumn, apple leaves fall and *V. inaequalis* survives by growing as a saprophyte inside fallen apple leaves, where it sexually reproduces and forms the fruiting

bodies, pseudothecia [5]. *V. inaequalis* is a heterothallic fungus, meaning that sexual reproduction only occurs between opposite mating types [5]. In spring, the infection cycle starts again, when rain promotes the discharge of sexual ascospores from mature pseudothecia.

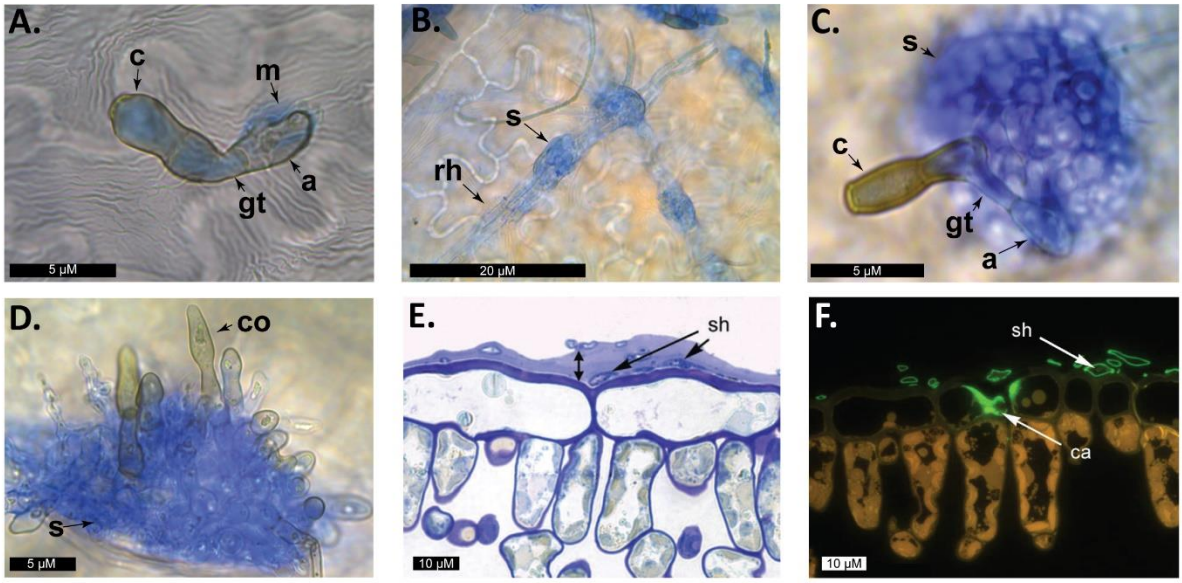

Figure 1-2. Cytology of *Venturia inaequalis* during colonization of leaves from susceptible apple cultivar 'Royal Gala'. **A.** Germinated *V. inaequalis* conidium (c) on the leaf cuticle that has formed a germ tube (gt) and appressorium (a), with the latter attached to the apple cuticle by an extracellular mucilage (m), at 12 hours post-inoculation (hpi). **B.** Wide runner hyphae (rh) differentiated in the subcuticular environment. Micrograph taken at 5 days post-inoculation (dpi). **C.** Stroma (s) differentiated in the subcuticular environment. Micrograph taken at 6 dpi. **D.** Conidiophore (co) produced from a stroma that has broken through the leaf cuticle. Micrograph taken at 7 dpi. Micrographs from A. to D. taken by J.K. Bowen, Plant and Food Research, Auckland, New Zealand [29]. **E.** Cross section of an infected leaf at 14 dpi showing subcuticular hyphae (sh) in the subcuticular environment and the associated increased leaf cuticle thickness (double arrow). **F.** Cross section of infected leaf observed under fluorescence microscopy with ultraviolet (UV) excitation showing subcuticular hyphae (sh) and callose (ca) deposition on leaf epidermal cells under the area colonized by *V. inaequalis*. Cross sections E. and F. extracted from Kucheryava et al. [25], copyright Elsevier, reproduced with permission.

1.2. Apple scab control

The characteristic apple scab lesions can render apples unmarketable by causing fruit blemishes and deformation. As a consequence, under favourable conditions, this disease can cause the loss of 70% or more of the crop [7]. Additionally, scab can reduce both the growth and yield of the

plant by causing repeated defoliation of apple trees over several seasons and making the tree more susceptible to abiotic stress [5,30].

Control of apple scab disease is very costly as it relies on the intensive use of fungicides, which might involve up to 20 treatments per year [5,6,31]. Monitoring of weather conditions during early spring is crucial to facilitate timing of fungicide applications to prevent scab infections. Mostly, fungicide treatments are applied during early spring as wet conditions are conducive for infection and young unfurling leaves are very susceptible to scab disease [17]. Unfortunately, the intensive use of fungicides accelerates the development of fungicide-resistant strains of *V. inaequalis* and increases production costs for growers [19]. Indeed, this pathogen is classified as a high-risk pathogen for the development of fungicide resistance by the Fungicide Resistance Action Committee [32]. Common fungicides used for scab control are demethylation inhibitors (DMIs), methyl benzimidazole carbamate (MBC) and quinone outside inhibitors (QoIs). However, many *V. inaequalis* strains resistant to these fungicides have been reported. For example, in Turkey, 65% of *V. inaequalis* strains tested were resistant to all three fungicides mentioned above [33].

To counter the emergence of fungicide-resistant strains, an integrated disease management programme should be employed [34]. Management programmes should include cultural practices, such as leaf litter sanitation, to reduce the amount of primary inoculum, and pruning of trees, to reduce the humidity required for ascospore germination in tree canopies [31]. Additionally, biological control strategies should also be considered. One strategy is to use fungal antagonists that interfere with *V. inaequalis* development during winter, which reduces the amount of primary inoculum for the next infection cycle [35]. Another strategy is to spray fungal antagonists onto apple trees during spring, which has been shown to significantly reduce the incidence of apple scab in orchards [36]. However, these biological control methods are not

commercially available yet and much work is needed to integrate biological control in scab management [35,36]. Another promising alternative to achieve a more sustainable apple production, is to use scab-resistant apple cultivars. However, the use of these cultivars has been limited due to relatively poor fruit quality [5,37]. Additionally, multiple strains of *V. inaequalis* that can overcome the resistance provided by the cultivar have emerged in the field (see section 5).[38]. Therefore, the development of more durable scab-resistant cultivars with high fruit quality is required for successful scab control.

Finally, the subcuticular lifestyle of *V. inaequalis* renders the control of this pathogen difficult, as it grows in the subcuticular environment without causing symptoms until sporulation, when conidia break through the cuticle generating visible lesions [5,39]. This long latency phase renders eradication of *V. inaequalis* and other subcuticular pathogens difficult, as symptoms only appear when dispersal of the secondary inoculum has already started [39].

2. Colonization of the subcuticular plant environment

Plant-pathogenic fungi that exhibit subcuticular growth are characterized by their ability to grow between the cuticle and underlying epidermal cells of host tissues. The subcuticular environment is a continuous extracellular matrix composed of multiple cuticular layers on top of the epidermal cells [40]. In terms of composition, the cuticle is mostly made up of lipids such as cutin and waxes, with a lower proportion of polysaccharides like pectin also present [40,41].

Little is known about the mechanisms underpinning the colonization of the subcuticular environment, as this parasitic strategy is often overlooked, with only a few subcuticular pathogens having been described. Notably, many of these species are economically important plant pathogens, such as species from the *Venturia*, *Rhynchosporium* and *Diplocarpon* genera. All species from the previously described *Venturia* genus are suspected to be subcuticular. However, microscopic evidence of their colonisation strategy is only available for *V. inaequalis* [25,26], *V. asperata* [8], *V. pirina* [8], *V. effusa* [42], *V. oleaginea* [43] and *V. paralias* [16].

The *Rhynchosporium* genus contains five described species, all of which cause leaf scald disease in economically important cereal crops, such as barley or rye [44,45]. In all cases, these species have been observed to extensively colonize the subcuticular environment of their hosts [45]. The most well-studied is *R. commune*, the causal agent of leaf scald, which is one of the most devastating diseases of barley, causing yield losses in the range of 10 to 45% [46]. *Rhynchosporium* species grow in the subcuticular environment during the biotrophic phase of their life cycle, and later during infection, when epidermal cells collapse, they initiate intracellular colonization of the underlying host mesophyll cells [47].

Species from the *Diplocarpon* genus are also important pathogens with a subcuticular phase. Examples include *D. rosae*, the causal agent of rose black spot, the most important disease in garden roses, and *D. mali*, the causal agent of leaf blotch disease in apple [48-

51]. *Diplocarpon* species grow extensively in the subcuticular environment; however, these pathogens can also develop inter- and intra-cellular hyphae that penetrate host cells, during the necrotrophic stage, when it kills and feeds from dead tissue [49-51]. Another economically important subcuticular pathogen is *Pyrenopeziza brassicae,* the causal agent of the devastating light leaf spot disease in oilseed rape [52] (**Table 1-1**). Some other plant-pathogenic fungal species have a lesser, more transitionary subcuticular host infection stage, such as some *Fusarium* spp. and *Colletrichum* spp. (**Table 1-1**). Usually, these species grow in the subcuticular environment before starting necrotrophic host-colonization [53,54]. This subcuticular stage is often described as quiescent and, for this reason, has been largely overlooked. Remarkably, subcuticular host-colonization is not only restricted to the fungal kingdom, as some plant-pathogenic oomycete species, such as *Phytophthora ramorum*, have also been described to colonize the subcuticular environment of different hosts [55].

Studies with a focus on the subcuticular mode of host-colonization by plant-pathogenic microbes are very limited. However, based on the few cytology studies that are available, an intriguing observation is that most of these pathogens develop visually similar infection structures. For example, *R. commune* and *R. secalis* develop subcuticular hyphae that fuse laterally along their length, similar to the runner hyphae of *V. inaequalis*. Furthermore, these pathogens develop dense stromata in the subcuticular environment [46]. *D. rosae* and *D. mali* also develop subcuticular hyphae that fuse along their length, referred to in the literature as subcuticular hyphal strands (SHS) [49,51]. Again, these SHS are morphologically similar to the runner hyphae described for *V. inaequalis* (**Figure 1-3)**. In addition to this, *D. rosae* and *D. mali* form finger-like pseudoparenchymatous structures in the subcuticular environment, which become the base for acervuli (asexual fruiting body) formation [50,51,56] (**Figure 1-3**). In terms of *Fusarium graminearum*, the causal agent of Fusarium head blight, coral-like hyphae are formed in the subcuticular environment prior to the development of intracellular hyphae [57].

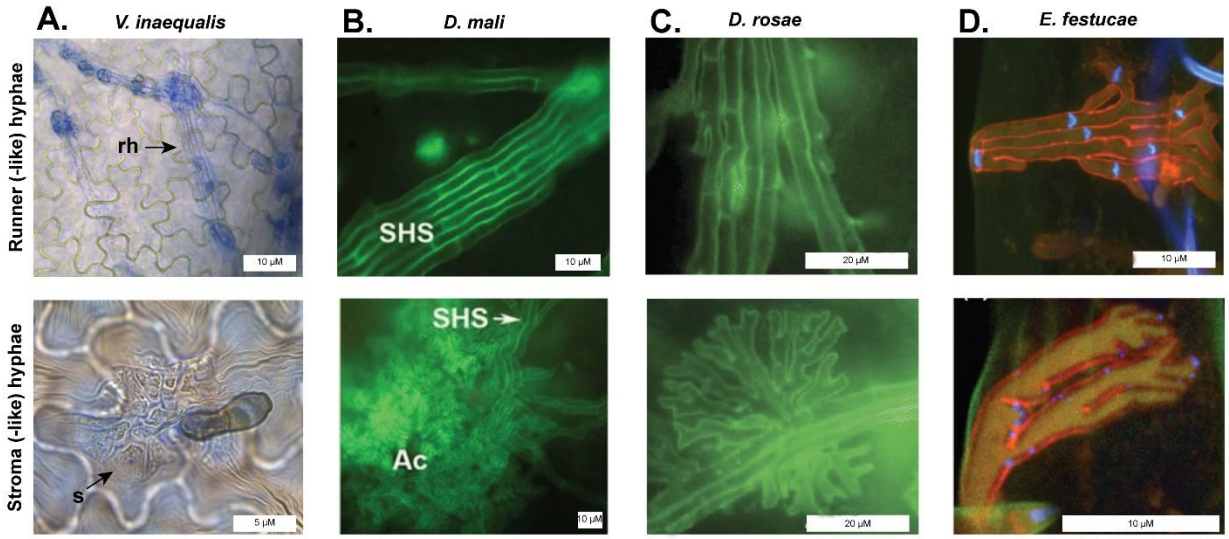

Figure 1-3. Subcuticular infection structures developed by different fungi. **A.** Runner hyphae (rh) and stroma (s) of *Venturia inaequalis* developed in apple leaves, stained with aniline blue. Micrographs taken by J.K. Bowen, Plant and Food Research, Auckland, New Zealand [29]. **B.** Runner-like hyphae from *Diplocarpon mali*, also referred to as subcuticular hyphal strands (SHS) developed in apple leaves. Stroma-like structure, referred to as the base of acervuli (Ac). Pictures extracted from Zhao et al. [51], with permission from Springer Nature. **C.** Runner-like hyphae and stroma-like (s) structures from *Diplocarpon rosae* developed in rose leaves. Pictures extracted from Gachomo et al. [50] with permission from John Wiley and Sons. **D.** Runner-like hyphae and stroma-like structures developed by *Epichloë festucae* mutant Δ*noxAB* developed inside the subcuticular environment of the *Lollium perenne* leaf blade expansion zone. Samples labelled with aniline blue (orange pseudocolour) and WGA-AF488 (blue pseudocolour). Micrographs extracted from Becker et al. [58] with permission from John Wiley and Sons.

Subcuticular infection structures are also found in endophytic fungi. Indeed, *Epichloë festucae*, the mutualistic symbiont of temperate grasses (*Lolium* and *Festuca* genera) develops infection structures in the subcuticular environment of the leaf blade expansion zone (**Figure 1-3**). Interestingly, mutants deleted for both of the *NADPH oxidase* complex genes, *NoxA* and *NoxB*, display more extensive subcuticular growth than the wild type fungus [58]. The *E. festucae* subcuticular infection structures consist of hyphae fused laterally, similar to *V. inaequalis* runner hyphae, and coral-like hyphae that resemble *V. inaequalis* stromata (**Figure 1-3**) [58]. Collectively, most subcuticular fungi appear to develop similar specialized infection structures to colonize the subcuticular environment (**Figure 1-3**). However, these structures are named differently in the literature and their function during host-colonization is, to date, unknown.

Table 1-1. Plant-associated microbes that colonize the subcuticular environment.

Organism	Disease	Lifestyle	Host	Niche	References
Venturia inaequalis	Apple scab	Biotroph	*Malus* x *domestica*	Subcuticular	[25]
Pyrenopeziza brassicae	Oilseed rape light leaf spot	Hemibiotroph	*Brassica napus*	Subcuticular	[52]
Rhynchosporium commune	Barley leaf blotch	Hemibiotroph	*Hordeum vulgare*	Subcuticular + Inter/intracellular	[46]
Rhynchosporium secalis	Leaf scald of barley	Hemibiotroph	*Hordeum vulgare*	Subcuticular + Inter/intracellular	[59]
Diplocarpon rosae	Rose black spot disease	Hemibiotroph	*Rosa* spp.	Subcuticular + Inter/intracellular	[49,50,56]
Diplocarpon mali	*Marssonina* leaf blotch of apple	Hemibiotroph	*Malus* x *domestica*	Subcuticular + Inter/intracellular	[51]
Fusarium graminearum	Fusarium head blight	Hemibiotroph	Cereal crops (e.g. *Hordeum vulgare*)	Subcuticular + Inter/Intracellular	[57,60,61]
Epichloë festucae	-	Mutualistic symbiont	Temperate grasses	Subcuticular and Intercellular	[58]
Colletotrichum acutatum	Anthracnose	Hemibiotroph	Wide host range	Subcuticular + Inter/intracellular	[62]
Colletotrichum capsici	Leaf spot of peppers	Hemibiotrophic	*Gossypium hirsutum, Vigna unguiculata*	Subcuticular + Inter/intracellular	[63]
Colletotrichum circinans	Onion smudge	Hemibiotrophic	*Allium* spp.	Subcuticular + Inter/intracellular	[63]
Colletotrichum gloeosporioides	Anthracnose	Hemibiotrophic	Wide host range	Subcuticular + Inter/intracellular	[53,63]
Phytophthora ramorum	Sudden oak death	Hemibiotrophic	Wide host range	Subcuticular + Inter/intracellular	[55]

2.1. Cellophane membranes: a potential in culture model to study subcuticular host-colonization by *V. inaequalis*

V. inaequalis can serve as a model pathogen to study the morphological differentiation of subcuticular infection structures, as this pathogen can develop infection-like structures inside cellophane membranes (CMs) overlaying potato dextrose agar (PDA) in culture. Remarkably, the infection structures developed in culture resemble the infection structures developed by the fungus during colonization of the subcuticular environment of apple (**Figure 1-4**) [25]. On top of a CM, *V. inaequalis* conidia germinate and develop a germ tube and, sometimes, an appressorium (**Figure 1-4. A**). Inside the CM, *V. inaequalis* develops subcuticular-like hyphae that, similar to those observed *in planta*, are wider than surface hyphae (**Figure 1-4. B**). These hyphae are swollen and fused longitudinally, again like the runner hyphae observed *in planta* (**Figure 1-4. C**). *V. inaequalis* also develops stroma-like structures inside the CM (**Figure 1-4**. **D**). These structures display a coral-like morphology that resemble the stromata developed in apple (**Figure 1-4**. **D**) [25]. Cross sections of the CM have confirmed that the stroma-like structures are formed within the CM membrane itself (**Figure 1-4**. **E**).

However, the structures developed in CMs are not identical to the structures developed *in planta*. For example, the stroma-like and runner-like hyphae developed in CMs are larger and wider than the stromata and runner hyphae developed in apple, which could be the result of an excess of nutrients available on PDA, and the lack of spatial limitations inside CMs. The trigger for the morphogenesis of infection-like structures in CMs is, to date, still unknown. However, the observation that these structures only develop inside the CM, indicates a potential sensing mechanism that recognizes the texture and/or pressure of the environment [25]. Future work will allow the similarities and differences between the infection structures developed in CMs and *in planta* to be determined. Altogether, the ability of *V. inaequalis* to grow inside CMs renders

it a perfect model species for studying the morphological differentiation of subcuticular infection structures by this fungus and other subcuticular fungal species.

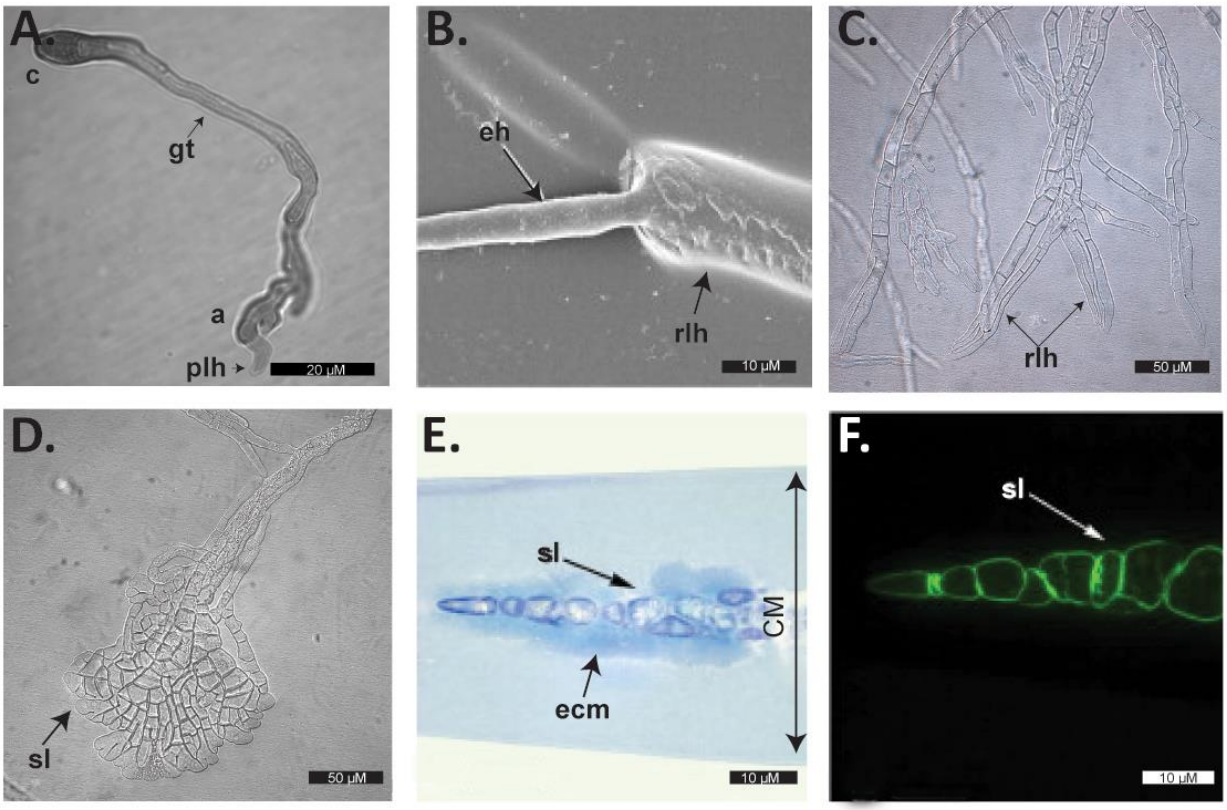

Figure 1-4. Growth of *Venturia inaequalis* in and on cellophane membranes (CMs) mimics growth of this fungus in and on apple tissue. A. Germination of a *V. inaequalis* conidium (c), germ tube (gt) and formation of an appressorium (a) on the surface of a CM. After penetration, a primary-like hypha (plh) is formed inside the CM. **B.** Scanning electron micrograph of a hypha emerging out of a CM. Note that the emerging hypha (eh) has a reduction of diameter compared with the runner-like hypha (rlh) formed inside the CM. Micrograph from B. extracted from Kucheryava et al. [25] with permission from Elsevier. **C.** rlh formed inside a CM. **D.** A stroma-like structure (sl) formed inside a CM. **E.** Cross section of a sl structure formed inside a CM stained with aniline blue, surrounded by an extracellular matrix (ecm). Arrow indicates the width of the CM. **F.** Cross section of a sl structure formed inside a CM labelled with a (1-3)-β-glucan antibody and observed by fluorescence microscopy under UV excitation. Micrographs from E. and F. extracted from Kucheryava et al. [25] with permission from Elsevier.

3. The fungal cell wall: composition and structure

The fungal cell wall is a dynamic interface with a crucial role in maintaining cell integrity and in mediating interactions with the environment [64]. As the first physical structure to make contact with the hostile environment of the plant, the fungal cell wall plays an important role in pathogenesis and is a promising target for the development of fungicides [65]. The composition and organization of the fungal cell wall have been extensively studied in model species, mostly human pathogens. However, research on the cell wall composition of fungal plant pathogens is very limited, with only a few studies focusing on the cell wall of the wilt fungus, F*usarium. oxysporum* [66], the grey mould fungus *Botrytis cinerea* [67] and *R. secalis* [68]. In addition, one study from 1965 investigated the gross *V. inaequalis* cell wall composition [69].

Research on model species has shown that the cell wall varies greatly between and within species, as illustrated in **Figure 1-5**. In general terms, the fungal cell wall contains around 90% polysaccharide (glucans, chitin and mannan) and 2–3% protein (glycoproteins and mannoproteins) [70]. Glucan is the main structural polysaccharide and represents around 50% of the total cell wall dry weight [71]. Glucans are classified based on their type of linkage: α-bound glucans and β-bound glucans [72]. The majority of glucans in the fungal cell wall are β-1,3-glucans and, in some cases, β-1,6-glucan linkages can also be found. Most authors consider the β-1,4-linkage to be absent from fungal cell walls, as β-1,4-glucan has only been reported from *Microdichium nivale* [73] and, more recently, *Aspergillus fumigatus* [72,74]. Additionally, some fungal species also contain α-1,3-glucans. In contrast, chitin represents only around 1–2% of the cell wall dry weight of yeast and around 10–20% of filamentous fungi [71].

The structure of the fungal cell wall varies greatly between fungal species. However, in general, the fungal cell wall of Ascomycetes is made of two layers: a polysaccharide-rich core layer and a protein-rich outer layer [75]. In most fungal species, the inner layer consists

of covalently linked β-1,3-glucan and chitin, with these carbohydrates forming a basket-like scaffold that serves as an exoskeleton around fungal cells [75]. The outer layer of the cell wall is more variable than the inner layer. The outer layer is usually rich in mannosylated glycoproteins, in particular glycosylphosphatidylinositol (GPI)-anchored proteins [76] and proteins with internal repeats (Pir) [77,78] as well as agglutinins [79] and hydrophobins [80,81]. Some fungal species, such as *Histoplasma capsulatum*, have an outer layer with α-1,3-glucan (**Figure 1-5**) and others, like *Cryptococcus* spp., have a distinct polysaccharide capsule surrounding their cell wall, composed of glucuronoxylomannan and galactoxylomannan (**Figure 1-5**) [75].

Even though many models about the structural distribution of the different components of the cell wall in different fungal species are available, information about the cell wall of plant pathogenic fungi is scarce. Additionally, the cell wall carbohydrate distribution is still unclear, due to the lack of non-destructive techniques to study the cell wall and the variability between the cell wall of different species. However, recent studies have started to re-define our current knowledge on the fungal cell wall structure. In *A. fumigatus*, chitin and α-1,3-glucan have been reported to form a cross-linked hydrophobic core which is surrounded by a mobile matrix of β-glucans and a hyper-mobile matrix of α-1,3-glucan and glycoproteins [74]. This structural role of α-1,3-glucan is novel and highlights the limitations of our current understanding of the fungal cell wall structure. Applications of novel non-destructive techniques will greatly change our current knowledge of fungal cell walls in the years to come [74].

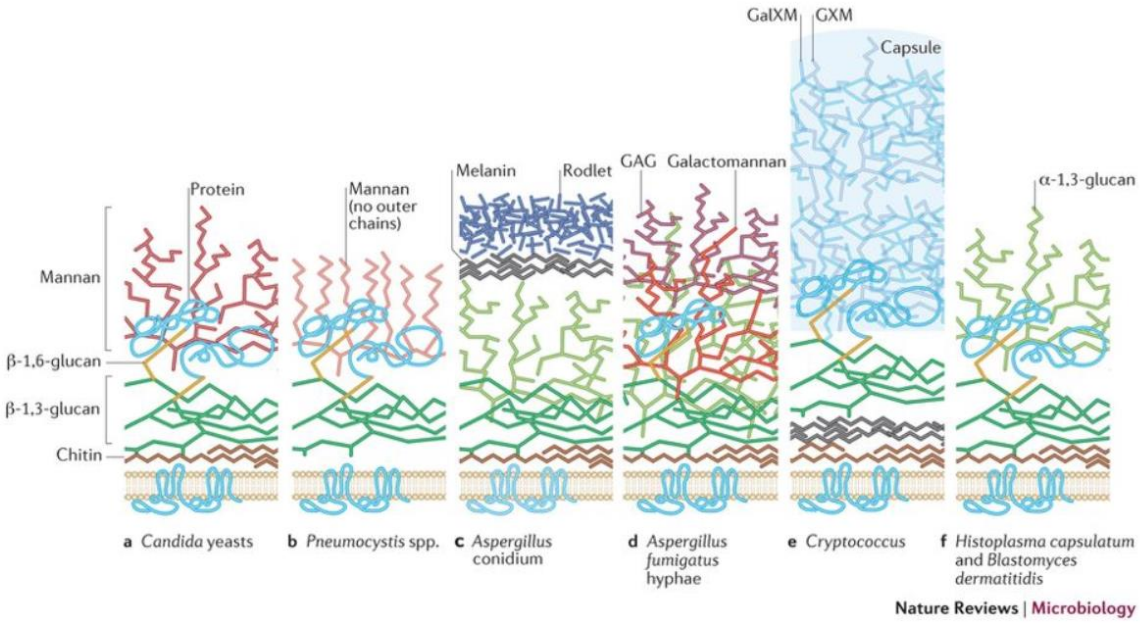

Figure 1-5. Cell wall composition of fungi with different lifestyles. The inner cell wall layer is usually composed of chitin and β-1,3-glucan and the outer cell wall layer is usually comprised of a matrix of polysaccharides and glycoproteins. GAG, Glycosaminoglycan; GalXM, Galactoxylomannan; GXM, Glucuronoxylomannan. Figure extracted from LP Erwig and NAR Gow [82] with permission from Nature.

3.1. Fungal cell wall biosynthesis

Chitin is a polymer of N-acetylglucosamine that is synthesized as microfibrils by plasma membrane-associated enzymes named chitin synthases (CHSs). These enzymes synthesize chitin from the cytosol by the addition of N-acetylglucosamine to the non-reducing end of the polymer and transfers the elongating chitin polymer to the cell wall space through a plasma membrane channel [83]. Chitin synthesis occurs mostly at the active sites of cell growth (e.g. the hyphal apex) and at sites of cell wall remodelling [84]. The number of *CHS* genes greatly differs between species; yeast species usually have one to three *CHS* genes, while filamentous fungi typically have more than ten [85]. *CHS*s genes could have expanded in filamentous fungi as a result of their complex life cycle stages of vegetative and sexual growth compared with yeasts [86].

Different methods to classify CHS enzymes exist and there are multiple discrepancies in the nomenclature [87,88]. In the current nomenclature by Mandel et al. [87] from

2006, division I consists of CHSs from classes I, II and III. CHSs from division I are characterized by the presence of short 'chitin synthase domain 2' module (PF03142) with a hydrophilic amino (N)-terminus and a hydrophobic carboxyl (C)-terminus (**Figure 1-6**). Division II contains CHSs from classes IV, V and VII. CHSs from division II are characterized by the presence of an N-terminal 'myosin motor-like domain' (PF00063) and a 'cytochrome b5-binding domain' (PF00173) before a C-terminal 'chitin synthase domain 2' module (**Figure 1-6**). Finally, division III consists of class VI. This class only has a 'chitin synthase domain 2' module, which is shared among all CHSs [85,86,88,89] (**Figure 1-6**). It is important to note that the previous classification from 2004 by Choquer et al. [88] placed class VI in division II.

All fungal CHSs contain four to seven transmembrane domains and the conserved motifs QXRRW, EDRXL, and QXXEY [86,88,90]. Remarkably, CHSs are very diverse and enzymes from the same class do not share the same function in all species. In general, CHSs with a 'myosin motor-like domain' (class V and VII), are important for apical growth, morphogenesis and pathogenicity as seen in the phenotype of deletion mutants [85,91-94]. However, there are a few exceptions and in some plant-pathogenic fungi, such as *B. cinerea*, deletion of a gene encoding a class V CHS with a 'myosin motor-like domain' did not affect virulence [95].

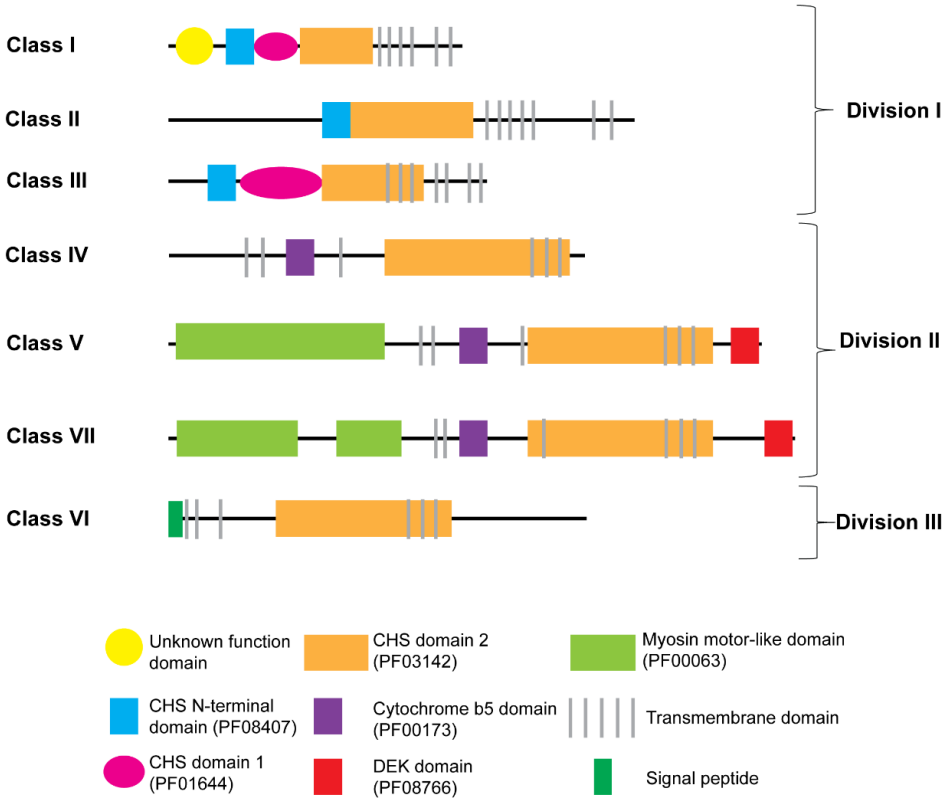

Figure 1-6. Schematic representation of the seven fungal chitin synthase (CHS) classes. Figure depicts CHSs identified from *Neurospora crassa* and was modified from Fajardo et al. [85]. CHSs are classified using nomenclature by Mandel et al. [87].

β-1,3-glucan is synthesized by a glucan synthase complex composed of the plasma membrane catalytic subunit Fks1, and the regulatory subunit Rho1. Here, the Rho GTPase acts as a molecular switch regulating the synthesis of β-1,3-glucan [64,83]. Many fungal species such as the filamentous fungi *A. fumigatus* and *Neurospora crassa*, as well as the yeast *Candida albicans*, have only one copy of the *Fks1* gene, while other fungal species have up to three or four copies [83]. The glucan synthase complex is crucial for cell wall biogenesis and fungal viability and, for this reason, this complex is the target of many antifungal chemicals, such as echinocandins [83]. The genes responsible for β-1,6-glucan synthesis in fungi are still undetermined; however, some genes are known to affect β-1,6-glucan synthesis, such as *Kre1* and *Kre6* [71,83,96].

In contrast to those described above, the synthesis of other polysaccharides that make up the cell wall of fungi is less well understood. One such example is α-1,3-glucan synthesis, as only some species have been reported to be able to synthesize this carbohydrate. In *A. fumigatus*, α-1,3-glucan is an important cell wall component, with this fungus having three α-1,3-glucan synthase-encoding genes (*AGS1*, *AGS2*, *AGS3*). Other species, however, might have none or only one α-1,3-glucan synthase-encoding gene [71,83].

4. Plant-microbe interactions: how plant pathogens achieve infection

Plants interact with a plethora of microbes over the course of their life. However, these interactions rarely result in disease, as the plant innate immune system has multiple immune receptors capable of recognizing pathogens and eliciting plant defences to stop infection [97,98]. Multiple models have been generated to summarize plant-pathogen interactions. The most well-known is the 'zigzag model' that describes two layers of plant immunity [99] (**Figure 1-7**). In brief, in this model, the first layer of immunity is thought to consist of cell-surface pattern recognition receptors (PRRs) that detect microbial elicitors, known as pathogen- or microbe-associated molecular patterns (PAMPs/MAMPs). These PAMPs/MAMPs are usually conserved molecules that are important for pathogen survival, such as cell wall-derived chitin fragments from fungal microbes [98]. Recognition of PAMPs/MAMPs by the PRRs elicits a broad-spectrum plant immune response known as PAMP/MAMP-triggered immunity (PTI/MTI), that halts or slows host infection. In turn, pathogens secrete effector molecules to stop PTI/MTI, providing effector-triggered susceptibility (ETS). In this model, the second layer of immunity relies on intracellular receptors termed resistance (R) proteins that recognize specific pathogen effector molecules to elicit effector-triggered immunity (ETI). Pathogen effector molecules that are recognized by R proteins are termed avirulence (Avr) effector proteins because their recognition typically renders the pathogen avirulent. In general, ETI is considered a stronger and faster immune response than PTI/MTI and induces a localized cell death response to prevent pathogen spread, known as the hypersensitive response (HR) [97,99]. Finally, to circumvent ETI and reinstate ETS, pathogens may delete or modify the gene encoding the recognized Avr effector to avoid recognition by the corresponding R protein. In turn, during this ongoing evolutionary battle, the host plant may evolve new R proteins that can recognize the mutated or new Avr effectors, triggering plant defences and restoring ETI [97,99].

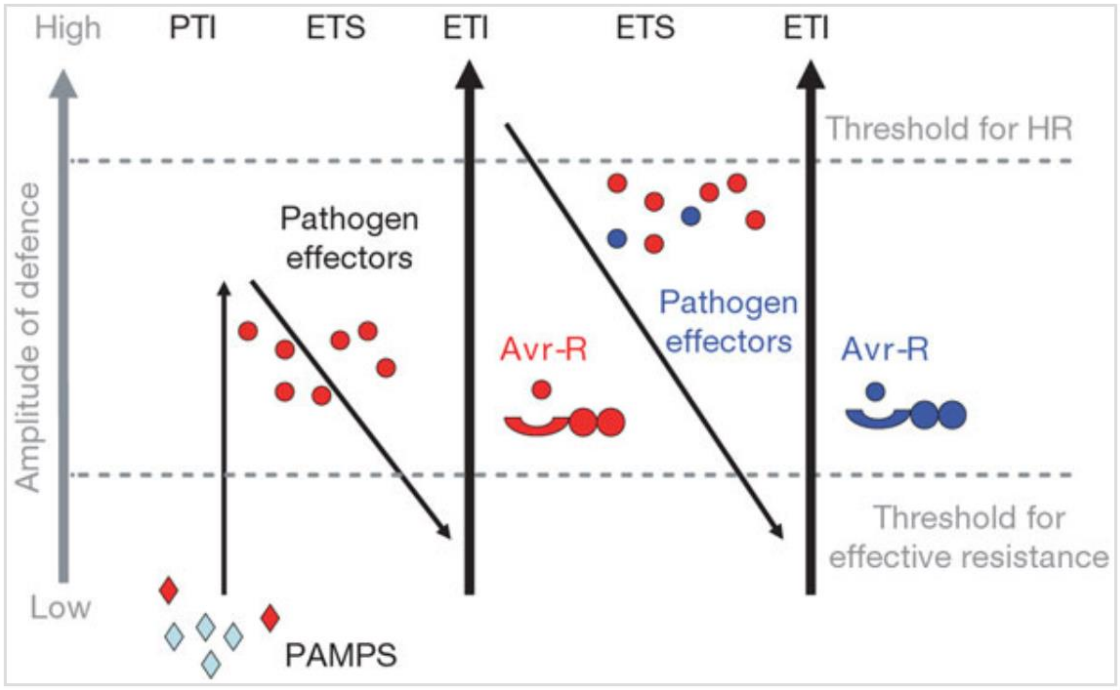

Figure 1-7. The 'zigzag model' illustrating the immune response of plants originally described by Jones & Dangl (2006). First, in this model, pathogen- or microbe-associated molecular patterns (PAMPs/MAMPs) (red diamonds) are detected by plants using cell surface-localized pattern recognition receptors (PRRs), triggering PAMP/MAMP-triggered immunity (PTI/MTI). Second, successful pathogens secrete virulence factors termed effectors to inhibit or suppress PTI, resulting in effector-triggered susceptibility (ETS). Third, an effector is recognized by an intracellular resistance (R) protein (in this model), triggering effector-triggered immunity (ETI), a more intense plant defence response that often involves a hypersensitive cell death response (HR). Here, the recognized effector is termed an avirulence effector (Avr), as recognition results in the pathogen being unable to cause disease. Fourth, the pathogen circumvents ETI, either by loss or mutation of the Avr effector, or by acquiring or repurposing another effector to suppress ETI, resulting in ETS once more. In this continuing arms-race, the plant is under selection pressure to evolve novel R proteins that can recognize the new or mutated Avr effectors, resulting again in ETI. Figure extracted from Jones & Dangl [99] with permission from Nature.

The 'zigzag model' is a great starting point to understand plant immunity. However, it is only applicable to biotrophic plant pathogens and does not incorporate necrotrophic pathogens or symbionts [100]. For example, necrotrophic pathogens can activate PRRs to trigger the cell death response to obtain nutrients from dead tissue, as shown for the causal agent of Septoria nodorum blotch, *Parastagonospora nodorum* [101]. Additionally, this model does not account for the recognition by the plant immune system of host-derived fragments generated by the pathogen during infection, so-called damage-associated molecular patterns (DAMPs) [100]. Finally, the

'zigzag model' excessively compartmentalizes the two layers of immunity [100]. Since the publication of this model, multiple Avr effectors have been shown to be recognized by PRRs and activate a strong immune defence response that can be classified as ETI [100,102]. Therefore, PRRs do not exclusively recognize PAMPs/MAMPs, but these cell surface receptors can also recognize DAMPs and Avr effectors. Finally, recent studies have shown that PTI and ETI work together to elicit strong immune defence responses [102,103]. For example, it has been observed that the HR triggered by intracellular receptors (ETI) is enhanced by the activation of PRRs (PTI), highlighting how PTI potentiates the immune response elicited by ETI [103].

These limitations led to the creation of a simpler model known as the 'invasion model', which incorporates all types of symbiotic interactions, from pathogenesis to mutualism [100] (**Figure 1-8**). In the 'invasion model', plant immune receptors, termed invasion pattern receptors (IPRs), recognize invasion patterns (IPs) (**Figure 1-8**). IPs are any microbe- or plant-derived molecules, including MAMPs, DAMPs and Avr effectors (**Figure 1-8**) [100]. Recognition of IPs by IPRs leads to activation of an invasion pattern-triggered response (IPTR). For biotrophic pathogens, failure to suppress this IPTR leads to cessation of the symbiosis (infection). In contrast, necrotrophic pathogens might utilize this IPTR to continue host-invasion.

Rapid plant defences associated with the IPTR consist of changes in ion fluxes, an increase of cytosolic calcium concentration, and an oxidative burst characterized by the accumulation apoplastic reactive oxygen species (ROS). Additionally, the IPTR is characterized by callose deposition and activation of defence-related kinases that trigger a transcriptional reprogramming of the host, which leads to the production of pathogenesis-related (PR) proteins with antimicrobial activities, such as chitinases and glucanases that hydrolase the fungal cell wall [104-106].

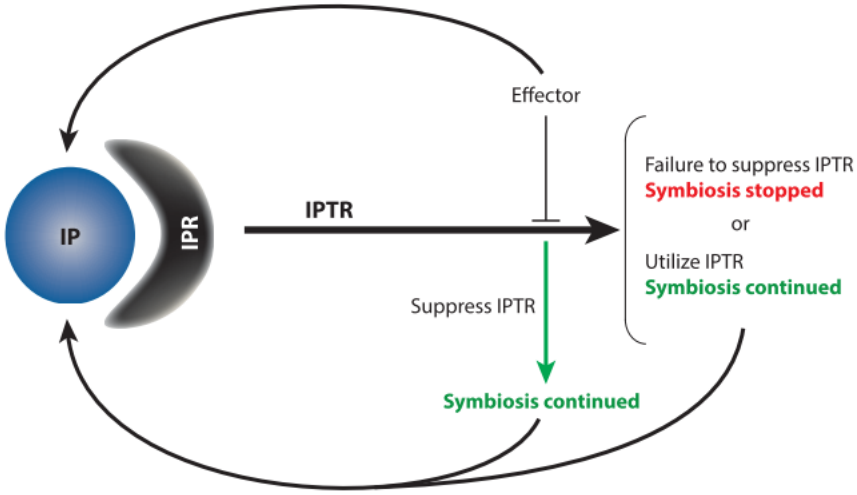

Figure 1-8. Schematic representation of the 'invasion model'. Invasion patterns (IPs) are recognized by plant invasion pattern receptors (IPRs) inducing a plant defence response known as the IP-triggered response (IPTR). Plant-associated microbes can use effectors to supress the IPTR. However, one or more of these effectors may be recognized by IPRs to activate an IPTR. Biotrophic infection is stopped if the microbe is unable to suppress the IPTR (symbiosis stopped). Contrarily, some microbes, such as necrotrophic pathogens, can exploit this IPTR to continue host infection (symbiosis continued). Figure adapted from Cook et al. [100], with permission from Annual Reviews in Phytopathology.

4.1. Plant immune receptors

Plant immune receptors are classified based on their subcellular localization and amino acid sequences. PRRs are cell surface-localized extracellular receptor-like kinases (RLKs) or receptor-like proteins (RLPs) [107,108]. RLKs contain an extracellular domain for ligand recognition (ectodomain) and an intracellular kinase domain for activation of plant defences. Ectodomains for ligand recognition include leucine-rich repeat (LRR), lysin motif (LysM), lectin, malectin and epidermal growth factor-like domains [108]. In contrast, RLPs only have an extracellular ectodomain and lack an intracellular kinase domain; therefore, they depend on RLK proteins to active plant defences [107,108]. Intracellular immune receptors are NLR receptors with a central nucleotide-binding (NB) domain and a leucine-rich repeat (LRR) domain that determines the specificity of the Avr effector recognition [109]. There are three types of NLR receptors based on

their N-terminal domain: NLRs with a coiled-coil (CC) domain, NLRs with Toll/Interleukin-1 (TIR) domain, and NLRs with an RPW8-like CC domain (RPW8) [102,109]. Additionally, some NLRs also have other noncanonical integrated domains that function as an effector bait; this is known as the 'decoy model'[110]. In some cases, these domains have originated by duplication of a host protein targeted by an effector [110]. A well-known example of an integrated domain is the heavy metal-associated (HMA) domain, integrated in rice NLRs that recognizes multiple Avr effectors from the rice blast fungus *Magnaporthe oryzae* [111,112].

4.1.1. Glycan-triggered immunity

Structural components of the fungal cell wall such as β-glucan oligosaccharides and chitin, function as PAMPs/MAMPs that elicit plant defences to activate glycan-triggered immunity [113]. Plants recognize chitin and β-1,3-glucan through PRRs. Little is known about β-glucan perception in plants, and a β-glucan receptor in plant species remains elusive [114]. In contrast, chitin perception in plants is better understood. Chitin is recognized by LysM-RLKs. In rice, the chitin RLP OsCEbiP is known to bind chitin and recruit the receptor kinase OsCERK1 to induce plant defence signalling [113]. As part of the plant defence response, plants secrete hydrolytic enzymes to interfere with fungal colonization. Hydrolytic enzymes stop fungal growth by compromising the integrity of the fungal cell wall. Additionally, hydrolysis of the fungal cell wall releases cell wall oligomers that can further function as PAMPs/MAMPs. To achieve host-colonization, pathogens use different strategies to avoid the elicitation of plant defences, including the secretion of effectors and the chemical modification of the fungal cell wall [113,115]. A literature review of apoplastic effectors with a focus on effectors that inhibit glycan-triggered immunity is presented in Chapter 2 of this thesis.

4.2. Chemical modifications of the fungal cell wall

Pathogenic fungal species use different strategies to avoid triggering plant defences and to protect themselves from the hostile host-environment [65,113,116-118]. One proposed strategy to avoid recognition by the plant immune system is to deacetylate chitin to chitosan, with the help of chitin deacetylases (CDAs), as chitosan is a poor elicitor of plant defences [119-121] and a weak substrate for plant chitinases [122,123]. CDAs can be bound to the fungal cell wall or secreted to the extracellular space. CDAs with a GPI anchor are likely to function with CHSs in nascent chitin polymers. In contrast, secreted CDAs without a GPI anchor might be involved in deacetylation/inactivation of chitin fragments to avoid triggering plant defences [124,125]. Secreted CDAs from the plant-pathogenic fungal species have been shown to deacetylate chitin oligomers to avoid chitin-triggered immunity [124,126] (reviewed in Chapter 2).

To date, chitosan has been observed to accumulate on the outer layer of the cell wall of the stem rust fungus *Puccinia graminis*, the broad bean rust fungus *Uromyces fabae*, the anthracnose pathogen *Colletotrichum graminicola* [127], *M. oryzae* [128], the corn smut fungus *Ustilago maydis* [129] and the endophyte *E. festucae* [130]. However, direct experimental evidence showing the benefits of chitosan accumulation on the cell wall to protect fungal cell walls from host chitinases has not yet been shown [131].

In addition to the role of chitosan in infection, chitosan has also been reported to be important for the morphogenesis of infection structures. In *M. oryzae*, chitosan was found to be required for appressorium formation by mediating germling adhesion and sensing of stimuli [132-134]. Finally, chitosan has also been shown to be crucial for sporulation in the filamentous fungal plant pathogen *Ashbya gossypii* [135] as well as for vegetative growth in the yeast human pathogen *Cryptococcus neoformans* [136]. Nevertheless, the diverse distribution of chitosan in the cell wall

of different fungal species indicates that chitosan may play multiple functions depending on the species and cellular morphotype [128].

Another strategy to avoid glycan-triggered immunity is the accumulation of α-1,3-glucan on the cell wall surface. The role of α-1,3-glucan in pathogenesis was first discovered in the fungal mammal pathogen *Histoplasma capsulatum* where α-1,3-glucan was found to shield chitin to evade host defences [137,138]. Then, Fujikawa et al. [139] reported an accumulation of α-1,3-glucan on the appressoria and germ tubes of the plant pathogen *M. oryzae* and showed that α-1,3-glucan accumulation on the surface of fungal hyphae increased hyphal resistance against plant chitinases [139]. More recently, in some fungal species α-1,3-glucan synthesis has been observed to occur during hyphal growth and conidial aggregation, highlighting the potential importance of α-1,3-glucan in fungal morphogenesis [140].

4.3. Fungal effectors

4.3.1. Fungal effector functions

Plant-associated microbes secrete effectors to successfully establish infection [115,141,142]. Effectors are defined as any molecule that promotes host-colonization, including enzymatic and non-enzymatic proteins, secondary metabolites and small RNAs [115,141,142]. Traditionally, fungal proteinaceous effectors are identified based on the presence of an N-terminal signal peptide for secretion to the apoplast and the presence of many cysteine residues in their sequence, which often form disulphide bonds to provide stability in the harsh apoplastic environment [115,141]. However, effectors without a signal peptide have also been observed to be translocated and function inside host cells, suggesting that some effectors are unconventionally secreted [143]. Effectors can be classified based on the location where they function in the plant cells. Apoplastic effector proteins (AEPs) perform their function in the host apoplast, while intracellular effectors

function inside plant cells [142]. Additionally, some effectors might have a dual function/location in both compartments [141].

The molecular basis of effector delivery and translocation into host cells is still poorly understood [142,144]. In *M. oryzae*, effectors that are translocated to the plant cell are observed to first localize to a biotrophic interfacial complex (BIC) on the hyphal tip that appears to be essential for effector delivery [145]. Interestingly, in *U. maydis*, a protein complex of seven effectors has been identified to be potentially associated with the delivery of effectors [146]. The protein complex is composed of the effectors Pep1, Cce1 (Stp4), Stp1, Stp3, Stp6, Sp2 and Stp5. This effector complex is located on the surface of biotrophic hyphae and is essential for suppressing plant defence responses, making it likely to be involved in the delivery of effector proteins during host infection [146].

The functions of AEPs from plant-associated fungi and oomycetes are reviewed in Chapter 2 of this thesis; therefore, this section only focuses on the function of intracellular effectors (**Table 1-2**). Most intracellular fungal effectors identified to date are small, non-enzymatic proteins [147]. Some exceptions are the effectors Cmu1 from *U. maydis* [148] and VdIsc1 from *Verticillium dahliae*, the causal agent of Verticillium wilt [143] (**Table 1-2**). These effectors are enzymes that suppress salicylic acid synthesis by hydrolysing a salicylic acid precursor [143,148]. Many intracellular fungal effectors manipulate plant defences at the transcription level, for example by interacting with transcription factors (e.g. VdSCP41 from *V. dahliae*) [149] (**Table 1-2**) or at the posttranslational level, by manipulating the ubiquitin proteosome system. For example, AvrPiz-t from *M. oryzae* suppresses the activity of a ubiquitin ligase [150], while Tin2 from *U. maydis* masks a ubiquitin-proteasome motif to stabilize a host protein that induces anthocyanin biosynthesis [151] (**Table 1-2**). Other effectors can suppress plant defences by directly inhibiting

plant defence kinases such as BAK1 and BIK1, as reported for the widely conserved fungal effector, NIS1[152] (**Table 1-2**).

Table 1-2. Selected intracellular effectors of biotrophic and hemibiotrophic plant-pathogenic fungi with characterized biological functions.

Effector protein	Fungal plant pathogen	Characterized biological function inside host cell	References
Cmu1	*Ustilago maydis*	Reduces levels of chorismate, a salicylic acid precursor.	[148]
Tin2	*U. maydis*	Promotes anthocyanin biosynthesis to inhibit cell wall lignification.	[151]
See1	*U. maydis*	Activates plant DNA synthesis to induce tumour formation.	[153]
Jsi1	*U. maydis*	Induces jasmonate/ethylate signalling to induce biotrophic susceptibility.	[154]
Pst18363	*Puccinia striiformis* f. sp. *tritici*	Suppresses accumulation of reactive oxygen species (ROS) by stabilizing the negative regulator of defense, TaNUDX3.	[155]
AvrL567	*Melampsora lini*	Modulates cytokinin levels.	[156,157]
BEC1054	*Blumeria graminis* f. sp. *hordei*	Suppresses cell death by inhibiting host ribosome-inactivation proteins.	[158]
BEC4	*B. graminis* f. sp. *hordei*	Interferes with host-associated vesicle trafficking.	[159]
AvrPiz-t	*Magnaporthe oryzae*	Suppresses plant immunity by modulating the activity of ubiquitin ligase and host potassium channels.	[150,160-162]
Avr-Pii	*M. oryzae*	Suppresses plant immune responses by inhibiting the malic enzyme NADP-ME2 and by interacting with an exocytosis complex.	[163,164]

Effector protein	Fungal plant pathogen	Characterized biological function inside host cell	References
Avr-Pita	*M. oryzae*	Inhibits ROS by increasing cytochrome c oxidase (COX) activity, an enzyme that scavenges ROS.	[165]
VdIsc1	*Verticillium dahliae*	Hydrolyses isochorismate, a salicylic acid precursor.	[143]
VdSCP41	*V. dahliae*	Inhibits a transcription factor to suppress host immunity.	[149]
NIS1	Conserved in Ascomycota and Basidiomycota fungi	Inhibits BAK1 and BIK1 kinases to suppress plant defences.	[152]

4.3.2. Structural effector families of fungi

Most fungal effector proteins do not share sequence similarity to proteins of known function; this is likely due to the evolutionary pressure on these proteins to evade recognition by corresponding R proteins [166]. The lack of sequence similarity and absence of known domains make the identification and functional characterization of fungal effector proteins difficult. However, protein tertiary structures are more conserved than amino acid sequences due to the strong evolutionary relationship between structure and function [166]. Therefore, investigation of effector protein tertiary structures can help researchers to understand their function. Recent advances in structural biology have shown that many effector proteins share structural commonalities with effectors proteins seemingly unrelated at the amino acid level [166-170].

A family of effector proteins with a common fold was identified in *M. oryzae*, the '*Magnaporthe* Avrs and ToxB-like' (MAX) family. The MAX family is composed of effectors with a six-stranded β-fold with at least one disulphide bond. Remarkably, many *M. oryzae* Avrs belong to the MAX effector family (**Table 1-3**). A number of these MAX effectors, such as Avr-Pik, Avr-Pia and Avr1-CO39, interact with an integrated HMA domain in NLR receptors (**Table**

1-3), indicating that this structure could be a scaffold suited to interact with these HMA domains [166,167,171]. Interestingly, the MAX family also includes the ToxB protein from *Pyrenophora tritici-repentis*, the causal agent of tan spot disease in wheat [167,172]. The ToxB effector protein is a host-selective toxin that induces cell death; however, its mode of action and interacting partner(s) are, to date, still unknown [172]. With the advent of highly accurate *de novo* protein structure prediction [173], a high-throughput analysis of the *M. oryzae* secretome has now shown that the MAX effectors in *M. oryzae* are more abundant than previously thought [168,174], with transcriptome data also highlighting that these effectors are co-expressed during host-colonization [175].

Another structural effector family was predicted in the powdery mildew fungus, *Blumeria graminis*. A large-scale structural prediction of effector candidates (ECs) from *B. graminis*, prior to the development of AlphaFold2, led to the identification of a subset of ECs with an RNAse-like fold and were named 'RNAse-like proteins expressed in haustoria' (RALPH) proteins [176-178]. A subsequent large-scale structural study of effectors from multiple plant pathogens, based on AlphaFold2, has now shown that RALPH effectors are particularly expanded in *B. graminis*, where they represent 43% of the secretome [168]. RALPH effectors have been shown to promote virulence (e.g. the RALPH effector BEC1054) [158,177] (**Table 1-2**) or to be Avr effectors recognized by NLRs in wheat (**Table 1-3**).

Another family of structurally related effectors is the '*Leptosphaeria* AviRulence-Suppressing' (LARS) effector family, which was identified in *Leptosphaeria maculans*, the causal agent of oilseed rape stem canker. Members of the LARS family are characterized by a tertiary structure with four β-sheets and one α-helix, stabilized by three conserved disulphide bridges [169]. To date, the LARS family includes the Avr effectors AvrLm3, AvrLm4-7 and AvrLm5-9 from *L. maculans*, as well as the candidate Avr effector Ecp11-1 [179] from the tomato leaf mould

pathogen *Fulvia fulva* (synonym: *Cladosporium fulvum*) [169]. Additionally, the recent large scale AlphaFold2 study mentioned above predicted that many effectors of different fungal pathogens adopt a LARS-like fold [168].

Another known structural effector family is the 'ToxA-like' family. This family was identified when the crystal structure of the AvrL567 Avr effector protein from the flax rust pathogen *Melampsora lini* was solved [180]. Remarkably, it was observed that AvrL567 adopted a compact β-fold that resembled the structure of the host-selective toxin effector ToxA from *P. tritici-repentis* [181]. Recently, the structure of the Avr2 (also known as Six3) Avr effector from *F. oxysporum* f. sp. *lycopersici,* the causal agent of tomato wilt disease, was crystallized and intriguingly, this protein also adopted the compact β-fold of the ToxA-Like family [182].

Finally, a new structural class of effectors has been recently discovered in *F. oxysporum* f. sp. *lycopersici*, the Fol dual-domain (FOLD) effectors [170]. The tertiary structure of the Avr effectors Avr1 (Six4) and Avr3 (Six1) have been solved by X-ray crystallography and shown to adopt a unique two-domain fold. Using AlphaFold2, other *F. oxysporum* f. sp. *lycopersici* ECs were also predicted to belong to the FOLD family [170].

Table 1-3. Avirulence (Avr) effectors from plant-pathogenic fungi with an experimentally determined protein tertiary structure that belongs to a structural family.

Avr effector	Fungal plant pathogen	Immune receptor[a]	Mode of recognition[b]	Structural family[c]	References
AvrL567	*Melampsora lini*	L5, L6 and L7 (NLR)	Direct	ToxA-like	[157,180,183]
AvrPiz-t	*Magnaporthe oryzae*	Piz-t (NLR)	Indirect	MAX	[150,184-186]
Avr-CO39	*M. oryzae*	CO39, RGA4/RGA5 (NLR-HMA)	Direct	MAX	[167,187,188]
Avr-Pia	*M. oryzae*	RGA4/RGA5 (NLR-HMA)	Direct	MAX	[167,187]
Avr-Pik	*M. oryzae*	Pik-1/Pik-2 (NLR-HMA)	Direct	MAX	[112,189-191]
Avr-Pib	*M. oryzae*	Pib (NLR)		MAX	[192]
AvrLm3	*Leptosphaeria maculans*	Rlm3 (NLR)		LARS	[169,193,194]
AvrLm5-9	*L. maculans*	Rlm9 (WAKL)	Indirect?	LARS	[169,195]
AvrLm4-7	*L. maculans*	Rlm4, Rlm7 (WAKL)		LARS	[196,197]
Avr1 (Six4)	*Fusarium oxysporum* f. sp. *lycopersici*	I (LRR-RLP)		FOLD	[170,198,199]
Avr2	*F. oxysporum* f. sp. *lycopersici*	I-2 (NLR)	Direct?	ToxA-Like	[182,200]
Avr3 (Six1)	*F. oxysporum* f. sp. *lycopersici*	I-3 (S-RLK)	Indirect?	FOLD	[170,201,202]

[a] NLR: Nucleotide-binding domain and Leucine-rich Repeat domain receptor; HMA: Heavy Metal-Associated domain; WAKL: Wall-Associated Kinase-Like, RLP: Receptor Like Protein, RLK: Receptor Like Kinase, S-RLK: RLK with an S domain homologous to self-incompatibility-locus glycoproteins of *Brassica oleracea*.

b Mode of apoplastic effector protein recognition by the corresponding cell surface immune receptor. Hypothesized modes of recognition based on current experimental data are denoted with a question mark (?).

c MAX: *Magnaporthe* Avrs and ToxB like; LARS: *Leptosphaeria* AviRulence-Suppressing; FOLD: *Fusarium oxysporum* f. sp. *lycopersici* dual-domain.

5. Resistance and susceptibility in the *Venturia–Malus* pathosystem

V. inaequalis is a model pathogen of woody tree hosts, as well as a model species for understanding subcuticular host-colonization by fungi, as this pathogen is restricted to the subcuticular environment during all stages of biotrophic host-colonization. As a result, the genome sequences of multiple *V. inaequalis* isolates have been sequenced [6,27,203,204]. These *V. inaequalis* genomes have an assembly size from 30 to 73 Mb, and a mosaic genome structure with a combination of GC-stabilized and AT-rich regions [6].

Genetic studies investigating the interaction between *Malus* and *V. inaequalis* have led to the genetic identification of many scab-*R* genes [37,38]. In this pathosystem, *R* genes are named *Resistance to V. inaequalis* (*Rvi*) and the corresponding *Avr* gene are named *Avirulence to Rvi* (*AvrRvi*). *V. inaequalis* isolates that can overcome resistance by an *R* gene are defined as a race [5,205]. Recognition of an AvrRvi effector by an Rvi R protein leads to an HR that stops or significantly slows pathogen infection. The strength of this HR is different depending on the R protein and can be divided into three classes [206] (**Figure 1-9**). The class 1 HR is the fastest and strongest of the HRs involving *V. inaequalis* and is characterized by rapid cell death that is visible as a 'pinpoint pit'. In contrast, class 2 HR involves stellate necrosis, while class 3 HR is characterized by chlorosis and reduced sporulation [205,206] (**Figure 1-9**).

To date, even though 19 *AvrRvi–Rvi* gene pairs have been genetically identified [38,205], only two *R* genes, *Rvi6* and *Rvi15*, have been cloned. The *Rvi6* gene encodes an extracellular RLP-type R protein [207], while *Rvi15* encodes an intracellular TIR-NLR-type R protein [208]. Notably, races of *V. inaequalis* that can overcome *Rvi6*-, but not *Rvi15*-mediated resistance, have been identified [38,205]. Furthermore, races of *V. inaequalis* that have overcome most single scab *R* genes used in breeding have now been discovered [38], highlighting the urgent need to identify and develop novel scab-resistant apple cultivars. Given the large number of *V.*

inaequalis races that have broken resistance mediated by single *R* genes, it is anticipated that multiple *R* genes will now need to be stacked into each apple cultivar to provide durable scab resistance [38]. However, before this can happen, the durability of individual *AvrRvi–Rvi* interactions needs to be assessed. This would involve the cloning of *AvrRvi* genes to determine whether their loss or mutation negatively impacts the fitness of *V. inaequalis*. Here, only those *Rvi* genes corresponding to *AvrRvi* genes that cannot be lost or mutated without a significant cost to fitness would be stacked [38]. To date, however, no *AvrRvi* genes have been published, although recent research suggests that *AvrRvi4*, corresponding to *Rvi4* (Silvia de la Rosa et al., in preparation), and *AvrRvi6*, corresponding to *Rvi6* (Bruno Le Cam et al., in preparation), have now been identified.

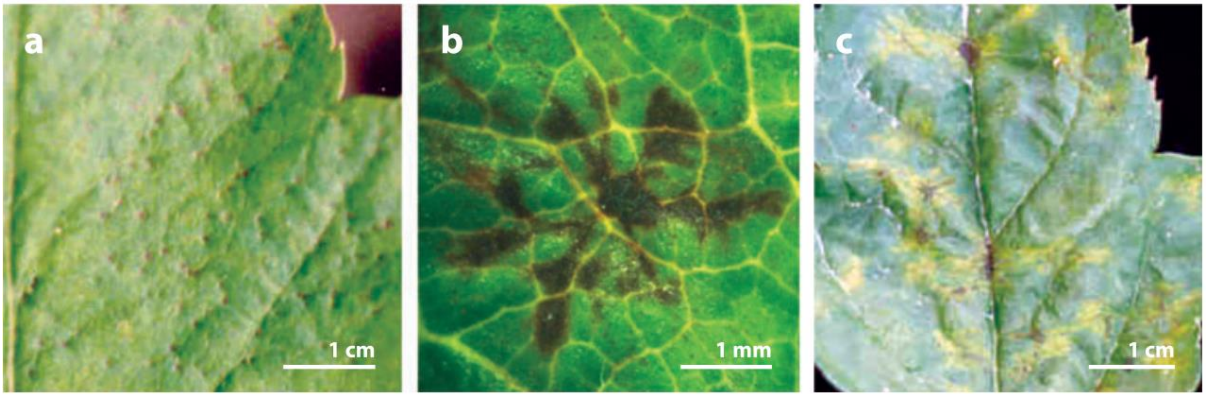

Figure 1-9. Different classes of hypersensitive response (HR) active against the scab pathogen, *Venturia inaequalis*, in apple. A. Class 1, 'pinpoint pit' cell death. **B.** Class 2, stellate necrosis. **C.** Class 3, chlorosis with limited sporulation. Figure adapted from Bus et al. [205] with permission from Annual Reviews of Phytopathology.

Different studies have attempted to predict ECs of *V. inaequalis* that play a crucial role during infection. First, one study used *V. inaequalis* growing on CMs to identify *EC* genes potentially up-regulated *in planta*. This study identified two *cellophane-induced* (*Cin*) genes, *Cin1* and *Cin3*. The proteins encoded by these genes were predicted to be novel and secreted, with an imperfect repeat domain structure [25]. Of these, Cin1 is a cysteine-rich protein with eight repeats of approximately 60 amino acids (C-X9/11C-X6C-X8/13C), that has homology to two other *V.*

inaequalis proteins, Cin1-L1 and Cin1-L2, which have only one repeat [209]. The tertiary structure of the first two repeat domains of Cin1 was determined by nuclear magnetic resonance spectroscopy, with each domain observed to adopt a three-helix disulphide-stabilized bundle with no structural similarity to other proteins [209].

Later, a bioinformatic analysis of expressed sequence tags (ESTs) from a cDNA library generated from a compatible interaction between *V. inaequalis* and *Malus* identified 16 ECs, named *V. inaequalis* candidate effectors (VICEs) [210]. Finally, a study analysed the predicted secretome of *V. inaequalis* together with RNA-seq gene expression data from two host-infection time points, to identify ECs in *V. inaequalis* [203]. This study identified that most of the ECs were novel and/or belonged to expanded effector families. Some of the expanded EC families had amino acid similarity to known effectors, for example, AvrLm6 from *L. maculans* and Ave1 from *V. dahliae* [27,203,211,212]. The *V. inaequalis* gene encoding the AvrLm6-like protein with the highest amino acid similarity to *L. maculans* AvrLm6 was observed to be up-regulated during infection and this protein was found to localize to *V. inaequalis* stromata [27]. Remarkably, most of the ECs were identified in low gene density areas of the genome and close to repetitive elements, indicating that transposable elements could be involved in effector family expansion [27,203].

6. Aims and Objectives

Scab disease management is challenging as fungicide-resistant strains of *V. inaequalis*, as well as strains of this fungus capable of overcoming one or multiple *Rvi* genes of apple, have emerged [38,213]. To develop novel control strategies against scab, a better understanding of how *V. inaequalis* colonizes its host at the molecular level is needed. In particular, more information is needed on the identity and function of effectors deployed by *V. inaequalis* as well as how this fungus develops and maintains infection structures required for subcuticular host-colonization. Given that several other fungal pathogens of economically important crop species demonstrate a subcuticular host-colonization infection strategy, and that subcuticular host-colonization is both massively understudied and not well-understood, this knowledge may also inform disease control programs involving other fungal species. With this in mind, this research project had the following specific objectives:

- **Objective 1 (Chapter 3)**: Identify biological processes and genes of *V. inaequalis* that may play a role in subcuticular host-colonization.
    1. Generate a more comprehensive transcriptome for *V. inaequalis* during subcuticular host-colonization using RNA-seq.
    2. Generate a new genome annotation for *V. inaequalis* isolate MNH120 using bioinformatics.
    3. Study the gene expression profile of *V. inaequalis* during subcuticular host-colonization.
    4. Identify proteinaceous ECs of *V. inaequalis* that are encoded by genes up-regulated during host-colonization using RNA-seq data.

5. Perform a large-scale tertiary structure prediction of proteinaceous effector candidates (ECs) from *V. inaequalis* that are encoded by genes up-regulated during host-colonization to shed light on their putative functions using AlphaFold2.
6. Initiate the functional characterization of proteinaceous ECs from *V. inaequalis* that have a predicted tertiary structure to shed light on their putative functions using *Agrobacterium tumefaciens*-mediated transient transformation assays.

- **Objective 2 (Chapter 4):** Determine how the cell wall polysaccharide composition of *V. inaequalis* dynamically changes during the differentiation of infection structures.
    1. Analyse the cell wall carbohydrate composition of *V. inaequalis* during growth in culture using a glycosidic linkage analysis.
    2. Identify and analyse the carbohydrate synthase-encoding genes in the *V. inaequalis* genome using bioinformatics.
    3. Determine which carbohydrate synthase-encoding genes of *V. inaequalis* have proteomic support during growth of *V. inaequalis* in culture using mass spectrometry.
    4. Profile the gene expression dynamics of carbohydrate synthase-encoding genes during subcuticular host-colonization.
    5. Monitor the dynamics of cell-surface-exposed carbohydrates on the infection-like and infection structures of *V. inaequalis* developed in culture and during host-colonization using confocal laser scanning microscopy.
- **Objective 3 (Chapter 5)**: Develop a gene disruption method in *V. inaequalis* that will facilitate reverse genetic studies.
    1. Attempt different gene disruptions technologies in *V. inaequalis* based on homologous recombination and CRISPR-Cas9 methods.

2. Establish a high-throughput screening method for the detection of *V. inaequalis* mutants developed using gene disruption technologies.

7. Thesis structure

All chapters of this thesis, except the general introduction (**Chapter 1**) and concluding discussion (**Chapter 6**), are presented as manuscripts that are available online as a preprint in *BioRxiv* or as a peer-reviewed manuscript. For each published chapter, the "statement of contribution" form (DRC16) is shown as an appendix.

Chapter 2 is a literature review with a specific focus on apoplastic effector proteins from plant-associated fungi and oomycetes. This review represents an exciting and comprehensive compilation of all apoplastic effector functions described to the point of publication. Furthermore, this review summarizes methodologies for successful prediction and identification of effectors. This chapter has been formatted for the *Current Opinion in Plant Biology* journal and was published in August 2020.

Chapter 3 represents the first comprehensive RNA-seq transcriptome of *V. inaequalis* during colonization of apple. This study focuses on the gene expression profiles and tertiary structure predictions of ECs from *V. inaequalis*. This chapter bas been formatted for the *BMC Biology* journal and was published in November 2022. The manuscript version presented here has been slightly modified from its published version to accommodate the addition of extra data in appendices that could not be added in the published manuscript due to size constraints. Appendix A includes all the supplementary information associated with the manuscript. Appendix B contains information on the general biology and nutrition of *V. inaequalis*. Appendix C contains preliminary data on the functional characterization of the Nod19 EC family from *V. inaequalis*, identified as part of the chapter.

Chapter 4 reports the first characterization of the *V. inaequalis* cell wall carbohydrate composition by glycosidic linkage analysis and investigates cell surface modifications during morphogenesis of infection structures using different probes and antibodies

in conjunction with confocal laser scanning microscopy. This chapter is available as a preprint in *BioRxiv* and it has been formatted for the *mSystems* journal.

Chapter 5 describes the first application of CRISPR-Cas9 technology to *V. inaequalis* for the generation of gene-disrupted mutants. Additionally, this chapter reports the development of a novel methodology for the high-throughput screening of CRISPR-Cas9 mutants. This chapter has been formatted for the journal *Fungal Biology* and was published in January 2022.

Chapter 6 is the general discussion of this thesis. It provides an overview of the main findings from Chapters 2–5 and discusses how the research in these chapters has moved our knowledge on subcuticular host-colonization by *V. inaequalis* (and other plant-pathogenic fungi) forward. Finally, this chapter also highlights future experiments that can be carried out as a follow-up of this thesis.

8. References

1. Beck A, Ritschel A, Schubert K, Braun U, Triebel D: **Phylogenetic relationships of the anamorphic genus *Fusicladium* s. lat. as inferred by ITS nrDNA data**. *Mycological Progress* 2005, **4**:111-116.
2. Shen M, Zhang JQ, Zhao LL, Groenewald JZ, Crous PW, Zhang Y: **Venturiales**. *Studies in Mycology* 2020, **96**:185-308.
3. Zhang Y, Crous PW, Schoch CL, Bahkali AH, Guo LD, Hyde KD: **A molecular, morphological and ecological re-appraisal of Venturiales—a new order of Dothideomycetes**. *Fungal Diversity* 2011, **51**:249-277.
4. Sivanesan A: *The taxonomy and pathology of Venturia species*: Bibliotheca Mycologica; 1977.
5. Bowen JK, Mesarich CH, Bus VG, Beresford RM, Plummer KM, Templeton MD: ***Venturia inaequalis*: the causal agent of apple scab**. *Molecular Plant Pathology* 2011, **12**:105-122.
6. Le Cam B, Sargent D, Gouzy J, Amselem J, Bellanger M-N, Bouchez O, Brown S, Caffier V, De Gracia M, Debuchy R, et al.: **Population genome gequencing of the scab fungal species *Venturia inaequalis*, *Venturia pirina*, *Venturia aucupariae* and *Venturia asperata***. *G3: Genes, Genomes, Genetics* 2019, **9**:2405-2414.
7. Jha G, Thakur K, Thakur P: **The *Venturia* apple pathosystem: pathogenicity mechanisms and plant defense responses**. *Journal of Biomedicine and Biotechnology* 2009, **2009**:680160.
8. Caffier V, Le Cam B, Expert P, Tellier M, Devaux M, Giraud M, Chevalier M: **A new scab-like disease on apple caused by the formerly saprotrophic fungus *Venturia asperata***. *Plant Pathology* 2012, **61**:915-924.
9. Shabi E: *Oxford Handbook of Innovation: Chapter pear scab*: American Phytopathological Society; 1990.
10. Park P, Ishii H, Adachi Y, Kanematsu S, Ieki H, Umemoto S: **Infection behavior of *Venturia nashicola*, the cause of scab on asian pears**. *Phytopathology* 2000, **90**:1209-1216.
11. Fisher EE: ***Venturia carpophila* sp.nov., the ascigerous state of the apricot freckle fungus**. *Transactions of the British Mycological Society* 1961, **44**:337-IN334.
12. Graniti A: **Olive scab: a review**. *EPPO Bulletin* 1993, **23**:377-384.
13. Schubert K, Braun U: ***Fusicladium effusum***. *IMI Descriptions of fungi and bacteria* 2002.
14. Sivanesan A, Holliday P: ***Venturia cerasi***. *Descriptions of Fungi and Bacteria* 1981:Sheet 706.
15. Braun U: **Taxonomy and nomenclature of *Sphaeria aucupariae* (*Mycosphaerella aucupariae*, *Venturia aucupariae*)–a story of confusion and misinterpretation**. *Schlechtendalia* 2019, **36**:61-69.
16. Hunter GC, Zeil-Rolfe I, Jourdan M, Morin L: **Exploring the host range and infection process of *Venturia paralias* isolated from *Euphorbia paralias* in France**. *European Journal of Plant Pathology* 2021, **159**:811-823.
17. González-Domínguez E, Armengol J, Rossi V: **Biology and epidemiology of *Venturia* species affecting fruit crops: a review**. *Frontiers in Plant Science* 2017, **8**.
18. MacHardy WE: *Apple Scab, Biology, Epidemiology, and Management*, vol 33: The Amercian Phytopathological Society 1996.
19. Manktelow D, Beresford R, Batchelor T, Walker J: **Use patterns and economics of fungicides for disease control in New Zealand apples**. In *International Conference on Integrated Fruit Production*: 1995:187-192.
20. Agrios GN: *Plant Pathology*: Elsevier Science; 2005.

21. Schumacher CF, Steiner U, Dehne HW, Oerke EC: **Localized adhesion of nongerminated *Venturia inaequalis* conidia to leaves and artificial surfaces**. *Phytopathology* 2008, **98**:760-768.
22. Smereka KJ, Kausch AP, MacHardy WE: **Intracellular junctional structures in germinating ascopores of *Venturia inaequalis***. *Protoplasma* 1988, **142**:1-4.
23. Koller W, Parker DM, Becker CM: **Role of cutinase in the penetration of apple leaves by *Venturia inaequalis.*** *Phytopathology* 1991, **81**:1375-1379.
24. Gessler C, Stumm D: **Infection and stroma formation by *Venturia inaequalis* on apple leaves with different degrees of susceptibility to scab**. *Journal of Phytopathology* 1984, **110**:119-126.
25. Kucheryava N, Bowen JK, Sutherland PW, Conolly JJ, Mesarich CH, Rikkerink EH, Kemen E, Plummer KM, Hahn M, Templeton MD: **Two novel *Venturia inaequalis* genes induced upon morphogenetic differentiation during infection and *in vitro* growth on cellophane**. *Fungal Genetics and Biology* 2008, **45**:1329-1339.
26. Nusbaum CJ, Keitt GW: **A cytological study of host-parasite relations of *Venturia inaequalis* on apple leaves**. *Journal of Agricultural Research* 1938, **56**:595-618.
27. Shiller J, Van de Wouw AP, Taranto AP, Bowen JK, Dubois D, Robinson A, Deng CH, Plummer KM: **A large family of *AvrLm6-like* genes in the apple and pear scab pathogens, *Venturia inaequalis* and *Venturia pirina***. *Frontiers in Plant Science* 2015, **6**.
28. Li B, Xu X: **Infection and development of apple scab *(Venturia inaequalis*) on old leaves**. *Journal of Phytopathology* 2002, **150**:687-691.
29. Rocafort M, Bowen JK, Hassing B, Cox MP, McGreal B, de la Rosa S, Plummer KM, Bradshaw RE, Mesarich CH: **The *Venturia inaequalis* effector repertoire is expressed in waves, and is dominated by expanded families with predicted structural similarity to avirulence proteins from other fungi**. *bioRxiv* 2022: 482717.
30. Thakur K, Chawla V, Bhatti S, Swarnkar MK, Kaur J, Shankar R, Jha G: ***De novo* transcriptome sequencing and analysis for *Venturia inaequalis*, the devastating apple scab pathogen**. *PLoS ONE* 2013, **8**:e53937.
31. Gauthier N: **Apple scab**. *The Plant Health Instructor* 2018.
32. FRAC: **FRAC pathogen risk list 2019**. 2019.
33. Polat Z, Bayraktar H: **Resistance of *Venturia inaequalis* to multiple fungicides in Turkish apple orchards**. *Journal of Phytopathology* 2021, **169**:360-368.
34. Gomez C, Brun L, Chauffour D, Vallée DDL: **Effect of leaf litter management on scab development in an organic apple orchard**. *Agriculture, Ecosystems and Environment* 2007, **118**:249-255.
35. Carisse O, Bernier J: **Effect of environmental factors on growth, pycnidial production and spore germination of *Microsphaeropsis* isolates with biocontrol potential against apple scab**. *Mycological Research* 2002, **106**:1455-1462.
36. Köhl J, Scheer C, Holb IJ, Masny S, Molhoek W: **Toward an integrated use of biological control by *Cladosporium cladosporioides* H39 in apple scab (*Venturia inaequalis*) management**. *Plant Disease* 2014, **99**:535-543.
37. Khajuria YP, Kaul S, Wani AA, Dhar MK: **Genetics of resistance in apple against *Venturia inaequalis* (Wint.) Cke**. *Tree Genetics & Genomes* 2018, **14**:16.
38. Patocchi A, Wehrli A, Dubuis PH, Auwerkerken A, Leida C, Cipriani G, Passey T, Staples M, Didelot F, Philion V, et al.: **Ten years of VINQUEST: first insight for breeding new apple cultivars with durable apple scab resistance**. *Plant Disease* 2020, **104**:2074-2081.
39. Zhan J, Fitt BDL, Pinnschmidt HO, Oxley SJP, Newton AC: **Resistance, epidemiology and sustainable management of *Rhynchosporium secalis* populations on barley**. *Plant Pathology* 2008, **57**:1-14.

40. Riederer M, Jeffree CE: **Introduction: Biology of the plant cuticle the fine structure of the plant cuticle**. *Annual Plant Reviews* 2006, **23**:1-10.
41. Fernández V, Guzmán-Delgado P, Graça J, Santos S, Gil L: **Cuticle structure in relation to chemical composition: re-assessing the prevailing model**. *Frontiers in Plant Science* 2016, **7**: 427.
42. Latham AJR, A. E.: **Development of *Cladosporium caryigenum* in pecan leaves**. *Phytopathology* 1988, **78**:1104-1108.
43. Lanza B, Ragnelli AM, Priore M, Aimola P: **Morphological and histochemical investigation of the response of *Olea europaea* leaves to fungal attack by *Spilocaea oleagina***. *Plant Pathology* 2017, **66**:1239-1247.
44. Zaffarano PL, McDonald BA, Linde CC: **Two new species of *Rhynchosporium***. *Mycologia* 2011, **103**:195-202.
45. King KM, West JS, Brunner PC, Dyer PS, Fitt BDL: **Evolutionary relationships between *Rhynchosporium lolii* sp. nov. and other *Rhynchosporium* species on grasses**. *PLoS ONE* 2013, **8**:e72536-e72536.
46. Avrova A, Knogge W: ***Rhynchosporium commune*: a persistent threat to barley cultivation**. *Molecular Plant Pathology* 2012, **13**:986-997.
47. Linsell KJ, Keiper FJ, Forgan A, Oldach KH: **New insights into the infection process of *Rhynchosporium secalis* in barley using GFP**. *Fungal Genetics and Biology* 2011, **48**:124-131.
48. Dohm A: **Biotechnologies for breeding | Genetic transformation**. In *Encyclopedia of Rose Science*. Edited by Roberts AV: Elsevier; 2003:15-25.
49. Blechert O, Debener T: **Morphological characterization of the interaction between *Diplocarpon rosae* and various rose species**. *Plant Pathology* 2005, **54**:82-90.
50. Gachomo EW, Kotchoni SO: **Detailed description of developmental growth stages of *Diplocarpon rosae* in Rosa: a core building block for efficient disease management**. *Annals of Applied Biology* 2007, **151**:233-243.
51. Zhao H, Han Q, Wang J, Gao X, Xiao C-L, Liu J, Huang L: **Cytology of infection of apple leaves by *Diplocarpon mali***. *European Journal of Plant Pathology* 2013, **136**:41-49.
52. Dewage CSK, Klöppel CA, Stotz HU, Fitt BDL: **Host–pathogen interactions in relation to management of light leaf spot disease (caused by *Pyrenopeziza brassicae*) on *Brassica* species**. *Crop and Pasture Science* 2018, **69**:9-19.
53. Alkan N, Friedlander G, Ment D, Prusky D, Fluhr R: **Simultaneous transcriptome analysis of *Colletotrichum gloeosporioides* and tomato fruit pathosystem reveals novel fungal pathogenicity and fruit defense strategies**. *New Phytologist* 2015, **205**:801-815.
54. Prusky D, Alkan N, Mengiste T, Fluhr R: **Quiescent and necrotrophic lifestyle choice during postharvest disease development**. *Annual Review of Phytopathology* 2013, **51**:155-176.
55. Moralejo E, Puig M, García JA, Descals E: **Stromata, sporangiomata and chlamydosori of *Phytophthora ramorum* on inoculated Mediterranean woody plants**. *Mycological Research* 2006, **110**:1323-1332.
56. Wolf F: **The perfect stage of *Actinonema rosae***. *Botanical Gazette* 1912, **54**:218-234.
57. Rittenour WR, Harris SD: **An *in vitro* method for the analysis of infection-related morphogenesis in *Fusarium graminearum***. *Molecular Plant Pathology* 2010, **11**:361-369.
58. Becker M, Becker Y, Green K, Scott B: **The endophytic symbiont *Epichloë festucae* establishes an epiphyllous net on the surface of *Lolium perenne* leaves by development of an expressorium, an appressorium-like leaf exit structure**. *New Phytologist* 2016, **211**:240-254.

59. Jones P, Ayres PG: ***Rhynchosporium*** **leaf blotch of barley studied during the subcuticular phase by electron microscopy**. *Physiological Plant Pathology* 1974, **4**:229-233.
60. Pritsch C, Muehlbauer GJ, Bushnell WR, Somers DA, Vance CP: **Fungal development and induction of defense response genes during early infection of wheat spikes by *Fusarium graminearum***. *Molecular Plant-Microbe Interactions* 2000, **13**:159-169.
61. Guenther JC, Trail F: **The development and differentiation of *Gibberella zeae* (anamorph: *Fusarium graminearum*) during colonization of wheat**. *Mycologia* 2005, **97**:229-237.
62. Diéguez-Uribeondo J, Förster H, Soto-Estrada A, Adaskaveg JE: **Subcuticular-intracellular hemibiotrophic and intercellular necrotrophic development of *Colletotrichum acutatum* on almond**. *Phytopathology* 2005, **95**:751-758.
63. Perfect SE, Hughes HB, O'Connell RJ, Green JR: ***Colletotrichum*****: a model genus for studies on pathology and fungal–plant interactions**. *Fungal Genetics and Biology* 1999, **27**:186-198.
64. Verdín J, Sánchez-León E, Rico-Ramírez AM, Martínez-Núñez L, Fajardo-Somera RA, Riquelme M: **Off the wall: The rhyme and reason of *Neurospora crassa* hyphal morphogenesis**. *The Cell Surface* 2019, **5**:100020.
65. Sánchez-Vallet A, Mesters JR, Thomma BP: **The battle for chitin recognition in plant-microbe interactions**. *FEMS Microbiology Reviews* 2015, **39**:171-183.
66. Schoffelmeer EAM, Klis FM, Sietsma JH, Cornelissen BJC: **The cell wall of *Fusarium oxysporum***. *Fungal Genetics and Biology* 1999, **27**:275-282.
67. Cantu D, Carl Greve L, Labavitch JM, Powell ALT: **Characterization of the cell wall of the ubiquitous plant pathogen *Botrytis cinerea***. *Mycological Research* 2009, **113**:1396-1403.
68. Pettolino F, Sasaki I, Turbic A, Wilson SM, Bacic A, Hrmova M, Fincher GB: **Hyphal cell walls from the plant pathogen *Rhynchosporium secalis* contain (1,3/1,6)-β-d-glucans, galacto- and rhamnomannans, (1,3;1,4)-β-d-glucans and chitin**. *The FEBS Journal* 2009, **276**:3698-3709.
69. Jaworski C, Wang L: **Gross cell wall composition of *V. inaequalis* cell wall**. *Phytopathology* 1965, **55**:401-403.
70. Latgé J-P: **The cell wall: a carbohydrate armour for the fungal cell**. *Molecular Microbiology* 2007, **66**:279-290.
71. Garcia-Rubio R, de Oliveira HC, Rivera J, Trevijano-Contador N: **The fungal cell wall: *Candida, Cryptococcus,* and *Aspergillus* species**. *Frontiers in Microbiology* 2020, **10**, 2993.
72. Ruiz-Herrera J, Ortiz-Castellanos L: **Cell wall glucans of fungi. A review**. *The Cell Surface* 2019, **5**:100022.
73. Schweiger-Hufnagel U, Ono T, Izumi K, Hufnagel P, Morita N, Kaga H, Morita M, Hoshino T, Yumoto I, Matsumoto N, et al.: **Identification of the extracellular polysaccharide produced by the snow mold fungus *Microdochium nivale***. *Biotechnology Letters* 2000, **22**:183-187.
74. Kang X, Kirui A, Muszyński A, Widanage MCD, Chen A, Azadi P, Wang P, Mentink-Vigier F, Wang T: **Molecular architecture of fungal cell walls revealed by solid-state NMR**. *Nature Communications* 2018, **9**:2747.
75. Gow NAR, Latge JP, Munro CA: **The fungal cell wall: structure, biosynthesis, and function**. *Microbiology Spectrum* 2017, **5**: 3-5.
76. Caro LH, Tettelin H, Vossen JH, Ram AF, van den Ende H, Klis FM: ***In silicio*** **identification of glycosyl-phosphatidylinositol-anchored plasma-membrane and cell wall proteins of *Saccharomyces cerevisiae***. *Yeast* 1997, **13**:1477-1489.

77. Mrsa V, Tanner W: **Role of NaOH-extractable cell wall proteins Ccw5p, Ccw6p, Ccw7p and Ccw8p (members of the Pir protein family) in stability of the *Saccharomyces cerevisiae* cell wall**. *Yeast* 1999, **15**:813-820.
78. Ecker M, Deutzmann R, Lehle L, Mrsa V, Tanner W: **Pir proteins of *Saccharomyces cerevisiae* are attached to β-1,3-Glucan by a new protein-carbohydrate linkage**. *Journal of Biological Chemistry* 2006, **281**:11523-11529.
79. Cappellaro C, Baldermann C, Rachel R, Tanner W: **Mating type-specific cell-cell recognition of *Saccharomyces cerevisiae*: cell wall attachment and active sites of a- and alpha-agglutinin**. *The EMBO journal* 1994, **13**:4737-4744.
80. Kershaw MJ, Talbot NJ: **Hydrophobins and repellents: Proteins with fundamental roles in fungal morphogenesis**. *Fungal Genetics and Biology* 1998, **23**:18-33.
81. Lacroix H, Whiteford JR, Spanu PD: **Localization of *Cladosporium fulvum* hydrophobins reveals a role for HCf-6 in adhesion**. *FEMS Microbiology Letters* 2008, **286**:136-144.
82. Erwig LP, Gow NAR: **Interactions of fungal pathogens with phagocytes**. *Nature Reviews Microbiology* 2016, **14**:163-176.
83. Free SJ: **Chapter two - Fungal cell wall organization and biosynthesis**. In *Advances in Genetics*. Edited by Friedmann T, Dunlap JC, Goodwin SF: Academic Press; 2013:33-82. vol 81.]
84. Merzendorfer H: **The cellular basis of chitin synthesis in fungi and insects: common principles and differences**. *European Journal of Cell Biology* 2011, **90**:759-769.
85. Fajardo-Somera RA, Jöhnk B, Bayram Ö, Valerius O, Braus GH, Riquelme M: **Dissecting the function of the different chitin synthases in vegetative growth and sexual development in *Neurospora crassa***. *Fungal Genetics and Biology* 2015, **75**:30-45.
86. Riquelme M, Bartnicki-García S: **Advances in understanding hyphal morphogenesis: ontogeny, phylogeny and cellular localization of chitin synthases**. *Fungal Biology Reviews* 2008, **22**:56-70.
87. Mandel AM, Galgiani JN, Scott K, Orbach MJ: ***Coccidioides posadasii* contains single chitin synthase genes corresponding to classes I to VII**. *Fungal Genetics and Biology* 2006, **43**:775-788.
88. Choquer M, Boccara M, Gonçalves IR, Soulié MC, Vidal-Cros A: **Survey of the *Botrytis cinerea* chitin synthase multigenic family through the analysis of six euascomycetes genomes**. *European Journal of Biochemistry* 2004, **271**:2153-2164.
89. Sheng W, Yamashita S, Ohta A, Horiuchi H: **Functional differentiation of chitin synthases in *Yarrowia lipolytica***. *Biosciencie, Biotechnology, and Biochemistry* 2013, **77**:1275-1281.
90. Ruiz-Herrera J, Manuel González-Prieto J, Ruiz-Medrano R: **Evolution and phylogenetic relationships of chitin synthases from yeasts and fungi**. *FEMS Yeast Research* 2002, **1**:247-256.
91. Amnuaykanjanasin A, Epstein L: **A class V chitin synthase gene, *chsA* is essential for conidial and hyphal wall strength in the fungus *Colletotrichum graminicola* (*Glomerella graminicola*)**. *Fungal Genetics and Biology* 2003, **38**:272-285.
92. Larson TM, Kendra DF, Busman M, Brown DW: ***Fusarium verticillioides* chitin synthases *CHS5* and *CHS7* are required for normal growth and pathogenicity**. *Current Genetics* 2011, **57**:177-189.
93. Kong LA, Yang J, Li GT, Qi LL, Zhang YJ, Wang CF, Zhao WS, Xu JR, Peng YL: **Different chitin synthase genes are required for various developmental and plant infection processes in the rice blast fungus *Magnaporthe oryzae***. *PLoS Pathogens* 2012, **8**:e1002526.
94. Werner S, Sugui JA, Steinberg G, Deising HB: **A chitin synthase with a myosin-like motor domain is essential for hyphal growth, appressorium differentiation, and**

pathogenicity of the maize anthracnose fungus *Colletotrichum graminicola*. *Molecular Plant-Microbe Interactions* 2007, **20**:1555-1567.
95. Cui Z, Ding Z, Yang X, Wang K, Zhu T: **Gene disruption and characterization of a class V chitin synthase in *Botrytis cinerea***. *Canadian Journal of Microbiology* 2009, **55**:1267-1274.
96. Levinson JN, Shahinian S, Sdicu A-M, Tessier DC, Bussey H: **Functional, comparative and cell biological analysis of *Saccharomyces cerevisiae Kre5p***. *Yeast* 2002, **19**:1243-1259.
97. Dodds PN, Rathjen JP: **Plant immunity: towards an integrated view of plant–pathogen interactions**. *Nature Reviews Genetics* 2010, **11**:539-548.
98. Saijo Y, Loo EPi, Yasuda S: **Pattern recognition receptors and signaling in plant–microbe interactions**. *The Plant Journal* 2018, **93**:592-613.
99. Jones JDG, Dangl JL: **The plant immune system**. *Nature* 2006, **444**:323-329.
100. Cook DE, Mesarich CH, Thomma BPHJ: **Understanding plant immunity as a surveillance system to detect invasion**. *Annual Review of Phytopathology* 2015, **53**:541-563.
101. Shi G, Zhang Z, Friesen Timothy L, Raats D, Fahima T, Brueggeman Robert S, Lu S, Trick Harold N, Liu Z, Chao W, et al.: **The hijacking of a receptor kinase–driven pathway by a wheat fungal pathogen leads to disease**. *Science Advances* 2016, **2**:e1600822.
102. Ngou BPM, Ding P, Jones JDG: **Thirty years of resistance: Zig-zag through the plant immune system**. *Plant Cell* 2022, **34**:1447-1478.
103. Ngou BPM, Ahn H-K, Ding P, Jones JDG: **Mutual potentiation of plant immunity by cell-surface and intracellular receptors**. *Nature* 2021, **592**:110-115.
104. Pitzschke A, Schikora A, Hirt H: **MAPK cascade signalling networks in plant defence**. *Current Opinion in Plant Biology* 2009, **12**:421-426.
105. Meng X, Zhang S: **MAPK cascades in plant disease resistance signaling**. *Annual Review of Phytopathology* 2013, **51**:245-266.
106. Zipfel C, Oldroyd GED: **Plant signalling in symbiosis and immunity**. *Nature* 2017, **543**:328-336.
107. Zipfel C: **Pattern-recognition receptors in plant innate immunity**. *Current Opinion in Immunology* 2008, **20**:10-16.
108. Boutrot F, Zipfel C: **Function, discovery, and exploitation of plant pattern recognition receptors for broad-spectrum disease resistance**. *Annual Review of Phytopathology* 2017, **55**:257-286.
109. Lolle S, Stevens D, Coaker G: **Plant NLR-triggered immunity: from receptor activation to downstream signaling**. *Current Opinion in Immunology* 2020, **62**:99-105.
110. cesari S, Bernoux M, Moncuquet P, Kroj T, Dodds P: **A novel conserved mechanism for plant NLR protein pairs: the 'integrated decoy' hypothesis**. *Frontiers in Plant Science* 2014, **5**.
111. Białas A, Zess EK, De la Concepcion JC, Franceschetti M, Pennington HG, Yoshida K, Upson JL, Chanclud E, Wu C-H, Langner T, et al.: **Lessons in effector and NLR biology of plant-microbe systems**. *Molecular Plant-Microbe Interactions* 2017, **31**:34-45.
112. Maqbool A, Saitoh H, Franceschetti M, Stevenson CEM, Uemura A, Kanzaki H, Kamoun S, Terauchi R, Banfield MJ: **Structural basis of pathogen recognition by an integrated HMA domain in a plant NLR immune receptor**. *eLife* 2015, **4**:e08709.
113. Rovenich H, Zuccaro A, Thomma BPHJ: **Convergent evolution of filamentous microbes towards evasion of glycan-triggered immunity**. *New Phytologist* 2016, **212**:896-901.
114. Fesel PH, Zuccaro A: **β-glucan: crucial component of the fungal cell wall and elusive MAMP in plants**. *Fungal Genetics and Biology* 2016, **90**:53-60.
115. Rovenich H, Boshoven JC, Thomma BPHJ: **Filamentous pathogen effector functions: of pathogens, hosts and microbiomes**. *Current Opinion in Plant Biology* 2014, **20**:96-103.

116. Mentlak TA, Kombrink A, Shinya T, Ryder LS, Otomo I, Saitoh H, Terauchi R, Nishizawa Y, Shibuya N, Thomma BPHJ, et al.: **Effector-mediated suppression of chitin-triggered immunity by *Magnaporthe oryzae* is necessary for rice blast disease**. *The Plant Cell* 2012, **24**:322.
117. O'Connell RJ, Pain NA, Hutchison KA, Jones GL, Green JR: **Ultrastructure and composition of the cell surfaces of infection structures formed by the fungal plant pathogen *Colletotrichum lindemuthianum***. *Journal of Microscopy* 1996, **181**:204-212.
118. Freytag S, Mendgen K: **Surface carbohydrates and cell wall structure of *in vitro*-induced uredospore infection structures of *Uromyces viciae-fabae* before and after treatment with enzymes and alkali**. *Protoplasma* 1991, **161**:94-103.
119. Vander P, KM Vr, Domard A, Eddine El Gueddari N, Moerschbacher BM: **Comparison of the ability of partially N-acetylated chitosans and chitooligosaccharides to elicit resistance reactions in wheat leaves**. *Plant Physiology* 1998, **118**:1353-1359.
120. Iriti M, Faoro F: **Chitosan as a MAMP, searching for a PRR**. *Plant Signaling & Behavior* 2009, **4**:66-68.
121. Gubaeva E, Gubaev A, Melcher RLJ, Cord-Landwehr S, Singh R, El Gueddari NE, Moerschbacher BM: **'Slipped Sandwich' model for chitin and chitosan perception in *Arabidopsis***. *Molecular Plant-Microbe Interactions* 2018, **31**:1145-1153.
122. Lopez-Moya F, Suarez-Fernandez M, Lopez-Llorca LV: **Molecular mechanisms of chitosan interactions with fungi and plants**. *International Journal of Molecular Sciences* 2019, **20**:332.
123. Ride JP, Barber MS: **Purification and characterization of multiple forms of endochitinase from wheat leaves**. *Plant Science* 1990, **71**:185-197.
124. Cord-Landwehr S, Melcher RLJ, Kolkenbrock S, Moerschbacher BM: **A chitin deacetylase from the endophytic fungus *Pestalotiopsis* sp. efficiently inactivates the elicitor activity of chitin oligomers in rice cells**. *Scientific Reports* 2016, **6**:38018.
125. Gao F, Zhang B-S, Zhao J-H, Huang J-F, Jia P-S, Wang S, Zhang J, Zhou J-M, Guo H-S: **Deacetylation of chitin oligomers increases virulence in soil-borne fungal pathogens**. *Nature Plants* 2019, **5**:1167-1176.
126. Naqvi S, Cord-Landwehr S, Singh R, Bernard F, Kolkenbrock S, El Gueddari NE, Moerschbacher BM: **A recombinant fungal chitin deacetylase produces fully defined chitosan oligomers with novel patterns of acetylation**. *Applied Environmental Microbiology* 2016, **82**:6645-6655.
127. El Gueddari NE, Rauchhaus U, Moerschbacher BM, Deising HB: **Developmentally regulated conversion of surface-exposed chitin to chitosan in cell walls of plant pathogenic fungi**. *New Phytologist* 2002, **156**:103-112.
128. Geoghegan IA, Gurr SJ: **Investigating chitin deacetylation and chitosan hydrolysis during vegetative growth in *Magnaporthe oryzae***. *Cellular Microbiology* 2017, **19**:e12743.
129. Rizzi Y S, Happel P, Lenz S, Urs M J, Bonin M, Cord-Landwehr S, Singh R, Moerschbacher B M, Kahmann R: **Chitosan and chitin deacetylase activity are necessary for development and virulence of *Ustilago maydis***. *mBio* 2021, **12**:e03419-03420.
130. Noorifar N, Savoian MS, Ram A, Lukito Y, Hassing B, Weikert TW, Moerschbacher BM, Scott B: **Chitin deacetylases are required for *Epichloë festucae* endophytic cell wall remodeling during establishment of a mutualistic symbiotic interaction with *Lolium perenne***. *Molecular Plant-Microbe Interactions* 2021, **34**:1181-1192.
131. Tanaka S, Kahmann R: **Cell wall–associated effectors of plant-colonizing fungi**. *Mycologia* 2021, **113**:247-260.
132. Kuroki M, Okauchi K, Yoshida S, Ohno Y, Murata S, Nakajima Y, Nozaka A, Tanaka N, Nakajima M, Taguchi H, et al.: **Chitin-deacetylase activity induces appressorium**

differentiation in the rice blast fungus *Magnaporthe oryzae*. *Scientific Reports* 2017, **7**:9697-9697.
133. Kamakura T, Yamaguchi S, Saitoh K, Teraoka T, Yamaguchi I: **A novel gene, *CBP1*, encoding a putative extracellular chitin-binding protein, may play an important role in the hydrophobic surface sensing of *Magnaporthe grisea* during appressorium differentiation**. *Molecular Plant-Microbe Interactions* 2002, **15**:437-444.
134. Geoghegan IA, Gurr SJ: **Chitosan mediates germling adhesion in *Magnaporthe oryzae* and is required for surface sensing and germling morphogenesis**. *PLoS Pathogens* 2016, **12**:e1005703-e1005703.
135. Lickfeld M, Schmitz HP: **A network involving Rho-type GTPases, a paxillin and a formin homologue regulates spore length and spore wall integrity in the filamentous fungus *Ashbya gossypii***. *Molecular Microbiology* 2012, **85**:574-593.
136. Banks IR, Specht CA, Donlin MJ, Gerik KJ, Levitz SM, Lodge JK: **A chitin synthase and its regulator protein are critical for chitosan production and growth of the fungal pathogen *Cryptococcus neoformans***. *Eukaryotic Cell* 2005, **4**:1902-1912.
137. Rappleye CA, Eissenberg LG, Goldman WE: ***Histoplasma capsulatum* alpha-(1,3)-glucan blocks innate immune recognition by the beta-glucan receptor**. *Proceedings of the National Academy of Sciences* 2007, **104**:1366-1370.
138. Rappleye CA, Engle JT, Goldman WE: **RNA interference in *Histoplasma capsulatum* demonstrates a role for α-(1,3)-glucan in virulence**. *Molecular Microbiology* 2004, **53**:153-165.
139. Fujikawa T, Kuga Y, Yano S, Yoshimi A, Tachiki T, Abe K, Nishimura M: **Dynamics of cell wall components of *Magnaporthe grisea* during infectious structure development**. *Molecular Microbiology* 2009, **73**:553-570.
140. Yoshimi A, Miyazawa K, Abe K: **Function and biosynthesis of cell wall α-1,3-glucan in fungi**. *Journal of Fungi* 2017, **3**:63.
141. Rocafort M, Fudal I, Mesarich CH: **Apoplastic effector proteins of plant-associated fungi and oomycetes**. *Current Opinion in Plant Biology* 2020, **56**:9-19.
142. Lo Presti L, Lanver D, Schweizer G, Tanaka S, Liang L, Tollot M, Zuccaro A, Reissmann S, Kahmann R: **Fungal effectors and plant susceptibility**. *Annual Review of Plant Biology* 2015, **66**:513-545.
143. Liu T, Song T, Zhang X, Yuan H, Su L, Li W, Xu J, Liu S, Chen L, Chen T, et al.: **Unconventionally secreted effectors of two filamentous pathogens target plant salicylate biosynthesis**. *Nature Communications* 2014, **5**:4686.
144. Khan M, Seto D, Subramaniam R, Desveaux D: **Oh, the places they'll go! A survey of phytopathogen effectors and their host targets**. *Plant Journal* 2018, **93**:651-663.
145. Khang CH, Berruyer R, Giraldo MC, Kankanala P, Park SY, Czymmek K, Kang S, Valent B: **Translocation of *Magnaporthe oryzae* effectors into rice cells and their subsequent cell-to-cell movement**. *Plant Cell* 2010, **22**:1388-1403.
146. Ludwig N, Reissmann S, Schipper K, Gonzalez C, Assmann D, Glatter T, Moretti M, Ma L-S, Rexer K-H, Snetselaar K, et al.: **A cell surface-exposed protein complex with an essential virulence function in *Ustilago maydis***. *Nature Microbiology* 2021, **6**:722-730.
147. He Q, McLellan H, Boevink PC, Birch PRJ: **All roads lead to susceptibility: The many modes of action of fungal and oomycete intracellular effectors**. *Plant Communications* 2020, **1**:100050.
148. Djamei A, Schipper K, Rabe F, Ghosh A, Vincon V, Kahnt J, Osorio S, Tohge T, Fernie AR, Feussner I, et al.: **Metabolic priming by a secreted fungal effector**. *Nature* 2011, **478**:395-398.

149. Qin J, Wang K, Sun L, Xing H, Wang S, Li L, Chen S, Guo HS, Zhang J: **The plant-specific transcription factors CBP60g and SARD1 are targeted by a *Verticillium* secretory protein VdSCP41 to modulate immunity**. *eLIFE* 2018, **7**.
150. Park C-H, Chen S, Shirsekar G, Zhou B, Khang CH, Songkumarn P, Afzal AJ, Ning Y, Wang R, Bellizzi M, et al.: **The *Magnaporthe oryzae* effector AvrPiz-t targets the RING E3 ubiquitin ligase APIP6 to suppress pathogen-associated molecular pattern-triggered immunity in rice**. *The Plant cell* 2012, **24**:4748-4762.
151. Tanaka S, Brefort T, Neidig N, Djamei A, Kahnt J, Vermerris W, Koenig S, Feussner K, Feussner I, Kahmann R: **A secreted *Ustilago maydis* effector promotes virulence by targeting anthocyanin biosynthesis in maize**. *eLife* 2014, **3**:e01355-e01355.
152. Irieda H, Inoue Y, Mori M, Yamada K, Oshikawa Y, Saitoh H, Uemura A, Terauchi R, Kitakura S, Kosaka A, et al.: **Conserved fungal effector suppresses PAMP-triggered immunity by targeting plant immune kinases**. *Proceedings of the National Academy of Sciences* 2019, **116**:496.
153. Redkar A, Hoser R, Schilling L, Zechmann B, Krzymowska M, Walbot V, Doehlemann G: **A secreted effector protein of *Ustilago maydis* guides maize leaf cells to form tumors**. *The Plant Cell* 2015, **27**:1332-1351.
154. Darino M, Chia K-S, Marques J, Aleksza D, Soto-Jiménez LM, Saado I, Uhse S, Borg M, Betz R, Bindics J, et al.: ***Ustilago maydis* effector Jsi1 interacts with Topless corepressor, hijacking plant jasmonate/ethylene signaling**. *New Phytologist* 2021, **229**:3393-3407.
155. Yang Q, Huai B, Lu Y, Cai K, Guo J, Zhu X, Kang Z, Guo J: **A stripe rust effector Pst18363 targets and stabilises TaNUDX23 that promotes stripe rust disease**. *New Phytologist* 2020, **225**:880-895.
156. Wan L, Koeck M, Williams SJ, Ashton AR, Lawrence GJ, Sakakibara H, Kojima M, Böttcher C, Ericsson DJ, Hardham AR, et al.: **Structural and functional insights into the modulation of the activity of a flax cytokinin oxidase by flax rust effector AvrL567-A**. *Molecular Plant Pathology* 2019, **20**:211-222.
157. Dodds PN, Lawrence GJ, Catanzariti A-M, Ayliffe MA, Ellis JG: **The *Melampsora lini AvrL567* avirulence genes are expressed in haustoria and their products are eecognized inside plant cells**. *The Plant Cell* 2004, **16**:755-768.
158. Pennington HG, Jones R, Kwon S, Bonciani G, Thieron H, Chandler T, Luong P, Morgan SN, Przydacz M, Bozkurt T, et al.: **The fungal ribonuclease-like effector protein CSEP0064/BEC1054 represses plant immunity and interferes with degradation of host ribosomal RNA**. *PLoS Pathogens* 2019, **15**:e1007620.
159. Schmidt SM, Kuhn H, Micali C, Liller C, Kwaaitaal M, Panstruga R: **Interaction of a B*lumeria graminis* f. sp. *hordei* effector candidate with a barley ARF-GAP suggests that host vesicle trafficking is a fungal pathogenicity target**. *Molecular Plant Pathology* 2014, **15**:535-549.
160. Shi X, Long Y, He F, Zhang C, Wang R, Zhang T, Wu W, Hao Z, Wang Y, Wang G-L, et al.: **The fungal pathogen *Magnaporthe oryzae* suppresses innate immunity by modulating a host potassium channel**. *PLoS Pathogens* 2018, **14**:e1006878.
161. Tang M, Ning Y, Shu X, Dong B, Zhang H, Wu D, Wang H, Wang GL, Zhou B: **The Nup98 homolog APIP12 targeted by the effector AvrPiz-t is involved in rice basal resistance against *Magnaporthe oryzae***. *Rice* 2017, **10**:5.
162. Park CH, Shirsekar G, Bellizzi M, Chen S, Songkumarn P, Xie X, Shi X, Ning Y, Zhou B, Suttiviriya P, et al.: **The E3 ligase APIP10 connects the effector AvrPiz-t to the NLR receptor Piz-t in rice**. *PLoS Pathogens* 2016, **12**:e1005529.

163. Singh R, Dangol S, Chen Y, Choi J, Cho YS, Lee JE, Choi MO, Jwa NS: ***Magnaporthe oryzae*** **effector AVR-Pii helps to establish compatibility by inhibition of the rice NADP-malic enzyme resulting in disruption of oxidative burst and host innate immunity**. *Molecules and Cells* 2016, **39**:426-438.
164. Fujisaki K, Abe Y, Ito A, Saitoh H, Yoshida K, Kanzaki H, Kanzaki E, Utsushi H, Yamashita T, Kamoun S, et al.: **Rice Exo70 interacts with a fungal effector, AVR-Pii, and is required for AVR-Pii-triggered immunity**. *Plant Journal* 2015, **83**:875-887.
165. Han J, Wang X, Wang F, Zhao Z, Li G, Zhu X, Su J, Chen L: **The fungal effector Avr-Pita suppresses innate immunity by increasing COX activity in rice mitochondria**. *Rice* 2021, **14**:12.
166. Franceschetti M, Maqbool A, Jiménez-Dalmaroni Maximiliano J, Pennington Helen G, Kamoun S, Banfield Mark J: **Effectors of filamentous plant pathogens: commonalities amid diversity**. *Microbiology and Molecular Biology Reviews* 2017, **81**:e00066-00016.
167. de Guillen K, Ortiz-Vallejo D, Gracy J, Fournier E, Kroj T, Padilla A: **Structure analysis uncovers a highly diverse but structurally conserved effector family in phytopathogenic fungi**. *PLoS Pathogens* 2015, **11**:e1005228.
168. Seong K, Krasileva KV: **Comparative computational structural genomics highlights divergent evolution of fungal effectors**. *bioRxiv* 2022: 490317.
169. Lazar N, Mesarich CH, Petit-Houdenot Y, Talbi N, Li de la Sierra-Gallay I, Zélie E, Blondeau K, Gracy J, Ollivier B, Blaise F, et al.: **A new family of structurally conserved fungal effectors displays epistatic interactions with plant resistance proteins**. *PLoS Pathogens* 2022, **18**:e1010664.
170. Yu DS, Outram MA, Smith A, McCombe CL, Khambalkar PB, Rima SA, Sun X, Ma L, Ericsson DJ, Jones DA, et al.: **The structural repertoire of *Fusarium oxysporum* f. sp. *lycopersici* effectors revealed by experimental and computational studies**. *bioRxiv* 2021: 472499.
171. Maidment JHR, Franceschetti M, Maqbool A, Saitoh H, Jantasuriyarat C, Kamoun S, Terauchi R, Banfield MJ: **Multiple variants of the fungal effector AVR-Pik bind the HMA domain of the rice protein OsHIPP19, providing a foundation to engineer plant defense**. *Journal of Biological Chemistry* 2021, **296**:100371.
172. Nyarko A, Singarapu KK, Figueroa M, Manning VA, Pandelova I, Wolpert TJ, Ciuffetti LM, Barbar E: **Solution NMR structures of *Pyrenophora tritici-repentis* ToxB and its inactive homolog reveal potential determinants of toxin activity**. *The Journal of Biological Chemistry* 2014, **289**:25946-25956.
173. Jumper J, Evans R, Pritzel A, Green T, Figurnov M, Ronneberger O, Tunyasuvunakool K, Bates R, Žídek A, Potapenko A, et al.: **Highly accurate protein structure prediction with AlphaFold**. *Nature* 2021, **596**:583-589.
174. Seong K, Krasileva KV: **Computational structural genomics unravels common folds and novel families in the secretome of fungal phytopathogen *Magnaporthe oryzae***. *Molecular Plant-Microbe Interactions* 2021:MPMI-03-21-0071-R.
175. Yan X, Tang B, Ryder LS, MacLean D, Were VM, Eseola AB, Cruz-Mireles N, Foster AJ, Osés-Ruiz M, Talbot NJ: **The transcriptional landscape of plant infection by the rice blast fungus *Magnaporthe oryzae* reveals distinct families of temporally co-regulated and structurally conserved effectors**. *bioRxiv* 2022: 500532.
176. Pedersen C, van Themaat EVL, McGuffin LJ, Abbott JC, Burgis TA, Barton G, Bindschedler LV, Lu X, Maekawa T, Weßling R, et al.: **Structure and evolution of barley powdery mildew effector candidates**. *BMC Genomics* 2012, **13**:694.
177. Pliego C, Nowara D, Bonciani G, Gheorghe DM, Xu R, Surana P, Whigham E, Nettleton D, Bogdanove AJ, Wise RP, et al.: **Host-induced gene silencing in barley powdery mildew**

reveals a class of ribonuclease-like effectors. *Molecular Plant-Microbe Interactions* 2013, **26**:633-642.
178. Spanu PD: **RNA-protein interactions in plant disease: hackers at the dinner table**. *New Phytologist* 2015, **207**:991-995.
179. Mesarich CH, Ökmen B, Rovenich H, Griffiths SA, Wang C, Karimi Jashni M, Mihajlovski A, Collemare J, Hunziker L, Deng CH, et al.: **Specific hypersensitive response-associated recognition of new apoplastic effectors from *Cladosporium fulvum* in wild tomato**. *Molecular Plant-Microbe Interactions* 2018, **31**:145-162.
180. Wang C-IA, Gunčar G, Forwood JK, Teh T, Catanzariti A-M, Lawrence GJ, Loughlin FE, Mackay JP, Schirra HJ, Anderson PA, et al.: **Crystal structures of flax rust avirulence proteins AvrL567-A and -D reveal details of the structural basis for flax disease resistance specificity**. *The Plant Cell* 2007, **19**:2898-2912.
181. Manning VA, Ciuffetti LM: **Localization of Ptr ToxA produced by *Pyrenophora tritici-repentis* reveals protein import into wheat mesophyll cells**. *The Plant Cell* 2005, **17**:3203-3212.
182. Di X, Cao L, Hughes RK, Tintor N, Banfield MJ, Takken FLW: **Structure-function analysis of the *Fusarium oxysporum* Avr2 effector allows uncoupling of its immune-suppressing activity from recognition**. *New Phytologist* 2017, **216**:897-914.
183. Dodds PN, Lawrence GJ, Catanzariti A-M, Teh T, Wang C-IA, Ayliffe MA, Kobe B, Ellis JG: **Direct protein interaction underlies gene-for-gene specificity and coevolution of the flax resistance genes and flax rust avirulence genes**. *Proceedings of the National Academy of Sciences* 2006, **103**:8888.
184. Li W, Wang B, Wu J, Lu G, Hu Y, Zhang X, Zhang Z, Zhao Q, Feng Q, Zhang H, et al.: **The *Magnaporthe oryzae* avirulence gene *AvrPiz-t* encodes a predicted secreted protein that triggers the immunity in rice mediated by the blast resistance gene *Piz-t***. *Molecular Plant-Microbe Interactions* 2009, **22**:411-420.
185. Zhou B, Qu S, Liu G, Dolan M, Sakai H, Lu G, Bellizzi M, Wang GL: **The eight amino-acid differences within three leucine-rich repeats between Pi2 and Piz-t resistance proteins determine the resistance specificity to *Magnaporthe grisea***. *Molecular Plant-Microbe Interactions* 2006, **19**:1216-1228.
186. Zhang ZM, Zhang X, Zhou ZR, Hu HY, Liu M, Zhou B, Zhou J: **Solution structure of the *Magnaporthe oryzae* avirulence protein AvrPiz-t**. *Journal of Biomolecular NMR* 2013, **55**:219-223.
187. Cesari S, Thilliez G, Ribot C, Chalvon V, Michel C, Jauneau A, Rivas S, Alaux L, Kanzaki H, Okuyama Y, et al.: **The rice resistance protein pair RGA4/RGA5 recognizes the *Magnaporthe oryzae* effectors AVR-Pia and AVR1-CO39 by direct binding**. *The Plant Cell* 2013, **25**:1463-1481.
188. Ribot C, Césari S, Abidi I, Chalvon V, Bournaud C, Vallet J, Lebrun M-H, Morel J-B, Kroj T: **The *Magnaporthe oryzae* effector AVR1–CO39 is translocated into rice cells independently of a fungal-derived machinery**. *The Plant Journal* 2013, **74**:1-12.
189. Yoshida K, Saitoh H, Fujisawa S, Kanzaki H, Matsumura H, Yoshida K, Tosa Y, Chuma I, Takano Y, Win J, et al.: **Association genetics reveals three novel avirulence genes from the rice blast fungal pathogen *Magnaporthe oryzae*.** *The Plant Cell* 2009, **21**:1573-1591.
190. Wu W, Wang L, Zhang S, Li Z, Zhang Y, Lin F, Pan Q: **Stepwise arms race between *AvrPik* and *Pik* alleles in the rice blast pathosystem**. *Molecular Plant-Microbe Interactions* 2014, **27**:759-769.
191. Kanzaki H, Yoshida K, Saitoh H, Fujisaki K, Hirabuchi A, Alaux L, Fournier E, Tharreau D, Terauchi R: **Arms race co-evolution of *Magnaporthe oryzae AVR-Pik* and rice *Pik* genes driven by their physical interactions**. *The Plant Journal* 2012, **72**:894-907.

192. Zhang S, Wang L, Wu W, He L, Yang X, Pan Q: **Function and evolution of *Magnaporthe oryzae* avirulence gene *AvrPib* responding to the rice blast resistance gene *Pib***. *Scientific Reports* 2015, **5**:11642.
193. Staal J, Dixelius C: **RLM3, a potential adaptor between specific TIR-NB-LRR receptors and DZC proteins**. *Communicative & integrative biology* 2008, **1**:59-61.
194. Plissonneau C, Daverdin G, Ollivier B, Blaise F, Degrave A, Fudal I, Rouxel T, Balesdent M-H: **A game of hide and seek between avirulence genes *AvrLm4-7* and *AvrLm3* in *Leptosphaeria maculans***. *New Phytologist* 2016, **209**:1613-1624.
195. Larkan NJ, Ma L, Haddadi P, Buchwaldt M, Parkin IAP, Djavaheri M, Borhan MH: **The *Brassica napus* wall-associated kinase-like (WAKL) gene *Rlm9* provides race-specific blackleg resistance**. *The Plant Journal* 2020, **104**:892-900.
196. Blondeau K, Blaise F, Graille M, Kale SD, Linglin J, Ollivier B, Labarde A, Lazar N, Daverdin G, Balesdent MH, et al.: **Crystal structure of the effector AvrLm4-7 of *Leptosphaeria maculans* reveals insights into its translocation into plant cells and recognition by resistance proteins**. *The Plant Journal* 2015, **83**:610-624.
197. Haddadi P, Larkan NJ, Van de Wouw A, Zhang Y, Neik TX, Beynon E, Bayer P, Edwards D, Batley J, Borhan MH: ***Brassica napus* genes *Rlm4* and *Rlm7* conferring resistance to *Leptosphaeria maculans* are alleles of the *Rlm9* wall-associated kinase-like resistance locus**. *Plant Biotechnology Journal* 2022, **20**:1229-1231.
198. Houterman PM, Cornelissen BJC, Rep M: **Suppression of plant resistance gene-based immunity by a fungal effector**. *PLoS Pathogens* 2008, **4**:e1000061.
199. Catanzariti AM, Do HT, Bru P, de Sain M, Thatcher LF, Rep M, Jones DA: **The tomato *I* gene for Fusarium wilt resistance encodes an atypical leucine-rich repeat receptor-like protein whose function is nevertheless dependent on SOBIR1 and SERK3/BAK1**. *Plant Journal* 2017, **89**:1195-1209.
200. Simons G, Groenendijk J, Wijbrandi J, Reijans M, Groenen J, Diergaarde P, Van der Lee T, Bleeker M, Onstenk J, de Both M, et al.: **Dissection of the Fusarium *I2* gene cluster in tomato reveals six homologs and one active gene copy**. *The Plant Cell* 1998, **10**:1055-1068.
201. Rep M, Van Der Does HC, Meijer M, Van Wijk R, Houterman PM, Dekker HL, De Koster CG, Cornelissen BJC: **A small, cysteine-rich protein secreted by *Fusarium oxysporum* during colonization of xylem vessels is required for I-3-mediated resistance in tomato**. *Molecular Microbiology* 2004, **53**:1373-1383.
202. Catanzariti AM, Dodds PN, Ve T, Kobe B, Ellis JG, Staskawicz BJ: **The AvrM effector from flax rust has a structured C-terminal domain and interacts directly with the M resistance protein**. *Molecular Plant-Microbe Interactions* 2010, **23**:49-57.
203. Deng CH, Plummer KM, Jones DAB, Mesarich CH, Shiller J, Taranto AP, Robinson AJ, Kastner P, Hall NE, Templeton MD, et al.: **Comparative analysis of the predicted secretomes of Rosaceae scab pathogens *Venturia inaequalis* and *V. pirina* reveals expanded effector families and putative determinants of host range**. *BMC Genomics* 2017, **18**:339.
204. Passey TAJ, Armitage AD, Xu X: **Annotated draft genome sequence of the apple scab pathogen *Venturia inaequalis***. *Microbiology Resource Announcements* 2018, **7**:e01062-01018.
205. Bus VGM, Rikkerink EHA, Caffier V, Durel C-E, Plummer KM: **Revision of the nomenclature of the differential host-pathogen interactions of *Venturia inaequalis* and *Malus***. *Annual Review of Phytopathology* 2011, **49**:391-413.
206. Gessler C, Patocchi A, Sansavini S, Tartarini S, Gianfranceschi L: ***Venturia inaequalis* resistance in apple**. *Critical Reviews in Plant Sciences* 2006, **25**:473-503.

207. Belfanti E, Silfverberg-Dilworth E, Tartarini S, Patocchi A, Barbieri M, Zhu J, Vinatzer BA, Gianfranceschi L, Gessler C, Sansavini S: **The *HcrVf2* gene from a wild apple confers scab resistance to a transgenic cultivated variety**. *Proceedings of the National Academy of Sciences of the United States of America* 2004, **101**:886-890.
208. Schouten HJ, Brinkhuis J, Burgh AMvd, Schaart JG, Groenwold R, Broggini GAL, Gessler C: **Cloning and functional characterization of the *Rvi15* (*Vr2*) gene for apple scab resistance**. *Tree Genetics & Genomes* 2013, **10**:251-260.
209. Mesarich CH, Schmitz M, Tremouilhac P, McGillivray DJ, Templeton MD, Dingley AJ: **Structure, dynamics and domain organization of the repeat protein Cin1 from the apple scab fungus**. *Biochimica et Biophysica Acta* 2012, **1824**:1118-1128.
210. Bowen JK, Mesarich CH, Rees-George J, Cui W, Fitzgerald A, Win j, Plummer KM, Templeton MD: **Candidate effector gene identification in the ascomycete fungal phytopathogen *Venturia inaequalis* by expressed sequence tag analysis**. *Molecular Plant Pathology* 2009, **10**:431-448.
211. Fudal I, Ross S, Gout L, Blaise F, Kuhn ML, Eckert MR, Cattolico L, Bernard-Samain S, Balesdent MH, Rouxel T: **Heterochromatin-like regions as ecological niches for avirulence genes in the *Leptosphaeria maculans* genome: map-based cloning of *AvrLm6***. *Molecular Plant-Microbe Interactions* 2007, **20**:459-470.
212. de Jonge R, Peter van Esse H, Maruthachalam K, Bolton MD, Santhanam P, Saber MK, Zhang Z, Usami T, Lievens B, Subbarao KV, et al.: **Tomato immune receptor Ve1 recognizes effector of multiple fungal pathogens uncovered by genome and RNA sequencing**. *Proceedings of the National Academy of Sciences* 2012, **109**:5110.
213. Cox KD: **Fungicide resistance in *Venturia inaequalis*, the causal agent of apple scab, in the United States**. In *Fungicide resistance in plant pathogens: principles and a guide to practical management*. Edited by Ishii H, Hollomon DW: Springer Japan; 2015:433-447.

Chapter 2:

Apoplastic effector proteins of plant-associated fungi and oomycetes

Mercedes Rocafort[a], Isabelle Fudal[b] and Carl H. Mesarich[a,c,†]

[a]Laboratory of Molecular Plant Pathology, School of Agriculture and Environment, Massey University, Private Bag 11222, Palmerston North 4442, New Zealand (m.rocafort.ferrer@massey.ac.nz; c.mesarich@massey.ac.nz).

[b]Université Paris-Saclay, INRAE, AgroParisTech, UMR BIOGER, 78850, Thiverval-Grignon, France (Isabelle.Fudal@inrae.fr).

[c]Bio-Protection Research Centre, Massey University, Private Bag 11222, Palmerston North 4442, New Zealand.

[†]Corresponding author: Carl H. Mesarich

A slightly modified version of this chapter was published in Current Opinion in Plant Biology, 56, 9-19 (2020)

DOI: 10.1016/j.pbi.2020.02.004

1. Abstract

The outcome of an interaction between a plant and a fungus or an oomycete, whether compatibility or incompatibility, is often determined in the hostile extracellular spaces and matrices of the apoplast. Indeed, for compatibility to occur, many plant-associated fungi and oomycetes must first neutralize the apoplast, which is both monitored by plant cell-surface immune receptors, and enriched in plant (and frequently, competitor)-derived antimicrobial compounds. Research is highlighting the diverse roles that fungal and oomycete effector proteins play in the apoplast to promote compatibility, with most recent progress made towards understanding the role of these proteins in evading chitin-triggered immunity. Research is also showcasing the ability of apoplastic effector proteins to bring about incompatibility upon recognition by diverse plant cell-surface immune receptors, and the use of effectoromics to rapidly identify apoplastic effector protein–cell-surface immune receptor interactions.

2. Introduction

Filamentous microbes develop interactions with plants that range from mutualistic (fungi) to pathogenic (fungi and oomycetes). The outcome of these interactions, be that compatibility or incompatibility, is often determined in the apoplast, where first contact between microbial and plant cells is made [1]. Very broadly, the apoplast is made up of all extracellular spaces and matrices beyond the plant plasma membrane, and is bordered by the rhizoplane and cuticle of the outer plant surface [2]. As such, the apoplast consists of all interfibrillar and intermicellar cell wall spaces, the intercellular spaces and xylem [2], as well as all spaces and matrices generated between the plant plasma membrane and fungal or oomycete cell wall during infection (**Figure 2-1**).

The apoplast is a hostile environment, with proteases, protease inhibitors, secondary metabolites and hydrolytic enzymes constitutively produced by plants to impede fungal and oomycete growth [1]. The apoplast is also monitored by cell surface-localized immune receptors that recognize invasion patterns to activate the plant immune system [3,4]. This activation slows or halts fungal and oomycete growth through the production of additional defensive compounds (similar to those mentioned above) and reactive oxygen species (ROS), as well as callose and lignin deposition, and in some cases, the hypersensitive response (HR). Notably, the apoplast is not a sterile environment, with other microbes present that compete for space and nutrients [5,6]. These microbes deploy hydrolytic enzymes, antibiotics, toxins and volatiles that can further impede fungal and oomycete growth [7].

To neutralize the apoplast and further promote colonization, fungi and oomycetes must deliver a suite of virulence factors, termed effectors, into their hosts. These effectors can be enzymatic or non-enzymatic proteins, secondary metabolites and small RNAs [8,9]. Of note, all effectors are initially delivered into the apoplast, with a subset performing their virulence function in the apoplast only. Others are translocated from the apoplast to the plant cell cytoplasm, where

they carry out their virulence function in a specific cell compartment. A third subset is anticipated, although not yet shown, to have dual virulence functions in the apoplast and the plant cell. In this review, we highlight recent progress towards the identification and functional characterization of effector proteins from plant-associated fungi and oomycetes that carry out their virulence function in the apoplast, or that are recognized by cell-surface immune receptors in this environment (hereafter referred to as apoplastic effector proteins [AEPs]).

3. Prediction and identification of apoplastic effector proteins

Most characterized effector proteins from plant-associated fungi and oomycetes are non-enzymatic, <300 amino acid residues in length, and have a signal peptide for secretion. However, larger proteins, enzymatic proteins, and proteins without a signal peptide (i.e. non-conventionally secreted proteins) can also function as effectors (e.g. [10,11,12,13]). Predicting which of these effector proteins function in the apoplast is often challenging. One feature that is frequently used as a predictor for apoplastic function is cysteine content, as many of the cysteines present in fungal and oomycete AEPs likely form intramolecular disulfide bonds required for stability and function in the protease-rich apoplast. Recently, a data-driven machine learning approach was used to develop ApoplastP, a tool for the prediction of apoplastic proteins, including conventionally and non-conventionally secreted effectors [14]. ApoplastP determined that, in addition to having a high cysteine content, AEPs tend to be rich in small amino acids, but depleted in glutamic acid, as well as acidic and charged amino acids [14]. In the case of fungi, ApoplastP is increasingly being used in conjunction with EffectorP, a powerful tool for the prediction of effector proteins, irrespective of whether they are apoplastic or non-apoplastic [15,16].

Plant-associated fungi and oomycetes deliver effector proteins into diverse apoplastic environments (**Figure 2-1**). While fluorescence microscopy is frequently used to determine whether a protein is localized to the apoplast, many are shown to reside in the apoplast through a

proteomic analysis of apoplastic wash fluid (AWF). For example, 75 small secreted proteins, made up of known and candidate effectors, were recently identified in AWF from tomato leaves infected with the fungal leaf mold pathogen, *Fulvia fulva* [17]. In other recent examples, 43 secreted proteins were identified in AWF from maize roots infected with the fungal beneficial endophyte, *Trichoderma virens* [18], while 102 proteins were identified in AWF from barley roots infected with the fungal beneficial root endophyte, *Serendipita indica* [19]. These studies, combined with previous research on the fungal rice blast pathogen, *Magnaporthe oryzae* (441 proteins identified) [20], and the fungal tomato vascular wilt pathogen, *Fusarium oxysporum* f. sp. *lycopersici* (14 secreted in xylem [SIX] proteins identified) [21,22], are providing valuable insights into the types and numbers of AEPs delivered by plant-associated fungi into the apoplast. How many of these AEPs are subsequently translocated into the plant cell cytoplasm, however, remains to be determined. Interestingly, some of the proteins identified above lack a predicted signal peptide, suggesting that a subset of AEPs are delivered into the apoplast using a non-conventional secretion system independent of the classical endoplasmic reticulum-Golgi secretory pathway [18,19,20,22]. It is anticipated that fungal and oomycete extracellular vesicles, which are membrane-enclosed cytosol-containing spheres released into the extracellular environment, will play a role in delivering many of these proteins into the apoplast, as has already been proposed for similar proteins involved in apoplastic defense from plants [23,24].

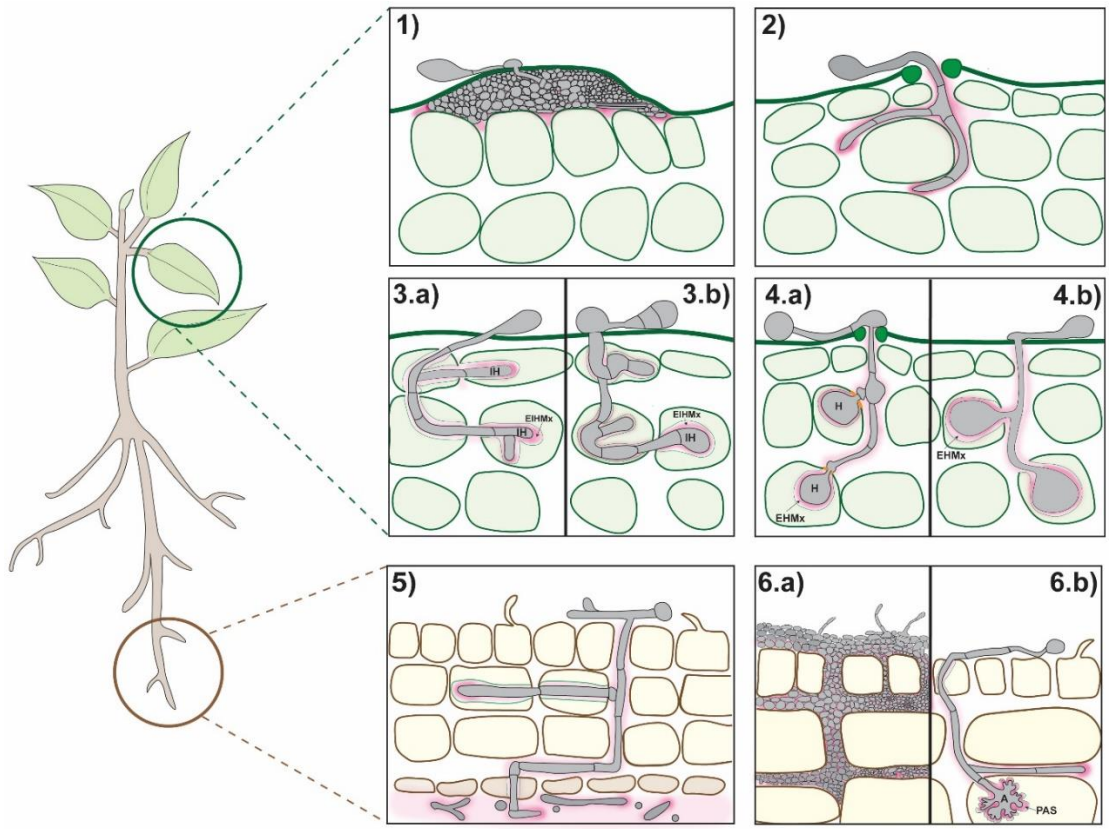

Figure 2-1. Effector proteins of plant-associated fungi and oomycetes are delivered into diverse apoplastic environments. Effector proteins of filamentous plant-associated microbes can be delivered into: **1)** the subcuticular environment between the plant cuticle and epidermal cells (e.g. during colonization of apple leaves and fruit by the fungal scab pathogen, *Venturia inaequalis*); **2)** between plant mesophyll cells (e.g. during colonization of tomato by the fungal leaf mold pathogen, *Fulvia fulva*); **3)** the extrainvasive hyphal matrix (EIHMx) developed between an intracellular invasive hypha (IH) and the host plasma membrane, which can be continuous with the apoplast (e.g. during colonization of maize leaf cells by the fungal corn smut pathogen, *Ustilago maydis* [3.a]), or sealed and separated from the bulk apoplast (e.g. during colonization of rice leaf cells by the fungal blast pathogen, *Magnaporthe oryzae* [3.b]); **4)** the extrahaustorial matrix (EHMx) developed between a haustorium (H) of an obligate biotrophic fungus or oomycete and a host-derived extrahaustorial membrane, which is separated from the bulk apoplast by a neckband (e.g. during colonization of cereal crop leaf cells by the rust pathogen, *Puccinia graminis* [4.a]), or is continuous with the bulk apoplast (e.g. during colonization of potato leaf cells by the oomycete late blight pathogen, *Phytophthora infestans* [4.b]); **5)** between cortex cells and in xylem spaces (e.g. during colonization of plant roots by the fungal wilt pathogen, *Verticillium dahliae*); **6)** between cortex cells (e.g. during colonization of plant roots by the ectomycorrhizal fungus *Laccaria bicolor* [6.a]), or in the periarbuscular space (PAS) developed between an arbuscule (A) of an endomycorrhizal fungus and the host-derived periarbuscular membrane (e.g. during colonization of plant roots by the fungus, *Rhizophagus irregularis* [6.b]). Please note that the EIHMx in 3.b and the EHMx in 4.a, which are sealed off from the bulk apoplast, are here hypothesized to be apoplastic environments. Further research is required to better understand the nature of these environments. Pathogen cell wall: black line; plant cell wall: dark green or brown line; plant cytosol: light green or brown; plant plasma membrane: light green line; haustorial neckband: orange; AEPs: pink. Figure not to scale.

4. Functional characterization of apoplastic effector proteins

4.1.Apoplastic effector proteins with roles in evading glycan-triggered immunity

AEPs from filamentous plant-associated fungi and oomycetes perform diverse biological functions to promote host-colonization (**Figure 2-2** and **Table 2-1**). Notably, many that have been functionally characterized to date play a role in deregulating glycan-triggered immunity. This is not surprising, as the apoplast is rich in chitinases and β-glucanases that disrupt microbial cell wall integrity and release chitin (fungi) and β-glucan oligomers (fungi and oomycetes) that can then be recognized by cell-surface immune receptors to activate the plant immune system [25]. Examples include Avr4, a carbohydrate-binding module family 14 (CBM14) protein from *F. fulva*, and SnTox1, a protein with similarity to plant chitin-binding proteins from the septoria nodorum blotch pathogen of wheat, *Parastagonospora nodorum*, that both shield cell wall chitin against hydrolysis by host chitinases [26,27,28], as well as Ecp6, a CBM family 50 (CBM50)/lysin motif (LysM) protein from *F. fulva* that sequesters chitin oligomers to prevent recognition by chitin immune receptors [29,30], and FGB1 from *S. indica*, which suppresses β-glycan-triggered immunity [31,32].

In line with this pioneering research, many recent studies have focused on the functional characterization of AEPs involved in evading chitin-triggered immunity. One class that is receiving ongoing attention are the CBM50/LysM effector proteins from fungi. Perhaps most interestingly, it has recently been shown that two AEPs from this class, specifically Tal6 from the beneficial root-colonizing endophytic fungus, *Trichoderma atroviride*, and RiLysM from the root-colonizing arbuscular mycorrhizal fungus, *Rhizophagus irregularis*, perform analogous roles to both Avr4 and Ecp6 [33,34]. This research, together with research on FGB1, highlights that both mutualistic and pathogenic fungi deploy AEPs to modulate glycan-triggered immunity.

In addition to CBM14- and CBM50/LysM-containing proteins, other chitin-binding AEPs have now been identified. An example is VnaChtBP, an AEP with six CBM family 18 (CBM18) domains from the fungal xylem-invading pathogen, *Verticillium nonalfalfae*, which has recently been shown to protect cell wall chitin against hydrolysis by host chitinases and to sequester chitin oligomers for the prevention of chitin-triggered immune responses [35].

These functions are not restricted to non-enzymatic proteins. For example, MoChi1, a chitinase from *M. oryzae*, has recently been demonstrated to suppress chitin-triggered immunity [36,37]. Notably, MoChi1 interacts with the rice protein, OsMBL1, a chitin-binding, jacalin-related lectin localized to the plasma membrane that is involved in defense against *M. oryzae* [36]. It has been proposed that OsMBL1 is an additional receptor for the recognition of chitin oligomers in rice, and that MoChi1 and OsMBL1 compete with each other for chitin binding, with MoChi1 degrading or sequestering chitin oligomers to interfere with recognition by OsMBL1 [36]. Interestingly, MoChi1 also directly interacts with OsTPR1, a plasma membrane-localized tetratricopeptide repeat protein in rice [37]. Through this interaction, OsTPR1 allows free chitin that would otherwise be bound or degraded by MoChi1 to trigger immune responses [37].

Remarkably, chitinases with mutations that abolish their enzymatic activity can also function as AEPs. Indeed, this has recently been shown for MpChi and MrChi, two non-orthologous, enzymatically-inactive chitinases from the fungal pathogens of cacao, *Moniliophthora perniciosa* (witches' broom disease) and *Moniliophthora roreri* (frosty pod rot disease), which have retained their substrate-binding specificity to prevent chitin-triggered immunity [38]. Strikingly, these examples illustrate the role of neofunctionalization in the generation of AEPs with new functions. Other recent examples of enzymes that function as AEPs in deregulating glycan-triggered immunity are VdPDA1 and FovPDA, polysaccharide deacetylases from the xylem-invading fungal pathogens, *Verticillium dahliae* and *Fusarium oxysporum* f. sp. *vasinfectum*, that directly deacetylate chitin oligomers to chitosan to impede

chitin-triggered defense responses [39], and VdSSEP1, a serine protease from *V. dahliae* that removes the chitin-binding domain (CBD) of Chi28, a chitinase from cotton, to compromise chitin recognition [40]. Interestingly, in the case of VdSSEP1, a DUF26 protein from cotton, CRR1, has been shown to interact with Chi28 to prevent CBD removal [40]. It is speculated that CRR1 may achieve this through blockage of the CBD cleavage site [40].

4.1.1. Apoplastic effector proteins with other roles in promoting host-colonization

Progress has also been made towards the functional characterization of AEPs that are not involved in deregulating glycan-triggered immunity. An example is Rsp3 from *U. maydis*, which possesses a glutamate and proline-rich region, followed by a cysteine-rich region and a long repeat-rich domain [12]. Rsp3 decorates the surface of *U. maydis* hyphae *in planta*, where it interacts with at least two apoplastic DUF26 mannose-binding proteins of maize, AFP1 and AFP2 [12]. Through this decoration, Rsp3 protects the hyphae of *U. maydis* against the antifungal activity of AFP1 and AFP2 [12]. Notably, the antifungal activity of AFP1 is dependent upon its ability to bind mannose, suggesting that AFP1 may bind to mannose residues or mannosylated proteins of the cell wall surface to negatively impact fungal cell wall integrity [12].

Perhaps two of the more interesting recent examples are PsXEG1 and PsXLP1 from *Phytophthora sojae*, the oomycete stem and root rot pathogen of soybean [11,41]. Of these, PsXEG1 is a glycoside hydrolase family 12 (GH12) domain-containing AEP with xyloglucanase activity that is essential for full virulence of the pathogen [11]. During infection, the xyloglucanase activity of PsXEG1 is targeted for inhibition by the xyloglucan-specific endoglucanase inhibitor protein of soybean, GmGIP1 [41]. To prevent this inhibition, *P. sojae* deploys PsXLP1, a PsXEG1-like AEP with a truncated GH12 domain devoid of xyloglucanase activity [41]. Remarkably, PsXLP1 functions as a decoy to protect PsXEG1 from the inhibitory action of GmGIP1 [41]. This protection is achieved through occupation of the PsXEG1 binding sites of GmGIP1 to allow PsXEG1 to fulfill its virulence function [41].

Another interesting example is SiE5´NT, a glycophosphatidylinositol (GPI)-anchored and soluble ecto-5´-nucleotidase from *S. indica* [19]. In plants, the perception of apoplastic nucleotides such as eATP by cell-surface receptors is important for growth and development, as well as for responses to abiotic and biotic stresses. During colonization of *Arabidopsis* and barley roots by *S. indica*, especially at early symbiotic stages, eATP accumulates in the apoplast, which has a negative effect on plant colonization [19]. It has been shown that SiE5´NT, which is capable of hydrolyzing ATP, ADP and AMP to adenosine and phosphate, is able to modify apoplastic nucleotide levels to promote host-colonization [19]. However, the specific mechanism of how SiE5´NT promotes colonization is unclear, as this effector could favor fungal growth by promoting fungal nutrition or by manipulating plant defenses [19].

While many other biological functions are expected to be performed by AEPs (**Figure 2-2**), it is anticipated that a subset will play a role in promoting self-defense against antimicrobial microbe (competitor)-derived compounds, or in manipulating the apoplastic microbiome to promote host-colonization [5,6]. One class of peptides that we believe may be of high interest to this exciting emerging area of apoplastic effector biology, specifically with regards to antagonistic fungus–microbe interactions, are the dikaritins, which are ribosomally synthesized and post-translationally modified cyclic peptides (RiPPs) produced by both ascomycete and basidiomycete fungi [42]. This is based on the finding that many RiPPs, including members of the cyclotide class from plants, have potent antimicrobial activity [43]. In line with this hypothesis, deletion of either *GigA* or *SspN*, two highly-expressed dikaritin precursor peptide-encoding genes from the fungal endophyte, *Epichloë festucae*, does not disrupt the mutualistic symbiotic relationship that this fungus has with perennial ryegrass, suggesting a possible role outside of host modulation [44,45].

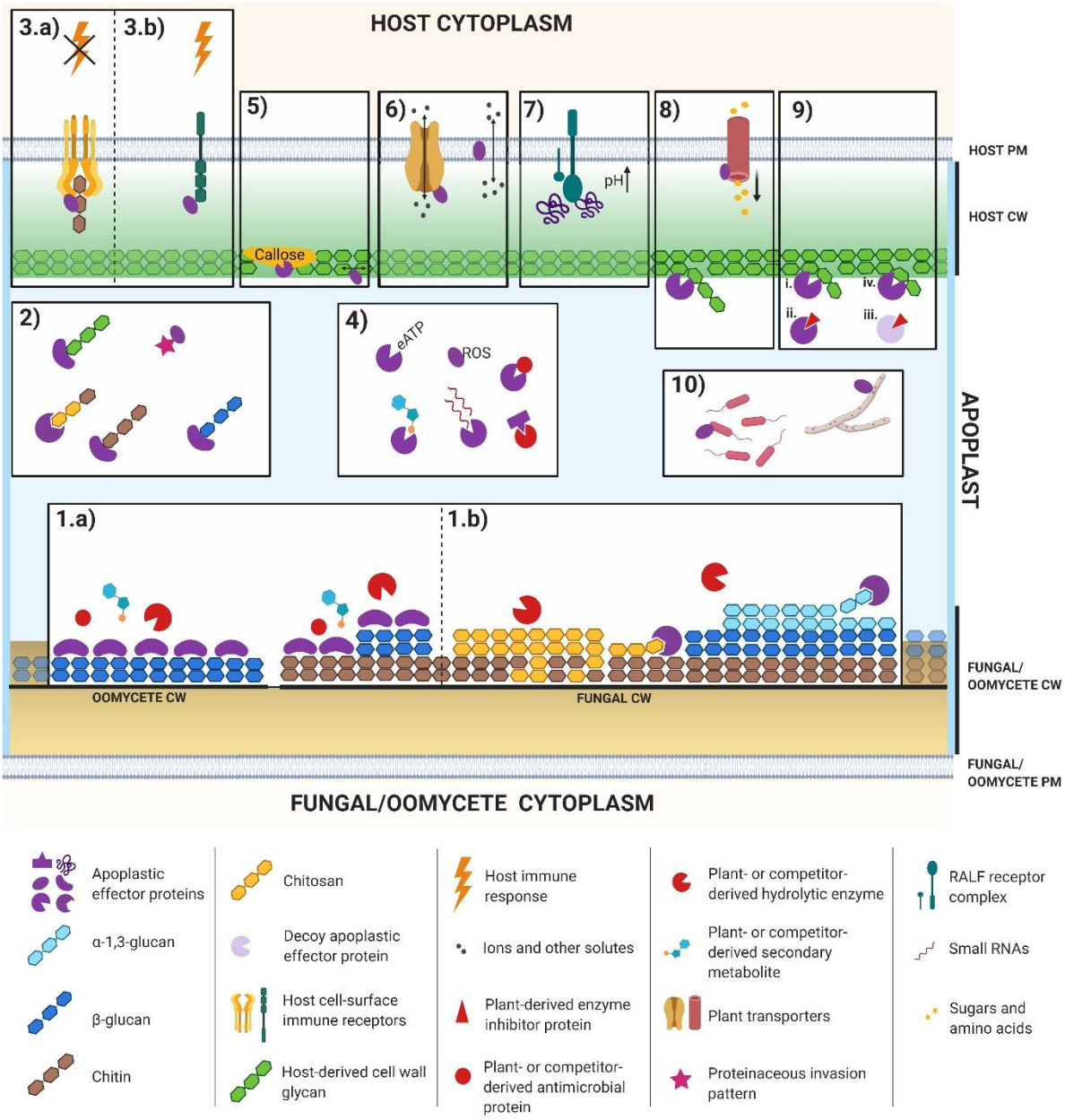

Figure 2-2. Characterized and anticipated biological functions of apoplastic effector proteins from plant-associated fungi and oomycetes. 1) Apoplastic effector proteins (AEPs) bind (**1.a**) or chemically modify (**1.b**) components of the fungal/oomycete cell surface (e.g. carbohydrates or proteins) to provide protection against plant- or competitor-derived antimicrobial compounds (e.g. enzymatic or non-enzymatic proteins and secondary metabolites), and to prevent the release of fungal/oomycete cell surface components (e.g. chitin oligomers, β-glucan oligomers or peptide fragments) that would otherwise be recognized as invasion patterns by plant cell-surface immune receptors. **2)** AEPs sequester, modify or break-down fungus/oomycete-, competitor- or plant-derived invasion patterns (e.g. chitin or β-glucan oligomers and peptide fragments) released into the apoplastic environment to prevent recognition by plant cell-surface immune receptors. **3.a)** AEPs from biotrophic fungi/oomycetes could interfere with cell-surface immune receptor complex assembly or activation. **3.b)** AEPs from necrotrophic fungi/oomycetes activate cell-surface immune receptors to enable cell death for nutrient acquisition. **4)** AEPs degrade, inhibit, modify, scavenge

or sequester plant- or competitor-derived antimicrobial compounds (e.g. enzymatic or non-enzymatic proteins and secondary metabolites) and other molecules (e.g. peroxidases, proteases, small RNAs, extracellular nucleotides and apoplastic signaling molecules) involved in plant defense. **5)** Enzymatic and non-enzymatic AEPs could increase plant cell wall extensibility or break down induced plant structural defenses (e.g. callose, tyloses and lignin). **6)** AEPs could interact with the plant plasma membrane or pumps/transporters to modulate ion fluxes (e.g. Ca^{2+}) involved in plant defense responses. **7)** AEPs could alter host physiology (e.g. by mimicking plant molecules such as rapid alkalinization factors that interact with cell-surface receptors to manipulate apoplastic pH for colonization [shown], or by interacting with cell-surface receptors to open or close stomata [not shown]). **8)** AEPs liberate nutrients from the plant cell surface, or interact with plant transporters for the export of nutrients from the plant cell, for nutrition. **9)** AEPs function as decoys that protect other important AEPs as bodyguards. For example, an enzymatic AEP could contribute to fungal/oomycete virulence by releasing nutrients from the plant cell wall **(i)**. In the presence of a plant-derived enzyme inhibitor protein, the enzymatic activity of the AEP could be inhibited, blocking its contribution to virulence **(ii)**. To prevent this inhibition, the fungus/oomycete could secrete a second AEP devoid of enzymatic activity that acts as a decoy for the plant-derived enzyme inhibitor protein. In this example, the decoy occupies the binding site of the plant-derived enzyme inhibitor protein so that it can no longer inhibit the enzymatic activity of the first AEP **(iii)**. In the presence of the decoy, the first AEP could then, once again, release nutrients from the plant cell wall **(iv)**. **10)** AEPs could manipulate the apoplastic microbiome (e.g. through the inhibition of competing or antagonistic microbes, or by attracting or promoting the growth of beneficial microbes). PM: plasma membrane, CW: cell wall.

Table 2-1. Selected apoplastic effector proteins from filamentous plant-associated fungi and oomycetes with characterized biological functions.

Apoplastic effector protein	Filamentous plant-associated microbe	Characterized biological function in the apoplast[1]	References
Avr2	*Fulvia fulva*	Inhibits host cysteine proteases	[46,47,48]
Avr4	*F. fulva*	CBM14 protein. Protects cell wall chitin against hydrolysis by host chitinases	[26,27]
CfTom1	*F. fulva*	GH10 protein. Degrades the tomato antifungal glycoalkaloid α-tomatine to the less-toxic tomatidine	[49]
Ecp6	*F. fulva*	CBM50/LysM protein. Sequesters chitin oligomers to prevent chitin-triggered immunity	[29,30]
(F)-RALF	*Fusarium oxysporum*	Promotes alkalinisation of the apoplast	[50,51]
FoMep1 and FoSep1	*F. oxysporum* f. sp. *lycopersici*	Metalloprotease and serine protease, respectively. Function synergistically to remove the CBD of host chitinases	[52]
MoChi1	*Magnaporthe oryzae*	GH18 chitinase. Prevents chitin-triggered immunity	[36]

MpChi	*Moniliophthora perniciosa*	Enzymatically-inactive GH18 chitinase. Sequesters chitin oligomers to prevent chitin-triggered immunity	[38]
SnToxA and SnTox3	*Parastagonospora nodorum*	Interact with host PR1 proteins	[53,54]
SnTox1	*P. nodorum*	Activates host cell death to acquire nutrients. Protects cell wall chitin against hydrolysis by host chitinases	[28,55]
PesCDA	*Pestalotiopsis* sp.	CE4 polysaccharide deacetylase with a CBM18 domain. Deacetylates chitin oligomers to chitosan to prevent chitin-triggered immunity	[56]
EPIC1 and EPIC2B	*Phytophthora infestans*	Inhibit host cysteine proteases	[57,58]
EPI1 and EPI10	*P. infestans*	Inhibit host serine proteases. EPI1 prevents plant subtilase-mediated cleavage of PC2 (an apoplastic effector protein) to dampen PC2-triggered immunity	[59,60,61[2]]
GIP1	*P. infestans*	Inhibits host endoglucanase to suppress β-glucan-triggered immunity	[62]
PsXEG1	*Phytophthora sojae*	GH12 xyloglucanase that can degrade xyloglucan and β-glucan. Promotes host-colonization through xyloglucanase activity	[11,41]
PsXLP1	*P. sojae*	Decoy that protects PsXEG1 from the inhibitory action of a host xyloglucan-specific endoglucanase inhibitor protein	[41]
SsCP1	*Sclerotinia slcerotiorum*	Cerato-platanin protein. Inhibits antifungal activity of PR1	[63]
FGB1	*Serendipita indica*	Suppresses β-glucan-triggered immunity and modifies fungal cell wall composition to increase resistance against cell wall stressors	[31,32]
SiE5´NT	*S. indica*	Ecto-5´-nucleotidase. Hydrolyses apoplast nucleotide levels to modulate host immunity or obtain nutrients	[19]
Pep1	*Ustilago maydis*	Inhibits host peroxidase to prevent peroxidase-mediated ROS production	[64]
Pit2	*U. maydis*	Inhibits host cysteine proteases	[65,66]

Rsp3	*U. maydis*	Protects hyphae from antifungal activity of host mannose-binding proteins	[12]
Ave1	*Verticillium dahliae*	Manipulates the host microbiome through the suppression of antagonistic bacteria	[67[2]]
VdPDA1	*Verticillium dahliae*	CE4 polysaccharide deacetylase. Deacetylates chitin oligomers to chitosan to prevent chitin-triggered immunity	[39]
VnaChtBP	*Verticillium nonalfalfae*	CBM18 protein. Protects hyphae from plant chitinases and prevents chitin-triggered immunity	[35]

[1]CBD, Chitin-Binding Domain; CBM14, Carbohydrate-Binding Module family 14; CBM18, CBM family 18; CBM50, CBM family 50; CE4, Carbohydrate Esterase family 4; GH10, Glycoside Hydrolase family 10; GH12, GH family 12; GH18, GH family 18; LysM, Lysin Motif; PR1; Pathogenesis-Related 1; ROS, Reactive Oxygen Species.

[2]Currently a preprint article.

5. Effectoromics and plant cell-surface immune receptors

Over several years, it has been demonstrated that effector proteins delivered into the apoplast by plant-associated fungi and oomycetes can be recognized as invasion patterns by cell-surface immune receptors to activate the plant immune system (**Table 2-2**). So far, these immune receptors have been shown to be either Leucine-Rich Repeat–Receptor-Like Proteins (LRR-RLPs) [68,69,70,71,72,73,74,75,76,77,78], an S–Receptor-Like Kinase (S-RLK) [79], or more recently, Wall-Associated receptor Kinase-Like (WAKL) proteins [80,81]. Notably, cell surface immune receptors can also be hijacked by AEPs of necrotrophs to activate host cell death for the acquisition of nutrients. Indeed, this has been shown for SnTox1 of *P. nodorum*, which is recognized by the WAK cell-surface immune receptor from wheat, Snn1 [55].

Increasingly, an effectoromics approach is being used to rapidly identify AEPs that are recognized by plant cell-surface immune receptors, and to identify (plants with) cell-surface immune receptors that recognize AEPs [82,83]. In both cases, this identification relies on activation of the plant immune system, usually in the form of an HR (cell death or chlorosis), following infiltration of the AEP into, or transient expression of the AEP in, the plant. For example, in a recent study, 14 of 63 tested AEP candidates from the fungal septoria leaf blotch pathogen of wheat, *Zymoseptoria tritici*, were shown to trigger cell death or chlorosis in the model non-host plant species, *Nicotiana benthamiana* [84]. In another recent study, nine of 41 tested AEP candidates from *F. fulva* were shown to trigger cell death or chlorosis in wild tomato species [17]. These studies set the foundation for understanding how plant-associated fungi and oomycetes activate apoplastic immune responses in non-host and host plants, and enable the identification of cell-surface immune receptors or plant material that can be used (or eliminated in the case of necrotrophic pathogens) to generate disease-resistant plants.

Table 2-2. Selected apoplastic effector proteins from filamentous plant-associated fungi and oomycetes that are recognized as invasion patterns by characterized plant cell-surface immune receptors.

Apoplastic effector protein	Filamentous plant-associated microbe	Corresponding plant cell-surface immune receptor[1]	Mode of recognition[2]	References
Avr2	*Fulvia fulva*	Cf-2.1 and Cf-2.2 (LRR-RLPs)	Indirect	[46,71,85]
Avr4	*F. fulva*	Cf-4 (LRR-RLP)	Direct?	[26,77,86]
Avr4E	*F. fulva*	Cf-4E (LRR-RLP)		[76,87]
Avr5	*F. fulva*	Cf-5 (LRR-RLP)		[70,88]
Avr9	*F. fulva*	Cf-9 (LRR-RLP)	Indirect?	[72,89,90,91]
Avr1 (Six4)	*Fusarium oxysporum* f. sp. *lycopersici*	I (LRR-RLP)		[69,92]
Avr3 (Six1)	*F. oxysporum* f. sp. *lycopersici*	I-3 (S-RLK)	Indirect?	[79,93]
AvrLm1	*Leptosphaeria maculans*	LepR3 (LRR-RLP)	Indirect?	[74,94]
AvrLm2	*L. maculans*	Rlm2 (LRR-RLP)		[75,95]
AvrLm5-9	*L. maculans*	Rlm9 (WAKL)	Indirect?	[80[3],96]
SnTox1	*Parastagonospora nodorum*	Snn1 (WAK)	Direct	[55,97]
PsXEG1	*Phytophthora sojae*	RXEG1 (LRR-RLP)	Direct	[11,78]
Ave1	*Verticillium dahliae*	Ve1 (LRR-RLP)		[73,98]
AvrStb6	*Zymoseptoria tritici*	Stb6 (WAKL)	Indirect?	[81,99]
NLPs	Various fungi and oomycetes	RLP23 (LRR-RLP)	Direct	[68,100]

[1]LRR, Leucine-Rich Repeats; NLP, Necrosis- and ethylene-inducing-Like Protein; RLK, Receptor-Like Kinase; RLP, Receptor-Like Protein; S-RLK, RLK with an S domain homologous to self-incompatibility-locus glycoproteins of *Brassica oleracea*; WAK, Wall-Associated Kinase; WAKL, WAK-Like.

[2]Mode of apoplastic effector protein recognition by the corresponding cell surface immune receptor. Hypothesized modes of recognition, based on current experimental data, are denoted with a question mark (?).

[3]Currently a preprint article.

6. Conclusions

Good progress continues to be made towards the identification and functional characterization of AEPs from plant-associated fungi and oomycetes, as well as the corresponding cell-surface immune receptors from plants that recognize them. However, a lot of research is still required to fully characterize the diversity of biological functions carried out by these proteins. Further research is also needed to understand the pathways and mechanisms responsible for the non-conventional secretion of AEPs, and for the translocation of effector proteins from the apoplast to the plant cell cytoplasm. It will be interesting to determine whether AEPs play a role in this translocation process.

7. Appendix A: Statement of contribution doctorate with publications/manuscripts (DRC16)

We, the candidate and the candidate's Primary Supervisor, certify that all co-authors have consented to their work being included in the thesis and they have accepted the candidate's contribution as indicated below in the *Statement of Originality*.

Name of candidate:	Mercedes Rocafort Ferrer
Name/title of Primary Supervisor:	Carl H. Mesarich
Name of Research Output and full reference:	
Apoplastic effector proteins of plant-associated fungi and oomycetes	
In which Chapter is the Manuscript /Published work:	Chapter 2
Please indicate:	
• The percentage of the manuscript/Published Work that was contributed by the candidate:	60
and	
• Describe the contribution that the candidate has made to the Manuscript/PublishedWork:	
The candidate performed the literature search and wrote the section entitled "Functional characterization of apoplastic effector proteins". The candidate alsogenerated both figures and the supplementary table.	
For manuscripts intended for publication please indicate target journal:	
Candidate's Signature:	Mercedes Rocafort Ferrer Ferrer Firmado digitalmente por Mercedes Rocafort Ferrer Fecha: 2022.09.23 09:23:17 +02'00'
Date:	23/09/2022
Primary Supervisor's Signature:	Carl Mesarich Digitally signed by Carl Mesarich Date: 2022.09.23 19:43:56 +12'00'
Date:	23/09/2022

Chapter 2_ DRC 16 -
V3 Online Statement

8. References

1. Doehlemann G, Hemetsberger C: **Apoplastic immunity and its suppression by filamentous plant pathogens**. *New Phytologist.* 2013, **198**:1001-1016.
2. Sattelmacher B: **The apoplast and its significance for plant mineral nutrition**. *New Phytologist.* 2001, **149**:167-192.
3. Cook DE, Mesarich CH, Thomma BPHJ: **Understanding plant immunity as a surveillance system to detect invasion**. *Annual Reviews of Phytopathology.* 2015, **53**:541-563.
4. van der Burgh AM, Joosten MHAJ: **Plant immunity: thinking outside and inside the box**. *Trends in Plant Science.* 2019, **24**:587-601.
5. Rovenich H, Boshoven JC, Thomma BPHJ: **Filamentous pathogen effector functions: of pathogens, hosts and microbiomes**. *Current Opinion in. Plant Biology.* 2014, **20**:96-103.
6. Snelders NC, Kettles GJ, Rudd JJ, Thomma BPHJ: **Plant pathogen effector proteins as manipulators of host microbiomes?** *Molecular Plant Pathology.* 2018, **19**:257-259.
7. Carrión VJ, Perez-Jaramillo J, Cordovez V, Tracanna V, de Hollander M, Ruiz-Buck D, Mendes LW, van Ijcken WFJ, Gomez-Exposito R, Elsayed SS, et al.: **Pathogen-induced activation of disease-suppressive functions in the endophytic root microbiome**. *Science* 2019, **366**:606-612.
8. Lo Presti L, Lanver D, Schweizer G, Tanaka S, Liang L, Tollot M, Zuccaro A, Reissmann S, Kahmann R: **Fungal effectors and plant susceptibility**. *Annual Reviews of Plant Biology.* 2015, **66**:513-545.
9. Wang Y, Tyler BM, Wang Y: **Defense and counterdefense during plant-pathogenic oomycete infection**. *Annual Reviews of Microbiology.* 2019, **73**:667-696.
10. Liu T, Song T, Zhang X, Yuan H, Su L, Li W, Xu J, Liu S, Chen L, Chen T, et al.: **Unconventionally secreted effectors of two filamentous pathogens target plant salicylate biosynthesis**. *Nature Communications.* 2014, **5**:4686.
11. Ma Z, Song T, Zhu L, Ye W, Wang Y, Shao Y, Dong S, Zhang Z, Dou D, Zheng X, et al.: **A *Phytophthora sojae* glycoside hydrolase 12 protein is a major virulence factor during soybean infection and is recognized as a PAMP**. *Plant Cell* 2015, **27**:2057-2072.
12. Ma L-S, Wang L, Trippel C, Mendoza-Mendoza A, Ullmann S, Moretti M, Carsten A, Kahnt J, Reissmann S, Zechmann B, et al.: **The *Ustilago maydis* repetitive effector Rsp3 blocks the antifungal activity of mannose-binding maize proteins**. *Nature Communications.* 2018, **9**:1711.
13. Salcedo A, Rutter W, Wang S, Akhunova A, Bolus S, Chao S, Anderson N, de Soto MF, Rouse M, Szabo L, et al.: **Variation in the *AvrSr35* gene determines *Sr35* resistance against wheat stem rust race Ug99**. *Science* 2017, **358**:1604-1606.
14. Sperschneider J, Dodds PN, Singh KB, Taylor JM: **ApoplastP: prediction of effectors and plant proteins in the apoplast using machine learning**. *New Phytologist.* 2018, **217**:1764-1778.
15. Sperschneider J, Dodds PN, Gardiner DM, Singh KB, Taylor JM: **Improved prediction of fungal effector proteins from secretomes with EffectorP 2.0**. *Molecular Plant Pathology.* 2018, **19**:2094-2110.
16. Sperschneider J, Gardiner DM, Dodds PN, Tini F, Covarelli L, Singh KB, Manners JM, Taylor JM: **EffectorP: predicting fungal effector proteins from secretomes using machine learning**. *New Phytologist.* 2016, 210:743-761.
17. Mesarich CH, Ökmen B, Rovenich H, Griffiths SA, Wang C, Karimi Jashni M, Mihajlovski A, Collemare J, Hunziker L, Deng CH, et al.: **Specific hypersensitive response-**

associated recognition of new apoplastic effectors from *Cladosporium fulvum* in wild tomato. *Molecular Plant-Microbe Interactions.* 2018, **31**:145-162.

18. Nogueira-Lopez G, Greenwood DR, Middleditch M, Winefield C, Eaton C, Steyaert JM, Mendoza-Mendoza A: **The apoplastic secretome of *Trichoderma virens* during interaction with maize roots shows an inhibition of plant defence and scavenging oxidative stress secreted proteins**. *Frontiers in Plant Science.* 2018, **9**:409.
19. Nizam S, Qiang X, Wawra S, Nostadt R, Getzke F, Schwanke F, Dreyer I, Langen G, Zuccaro A: ***Serendipita indica* E5′NT modulates extracellular nucleotide levels in the plant apoplast and affects fungal colonization**. *EMBO Reports.* 2019, **20**:e47430.
20. Kim SG, Wang Y, Lee KH, Park Z-Y, Park J, Wu J, Kwon SJ, Lee Y-H, Agrawal GK, Rakwal R, et al.: **In-depth insight into *in vivo* apoplastic secretome of rice-*Magnaporthe oryzae* interaction**. *Journal of Proteomics* 2013, **78**:58-71.
21. Houterman PM, Speijer D, Dekker HL, de Kloster CG, Cornelissen BJC, Rep M: **The mixed xylem sap proteome of *Fusarium oxysporum*-infected tomato plants**. *Molecular Plant Pathology.* 2007, **8**:215-221.
22. Schmidt SM, Houterman PM, Schreiver I, Ma L, Amyotte S, Chellappan B, Boeren S, Takken FLW, Rep M: **MITEs in the promoters of effector genes allow prediction of novel virulence genes in *Fusarium oxysporum***. *BMC Genomics* 2013, **14**:119.
23. Rybak K, Robatzek S: **Functions of extracellular vesicles in immunity and virulence**. *Plant Physiology* 2019, **179**:1236-1247.
24. Rutter BD, Innes RW: **Extracellular vesicles isolated from the leaf apoplast carry stress-response proteins**. *Plant Physiology* 2017, **173**:728-741.
25. Rovenich H, Zuccaro A, Thomma BPHJ: **Convergent evolution of filamentous microbes towards evasion of glycan-triggered immunity**. *New Phytologist.* 2016, **212**:896-901.
26. Hurlburt NK, Chen L-H, Stergiopoulos I, Fisher AJ: **Structure of the *Cladosporium fulvum* Avr4 effector in complex with $(GlcNAc)_6$ reveals the ligand-binding mechanism and uncouples its intrinsic function from recognition by the Cf-4 resistance protein**. *PLoS Pathogens.* 2018, **14**:e1007263.
27. van den Burg HA, Harrison SJ, Joosten MHAJ, Vervoort J, de Wit PJGM: ***Cladosporium fulvum* Avr4 protects fungal cell walls against hydrolysis by plant chitinases accumulating during infection**. *Molecular Plant-Microbe Interactions.* 2006, **19**:1420-1430.
28. Liu Z, Gao Y, Kim YM, Faris JD, Shelver WL, de Wit PJGM, Xu SS, Friesen TL: **SnTox1, a *Parastagonospora nodorum* necrotrophic effector, is a dual-function protein that facilitates infection while protecting from wheat-produced chitinases**. *New Phytologist.* 2016, **211**:1052-1064.
29. de Jonge R, Peter van Esse H, Kombrink A, Shinya T, Desaki Y, Bours R, van der Krol S, Shibuya N, Joosten MHAJ, Thomma BPHJ: **Conserved fungal LysM effector Ecp6 prevents chitin-triggered immunity in plants**. *Science* 2010, **329**:953-955.
30. Sánchez-Vallet A, Saleem-Batcha R, Kombrink A, Hansen G, Valkenburg D-J, Thomma BPHJ, Mesters JR: **Fungal effector Ecp6 outcompetes host immune receptor for chitin binding through intrachain LysM dimerization**. *eLife* 2013, **2**:e00790.
31. Wawra S, Fesel P, Widmer H, Neumann U, Lahrmann U, Becker S, Hehemann J-H, Langen G, Zuccaro A: **FGB1 and WSC3 are *in planta*-induced β-glucan-binding fungal lectins with different functions**. *New Phytologist.* 2019, **222**:1493-1506.
32. Wawra S, Fesel P, Widmer H, Timm M, Seibel J, Leson L, Kesseler L, Nostadt R, Hilbert M, Langen G, et al.: **The fungal-specific β-glucan-binding lectin FGB1 alters cell-wall composition and suppresses glucan-triggered immunity in plants**. *Nature Communications.* 2016, **7**:13188.

33. Romero-Contreras YJ, Ramírez-Valdespino CA, Guzmán-Guzmán P, Macías-Segoviano JI, Villagómez-Castro JC, Olmedo-Monfil V: **Tal6 from *Trichoderma atroviride* is a LysM effector involved in mycoparasitism and plant association**. *Frontiers in Microbiolology.* 2019, **10**:2231.
34. Zeng T, Rodriguez-Moreno L, Mansurkhodzaev A, Wang P, van den Berg W, Gasciolli V, Cottaz S, Fort S, Thomma BPHJ, Bono J-J, et al.: **A LysM effector subverts chitin-triggered immunity to facilitate arbuscular mycorrhizal symbiosis**. *New Phytologist.* 2019, **In Press**.
35. Volk H, Marton K, Flajšman M, Radišek S, Tian H, Hein I, Podlipnik Č, Thomma BPHJ, Košmelj K, Javornik B, et al.: **Chitin-binding protein of *Verticillium nonalfalfae* disguises fungus from plant chitinases and suppresses chitin-triggered host immunity**. *Molecular Plant-Microbe Interactions.* 2019, **32**:1378-1390.
36. Han Y, Song L, Peng C, Liu X, Liu L, Zhang Y, Wang W, Zhou J, Wang S, Ebbole D, et al.: **A *Magnaporthe* chitinase Interacts with a rice jacalin-related lectin to promote host colonization**. *Plant Physiology.* 2019, **179**:1416-1430.
37. Yang C, Yu Y, Huang J, Meng F, Pang J, Zhao Q, Islam MA, Xu N, Tian Y, Liu J: **Binding of the *Magnaporthe oryzae* chitinase MoChia1 by a rice tetratricopeptide repeat protein allows free chitin to trigger immune responses**. *Plant Cell* 2019, **31**:172-188.
38. Fiorin GL, Sanchéz-Vallet A, Thomazella DPdT, do Prado PFV, do Nascimento LC, Figueira AVdO, Thomma BPHJ, Pereira GAG, Teixeira PJPL: **Suppression of plant immunity by fungal chitinase-like effectors**. *Current Biology.* 2018, **28**:3023-3030.e5.
39. Gao F, Zhang B-S, Zhao J-H, Huang J-F, Jia P-S, Wang S, Zhang J, Zhou J-M, Guo H-S: **Deacetylation of chitin oligomers increases virulence in soil-borne fungal pathogens**. *Nature Plants* 2019. **5**: 1167-1176.
40. Han L-B, Li Y-B, Wang F-X, Wang W-Y, Liu J, Wu J-H, Zhong N-Q, Wu S-J, Jiao G-L, Wang H-Y, et al.: **The cotton apoplastic protein CRR1 stabilizes chitinase 28 to facilitate defense against the fungal pathogen *Verticillium dahliae***. *Plant Cell* 2019, **31**:520-536.
41. Ma Z, Zhu L, Song T, Wang Y, Zhang Q, Xia Y, Qiu M, Lin Y, Li H, Kong L, et al.: **A paralogous decoy protects *Phytophthora sojae* apoplastic effector PsXEG1 from a host inhibitor**. *Science* 2017, **355**:710-714.
42. Vogt E, Künzler M: **Discovery of novel fungal RiPP biosynthetic pathways and their application for the development of peptide therapeutics**. *Applied Microbiology and Biotechnology.* 2019, **31**:1-5.
43. Slazak B, Kapusta M, Strömstedt AA, Słomka A, Krychowiak M, Shariatgorji M, Andrén PE, Bohdanowicz J, Kuta E, Göransson U: **How does the sweet violet (*Viola odorata* L.) fight pathogens and pests – Cyclotides as a comprehensive plant host defense system**. *Frontiers in Plant Science.* 2018, **9**:1296.
44. Hassing B, Winter D, Becker Y, Mesarich CH, Eaton, CJ, Scott B: **Analysis of *Epichloë festucae* small secreted proteins in the interaction with *Lolium perenne***. *PLoS One* 2019, **14**:e0209463.
45. Johnson RD, Lane GA, Koulman A, Cao M, Fraser K, Fleetwood DJ, Voisey CR, Dyer JM, Pratt J, Christensen M, et al.: **A novel family of cyclic oligopeptides derived from ribosomal peptide synthesis of an *in planta*-induced gene, *gigA*, in *Epichloë* endophytes of grasses**. *Fungal Genetics and Biology.* 2015, **85**:14-24.
46. Rooney HCE, van't Klooster JW, van der Hoorn RAL, Joosten MHAJ, Jones JDG, de Wit PJGM: ***Cladosporium* Avr2 inhibits tomato Rcr3 protease required for *Cf-2*-dependent disease resistance**. *Science* 2005, **308**:1783-1786.

47. Shabab M, Shindo T, Gu C, Kaschani F, Pansuriya T, Chintha R, Harzen A, Colby T, Kamoun S, van der Hoorn RAL: **Fungal effector protein AVR2 targets diversifying defense-related Cys proteases of tomato**. *Plant Cell* 2008, **20**:1169-1183.
48. van Esse HP, van't Klooster JW, Bolton MD, Yadeta KA, van Baarlen P, Boeren S, Vervoort J, de Wit PJGM, Thomma BPHJ: **The *Cladosporium fulvum* virulence protein Avr2 inhibits host proteases required for basal defense**. *Plant Cell* 2008, **20**:1948-1963.
49. Ökmen B, Etalo DW, Joosten MHAJ, Bouwmeester HJ, de Vos RC, Collemare J, de Wit PJGM: **Detoxification of α-tomatine by *Cladosporium fulvum* is required for full virulence on tomato**. *New Phytologist.* 2013, **198**:1203-1214.
50. Masachis S, Segorbe D, Turrà D, Leon-Ruiz M, Fürst U, El Ghalid M, Leonard G, López-Berges MS, Richards TA, Felix G, et al.: **A fungal pathogen secretes plant alkalinizing peptides to increase infection**. *Nature Microbiology.* 2016, **1**:16043.
51. Thynne E, Saur IML, Simbaqueba J, Ogilvie HA, Gonzalez-Cendales Y, Mead O, Taranto A, Catanzariti A-M, McDonald MC, Schwessinger B, et al.: **Fungal phytopathogens encode functional homologues of plant rapid alkalinization factor (RALF) peptides**. *Molecular Plant Pathology.* 2017, **18**:811-824.
52. Karimi Jashni M, Dols IHM, Iida Y, Boeren S, Beenen HG, Mehrabi R, Collemare J, de Wit PJGM: **Synergistic action of a metalloprotease and a serine protease from *Fusarium oxysporum* f. sp. *lycopersici* cleaves chitin-binding tomato chitinases, reduces their antifungal activity, and enhances fungal virulence**. *Molecular Plant-Microbe Interactions.* 2015, **28**:996-1008.
53. Breen S, Williams SJ, Winterberg B, Kobe B, Solomon PS: **Wheat PR-1 proteins are targeted by necrotrophic pathogen effector proteins**. *The Plant Journal.* 2016, **88**:13-25.
54. Lu S, Faris JD, Sherwood R, Friesen TL, Edwards MC: **A dimeric PR-1-type pathogenesis-related protein interacts with ToxA and potentially mediates ToxA-induced necrosis in sensitive wheat**. *Molecular Plant Pathology.* 2014, **15**:650-663.
55. Shi G, Zhang Z, Friesen TL, Raats D, Fahima T, Brueggeman RS, Lu S, Trick HN, Liu Z, Chao W, et al.: **The hijacking of a receptor kinase-driven pathway by a wheat fungal pathogen leads to disease**. *Science Advances.* 2016, **2**:e1600822.
56. Cord-Landwehr S, Melcher RLJ, Kolkenbrock S, Moerschbacher BM: **A chitin deacetylase from the endophytic fungus *Pestalotiopsis* sp. efficiently inactivates the elicitor activity of chitin oligomers in rice cells**. *Scientific Reports.* 2016, **6**:38018.
57. Tian M, Benedetti B, Kamoun S: **A second Kazal-like protease inhibitor from *Phytophthora infestans* inhibits and interacts with the apoplastic pathogenesis-related protease P69B of tomato**. *Plant Physiology.* 2005, **138**:1785-1793.
58. Tian M, Huitema E, da Cunha L, Torto-Alalibo T, Kamoun S: **A Kazal-like extracellular serine protease inhibitor from *Phytophthora infestans* targets the tomato pathogenesis-related protease P69B**. *Journal of Biology and Chemistry.* 2004, **279**:26370-26377.
59. Song J, Win J, Tian M, Schornack S, Kaschani F, Ilyas M, van der Hoorn RAL, Kamoun S: **Apoplastic effectors secreted by two unrelated eukaryotic plant pathogens target the tomato defense protease Rcr3**. *Proceedings of the National Academy of Sciences.* 2009, **106**:1654-1659.
60. Tian M, Win J, Song J, van der Hoorn R, van der Knaap E, Kamoun S: **A *Phytophthora infestans* cystatin-like protein targets a novel tomato papain-like apoplastic protease**. *Plant Physiology.* 2007, **143**:364-377.

61. Wang S, Xing R, Wang Y, Shu H, Fu S, Paulus JK, Schuster M, Saunders DGO, Win J, Vleeshouwers V, et al.: **Cleavage of a pathogen apoplastic protein by plant subtilases activates immunity**. *bioRxiv* 2019:878272.
62. Rose JKC, Ham K-S, Darvill AG, Albersheim P: **Molecular cloning and characterization of glucanase inhibitor proteins: Coevolution of a counterdefense mechanism by plant pathogens**. *Plant Cell* 2002, **14**:1329-1345.
63. Yang G, Tang L, Gong Y, Xie J, Fu Y, Jiang D, Li G, Collinge DB, Chen W, Cheng J: **A cerato-platanin protein SsCP1 targets plant PR1 and contributes to virulence of *Sclerotinia sclerotiorum***. *New Phytologist.* 2018, **217**:739-755.
64. Hemetsberger C, Herrberger C, Zechmann B, Hillmer M, Doehlemann G: **The *Ustilago maydis* effector Pep1 suppresses plant immunity by inhibition of host peroxidase activity**. *PLoS Pathogens.* 2012, **8**:e1002684.
65. Mueller AN, Ziemann S, Treitschke S, Aßmann D, Doehlemann G: **Compatibility in the *Ustilago maydis*–maize interaction requires inhibition of host cysteine proteases by the fungal effector Pit2**. *PLoS Pathogens.* 2013, **9**:e1003177.
66. Misas Villamil JC, Mueller AN, Demir F, Meyer U, Ökmen B, Schulze Hüynck J, Breuer M, Dauben H, Win J, Huesgen PF, et al.: **A fungal substrate mimicking molecule suppresses plant immunity via an inter-kingdom conserved motif**. *Nature Communications.* 2019, **10**:1576.
67. Snelders NC, Rovenich H, Petti GC, Rocafort M, Vorholt JA, Mesters JR, Seidl MF, Nijland R, Thomma BPHJ: **An RLP23–SOBIR1–BAK1 complex mediates NLP-triggered immunity**. *Nature Plants* 2015, **1**:15140.
68. Albert I, Böhm H, Albert M, Feiler CE, Imkampe J, Wallmeroth N, Brancato C, Raaymakers TM, Oome S, Zhang H, et al.: **An RLP23–SOBIR1–BAK1 complex mediates NLP-triggered immunity**. *Nature Plants* 2015, **1**:15140.
69. Catanzariti A-M, Do HTT, Bru P, de Sain M, Thatcher LF, Rep M, Jones DA: **The tomato *I* gene for Fusarium wilt resistance encodes an atypical leucine-rich repeat receptor-like protein whose function is nevertheless dependent on SOBIR1 and SERK3/BAK1**. The *Plant Journal.* 2017, **89**:1195-1209.
70. Dixon MS, Hatzixanthis K, Jones DA, Harrison K, Jones JDG: **The tomato *Cf-5* disease resistance gene and six homologs show pronounced allelic variation in leucine-rich repeat copy number**. *Plant Cell* 1998, **10**:1915-1925.
71. Dixon MS, Jones DA, Keddie JS, Thomas CM, Harrison K, Jones JDG: **The tomato *Cf-2* disease resistance locus comprises two functional genes encoding leucine-rich repeat proteins**. *Cell* 1996, **84**:451-459.
72. Jones D, Thomas C, Hammond-Kosack K, Balint-Kurti P, Jones J: **Isolation of the tomato *Cf-9* gene for resistance to *Cladosporium fulvum* by transposon tagging**. *Science* 1994, **266**:789-793.
73. Kawchuk LM, Hachey J, Lynch DR, Kulcsar F, van Rooijen G, Waterer DR, Robertson A, Kokko E, Byers R, Howard RJ, et al.: **Tomato *Ve* disease resistance genes encode cell surface-like receptors**. *Proceedings of the National Academy of Sciences.* 2001, **98**:6511-6515.
74. Larkan NJ, Lydiate DJ, Parkin IAP, Nelson MN, Epp DJ, Cowling WA, Rimmer SR, Borhan MH: **The *Brassica napus* blackleg resistance gene *LepR3* encodes a receptor-like protein triggered by the *Leptosphaeria maculans* effector AVRLM1**. *New Phytologist.* 2013, **197**:595-605.
75. Larkan NJ, Ma L, Borhan MH: **The *Brassica napus* receptor-like protein RLM2 is encoded by a second allele of the *LepR3*/*Rlm2* blackleg resistance locus**. *Plant Biotechnology Journal.* 2015, **13**:983-992.

76. Takken FLW, Thomas CM, Joosten MHAJ, Golstein C, Westerink N, Hille J, Nijkamp HJJ, de Wit PJGM, Jones JDG: **A second gene at the tomato *Cf-4* locus confers resistance to *Cladosporium fulvum* through recognition of a novel avirulence determinant**. *The Plant Journal.* 1999, **20**:279-288.
77. Thomas CM, Jones DA, Parniske M, Harrison K, Balint-Kurti PJ, Hatzixanthis K, Jones JD: **Characterization of the tomato *Cf-4* gene for resistance to *Cladosporium fulvum* identifies sequences that determine recognitional specificity in Cf-4 and Cf-9**. *Plant Cell* 1997, **9**:2209-2224.
78. Wang Y, Xu Y, Sun Y, Wang H, Qi J, Wan B, Ye W, Lin Y, Shao Y, Dong S, et al.: **Leucine-rich repeat receptor-like gene screen reveals that *Nicotiana* RXEG1 regulates glycoside hydrolase 12 MAMP detection**. *Nature Communications.* 2018, **9**:594.
79. Catanzariti A-M, Lim GTT, Jones DA: **The tomato *I-3* gene: a novel gene for resistance to Fusarium wilt disease**. *New Phytologist.* 2015, **207**:106-118.
80. Larkan NJ, Ma L, Haddadi P, Buchwaldt M, Parkin IAP, Djavaheri M, Borhan MH: **The *Brassica napus* Wall-Associated Kinase-Like (WAKL) gene *Rlm9* provides race-specific blackleg resistance**. *bioRxiv* 2019:815845.
81. Saintenac C, Lee W-S, Cambon F, Rudd JJ, King RC, Marande W, Powers SJ, Bergès H, Phillips AL, Uauy C, et al.: **Wheat receptor-kinase-like protein Stb6 controls gene-for-gene resistance to fungal pathogen *Zymoseptoria tritici***. *Nature Genetics.* 2018, **50**:368-374.
82. Domazakis E, Lin X, Aguilera-Galvez C, Wouters D, Bijsterbosch G, Wolters PJ, Vleeshouwers VGAA: **Effectoromics-based identification of cell surface receptors in potato**. In *Plant Pattern Recognition Receptors: Methods and Protocols*. Edited by Shan L, He P: Springer New York; 2017:337-353.
83. Vleeshouwers VGAA, Oliver RP: **Effectors as tools in disease resistance breeding against biotrophic, hemibiotrophic, and necrotrophic plant pathogens**. *Molecular Plant-Microbe Interactions.* 2014, **27**:196-206.
84. Kettles GJ, Bayon C, Canning G, Rudd JJ, Kanyuka K: **Apoplastic recognition of multiple candidate effectors from the wheat pathogen *Zymoseptoria tritici* in the nonhost plant *Nicotiana benthamiana***. *New Phytologist.* 2017, **213**:338-350.
85. Luderer R, Takken FLW, Wit PJGMd, Joosten MHAJ: ***Cladosporium fulvum* overcomes Cf-2-mediated resistance by producing truncated AVR2 elicitor proteins**. *Molecular Microbiology.* 2002, **45**:875-884.
86. Joosten M, Cozijnsen T, de Wit P: **Host resistance to a fungal tomato pathogen lost by a single base-pair change in an avirulence gene**. *Nature* 1994, **367**:384-386.
87. Westerink N, Brandwagt B, de Wit P, Joosten M: ***Cladosporium fulvum* circumvents the second functional resistance gene homologue at the *Cf-4* locus (*Hcr9-4E*) by secretion of a stable avr4E isoform**. *Molecular Microbiology.* 2004, **54**:533-545.
88. Mesarich CH, Griffiths SA, van der Burgt A, Ökmen B, Beenen HG, Etalo DW, Joosten MHAJ, de Wit PJGM: **Transcriptome sequencing uncovers the *Avr5* avirulence gene of the tomato leaf mold pathogen *Cladosporium fulvum***. *Molecular Plant-Microbe Interactions.* 2014, **27**:846-857.
89. van Kan JA, van den Ackerveken G, de Wit P: **Cloning and characterization of cDNA of avirulence gene *avr9* of the fungal pathogen *Cladosporium fulvum*, causal agent of tomato leaf mold**. *Molecular Plant-Microbe Interactions.* 1991, **4**:52-59.
90. Kooman-Gersmann M, Honee G, Bonnema G, de Wit P: **A high-affinity binding site for the AVR9 peptide elicitor of *Cladosporium fulvum* is present on plasma membranes of tomato and other solanaceous plants**. *Plant Cell* 1996, **8**:929-938.

91. Luderer R, Rivas S, Nürnberger T, Mattei B, van den Hooven HW, van der Hoorn RAL, Romeis T, Wehrfritz J-M, Blume B, Nennstiel D, et al.: **No evidence for binding between resistance gene product Cf-9 of tomato and avirulence gene product AVR9 of *Cladosporium fulvum***. *Molecular Plant-Microbe Interactions.* 2001, **14**:867-876.
92. Houterman PM, Cornelissen BJC, Rep M: **Suppression of plant resistance gene-based immunity by a fungal effector**. *PLoS Pathogens.* 2008, **4**:e1000061.
93. Rep M, van der Does HC, Meijer M, van Wijk R, Houterman PM, Dekker HL, de Koster CG, Cornelissen BJC: **A small, cysteine-rich protein secreted by *Fusarium oxysporum* during colonization of xylem vessels is required for *I-3*-mediated resistance in tomato**. *Molecular Microbiology.* 2004, **53**:1373-1383.
94. Gout L, Fudal I, Kuhn M-L, Blaise F, Eckert M, Cattolico L, Balesdent M-H, Rouxel T: **Lost in the middle of nowhere: the *AvrLm1* avirulence gene of the Dothideomycete *Leptosphaeria maculans***. *Molecular Microbiology.* 2006, **60**:67-80.
95. Ghanbarnia K, Fudal I, Larkan NJ, Links MG, Balesdent M-H, Profotova B, Fernando WGD, Rouxel T, Borhan MH: **Rapid identification of the *Leptosphaeria maculans* avirulence gene *AvrLm2* using an intraspecific comparative genomics approach**. *Molecular Plant Pathology.* 2015, **16**:699-709.
96. Ghanbarnia K, Ma L, Larkan NJ, Haddadi P, Fernando WGD, Borhan MH: ***Leptosphaeria maculans* AvrLm9: a new player in the game of hide and seek with AvrLm4-7**. *Molecular Plant Pathology.* 2018, **19**:1754-1764.
97. Liu Z, Zhang Z, Faris JD, Oliver RP, Syme R, McDonald MC, McDonald BA, Solomon PS, Lu S, Shelver WL, et al.: **The cysteine rich necrotrophic effector SnTox1 produced by *Stagonospora nodorum* triggers susceptibility of wheat lines harboring *Snn1***. *PLoS Pathogens.* 2012, **8**:e1002467.
98. de Jonge R, Peter van Esse H, Maruthachalam K, Bolton MD, Santhanam P, Saber MK, Zhang Z, Usami T, Lievens B, Subbarao KV, et al.: **Tomato immune receptor Ve1 recognizes effector of multiple fungal pathogens uncovered by genome and RNA sequencing**. *Proceedings of the National Academy of Sciences.* 2012, **109**:5110-5115.
99. Zhong Z, Marcel TC, Hartmann FE, Ma X, Plissonneau C, Zala M, Ducasse A, Confais J, Compain J, Lapalu N, et al.: **A small secreted protein in *Zymoseptoria tritici* is responsible for avirulence on wheat cultivars carrying the *Stb6* resistance gene**. *New Phytologist.* 2017, **214**:619-631.
100. Oome S, Raaymakers TM, Cabral A, Samwel S, Böhm H, Albert I, Nürnberger T, van den Ackerveken G: **Nep1-like proteins from three kingdoms of life act as a microbe-associated molecular pattern in *Arabidopsis***. *Proceedings of the National Academy of Sciences.* 2014, **111**:16955-16960.

Chapter 3:

The *Venturia inaequalis* effector repertoire is expressed in waves and is dominated by expanded families with predicted structural similarity to avirulence proteins from other plant-pathogenic fungi

Mercedes Rocafort[1], Joanna K. Bowen[2], Berit Hassing[1], Murray P. Cox[3], Brogan McGreal[2], Silvia de la Rosa[1], Kim M. Plummer[4], Rosie E. Bradshaw[3] and Carl H. Mesarich[1,*]

[1]Laboratory of Molecular Plant Pathology/Bioprotection Aotearoa, School of Agriculture and Environment, Massey University, Private Bag 11222, Palmerston North 4442, New Zealand.

[2]The New Zealand Institute for Plant and Food Research Limited, Mount Albert Research Centre, Auckland 1025, New Zealand.

[3]Bioprotection Aotearoa, School of Natural Sciences, Massey University, Private Bag 11222, Palmerston North 4442, New Zealand.

[4]Department of Animal, Plant and Soil Sciences, La Trobe University, AgriBio, Centre for AgriBiosciences, La Trobe University, Bundoora, Victoria 3086, Australia.

[*]Corresponding author: Carl H. Mesarich (c.mesarich@massey.ac.nz).

A slightly modified version of this chapter was published in BMC Biology, 20, 246 (2022)

DOI: 10.1186/s12915-022-01442-9

1. Abstract

Background: Scab, caused by the biotrophic fungus *Venturia inaequalis*, is the most economically important disease of apples worldwide. During infection, *V. inaequalis* occupies the subcuticular environment, where it secretes virulence factors, termed effectors, to promote host-colonization. Consistent with other plant-pathogenic fungi, many of these effectors are expected to be non-enzymatic proteins, some of which can be recognized by corresponding host resistance proteins to activate plant defences, thus acting as avirulence determinants. To develop durable control strategies against scab, a better understanding of the roles that these effector proteins play in promoting subcuticular growth by *V. inaequalis*, as well as in activating, suppressing or circumventing resistance protein-mediated defences in apple, is required.

Results: We generated the first comprehensive RNA-seq transcriptome of *V. inaequalis* during colonization of apple. Analysis of this transcriptome revealed five temporal waves of gene expression that peaked during early, mid or mid-late infection. While the number of genes encoding secreted, non-enzymatic proteinaceous effector candidates (ECs) varied in each wave, most belonged to waves that peaked in expression during mid-late infection. Spectral clustering based on sequence similarity determined that the majority of ECs belonged to expanded protein families. To gain insights into function, the tertiary structures of ECs were predicted using AlphaFold2. Strikingly, despite an absence of sequence similarity, many ECs were predicted to have structural similarity to avirulence proteins from other plant-pathogenic fungi, including members of the MAX, LARS, ToxA and FOLD effector families. In addition, several other ECs, including an EC family with sequence similarity to the AvrLm6 avirulence effector from *Leptosphaeria maculans*, were predicted to adopt a KP6-like fold. Thus, proteins with a KP6-like fold represent another structural family of effectors shared among plant-pathogenic fungi.

Conclusions: Our study reveals the transcriptomic profile underpinning subcuticular growth by *V. inaequalis* and provides an enriched list of ECs that can be investigated for roles in virulence and avirulence. Furthermore, our study supports the idea that numerous sequence-unrelated effectors across plant-pathogenic fungi share common structural folds. In doing so, our study gives weight to the hypothesis that many fungal effectors evolved from ancestral genes through duplication, followed by sequence diversification, to produce sequence-unrelated but structurally similar proteins.

Keywords

Venturia inaequalis; apple scab fungus; biotrophic subcuticular pathogen; effectors and effector families; virulence and avirulence; RNA-seq transcriptome; AlphaFold2 protein tertiary structure predictions.

2. Introduction

Fungal pathogens are responsible for some of the most devastating diseases of crop plants worldwide, causing large economic losses, and threatening both food production and security [1]. Resistance to these pathogens is largely governed by the plant immune system, and is based on the recognition of invasion patterns (IPs) by plant immune receptors [2]. At the plant cell surface, many of these immune receptors are pattern recognition receptors (PRRs) of the receptor-like protein (RLP) or receptor-like kinase (RLK) classes, which recognize conserved IPs known as microbe-associated molecular patterns (MAMPs) [3]. Following the recognition of these MAMPs, plant defence responses that slow or halt growth of the fungal pathogen are initiated [3]. To circumvent or suppress these defence responses, plant-pathogenic fungi must secrete a collection of virulence factors, termed effectors, to the plant–pathogen interface, a subset of which may be taken up intracellularly. These effectors are predominantly non-enzymatic proteins, but can also be enzymes, secondary metabolites and small RNAs [4-7]. In some cases, however, effectors can be recognized as IPs by extracellular PRRs or intracellular nucleotide-binding leucine-rich repeat (NLR) immune receptors, collectively referred to as qualitative resistance (R) proteins, to activate plant defences [3,8]. Such effectors are termed avirulence (Avr) effectors because their recognition typically renders the fungal pathogen unable to cause disease.

Scab (or black spot), caused by *Venturia inaequalis*, is the most economically important disease of apple (*Malus* x *domestica*) worldwide [9,10]. Under favourable conditions, this disease can render the fruit unmarketable and cause a yield reduction of up to 70% [10]. During biotrophic host-colonization, *V. inaequalis* exclusively colonizes the subcuticular environment without penetrating the underlying plant epidermal cells [9,11,12]. It is here that the fungus develops specialized infection structures, known as stromata and runner hyphae [9,11]. Stromata give rise to asexual conidia, but are also likely required for nutrient acquisition and effector secretion

[9,11,13]. Runner hyphae, on the other hand, enable the fungus to radiate out from the initial site of host penetration, acting as a base from which additional stromata can be differentiated [11]. At the end of the season, in autumn, *V. inaequalis* switches to saprobic growth inside fallen leaves, where it undergoes sexual reproduction [9].

Scab disease is largely controlled through fungicides, which greatly accelerate the development of fungicide resistance in *V. inaequalis* [14,15]. Scab-resistant apple cultivars, developed through the incorporation of *R* genes, represent a more sustainable disease control option [16]. However, races of *V. inaequalis* that can overcome resistance in apple mediated by single *R* genes have been identified [16,17]. Therefore, it is likely that multiple 'unbroken' *R* genes, perhaps together with quantitative trait loci (QTL), will need to be stacked in each of these cultivars to provide durable disease resistance [16,17]. For this to be successful, prior knowledge of the molecular mechanisms used by the fungus to overcome *R* gene-mediated resistance, including an understanding of how these mechanisms impact effector function and pathogen fitness, will be required. So far, however, there have been no publications describing the cloning of *Avr* effector genes from *V. inaequalis.* Crucially, the genomes of multiple *V. inaequalis* isolates have been sequenced [18-23] and bioinformatic studies have identified a large catalogue of secreted, non-enzymatic proteinaceous effector candidates (ECs) from which candidate Avr effectors can be identified [19]. Most of these ECs belong to expanded (sequence-related) families [19]; however, the driving force behind the expansion of these families is not yet known. Nevertheless, many *EC* genes are located next to repetitive sequences in the genome of *V. inaequalis* and, therefore, it is possible that transposition is one of the mechanisms driving this expansion [19]. Examples where *EC* genes of *V. inaequalis* are located next to repetitive sequences include members of the *AvrLm6-like* family, which encode proteins with sequence similarity to AvrLm6 [13], an Avr effector from the fungal pathogen *Leptosphaeria maculans* (blackleg of canola) [24], as well as members of the

Ave1-like family [19], which encode proteins with sequence similarity to Ave1, an antimicrobial Avr effector from the fungal pathogen *Verticillium dahliae* (Verticillium wilt disease) [25,26].

To develop durable control strategies against scab disease, a better understanding of the roles that effectors play in promoting subcuticular growth by *V. inaequalis* is also required. To date, subcuticular growth has been largely understudied, even though it is exhibited by many plant-pathogenic fungi, including other crop-infecting members of the *Venturia* genus [11,27-29], as well as, for example, *Rhynchosporium* (scald disease of graminaceous plants) [30,31] and *Diplocarpon* (e.g. rose black spot) [32,33]. In recent years, host-colonization by plant-pathogenic fungi has been studied by transcriptomic analysis [34-36]. However, comprehensive transcriptomic studies focusing on the subcuticular parasitic strategy are not yet available. Indeed, while previous expression data from interactions between *V. inaequalis* and susceptible apple have been published [19,37], these data are only based on a limited number of infection time points with no biological replicates.

In this study, we provide the first comprehensive transcriptomic analysis of *V. inaequalis* during colonization of susceptible apple and identify infection-related temporal expression waves associated with *EC* genes of this fungus. Using recent advances in *de novo* protein folding algorithms, we also show that the EC repertoire of *V. inaequalis* is dominated by expanded families with predicted structural similarity to Avr proteins from other plant-pathogenic fungi. Collectively, this study furthers our understanding of subcuticular growth by *V. inaequalis* and provides an enriched list of ECs that can be investigated for potential roles in virulence and avirulence.

3. Results

3.1. The different stages of host infection by *V. inaequalis* observed by bright-field microscopy display distinct gene expression profiles

To investigate changes in *V. inaequalis* gene expression during host-colonization and relative to growth in culture, we set up an infection time course involving detached leaves of susceptible apple cultivar *M.* x *domestica* 'Royal Gala' and compared it to growth of the fungus on cellophane membranes overlying potato dextrose agar (PDA). Here, six *in planta* time points (12 and 24 hours post-inoculation [hpi], as well as 2, 3, 5 and 7 days post-inoculation [dpi]) and one in culture time point (7 dpi) were used.

Analysis of leaf material from the infection time course by bright-field microscopy revealed that, at 12 hpi, conidia of *V. inaequalis* had germinated and formed appressoria on the leaf surface (**Figure 3-1. A**). At 24 hpi, primary hyphae had developed, indicating that colonization of the subcuticular environment was underway. Then, by 2 and 3 dpi, stromata had differentiated from primary hyphae and, in many cases, these stromata had undergone a rapid expansion in size through non-polar division (**Figure 3-1. A**). Subcuticular runner hyphae had also started to radiate out from stromata (**Figure 3-1. A**). By 5 dpi, fungal biomass had accumulated extensively in the subcuticular environment and additional stromata had started to develop from runner hyphae (**Figure 3-1. A).** Often, these stromata had formed conidiophores, from which conidia had developed (**Figure 3-1. A**). Finally, at 7 dpi, conidia of *V. inaequalis* had started to rupture through the plant cuticle (**Figure 3-1. A**) and the first macroscopic olive-brown lesions, indicative of heavy sporulation, were apparent. This represented the end of the biotrophic infection stage, as detached apple leaves had started to decay after this time point.

Inspection of the RNA-seq data revealed that the percentage of reads mapping to the *V. inaequalis* genome [19] increased as the infection time course progressed (**Figure 3-1. B**,

Appendix A-Additional file 1: Table A 3-1). Furthermore, the biological replicates clustered robustly within time points and a clear distinction between the early and mid-late infection stages, as well as between the *in planta* and in culture growth conditions, was observed (**Figure 3-1. C**).

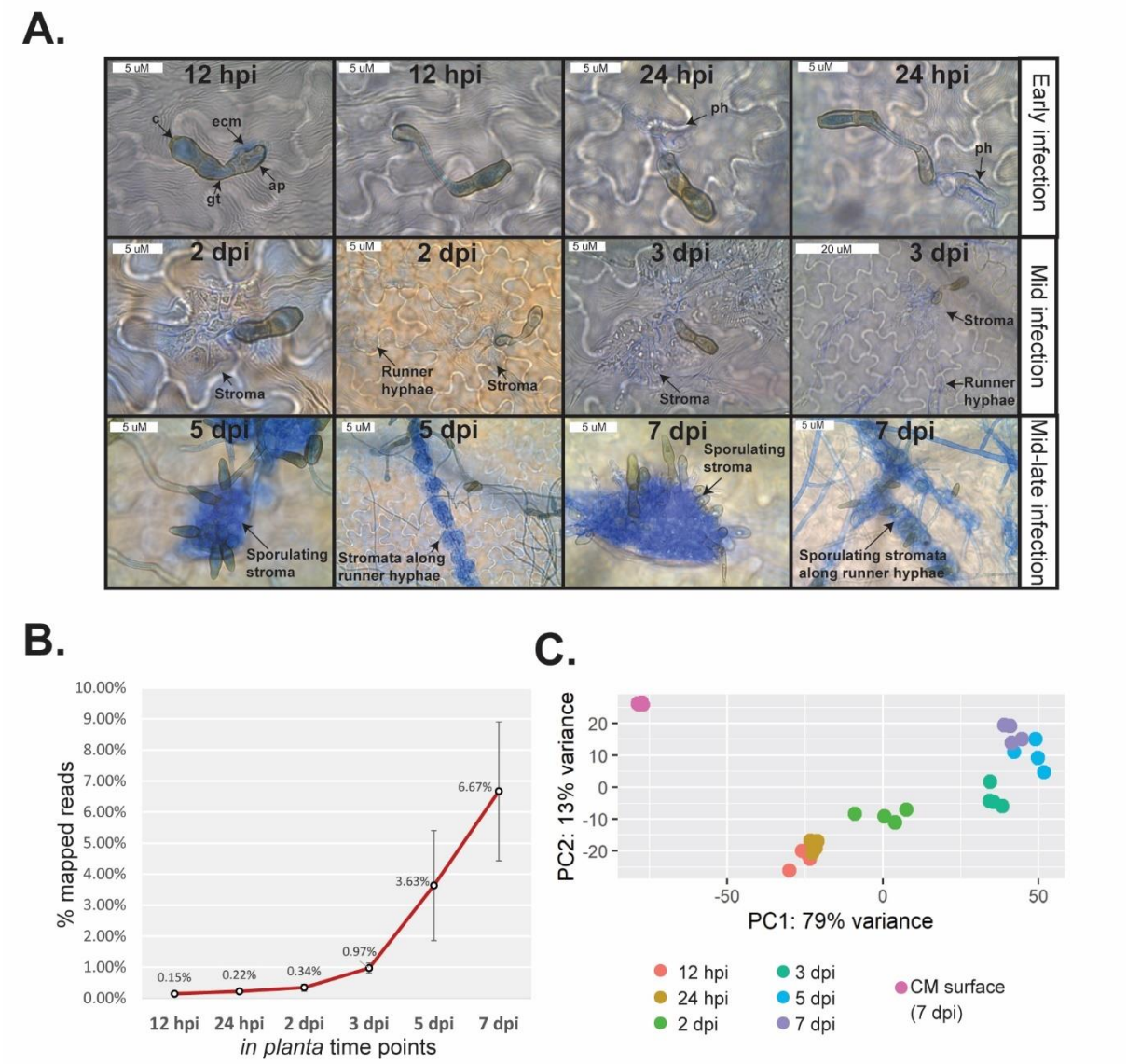

Figure 3-1. Microscopic and transcriptomic profile of *Venturia inaequalis* during infection of detached leaves from susceptible apple cultivar 'Royal Gala'. A. Microscopic evaluation of *V. inaequalis* during colonization of apple leaves. Infection structures observed by bright-field microscopy were stained with aniline blue. Infected leaves are representative of material used in the RNA-seq transcriptome sequencing experiment. c, conidium; gt, germ tube; ap, appressorium; ecm: extracellular matrix; ph: primary hyphae. **B.** Percentage (%) of paired RNA-seq reads mapped to the *V. inaequalis* genome relative to the total RNA-seq reads sequenced. Error bars represent standard deviation across four biological replicates. **C.** Principal component analysis (PCA) of RNA-seq data from *V. inaequalis* during colonization of apple leaves and in culture on the surface of cellophane membranes (CMs) overlaying potato dextrose agar. Four biological replicates per time point are shown. hpi: hours post-inoculation; dpi: days post-inoculation.

3.2. Genes of *V. inaequalis* are expressed in temporal waves during infection of apple leaves

We set out to identify which genes of *V. inaequalis* are up-regulated during infection of apple, when compared to growth in culture, as these genes are most likely to be required for promoting host-colonization. For this purpose, we updated the current gene catalogue for isolate MNH120 [19] to increase the total number of annotated genes, including those that encode ECs, which are notoriously difficult to predict in fungi (**Appendix A-Additional file 2: Figure A 3-1**). In total, 24,502 genes, excluding splice variants, were predicted and, of these, 3,563 were up-regulated and 1,462 were down-regulated at one or more *in planta* time points (*p* value of 0.01 and $\log_2$-fold change of 1.5) (**Appendix A-Additional file 3**). It must be pointed out here that our approach was used to predict as many genes as possible and, consequently, it is expected that some spurious genes were included in the annotation. However, as many of these spurious genes were anticipated to show a negligible level of expression, most would not have featured in our list of differentially expressed genes, which formed the central focus of our study. For example, of the 24,502 predicted genes, 9,284 had a maximum DESeq2-normalized gene expression count across growth conditions of <1, indicating that they were neither expressed under the conditions tested nor up-regulated *in planta*.

The total set of *in planta* up-regulated genes was used to identify temporal host infection-specific gene expression clusters, henceforth referred to as waves. Here, all expression data were scaled across all samples (Z-score) to visualize the gene expression deviation from the overall mean. For hierarchical clustering, the parameters were set to specifically identify the minimum number of waves for which a distinct gene expression profile could be observed (**Figure 3-2**). In total, five distinct gene expression waves (**Figure 3-2. A**), representing three separate infection stages (**Figure 3-2. B**), were identified. More specifically, genes of waves 1 and 2 peaked in

expression during early infection at 12 hpi, with expression largely plateauing (wave 1) or trending downwards (wave 2) throughout the remaining infection time points (**Figure 3-2**). Wave 3 contained genes that peaked in expression during mid infection at 2 dpi (**Figure 3-2**). Genes of wave 4 displayed their lowest level of expression at 12 and 24 hpi, with expression strongly increasing through 2 and 3 dpi, peaking at 5 dpi during mid-late infection (**Figure 3-2**). Finally, for genes of wave 5, a similar profile was observed to genes of wave 4, but with expression strongly increasing from 3 dpi and peaking during mid-late infection at 7 dpi (**Figure 3-2**).

To determine which biological processes are overrepresented in the five temporal gene expression waves, gene ontology (GO) (**Figure 3-2. B**) and protein family (Pfam) enrichment (**Appendix A-Additional file 4**) analyses were performed. Genes from waves 1 and 2 were mostly characterized by GO terms associated with high metabolic activity, responses to oxidative stress and cutinase activity. Here, cutinases of carbohydrate esterase family 5 (CE5) were abundant (**Appendix A-Additional file 5: Figure A 3-2**). In contrast, genes of wave 3 were mostly characterized by GO terms associated with transmembrane transport (**Figure 3-2. B**). Finally, genes of waves 4 and 5 were mostly characterized by GO terms associated with carbohydrate metabolism and transcription (**Figure 3-2. B**). In wave 4, for example, a GO enrichment for polygalacturonase activity was observed. This, together with the more general enrichment for carbohydrate metabolism, was supported by the high number of plant cell wall-degrading enzyme (PCWDE)-encoding genes in wave 4, most of which were predicted to encode polygalacturonase enzymes of glycoside hydrolase family 28 (GH28) (**Appendix A-Additional file 5: Figure A 3-2**). A more detailed analysis of the general fungal biology and transporters expressed in each temporal expression wave can be found in **Appendix B**.

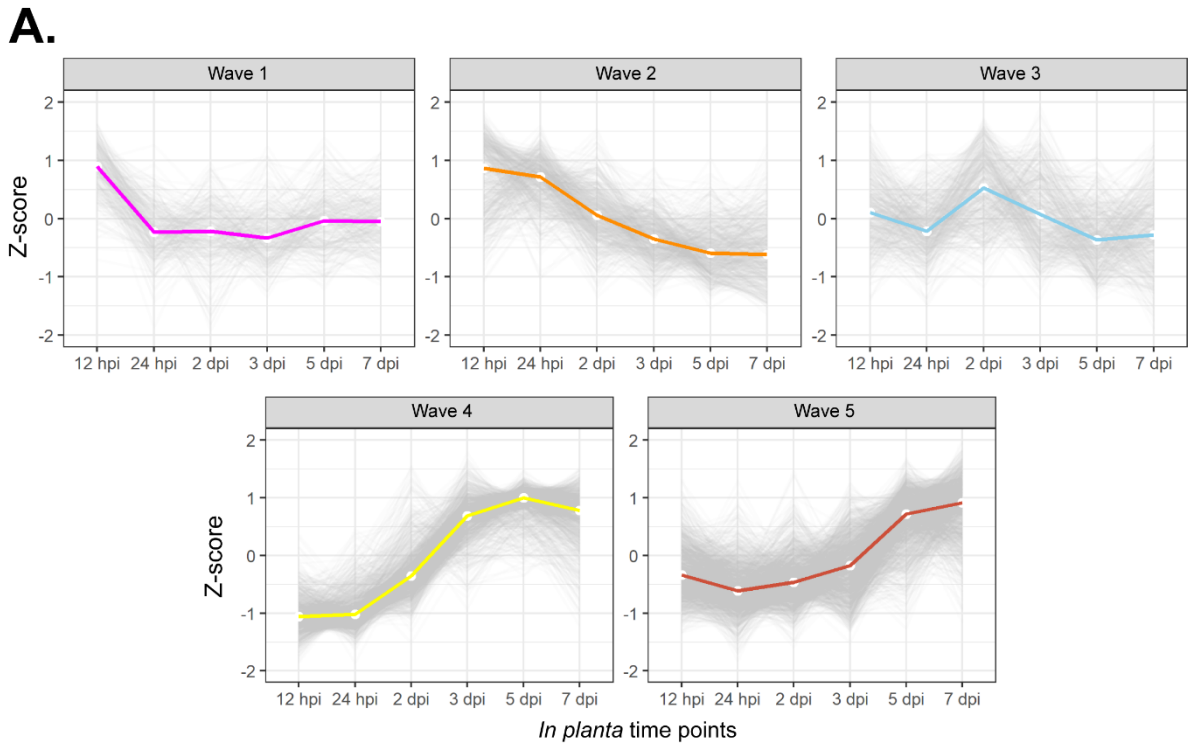
A.
Wave 1
Wave 2
Wave 3
Wave 4
Wave 5
Z-score
12 hpi 24 hpi 2 dpi 3 dpi 5 dpi 7 dpi
In planta time points

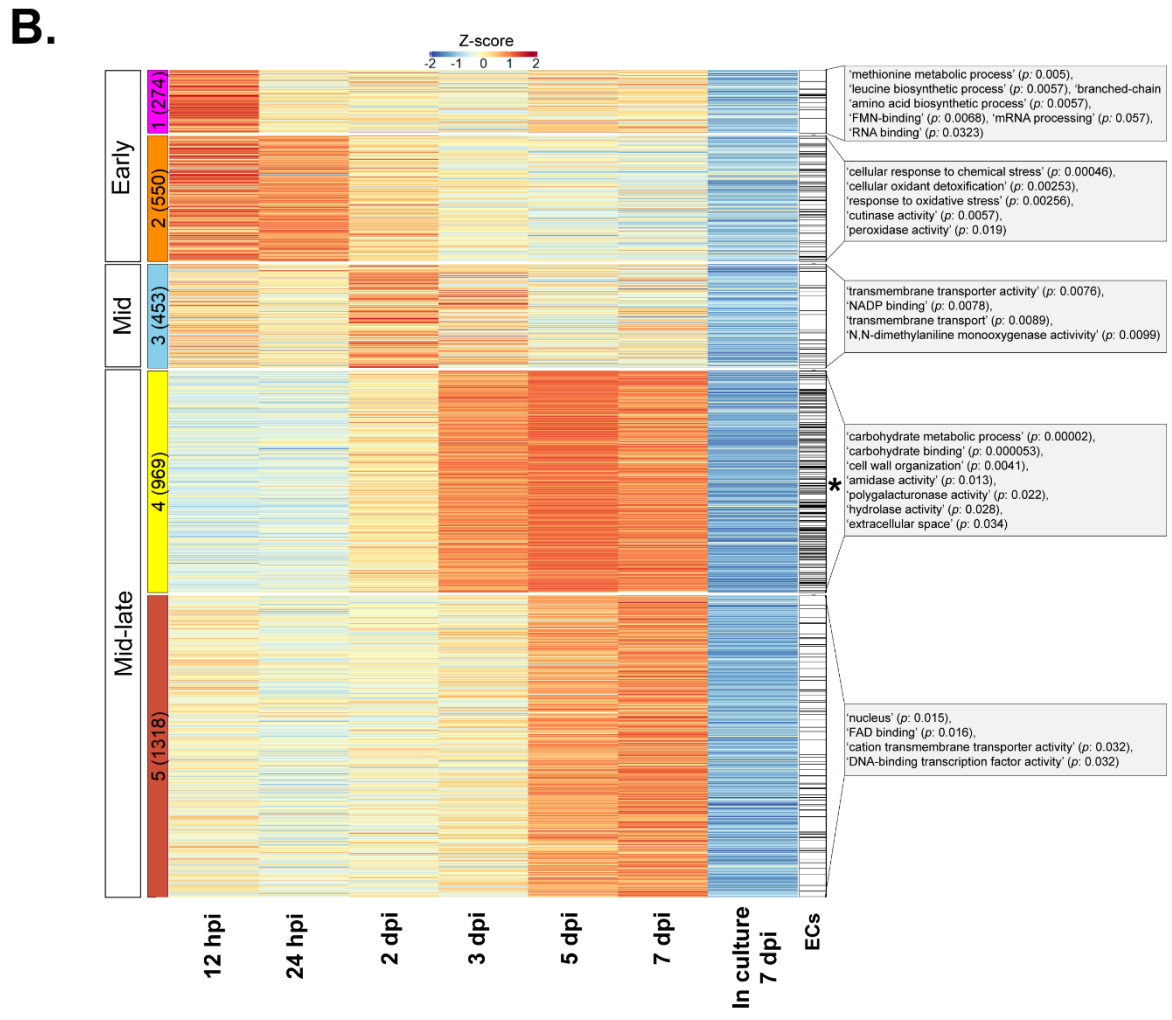
B.
Z-score
-2 -1 0 1 2
Early
Mid
Mid-late
1 (274)
2 (550)
3 (453)
4 (969)
5 (1318)
'methionine metabolic process' (p: 0.005), 'leucine biosynthetic process' (p: 0.0057), 'branched-chain 'amino acid biosynthetic process' (p: 0.0057), 'FMN-binding' (p: 0.0068), 'mRNA processing' (p: 0.057), 'RNA binding' (p: 0.0323)
'cellular response to chemical stress' (p: 0.00046), 'cellular oxidant detoxification' (p: 0.00253), 'response to oxidative stress' (p: 0.00256), 'cutinase activity' (p: 0.0057), 'peroxidase activity' (p: 0.019)
'transmembrane transporter activity' (p: 0.0076), 'NADP binding' (p: 0.0078), 'transmembrane transport' (p: 0.0089), 'N,N-dimethylaniline monooxygenase activivity' (p: 0.0099)
'carbohydrate metabolic process' (p: 0.00002), 'carbohydrate binding' (p: 0.000053), 'cell wall organization' (p: 0.0041), 'amidase activity' (p: 0.013), 'polygalacturonase activity' (p: 0.022), 'hydrolase activity' (p: 0.028), 'extracellular space' (p: 0.034)
*
'nucleus' (p: 0.015), 'FAD binding' (p: 0.016), 'cation transmembrane transporter activity' (p: 0.032), 'DNA-binding transcription factor activity' (p: 0.032)
12 hpi
24 hpi
2 dpi
3 dpi
5 dpi
7 dpi
In culture 7 dpi
ECs

Figure 3-2. Genes of *Venturia inaequalis* up-regulated during infection of susceptible apple cultivar 'Royal Gala', relative to growth of the fungus in culture on the surface of cellophane membranes overlying potato dextrose agar, belong to one of five distinct temporal waves of expression. A. Expression profile of the five distinct temporal expression waves at 12 and 24 hours post-inoculation (hpi), as well as 2, 3, 5 and 7 days post-inoculation (dpi), relative to growth in culture (7 dpi). **B.** Heatmap of all *V. inaequalis* genes up-regulated *in planta* when compared with growth in culture. Gene expression data are scaled rlog-normalized counts across all samples (Z-score), averaged from four biological replicates. Genes up-regulated *in planta* were clustered using hclust according to the Ward.D2 and Euclidean distance methods. Early (12 and 24 hpi), mid (2 and 3 dpi) and mid-late infection (5 and 7 dpi) refer to the stage of infection where peak gene expression was observed. Coloured block labels on the left indicate gene expression waves. Numbers in brackets indicate number of genes per wave. The black asterisk indicates the wave significantly enriched for genes encoding effector candidates (ECs) (*p* value: 3.644e-14). Grey boxes indicate enriched gene ontology (GO) terms. *p*: *p* value.

3.3. Genes encoding non-enzymatic proteinaceous effector candidates of *V. inaequalis* predominantly demonstrate peak expression during the mid-late infection stage of apple

From the 24,502 predicted genes of *V. inaequalis*, 1,955 genes were predicted to encode a secreted protein without a transmembrane domain and, of these, 1,369 were predicted to encode a non-enzymatic effector candidate (EC). Here, only small, secreted proteins of ≤400 amino acid residues in length, as well as larger secreted proteins with an effector prediction by EffectorP v3.0, were considered to be ECs (**Appendix A-Additional file 6: Figure A 3-3. A**). Of the 1,369 EC proteins, 518 were identical to proteins predicted by Deng et al. [19] (**Appendix A-Additional file 6: Figure A 3-3.B**). Sequence similarities within our predicted set of ECs were investigated using BLASTp, with the ECs then grouped into families using spectral clustering. Based on this analysis, 759 of the ECs were grouped into 118 families ranging in size from two to 75 members. Of these, 32 families were expanded with five or more members. Due to the observed similarity in sequence between family members, and the fact that expanded families had previously been predicted by Deng et al. [19], we do not expect the gene models encoding these ECs to be spurious. In contrast to the 759 ECs mentioned above, 610 of the ECs were predicted to be singletons that did not belong

to any family (**Appendix A-Additional file 7**). Interestingly, ~22% of the ECs that belonged to families were encoded by genes that either clustered together or were located in close proximity to each other (i.e. within 10 genes) in the genome of isolate MNH120 (**Appendix A-Additional file 7**).

Based on the differential gene expression analysis presented above, 686 of the 1,369 predicted *EC* genes from *V. inaequalis* were up-regulated *in planta*. To determine when these genes peaked in expression, their expression profile across the five temporal waves during host-colonization was investigated. In total, ~20% of the up-regulated genes peaked in expression during early infection, ~9% during mid infection, and ~71% during mid-late infection (**Figure 3-3**). In all cases, families made up the majority of ECs in each wave (**Figure 3-3**). Most of the *EC* genes that peaked in expression during early infection (121) encoded proteins that lacked predicted functional domains. Exceptions included: (1) a family that encoded proteins with an 'Egh16-like virulence factor' domain (PF11327) and had sequence similarity to the appressorium-specific Gas1 effector from the rice blast fungus *Magnaporthe oryzae* [38], hereafter named the Gas1-like family, (2) a family that encoded proteins with a 'stress-up regulated Nod19' domain (PF07712), hereafter named the Nod19 family, (3) a family that encoded proteins with a 'hydrophobic surface-binding protein A' (HsbA) domain (PF12296), hereafter named the HsbA family, and (4) a family that encoded proteins with a 'common fold in several fungal extracellular membrane proteins' (CFEM) domain (PF05730) [39], hereafter named the CFEM family.

While the *HsbA* and *CFEM* families possessed genes that mostly peaked in expression during early host-colonization (**Figure 3-3**), each of these families also had a smaller number of genes that peaked in expression during waves 4 and 5 of mid-late infection (**Appendix A-Additional file 8: Figure A 3-4**). Given that *HsbA* and *cutinase* genes have been shown to be regulated by the same transcription factor in *Aspergillus nidulans* [40,41], and that most *cutinase* and *HsbA* genes of *V. inaequalis* peaked in expression during wave 2 of the early infection stage

(**Figure 3-3, Appendix A-Additional file 5: Figure A 3-2**), we set out to determine whether the *cutinase* and *HsbA* genes of *V. inaequalis* were co-expressed. Based on the Pearson correlation coefficient, which was calculated between the *cutinases* and *HsbA* gene expression profiles during the early infection stage, the *cutinase* and *HsbA* genes were indeed found to be co-expressed ($R > 0.8$, $p < 0.01$). Another family with members exhibiting different expression profiles during host-colonization was the *Cin1* family (**Appendix A-Additional file 8: Figure A 3-4**), which is specific to the *Venturia* genus [42]. This family contains the *Cin1* gene (*g8385*), which encodes a cysteine-rich protein with eight repeats, and two *Cin1-like* genes, *Cin1-like 1* (*g10529*) and *Cin1-like 2* (*g13013*), which encode smaller proteins with only one repeat. *Cin1* peaked in expression during wave 4, and was the most highly expressed gene during mid-late host-colonization. In contrast, the *Cin1-like* genes peaked in expression during wave 2 of early infection (**Appendix A-Additional file 8: Figure A 3-4**).

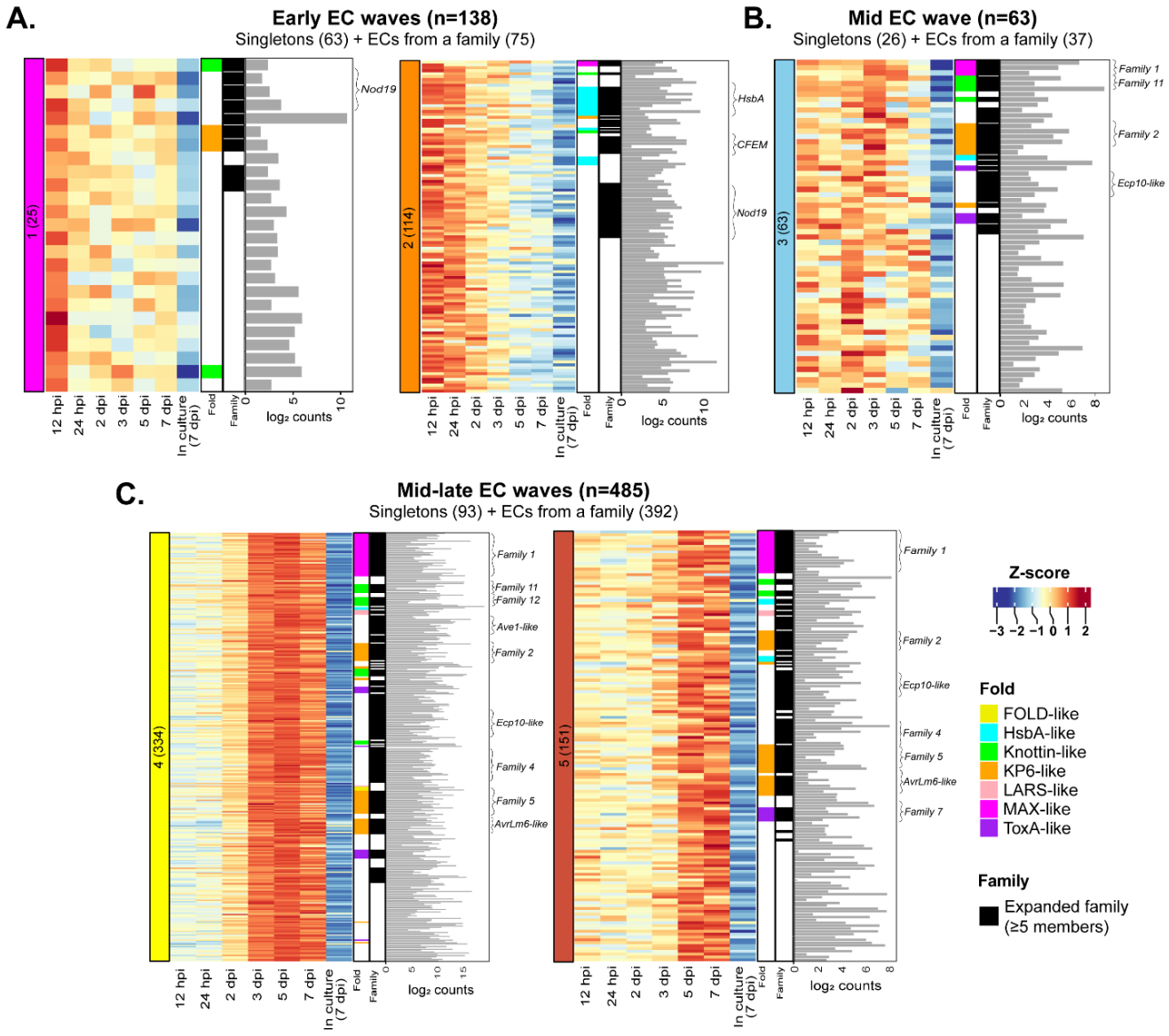

Figure 3-3. Genes encoding secreted, non-enzymatic proteinaceous effector candidates (ECs) of *Venturia inaequalis* are expressed in temporal waves during colonization of susceptible apple cultivar 'Royal Gala'. A. Heatmap of genes demonstrating peak expression during waves 1 and 2 of the early infection stage at 12 and 24 hours post-inoculation (hpi). **B.** Heatmap of genes demonstrating peak expression during wave 3 of the mid infection stage at 2 and 3 days post-inoculation (dpi). **C.** Heatmap of genes demonstrating peak expression during waves 4 and 5 of the mid-late infection stage at 5 and 7 dpi. Heatmap gene expression data are scaled rlog-normalized counts across all samples (Z-score). Bar plots depict the maximum $\log_2$ DESeq2-normalized count value across all *in planta* time points. Black annotations indicate genes encoding proteins that belong to an expanded EC family (≥5 members), with brackets highlighting large families and families with sequence similarity to avirulence (Avr) effector proteins from other plant-pathogenic fungi. CM: cellophane membrane.

The mid and mid-late waves were characterized by 513 genes that mostly encoded EC proteins without a functional domain. The main exception was for members of the Ave1-like family [19], which had an 'RlpA-like domain superfamily annotation (IPR036908). Notably, most of the expanded *EC* families that encoded proteins with sequence similarity to effectors or Avr effectors from other plant-pathogenic fungi, such as the *AvrLm6-like* [13] and *Ave1-like* [19] families, displayed a peak level of expression during waves 4 and 5 (**Figure 3-3, Appendix A-Additional file 9: Table A 3-2**). Other examples included the *Ecp10-like* family, which encoded proteins with sequence similarity to the Ecp10-1 Avr candidate from the tomato leaf mold fungus *Fulvia fulva* (formerly *Cladosporium fulvum*), as well as the *Ecp39-like* family, which encoded proteins with sequence similarity to the *F. fulva* EC Ecp39 [43]. An *Ecp6-like* gene (singleton), which encoded a protein with sequence similarity to the Ecp6 effector from *F. fulva* [19,44], also peaked in expression during wave 4. Interestingly, most expanded *EC* families that peaked in expression during waves 4 and 5 encoded proteins that lacked sequence similarity to other proteins. Examples included the most expanded *EC* family in *V. inaequalis*, family 1 (**Figure 3-4**), as well members from family 2 (**Appendix A-Additional file 15: Figure A 3-7**). In most cases, only one or a few family members were very highly expressed during host-colonization (**Figure 3-4**).

Finally, as it known that some fungal effectors are cyclic ribosomally-synthesized and post-translationally modified peptides (RiPPs) called dikaritins [45], and that dikaritin precursor peptides are often mistaken for standard secretory proteins, we set out to determine whether any of our 1,369 ECs were in fact dikaritin precursor peptides. A hallmark of dikaritin precursor peptides is an amino (N)-terminal signal peptide followed by multiple perfect or imperfect tandem repeats [46]. As the genes encoding these precursor peptides form part of a biosynthetic gene cluster that also includes a gene encoding a DUF3328 protein, we screened the *V. inaequalis* genome for *DUF3328* genes (and thus, dikaritin gene clusters) to determine which ECs could be dikaritins. In total, nine *dikaritin* gene clusters were identified, with each cluster containing one or

more *dikaritin* precursor genes. Based on this analysis, ten of the ECs were identified as putative dikaritin precursor peptides and, of these, four were encoded by genes that peaked in expression during mid-late infection (waves 4 and 5) (**Appendix A- Additional file 10: Figure A 3-5**). The most highly expressed dikaritin precursor gene (*g7830*, from the dikaritin-2 cluster) corresponded to the previously identified gene *Cin3*, which was formerly considered to encode a repeat-containing EC protein [11,19].

3.4. Several expanded effector candidate families of *V. inaequalis* have predicted structural similarity to Avr effector proteins from other plant-pathogenic fungi

To gain insights into the putative function of ECs, we predicted their tertiary structures using AlphaFold2 [47], and then investigated these structures for similarity to proteins of characterized tertiary structure (and in some cases, function) using the Dali server [48]. This analysis was specifically performed on the most highly expressed member from each EC family (referred to as the representative family member), as well as each singleton, expressed during the temporal host infection-specific waves. In total, the tertiary structure was confidently predicted for the representative family member of 71 (~76%) EC families and 118 (~65%) EC singletons (**Appendix A-Additional file 11**).

Strikingly, many EC families were predicted to be structurally similar to one or more ECs or Avr effector proteins with solved tertiary structures from other plant-pathogenic fungi (**Figure 3-4, Appendix A-Additional file 12: Table A 3-3**, **Appendix A-Additional file 13: Figure A 3-6**). More specifically, 12 EC families were predicted to be structurally analogous to ECs or Avr effector proteins (**Appendix A-Additional file 12: Table A 3-3**). Remarkably, many of these families were among the most expanded families in *V. inaequalis*. In contrast to the families, only three EC singletons had predicted structural similarity to ECs or Avr effector proteins from other plant-pathogenic fungi (**Appendix A-Additional file 12: Table A 3-3**).

The representative member of the most expanded EC family in *V. inaequalis*, family 1, was confidently predicted to adopt a six-stranded β-sandwich fold with structural similarity to seven '*Magnaporthe* Avr and ToxB-like' (MAX) effectors. The identified MAX effectors were the recently described MAX effector 6R5J [49] and the Avr effectors AvrPiz-t [50], Avr-Pia [51,52], Avr-Pib [53], Avr1-CO39 [51] and Avr-Pik [54] from *M. oryzae*, as well as the host-selective toxin effector ToxB from *Pyrenophora tritici-repentis* [55], the fungal pathogen responsible for tan spot of wheat (**Appendix A-Additional file 12: Table A 3-3**). A sequence alignment constructed from all family 1 members of *V. inaequalis*, as well as the identified MAX effectors from *M. oryzae*, revealed that these proteins lacked significant sequence similarity, with a maximum pairwise identity of only 13.9% observed between g13386 and Avr1-CO39 (**Appendix A-Additional file 14**). However, these sequence-diverse proteins did share the characteristic conserved disulphide bond between β1 and β5 that has previously been reported for MAX effectors [51] (**Figure 3-4. A**).

Similarly, two expanded families, families 7 and 28, as well as family 38 and a singleton, were predicted to share a common β-sandwich fold with structural similarity to the host-selective toxin effector ToxA from *P. tritici-repentis* [56], the Avr effector Avr2/Six3 from the wilt fungus *Fusarium oxysporum* [57,58], and the AvrL567 (AvrL567-A and/or AvrL567-D) Avr effectors from the flax rust fungus *Melampsora lini* [59,60] (**Figure 3-4. A, Appendix A-Additional file 12: Table A 3-3, Appendix A-Additional file 13: Figure A 3-6**). Notably, despite sharing an overall β-sandwich fold with similar topology, these proteins were very diverse at the amino acid level, with a maximum sequence identity of 12.7% (**Appendix A-Additional file 14**). All of the ToxA-like families had a different number of β-sheets (**Appendix A-Additional file 13: Figure A 3-6**).

Another two families, families 15 and 47, were predicted to have structural similarity to the AvrLm4-7 and AvrLm5-9 Avr effectors from *L. maculans*, as well as the Ecp11-1 Avr

candidate from *F. fulva* [61,62] (**Figure 3-4. A, Appendix A-Additional file 12: Table A 3-3, Appendix A-Additional file 13: Figure A 3-6**), which belong to the '*Leptosphaeria* AviRulence-Supressing (LARS)' structural effector family [62]. The *V. inaequalis* LARS-like effectors had the same predicted topology as AvrLm4-7 but with a variable number of β-sheets. At the amino acid level, the identified *V. inaequalis* LARS-like proteins shared only 7.8–16.9% sequence identity with AvrLm4-7, AvrLm5-9 and Ecp11-1 (**Appendix A-Additional file 14**). Interestingly, the *V. inaequalis* structures were predicted to be stabilized by a different number of disulfide bonds and lacked both the conserved disulfide bridge between the α-helix and β-strand, as well as the conserved WR(F/L/V)(R/K) motif, previously reported for the LARS effectors [62].

Finally, family 49 was predicted to adopt a two-domain fold similar to the Avr1/Six4 and Avr3/Six1 Avr effectors from *F. oxysporum* (**Figure 3-4. A, Appendix A-Additional file 12: Table A 3-3**), which are the founding members of the recently identified *Fol* dual-domain (FOLD) structural family of effectors [63]. Despite the *V. inaequalis* FOLD-like family representative sharing only 17.6% amino acid identity with Avr1/Six4 (**Appendix A-Additional file 14**), the cysteine spacing pattern was conserved.

Interestingly, many expanded EC families had a KP6-like fold similar to the KP6 protein of the P6 virus from the corn smut fungus *Ustilago maydis* (**Appendix A-Additional file 15: Figure A 3-7**) [64,65] and the Zt-KP6-1 EC from wheat blotch fungus *Zymoseptoria tritici* [66]. This included the AvrLm6-like family, families 2, 5, 23, and 26, as well as two singletons (**Appendix A-Additional file 15: Figure A 3-7**). All KP6-like proteins were predicted to have between two and four disulphide bridges, two α-helices and a variable number of β-sheets (**Figure 3-4. B, Appendix A-Additional file 15: Figure A 3-7**).

Unfortunately, many other EC proteins from *V. inaequalis* were too small to be included in RCSB PDB searches (or did not have a significant hit) using the Dali server. To gain further insights into their function, we investigated their general SCOPe fold classification and identified

three families and one singleton that were predicted to adopt a knottin-like fold (**Appendix A-Additional file 11**). The most highly expressed member of family 11 (**Appendix A-Additional file 16: Figure A 3-8**) and a singleton were predicted to adopt a knottin-like fold with two β-sheets and three disulfide bonds that form an intramolecular knot (**Appendix A-Additional file 16: Figure A 3-8**). Additionally, families 12, 24, and 35 were predicted to adopt a knottin-like fold using the SCOPe database [67] (**Appendix A-Additional file 16: Figure A 3-8**). However, these proteins were not predicted to have a true intramolecular knot characteristic of knottin proteins based on our current AlphaFold2 predictions. Instead, these proteins shared a common fold with cysteine-stabilized αβ defensins, which are made up of a single α-helix and three β-strands.

In addition to these knottin-like proteins, the Ecp10-like family, along with the candidate Avr effector Ecp10-1 from *F. fulva* [43], were predicted to adopt a small compact β-folded structure that is structurally similar to the PAF protein from *Penicillium chrysogenum* (**Appendix A-Additional file 17: Figure A 3-9**) [68-70]. Furthermore, the Ecp39-like family, along with the Ecp39 EC from *F. fulva* [43], were predicted to adopt a crambin-like fold (**Appendix A-Additional file 17: Figure A 3-9**). Unlike that observed for the Ecp10-like family, no analogous protein structures were identified for the Ecp39-like family in the RCSB PDB using the Dali server. Lastly, the Ave1-like family, together with the Ave1 Avr effector from *V. dahliae* [19,25], were predicted to adopt a double-psi β-barrel fold, stabilized by two conserved disulfide bonds, with high similarity to expansins (**Appendix A-Additional file 17: Figure A 3-9**).

Lastly, we investigated whether a relationship existed between the predicted fold types of EC proteins and the expression profiles of genes that encoded them. Consistent with the results mentioned above, ECs with a predicted HsbA-like fold were predominantly encoded by genes that peaked in expression during wave 2 of early infection (**Figure 3-3**). In contrast, ECs with structural similarity to ECs and Avr effector proteins from other plant-pathogenic fungi predominantly peaked in expression during mid and mid-late infection (**Figure 3-3**). Remarkably, all members of

the FOLD-like and LARS-like families peaked in expression during mid-late infection (wave 4 and wave 5). Similarly, the majority of members from the MAX-like (65%), ToxA-like (70%), KP6-like (~59%) and knottin-like (~66%) families peaked in expression during wave 4.

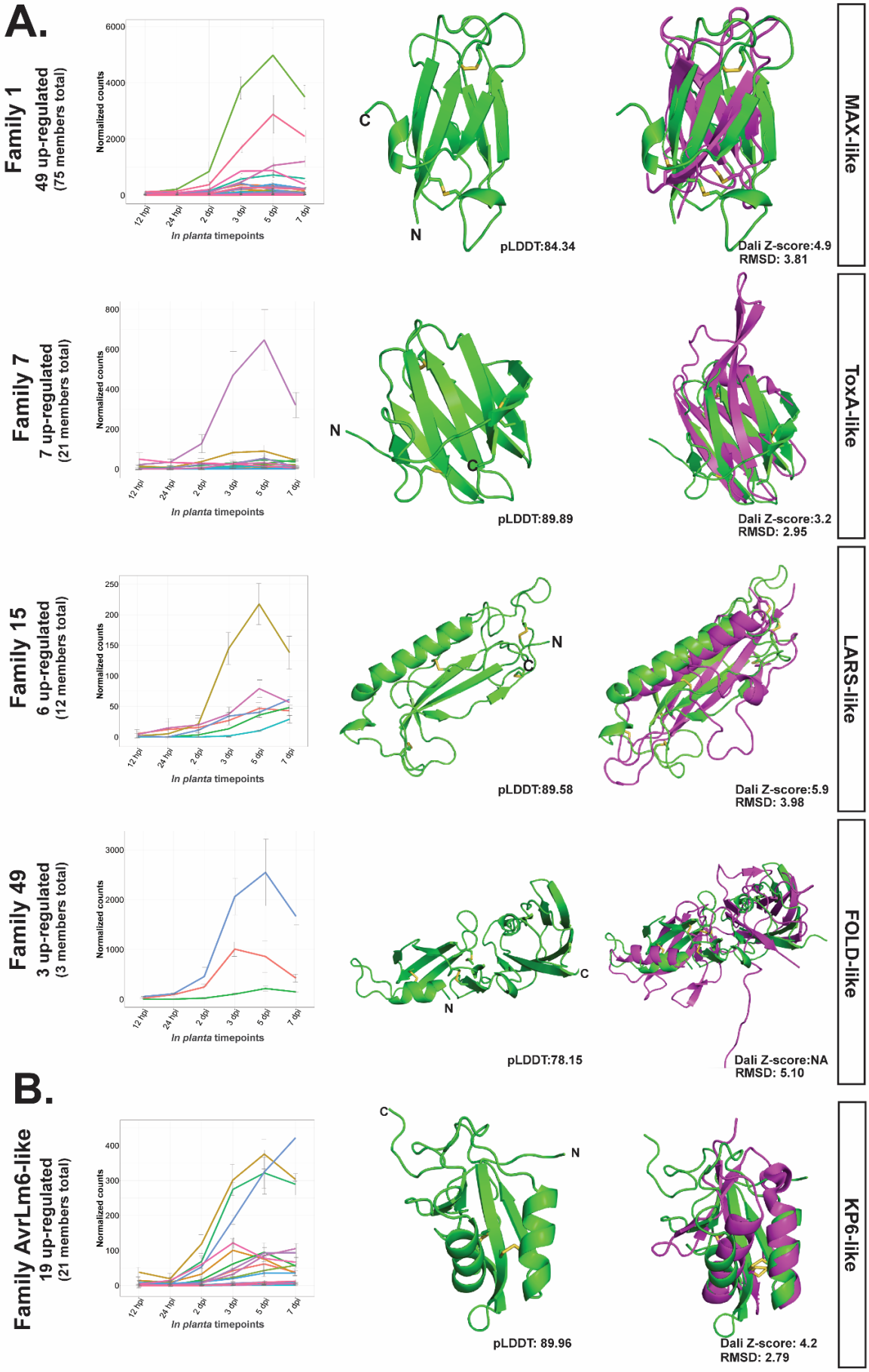
A.
Family 1
49 up-regulated
(75 members total)
Normalized counts
In planta timepoints
12 hpi
24 hpi
2 dpi
3 dpi
5 dpi
7 dpi
pLDDT:84.34
Dali Z-score:4.9
RMSD: 3.81
MAX-like
Family 7
7 up-regulated
(21 members total)
pLDDT:89.89
Dali Z-score:3.2
RMSD: 2.95
ToxA-like
Family 15
6 up-regulated
(12 members total)
pLDDT:89.58
Dali Z-score:5.9
RMSD: 3.98
LARS-like
Family 49
3 up-regulated
(3 members total)
pLDDT:78.15
Dali Z-score:NA
RMSD: 5.10
FOLD-like
B.
Family AvrLm6-like
19 up-regulated
(21 members total)
pLDDT: 89.96
Dali Z-score: 4.2
RMSD: 2.79
KP6-like

Figure 3-4. Predicted tertiary structures of secreted non-enzymatic proteinaceous effector candidates (ECs) from *Venturia inaequalis*. A. Representative EC family members with structural similarity to avirulence (Avr) effector proteins from other plant-pathogenic fungi. MAX-like: representative predicted family 1 protein structure (green; g13386) aligned to an uncharacterized MAX effector from *Magnaporthe oryzae* (6R5J) (purple). ToxA-like: representative predicted family 7 (green; g4781) protein structure aligned to ToxA from *Pyrenophora tritici-repentis* (1ZLE) (purple). LARS-like: representative predicted family 15 (green; g11097) protein structure aligned to AvrLm4-7 from *Leptosphaeria maculans* (7FPR) (purple). FOLD-like: representative predicted family 49 (green; g3787) protein structure aligned to Avr1/Six4 from *Fusarium oxysporum* (7T6A) (purple). **B**. Predicted EC family members with a KP6-like fold. KP6-like: representative predicted AvrLm6-like family (green; g20030) protein structure aligned to EC Zt-KP6-1 from *Zymoseptoria tritici* (6QPK). Expression data of up-regulated *EC* genes during colonization of susceptible apple cultivar 'Royal Gala' are DESeq2-normalized counts, averaged from four biological replicates, with error bars representing standard deviation (hpi: hours post-inoculation; dpi: days post-inoculation). Protein structures predicted by AlphaFold2 represent the most highly expressed member of each EC family from *V. inaequalis*. Disulfide bonds coloured in yellow. N: amino (N) terminus; C: carboxyl (C) terminus. pLDDT: predicted Local Distance Difference Test score (0–100). A pLDDT score of 70–100 is indicative of medium to high confidence. A Dali Z-score above 2 indicates 'significant similarities' between proteins. RMSD: root-mean-square deviation. The protein structure of Avr1/Six4 was not present in the Dali database at the time of writing this manuscript and therefore no Dali Z-score is shown.

4. Discussion

In this study, we present the first comprehensive transcriptome of *V. inaequalis* during colonization of apple, covering six biotrophic time points from early to late infection. In doing so, we have, to our knowledge, also provided the first comprehensive *in planta* transcriptome of a subcuticular fungal pathogen. Based on this transcriptome, we identified five temporal host infection-specific waves of gene expression for *in planta*-upregulated genes of *V. inaequalis*. Here, genes demonstrated peak expression during one of three stages of host-colonization corresponding to early (12 and 24 hpi; waves 1 and 2), mid (2 and 3 dpi; wave 3) and mid-late (5 and 7 dpi; waves 4 and 5) infection. These temporal gene expression waves were biologically distinct from each other and were enriched for different GO terms.

A key focus of our study was to understand the expression profile of *EC* genes that encode secreted, non-enzymatic proteins during host-colonization, as these genes make up the bulk of effectors identified from plant-pathogenic fungi to date [4,71]. Interestingly, during early host-colonization, when *V. inaequalis* is either growing on the leaf surface or has just initiated subcuticular growth, only around 20% of the up-regulated *EC* genes peaked in expression. In other plant-pathogenic fungi, however, the percentage of *EC* genes that peak in expression during early host-colonization is much higher. For instance, in *U. maydis*, ~40% of genes encoding secreted proteins were found to be specifically induced during early host-colonization [34]. One possible reason for this difference could be that, during the early infection stage, *V. inaequalis* predominantly colonizes the epicuticular wax above apple epidermal cells, perhaps on its way to colonizing the subcuticular environment. This may suggest that not all infections have yet resulted in close contact with the underlying epidermal cells and, consequently, the mass upregulation of genes encoding effector proteins with roles in suppressing host defences has not yet been initiated.

Among the *EC* genes that peaked in expression during early colonization, several belonged to the *HsbA* family. HsbA proteins have been suggested to recruit cutinases to hydrophobic

surfaces [41] and, in *A. nidulans*, *HsbA* and *cutinase* genes are co-regulated by the same transcription factor [40,41]. Consistent with this previous research, we observed that some *HsbA* and *cutinase* genes of *V. inaequalis* were co-expressed, suggesting that, as previously hypothesized, the HsbA proteins of *V. inaequalis* may recruit cutinases to facilitate the degradation and digestion of the hydrophobic apple cuticle during early host infection [19,41,72]. In line with this observation, early infection was enriched for the GO term 'cutinase activity' and many CE cutinase-encoding genes were up-regulated. Altogether, these observations support previous reports showing that localized enzymatic hydrolysis is needed for penetration of the apple cuticle by *V. inaequalis* to facilitate access to the subcuticular environment [9,73].

Other *EC* genes that peaked in expression during early host-colonization included members of the *Gas1-like* family, which encode proteins with a 'Egh16-like virulence factor' domain, and members of the *Nod19* family, which encode proteins with a 'stress up-regulated Nod19' domain. Recently, Gas1-like proteins have been shown to form part of the widely distributed fungal 'effectors with chitinase activity' (EWCA) family [74]. EWCA proteins are secreted chitinases without a characterized enzymatic domain in the CAZyme database that degrade immunogenic chitin fragments to prevent chitin-triggered immunity in plants [74]. Thus, it is tempting to speculate that members of the Gas1-like family from *V. inaequalis* play a similar role upon access to the subcuticular environment. The function of proteins with a stress up-regulated Nod19 domain is currently unknown. However, it has been suggested that these proteins are associated with responses to abiotic and biotic stress [75-78]. Based on these studies and the expression of the *Nod19* genes during early infection, the Nod19 family from *V. inaequalis* could play a role in modulating oxidative stress during early subcuticular colonization of apple. A more detailed analysis and efforts to functionally characterize this Nod19 EC family can be found in Appendix C. Crucially, other genes associated with oxidative stress tolerance, such as those encoding

peroxidases, were also enriched during early infection, suggesting that modulation of oxidative stress is crucial for early host-colonization by *V. inaequalis*.

Like the *HsbA* family, most members of the *CFEM* family peaked in expression during early host-colonization. The CFEM domain is found in several fungal proteins, including those of plant pathogens [79], where it has been shown to confer a diverse range of functions ranging from the promotion or suppression of plant cell death and chlorosis [80-82] to the development of appressoria [83]. Consistent with this functional diversity, and because some members of the CFEM family from *V. inaequalis* instead demonstrated a peak level of expression during mid-late infection, it is likely that the CFEM proteins also play a diverse range of roles in *V. inaequalis* during colonization of apple.

The mid infection stage, which was characterized by the large-scale expansion and continued differentiation of subcuticular infection structures (i.e. stromata and runner hyphae), was enriched for GO terms associated with transmembrane transport. Interestingly, while many *EC* genes of *V. inaequalis* were highly expressed during this mid infection stage, very few displayed their peak level of expression here. This may suggest that the expression of most *EC* genes is still increasing during mid infection. However, it is important to point out that the mid infection wave was not well defined, overlapping partially with the mid-late infection waves. This is presumably due to the asynchronous nature of *V. inaequalis* infection.

Finally, during the mid-late infection stage, when *V. inaequalis* is heavily colonizing the subcuticular space, most *EC* genes peaked in expression. Based on this expression profile, and the fact that their expression steadily ramped up from the onset of the infection process, we believe that these genes likely play a key role in the establishment and maintenance of biotrophy. Intriguingly, many genes encoding GH enzymes associated with the degradation of the plant cell wall, such as pectin-degrading GH28 proteins, also peaked in expression during this infection stage. As nutrients in the subcuticular environment are likely to be scarce throughout host-

colonization, it is anticipated that *V. inaequalis* meets a portion of its nutritional requirements through the degradation of the pectin-rich layer located between the cuticle and epidermal cells of apple using these enzymes [84]. Related to this, it is well known that fungal GH28 enzymes can be recognized as MAMPs, while host cell wall fragments released as a consequence of GH28 hydrolytic activity can be recognized as damaged-associated molecular patterns (DAMPs) by PRRs, to activate the plant immune system [7]. With this in mind, a subset of the ECs encoded by genes that peaked in expression during mid-late infection may function to suppress plant defences responses initiated by these GH28 enzymes.

Remarkably, many of the *EC* genes that peaked in expression during mid-late infection encoded proteins that belonged to expanded families. Such a phenomenon, where ECs are known to form part of expanded families, has also been observed in other lineage-specific pathogens, including *Blumeria graminis* [85,86]. Although the relevance of EC family expansion to *V. inaequalis* is not yet well understood, it is anticipated that this expansion facilitates the diversification of effector function and enables the avoidance of recognition by cognate host R proteins [19]. In any case, repetitive elements are expected to play a major role in the expansion process, enabling both *EC* gene duplication and subsequent transposition to other regions of the *V. inaequalis* genome [87,88]. In line with this, it has previously been shown that *ECs* of *V. inaequalis*, including members of the *Ave1-like* and *AvrLm6-like EC* families, tend to be closely associated with repetitive elements [13,19]. Moreover, some *EC* genes belonging to the same expanded families have been shown to cluster together in the *V. inaequalis* genome (this study), indicating that tandem duplication events might have occurred. To provide further insights into the process of *EC* family expansion in *V. inaequalis*, a chromosome-level genome assembly of this fungus is now required as, due to its highly fragmented nature (1,012 scaffolds) [19], the current Illumina genome provides an incomplete picture of repeat composition and gene clusters.

To gain insights into the function of EC proteins from *V. inaequalis*, we used the *de novo* folding algorithm AlphaFold2 to predict their tertiary structures, as AlphaFold2 has been successfully benchmarked against effectors of characterized tertiary structure from other plant-pathogenic fungi [63,89]. One of the main limitations when using AlphaFold2 is that proteins with a low number of homologous sequences in public databases normally result in predictions with low confidence scores. In an attempt to overcome this, we generated custom multiple sequence alignments (MSAs) that included the amino acid sequences of all EC family members identified in this study, many of which were not available in public sequence databases, which greatly improved prediction scores (**Appendix A-Additional file 18: Figure A 3-10**).

Strikingly, many of the EC families, especially the expanded EC families, demonstrated predicted structural similarity to Avr effector proteins from other plant-pathogenic fungi. The biggest of these was the MAX-like family, which had predicted structural similarity to one of the largest effector/EC families from *M. oryzae*, the MAX family [90,91]. Intriguingly, a recent computational study of secreted proteins from multiple plant pathogens based on AlphaFold2 concluded that the MAX fold was almost exclusive to *M. oryzae*, with a few members of this family also found in the vanilla black spot fungus *Colletotrichum orchidophilum* [91]. However, here we show that the MAX-like family has undergone massive expansion and diversification in *V. inaequalis*, highlighting the need for more comprehensive sampling of fungal species using AlphaFold2 to better understand the evolutionary origin and distribution of the MAX structural fold.

In *M. oryzae*, Avrs of the MAX effector family are translocated into host cells, where they are recognized by NLR R proteins [50,53,92-95]. Of these, Avr-PikD and Avr1-CO39 directly interact with their corresponding NLR R proteins; an interaction mediated through a heavy metal-associated (HMA) domain that is integrated into the R protein itself. Similarly, the MAX effector Avr-Pik binds and stabilizes an independent HMA protein to modulate host immunity [96].

Altogether, these studies suggest that the MAX fold could be well suited to interactions with HMA domains [97,98]. It is therefore tempting to speculate that ECs of the MAX-like family from *V. inaequalis* are translocated into host cells, where they interact with HMA domain-containing proteins of apple. Certainly, as Rvi15, an R protein of apple that recognizes the AvrRvi15 Avr effector of *V. inaequalis*, is an NLR [99], it seems likely that a subset of Avrs from this fungus are translocated into host cells.

EC families and singletons with predicted structural similarity to ECs and Avr proteins from the ToxA-like family were also identified in *V. inaequalis*. Interestingly, like that observed in *V. inaequalis*, the recent computational study by Seong and Krasileva [91] showed that ToxA-like ECs are greatly expanded in the cereal stem rust fungus *Puccinia graminis*. The same study also showed that a further four species, *F. oxysporum, C. orchidophilum, V. dahliae*, and *U. maydis*, have members of this family [91]. However, in the case of these four species, only a few members of the ToxA family could be identified. Thus, *V. inaequalis* appears to have one of the largest repertoires of ToxA-like ECs in fungal species investigated to date.

Like the MAX family, some members of the ToxA-like family (Avr2/Six3 and AvrL567) are translocated into plant cells, where they perform their virulence functions and are recognized by their corresponding R proteins [57,100,101]. For example, Avr2/Six3 of *F. oxysporum* functions together with another effector, Six5, to facilitate the cell-to-cell movement of effectors by increasing the size exclusion limit of plasmodesmata [102]. Other members, however, are thought to be apoplastic. For instance, an ortholog of ToxA from the wheat blotch fungus *Parastagonospora nodorum* interacts with an integral membrane protein of wheat from the apoplast to facilitate a cell death reaction that involves the intracellular protein, Tsn1 [103]. As all ToxA-like effectors functionally characterized to date display different virulence functions, no insights into the possible function of ToxA-like proteins from *V. inaequalis* can be made. However, as the Rvi6 R protein of apple, which recognizes the AvrRvi6 Avr effector protein of *V. inaequalis*,

is an RLP [104], it is possible that these or other ECs of this fungus identified in our study could be recognised as Avr determinants in the subcuticular environment.

Two other structural EC families in *V. inaequalis* were the LARS-like family [62] and the two-domain FOLD-like family [63]. Of note, only one small EC family of *V. inaequalis* was predicted to adopt the FOLD-like fold. However, it must be pointed out that proteins with this fold are known to be difficult to predict [90] and, as a consequence, some members may have been missed. Interestingly, while the precise functions of the LARS and FOLD effector families are currently unknown, both contain members that suppress the host immune response related to the recognition of another member. More specifically, in terms of the LARS family, AvrLm4-7 suppresses immune responses triggered by AvrLm3 and AvrLm5-9 [105,106], while for the FOLD family, Avr1/Six4 suppresses immune responses triggered by Avr3/Six1 [107]. Together, this suggests that these protein structures may play a role in molecular mimicry to prevent detection [62,63,108]. It will be interesting to determine whether similar relationships are observed for the LARS-like and FOLD-like ECs of *V. inaequalis*.

Aside from the folds described above, an intriguing observation was that many of the EC families and singletons from *V. inaequalis* were predicted to adopt a KP6-like or knottin-like fold. The KP6 fold was first described in the antifungal KP6 protein from the P6 virus from *U. maydis* [64,65] and, in our study, was predicted to be adopted by the AvrLm6-like family as well as AvrLm6 Avr effector protein from *L. maculans*. Notably, this fold is known to be adopted by the EC Zt-KP6-1 (6QPK) from *Z. tritici* [66] and has also been predicted to be adopted by many effectors such as the Avr effector AvrLm10 from *L. maculans* [90,109], the BAS4 effector from *M. oryzae* [90,110], the Ecp28 EC family and Ecp29 EC from *F. fulva* [43], and the CbNip1 necrosis-inducing effector from the sugar beet leaf spot fungus *Cercospora beticola* [111]. Even more interesting, as observed in *V. inaequalis*, the KP6-like fold has been predicted to be the most abundant fold in the *M. oryzae* secretome [90,91] and is widely shared among phytopathogens

[91]. Altogether, this suggests that this KP6-like fold is a widely conserved structural family of effectors in different phytopathogens.

In terms of ECs from *V. inaequalis* that had a predicted knottin-like fold, several families and a singleton were identified. Knottins are small, ultra-stable proteins with at least three disulfide bridges that form an intramolecular knot known to provide stability in hostile conditions such as the plant apoplast [112]. Current evidence suggests that multiple fungal effectors adopt this fold. Indeed, the Avr effector Avr9 from *F. fulva* has previously been suggested to adopt a knottin fold, based on NMR [113] and cysteine bond connectivity data [114]. Furthermore, an EC from the poplar rust fungus *Melampsora larici-populina*, MLP124266, which is a homolog of the AvrPm4 Avr effector from *M. lini*, was recently shown to adopt this fold [115]. Other knottin-like families identified in our study appear to adopt a fold resembling defensins, similar to the VdAMP3 effector of *V. dahliae*, which has antifungal activity and facilitates microsclerotia formation [116].

Curiously, the Ecp39-like EC family from *V. inaequalis*, along with the Ecp39 EC from *F. fulva*, were predicted to adopt a crambin fold, which is commonly found in antimicrobial proteins [117], while the Ecp10-like family from *V. inaequalis*, together with the Ecp10-1 Avr candidate from *F. fulva*, were predicted to adopt a fold with similarity to the antimicrobial PAF protein from *P. chrysogenum* [68-70]. The large number of proteins from *V. inaequalis* that are predicted to have structural (KP6-like, knottin-like, Ecp39-like and Ecp10-like) or sequence (Ave1-like) similarity to antimicrobial proteins suggests that a considerable proportion of the ECs from this fungus may be dedicated to antagonistic fungus–microbe interactions to ward off microbial competitors.

It should be noted that as part of our EC prediction pipeline, we also identified four putative dikaritin RiPP precursor peptides that were encoded by genes displaying a peak level of expression during late infection. Dikaritins are a class of cyclic bioactive peptides that have recently been discovered in fungi [118] and have been hypothesized to play a role as effectors in promoting host-

colonization [71]. In line with this, Victorin, a host-selective dikaritin toxin from the necrotrophic oat blight fungus *Cochliobolus victoriae*, has been shown to be essential for pathogenicity in oat cultivars resistant to the biotrophic crown rust fungus *Puccinia coronata* [45]. The late-expression profile of the *V. inaequalis* dikaritins, together with the finding that many RiPPs from plants have potent antimicrobial activity [71,119], may suggest that these peptides, perhaps in addition to some of the ECs described above, promote host-colonization through the eradication of microbial competitors in preparation for saprobic growth inside fallen leaf litter.

Taken together, our study on *V. inaequalis*, along with previous studies on effector proteins from *M. oryzae*, *F. oxysporum* and other fungi [51,62,63,90,91], reinforces the idea that many sequence-diverse fungal effectors share common structural folds. This provides weight to the hypothesis that many fungal effector proteins have in fact originated from ancestral folds and suggests that the genes encoding these effectors have evolved through duplication, followed by sequence diversification, to encode sequence-unrelated but structurally similar proteins. Under this hypothesis, the effector proteins have evolved rapidly to a point where almost all sequence similarity, with the exception of residues involved in the maintenance of the overall structural fold, has been lost [51]. It is of course possible, however, that the appearance of common folds, at least in some instances, could be the result of convergent evolution, whereby certain similar folds have evolved independently in different fungi [51].

Specific protein folds may be common across fungal effector proteins as they provide a stable structural scaffold on which surface or loop features can be altered to enable functional diversification [108]. For those Avr effectors that are directly recognized by their corresponding R proteins, it may also be possible that these alterations extend to the evasion of host recognition. Another possibility is that particular structural folds are well suited to certain functions or to interactions with specific host components [108]. Most likely, though, both above-mentioned scenarios are possible [108]. Future research focussing on the finer details of the distribution of

structural effector families among both pathogenic and non-pathogenic fungi, and on the functional characterization of members within these families, will shed more light on this intriguing topic.

5. Conclusions

In conclusion, we have performed the first comprehensive gene expression analysis of a subcuticular pathogen, with a specific focus on genes encoding non-enzymatic proteinaceous ECs, during host-colonization. In doing so, our study provides valuable new insights into the molecular mechanisms underpinning subcuticular host-colonization by this largely understudied class of fungi, including *V. inaequalis*. Notably, in conjunction with structural modelling, we have also provided an enriched list of ECs from which effectors and Avr effectors of *V. inaequalis* can be identified and functionally characterized. Such a resource is desperately needed as, to date, there have been no publications reporting the cloning of *Avr* effector genes from this fungus. Once identified, these *Avr* effector genes will enable the real-time detection of resistance-breaking strains in the orchard. Should Avr effectors of *V. inaequalis* belong to expanded protein families, it may then be possible to engineer their cognate R proteins to recognize features common to the structural fold (direct recognition) or to monitor specific host components targeted by multiple members of the Avr family (indirect recognition). Certainly, with the recent development of CRISPR-Cas9 technology in *V. inaequalis* [120], the functional characterization of ECs, and in particular those that form part of expanded EC families, is now possible. Finally, our study has provided further evidence that many sequence-diverse fungal effectors share common structural folds. Given that the genomes of many other *Venturia* species have now been sequenced [19,22,121-127], it will be interesting to determine whether specific effector folds are associated with subcuticular growth or the infection of specific host species.

6. Materials and methods

6.1. *V. inaequalis* isolates

V. inaequalis isolate MNH120, also known as ICMP 13258 and Vi1 [19,128], was used for all bright-field microscopy, transcriptome sequencing, gene predictions and AlphaFold2 protein structure predictions in this study. MNH120 is a race (1) isolate, meaning that it can only overcome resistance mediated by the *Rvi1* gene in apple [19]. This is presumably due to a mutated, absent, or non-expressed copy of the corresponding *AvrRvi1* gene (a functional copy of which is rare among isolates of *V. inaequalis* [129]). MNH120 is, however, anticipated to possess a functional copy of all other known *V. inaequalis Avr* effector genes (*AvrRvi2–20*), corresponding to all other known apple *R* genes (*Rvi2–20*) [19]. Gene predictions from *V. inaequalis* isolate 05/172 [21], which is of unknown race status [130], were used to assist the gene predictions in isolate MNH120.

6.2. Growth in culture for RNA sequencing

V. inaequalis isolate MNH120 was grown as a lawn culture from conidia on cellophane membranes (Waugh Rubber Bands, Wellington, New Zealand) [131] overlaying PDA (Difco™, NJ, USA) at 20°C for 7 days under white fluorescent lights (4,300 K) with a 16 h light/8 h dark photoperiod. Four culture plates, representing four independent biological replicates, were then flooded with 1 ml sterile distilled water and the fungal biomass was scraped from the membrane surface using a cell spreader. Following this step, fungal suspensions were transferred to independent microcentrifuge tubes, pelleted by centrifugation at 21,000 x g for 1 min, snap frozen in liquid nitrogen, and then ground to a powder in preparation for RNA extraction. The 7 dpi time point was chosen because *V. inaequalis* had produced enough biomass on the surface of cellophane membranes for adequate RNA extraction.

6.3. Plant infection assays for RNA sequencing and microscopy

Seeds from open-pollinated *M.* x *domestica* cultivar 'Royal Gala' (Hawke's Bay, New Zealand), which is a cultivar susceptible to scab disease caused by *V. inaequalis*, were germinated at 4°C in moist vermiculite with 100 mg/ml Thiram fungicide (Kiwicare Corporation Limited; Christchurch, New Zealand) for approximately two months in the dark. Germinated seedlings were planted in potting mix (Daltons^{TM} premium potting mix; Daltons, Matamata, New Zealand) and grown under a 16 h light/8 h dark cycle with a Philips SON-T AGRO 400 Sodium lamp, at 20°C with ambient humidity. Inoculations with *V. inaequalis* isolate MNH120 were performed on freshly un-furled detached leaves from 4- to 6-week old apple seedlings, as described previously [132], with the exception that 5 µl droplets of conidial suspension (1×10^5 ml^{-1}) were used to cover the entire leaf surface. At 12 and 24 hpi, as well as 2, 3, 5 and 7 dpi, four infected leaves, each from an independent seedling, were sampled to give four biological replicates. A microscopic evaluation of infection was then performed on harvested tips from these leaves. Here, leaf tips were cleared and stained according to a previously established protocol [133] and then visualised by bright-field microscopy, with images captured using a Leica DFC 295 digital camera and the Leica Application Suite X (LAS X). Immediately following tip harvesting, leaves were snap frozen in liquid nitrogen and then ground to a powder in preparation for RNA extraction.

6.4. RNA extraction and sequencing

Total RNA was extracted from samples of *V. inaequalis* isolate MNH120 grown in culture, as well as infected leaves, using a Spectrum™ Plant Total RNA Kit (Sigma-Aldrich, St. Louis, MO, USA), with DNA subsequently removed using DNase I (Invitrogen^{TM}, Thermo Fisher Scientific, MA, USA). RNA concentration and purity were quantified using a Nanodrop ND-1000 Spectrophotometer (NanoDrop Technologies, Rockland, DE, USA), while RNA integrity was

assessed on the Agilent 2100 Bioanalyser (Agilent Technologies, Waldbronn, Germany) using an Agilent RNA 6000 Nano Kit in conjunction with Agilent 2100 Bioanalyzer software. Genomic DNA contamination was excluded by visualisation of RNA on a 0.8% agarose gel and absence of polymerase chain reaction (PCR) amplification products specific to the *actin* gene of apple (GenBank Accession OU745002.1 [location 20,713,063–20,714,807]; primers RE45 [5´–TGACCGAATGAGCAAGGAAATTACT–3´] and RE64 [5´–TACTCAGCTTTGGCAATCCACATC–3´]) [11,134]. Following these quality control checks, total RNA from each of the samples was sequenced on a HiSeq X platform at Novogene (Beijing, China) via the Massey Genome Service facility (Palmerston North, New Zealand; project number MGS00286). Here, only those RNA samples with an RNA Integrity Number (RIN) value of ≥3.5 were sequenced.

6.5. Gene prediction

The genome sequence of *V. inaequalis* isolate MNH120 [19] was downloaded from the Joint Genome Institute (JGI) MycoCosm portal (https://mycocosm.jgi.doe.gov/Venin1/Venin1.home.html) and a new gene catalogue was predicted to accommodate those genes that may have been missed in the initial annotation by Deng et al. [19] (summarized in **Additional file 2: Figure A 3-1**). Here, we combined three sources of information to generate a more complete gene catalogue. More specifically, for the first source of information, the complete set of predicted genes (coding sequences; CDSs) for *V. inaequalis* isolate 05/172 was downloaded from the National Center for Biotechnology Information (NCBI; https://www.ncbi.nlm.nih.gov/nuccore/QFBF00000000.1/) and mapped to the MNH120 genome using GMAP v2021-02-22 [135] to generate a genome annotation file. Isolate 05/172 was used as the source of information for homology-based gene prediction, as it was deemed to have a more complete set of predicted *EC* genes than the previously predicted gene catalogue for isolate

MNH120 [19], based on a crude assessment of how many EC family members were present in the non-redundant (nr) protein database using a tBLASTn search. For the second source of information, we used the RNA-seq data generated from isolate MNH120 in this study to predict open reading frames (ORFs), and thus CDSs, from transcript sequences. More specifically, high quality RNA-seq reads (see the RNA-seq read analysis section below) from one biological replicate of each time point of *V. inaequalis* grown *in planta* and in culture were mapped to the MNH120 genome using HISAT2 v2.2.1 [136,137], with unmapped reads filtered out using SAMtools v9.2.0 [138]. Then, a genome-guided *de novo* transcriptome assembly was performed with the mapped reads using Trinity v2.12.0 [139]. Likely CDSs were identified using Transdecoder v5.5.0 (https://github.com/TransDecoder/TransDecoder), a program that predicts genes from transcript sequences, in conjunction with a minimum ORF length of 50 amino acids. To support gene predictions, a Pfam domain search was performed to ensure that translated ORFs with one or more characterized functional domains were retained. Additionally, to capture as many EC-encoding ORFs as possible, translated ORFs were scanned against a list of EC proteins identified in the previous gene annotation by Deng et al. [19], supplemented with an in-house database of putative MNH120 effector proteins (de la Rosa and Mesarich, unpublished). Here, a BLASTp e-value threshold of ≤0.05 was employed, with proteins identified using this analysis retained as likely CDSs. Finally, for the third source of information, the original gene catalogue predicted for isolate MNH120 by Deng et al. [19] was downloaded from the JGI MycoCosm portal as above. Together, the three sets of CDSs, derived from the three sources of information described above, were then loaded onto the MHN120 genome as different tracks in Geneious v9.05 [140], and manual curation was performed to create an updated gene catalogue based on a consensus prediction for each gene. More specifically, predictions that were identical across at least two of the three sets of CDSs for a given gene were accepted as correct. Likewise, if for a given gene predictions were different across all CDSs, only the CDS supported by mapped RNA-seq reads

(intron–exon boundaries) was selected. Finally, when a CDS was only predicted with one method it was accepted as correct.

6.6. Prediction of protein functions

Protein functional domains were predicted using InterProScan v5.51-85.0 in conjunction with the Pfam, HAMAP, MOBIDB, PIRSF, PROSITE and SUPERFAMILY tools [141], while GO class predictions were carried out using Pannzer2 [142]. N-terminal signal peptides were predicted using SignalP v5.0 [143] and transmembrane (TM) domains were predicted using TMHMM v2.0 [144]. CAZymes were predicted using dbCAN2 in conjunction with the Hotpep, HMMER and DIAMOND tools [145]. Only CAZymes predicted with at least two of the three tools were retained for further analysis. Putative PCWDEs were manually identified based on their CAZy classification (http://www.cazy.org) [146], KEGG description and InterPro annotation. *RiPP* gene clusters were manually identified in the *V. inaequalis* MNH120 genome (**Additional file 19: S1 Text**) through the presence of a gene encoding a protein with a DUF3328 domain in close proximity to a gene encoding a dikaritin precursor peptide with an N-terminal signal peptide, followed by one or more perfect or imperfect tandem sequence repeats of at least 10 amino acid residues in length separated by putative kexin protease cleavage sites.

6.7. Prediction of effector candidates and effector candidate families

Small proteins of ≤400 amino acid residues in length with a predicted N-terminal signal peptide, but without a predicted TM domain or endoplasmic reticulum (ER) retention motif (HDEL/KDEL), were annotated as ECs. This list of ECs was supplemented with proteins of >400 amino acids in length with a predicted N-terminal signal peptide, but no predicted TM domain or ER retention motif, provided that they were predicted to be an effector using EffectorP v3.0 [147]. ECs were grouped into protein families using spectral clustering SCPS v0.9.8 [148]. The identified

protein families were then manually curated by eye, taking into account conservation of the N-terminal signal peptide sequence, cysteine spacing, as well as conserved functional domains identified with InterProScan v5.51-85.0. To further refine the list of ECs, proteins with an enzymatic annotation by InterProScan v5.51-85.0 were discarded. In cases where only one or two ECs from a family were predicted to have an enzymatic domain, the EC was retained. To determine whether the ECs had sequence similarity to other proteins, a BLASTp analysis using an e-value threshold of 0.05 was performed against the nr protein database at NCBI.

6.8. RNA-seq read analysis

Methods associated with this section are summarized in **Additional file 2: Figure A 3-1**. As a starting point for the analysis of RNA-seq reads, all unique genes of *V. inaequalis* isolate MNH120 were identified, and any additional genes that were identical in sequence, representing paralogs (or false gene duplications generated as a consequence of incorrect genome assembly by Deng et al. [19]), were masked to avoid the multimapping of RNA-seq reads. Here, a gff3 file containing only the duplicated genes was generated using AGAT [149], with the sequences subsequently masked using BEDTools v2.30.0 (maskfasta) [150]. Finally, a mappability mask was applied to the MNH120 genome to prevent the multimapping of reads to repetitive genomic regions, including those genes of *EC* families that are known to be highly similar in sequence. To generate the mappability mask, the MNH120 genome was fragmented into all possible 150-bp stretches and mapped to the MNH120 genome using the Burrows-Wheeler Aligner (bwa) [151] with a gap open penalty of 3, gap extension penalty of 3 and max mismatch penalty of 3. Finally, the resulting SAM file from was used to generate the mappability mask (http://lh3lh3.users.sourceforge.net/download/seqbility-20091110.tar.bz2). Raw RNA-seq reads were then filtered, in which adapter sequences, as well as reads with >10% Ns or ≥50% low quality (Qscore: 5) bases, were removed, and the final quality of reads was checked using fastQC v0.11.9

[152]. Next, filtered RNA-seq reads from all samples were mapped to the masked MNH120 genome using HISAT2 v2.2.1 [136,137] and SAMtools v9.2.0 [138] was used to only keep those reads that mapped to the fungal genome. Uniquely mapped reads were counted using featureCounts from SubRead package v2.0.0 to generate a count matrix [153]. Results from all steps of the RNA-seq analysis were aggregated for quality control assessment using MultiQC v1.11 [154].

6.9. Differential gene expression and clustering

The count matrix (see section 6.8) was imported to R and a differential gene expression analysis was performed with DESeq2 package v1.32.0 [155]. Pairwise comparisons from all samples were performed and genes with a $\log_2$-fold change in expression of >1.5 and a *p*adj value of <0.01 during at least one *in planta* infection time point, relative to growth in culture, were considered significantly differentially expressed. Here, multiple testing correction was applied using the Benjamini-Hochberg (BH) method of the DESq2 package, in conjunction with a *p*adj value threshold of <0.01. A PCA plot was then generated using the PCA function of the DESeq2 package. Genes that were up-regulated at one or more *in planta* infection time points were selected for hierarchical clustering. For hierarchical clustering, RNA-seq read counts were first normalized using the rlog method from the DESeq2 package and scaled. Hierarchical clustering of the genes was performed using the hclust function according to the Ward.D2 and Euclidean distance methods, with the minimum number of clusters displaying a distinct expression profile during host infection identified in the resulting clustering dendrogram. Using quantitative guidance from the cutree function, the number of clusters was initially set to 10, then systematically reduced due to observed similarity between clusters, to give five distinct clusters with unique expression trends. Visualization of gene expression clusters (waves), with the expression trends plotted, was performed using ggplot2 v3.3.5 [156], while gene expression heatmaps were generated using

Complexheatmap v2.9.1 [157]. Pearson correlation coefficients were calculated to investigate the co-expression of genes inside specific clusters.

6.10. GO and Pfam term enrichment analysis

GO predictions from Pannzer2 [142] with a predictive positive value (PPV) >5 were used for a GO term enrichment analysis across the five distinct gene expression waves. The GO term enrichment analysis was performed with topGO package v2.44.0 [158], using the total set of genes employed for clustering as background and a Fisher's exact test for all GO terms: Biological Process (BP), Cellular Component (CC) and Molecular Function (MF). GO enrichment analysis results were visualized using ggplots2 v3.3.5 [156]. An enrichment test for Pfam domains was performed using a Fisher's exact test, with all genes targeted in the clustering analysis used as background.

6.11. Structural modelling of protein tertiary structures

AlphaFold2 [159], in conjunction with the ColabFold notebook [160], was used to predict the protein tertiary structures of EC family members from *V. inaequalis* isolate MNH120. Here, only those family members that were encoded by genes up-regulated *in planta*, relative to growth in culture, were used in this analysis, with only the most highly expressed member targeted for prediction (i.e. as a family representative). In each case, the mature amino acid sequence of the EC (i.e. without its predicted N-terminal signal peptide) was used as input. For the Avr1/Six4-like family, the published pro-domain [63] was also removed. For those ECs that had <30 proteins with sequence similarity in the NCBI database, as identified by a BLASTp analysis in conjunction with an e-value threshold of ≤0.05, a custom MSA was generated and used as input. These custom MSAs, which were built with up to 100 protein sequences, depending on how many protein sequences were available, included all mature EC family members that were unique to the updated

MNH120 annotation (i.e. that could not be accessed by the AlphaFold2 search algorithms), as well as similar protein sequences identified through the BLASTp analysis at NCBI. To build the custom MSAs, all sequences were aligned using Clustal Omega [161,162], with the alignments subsequently converted to the a3m format using ToolSeq [163,164]. The only exception was for members of the FOLD-like family. Here, in an attempt to improve the structural prediction, the *F. oxysporum* Avr1/Six4 and Avr2/Six3 proteins were manually added to the input sequences to generate a custom MSA, even though these proteins were not identified in the initial BLASTp similarity search. For EC singletons, protein tertiary structures were predicted using AlphaFold2 open source code v2.0.1 and v2.1.0 [159], with preset casp14, max_template_date: 2020-05-14, using mature protein sequences as input. Again, only those ECs that were encoded by genes up-regulated *in planta*, relative to growth in culture, were used in this analysis. All predicted protein tertiary structures with a pLDDT score of ≥70 were considered confident predictions. Protein structures with an pLDDT score of 50–60 that also had an intrinsically disordered region predicted with MobiDB-lite [165] or PrDos [166] were also considered confident predictions.

Predicted EC protein tertiary structures were screened against the Research Collaboratory for Structural Bioinformatics (RCSB) PDB database to identify proteins with similar folds using the Dali server [48]. Here, all hits with a Z-score of ≥2 were considered similar. Protein tertiary structures were visualized and aligned using PyMol v2.5, in conjunction with the alignment plugin tool CEalign [167]. To further investigate similarities between protein tertiary structures, TM-align [168] was used to calculate a root-mean-square deviation (RMSD) value. Finally, the general fold of confidently predicted protein tertiary structures was investigated using RUPEE [169,170] against the SCOPe v2.08 database [67,171]. Proteins predicted to have a knottin fold in the SCOPe database were assessed using Knotter 3D to determine whether they had a true knottin structure [112].

Declarations

Ethics approval and consent to participate

Not applicable.

Consent for publication

Not applicable.

Availability of data and materials

The raw RNA-seq data generated in this study, as well as the count matrix and DESEq2-normalized read counts, have been deposited in the NCBI Gene Expression Omnibus (GEO), and are accessible through GEO Series accession number (GSE198244). The *V. inaequalis* MNH120 gene annotations and associated proteins sequences generated in this study, as well as the output of AlphaFold2 (open source or ColabFold) with the PDB files for the predicted ECs tertiary structures are available at zenodo (10.5281/zenodo.6233645).

Competing interests

The authors declare that they have no competing interests.

Funding

MRF and CHM were supported by the Marsden Fund Council from Government funding (project ID 17-MAU-100), managed by Royal Society Te Apārangi. JKB and BM received funding from The New Zealand Institute for Plant and Food Research Limited, Strategic Science Investment Fund, Project number: 12070.

Authors' contributions

CHM, MR, JKB and KMP conceived the project. JKB, CHM and BM conducted plant infections and prepared samples for sequencing. MR, BH, BM and SdlR performed the bioinformatic analyses. CHM, JKB, MPC and REB provided critical input in experimental design and data

analysis. MR, CHM, BH and JKB wrote the manuscript. All authors read, revised, and approved the final manuscript.

Acknowledgements

We acknowledge use of the New Zealand eScience Infrastructure (NeSI) high-performance computing facilities, as well as their technical support and training services. In particular, we thank Dinindu Senanayake for his consulting support on the high-throughput prediction of protein tertiary structures. New Zealand's national computing facilities are provided by NeSI and are funded jointly by NeSI's collaborator institutions and through the Ministry of Science & Innovation's Research Infrastructure programme. URL:http://www.nesi.org.nz. We thank Drs Erik Rikkerink and Jay Jayaraman for critically reviewing the manuscript, and Dr Simon Williams for providing the *F. oxysporum* Avr1/Six4 and Avr3/Six1 protein structure files ahead of public release.

7. Appendix A: Supplementary material

This appendix contains all the supplementary information associated with the published manuscript in *bioRxiv*. All the supplementary files that are excel spreadsheets are available as a hyperlink to the "Supporting information" section of this particular manuscript.

Additional file 1: Table A 3-1. RNA-seq transcriptome sequencing read statistics from this study. Samples used for the RNA-seq transcriptome sequencing experiment were derived from an infection time course of *Venturia inaequalis* on detached leaves from susceptible apple cultivar 'Royal Gala' at 12 and 24 hours post-inoculation (hpi), as well as 2, 3, 5 and 7 days post-inoculation (dpi), and during growth of the fungus in culture on the surface of cellophane membranes overlying potato dextrose agar at 7 dpi.

Sample name	**Time point**	**Tissue**	**Total number of reads**	**Number of paired reads mapped to the *V. inaequalis* MNH120 genome**	**Overall alignment rate**
S12V2			72,515,775	91,069	0.13%
S12V3	12 hpi	Apple leaf	71,722,781	84,531	0.12%
S12V4		(*In planta*)	65,009,930	78,419	0.12%
S12V5			61,088,214	123,211	0.21%
S24V1			67,826,021	135,704	0.21%
S24V3	24 hpi	Apple leaf	67,811,505	134,126	0.20%
S24V4		(*In planta*)	75,706,837	205,908	0.28%
S24V5			78,244,648	148,265	0.20%
S2V1			47,424,653	125,061	0.27%
S2V2	2 dpi	Apple leaf	68,132,940	279,525	0.42%
S2V3		(*In planta*)	73,356,846	327,163	0.46%
S2V5			63,149,333	136,993	0.22%
S3V1		Apple leaf	46,736,839	475,239	1.05%
S3V2	3 dpi	(*In planta*)	48,406,231	341,262	0.73%

Sample name	**Time point**	**Tissue**	**Total number of reads**	**Number of paired reads mapped to the *V. inaequalis* MNH120 genome**	**Overall alignment rate**
S3V3			63,951,888	658,625	1.07%
S3V5			46,365,679	465,485	1.04%
S5V1			40,513,300	1,439,733	3.68%
S5V2	5 dpi	Apple leaf	36,798,369	494,654	1.39%
S5V3		(*In planta*)	53,569,444	2,965,281	5.73%
S5V4			46,221,769	1,666,765	3.73%
S7V2			47,760,909	3,482,001	7.55%
S7V3	7 dpi	Apple leaf	48,892,959	2,331,267	4.94%
S7V4		(*In planta*)	47,854,848	4,350,665	9.43%
S7V5			43,384,995	1,988,632	4.76%
SS1			24,522,994	22,249,229	93.77%
SS3b	7 dpi	Apple leaf	20,754,255	18,915,521	93.99%
SS4b		(*In planta*)	22,646,155	20,670,316	93.89%
SS8b			26,675,000	24,347,911	94.34%

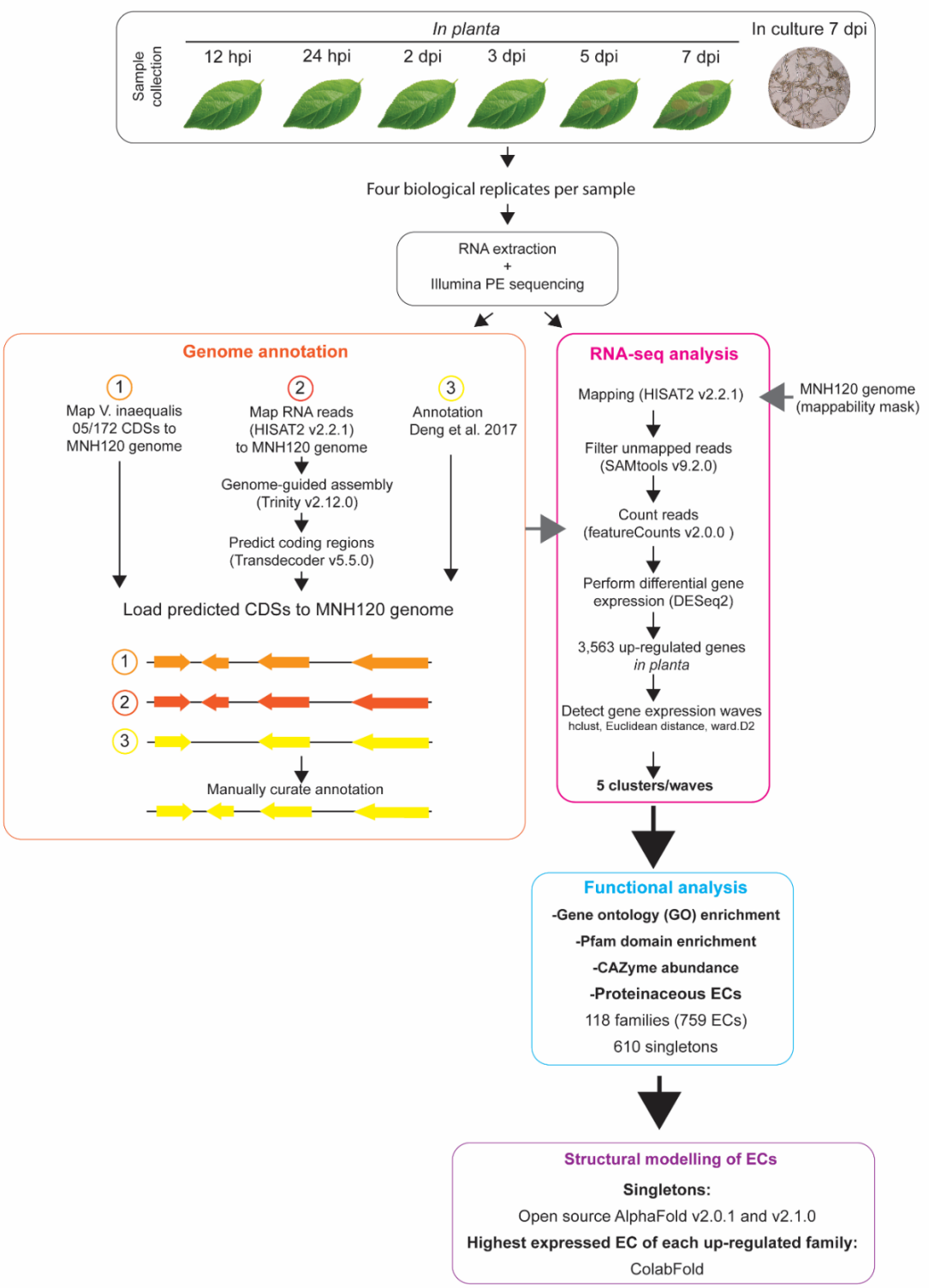

Additional file 2: Figure A 3-1. Bioinformatic pipeline used for transcriptome analysis and genome annotation. Total RNA was extracted from apple leaves infected with *Venturia inaequalis* at 12 and 24 hours post-inoculation (hpi), as well as 2, 3, 5 and 7 days post-inoculation (dpi). As a reference for growth in culture, total RNA was also extracted from *V. inaequalis* grown on the surface of cellophane membranes overlaying potato dextrose agar at 7 dpi. Four biological replicates were included per sample. PE: paired-end; CDS: coding sequence; CAZyme: carbohydrate-active enzyme; EC: effector candidate.

Additional file 3: Differentially expressed genes of *Venturia inaequalis* during infection of susceptible apple cultivar 'Royal Gala', when compared to growth of the fungus in culture on the surface of cellophane membranes overlying potato dextrose agar.

https://www.biorxiv.org/content/biorxiv/early/2022/09/22/2022.03.22.482717/DC2/embed/media-2.xlsx?download=true

Additional file 4: List of Pfam domains in proteins encoded by genes of the five distinct temporal expression waves of *Venturia inaequalis* that are up-regulated during colonization of susceptible apple cultivar 'Royal Gala', when compared to growth of the fungus in culture on the surface of cellophane membranes overlying potato dextrose agar.

https://www.biorxiv.org/content/biorxiv/early/2022/09/22/2022.03.22.482717/DC3/embed/media-3.xlsx?download=true

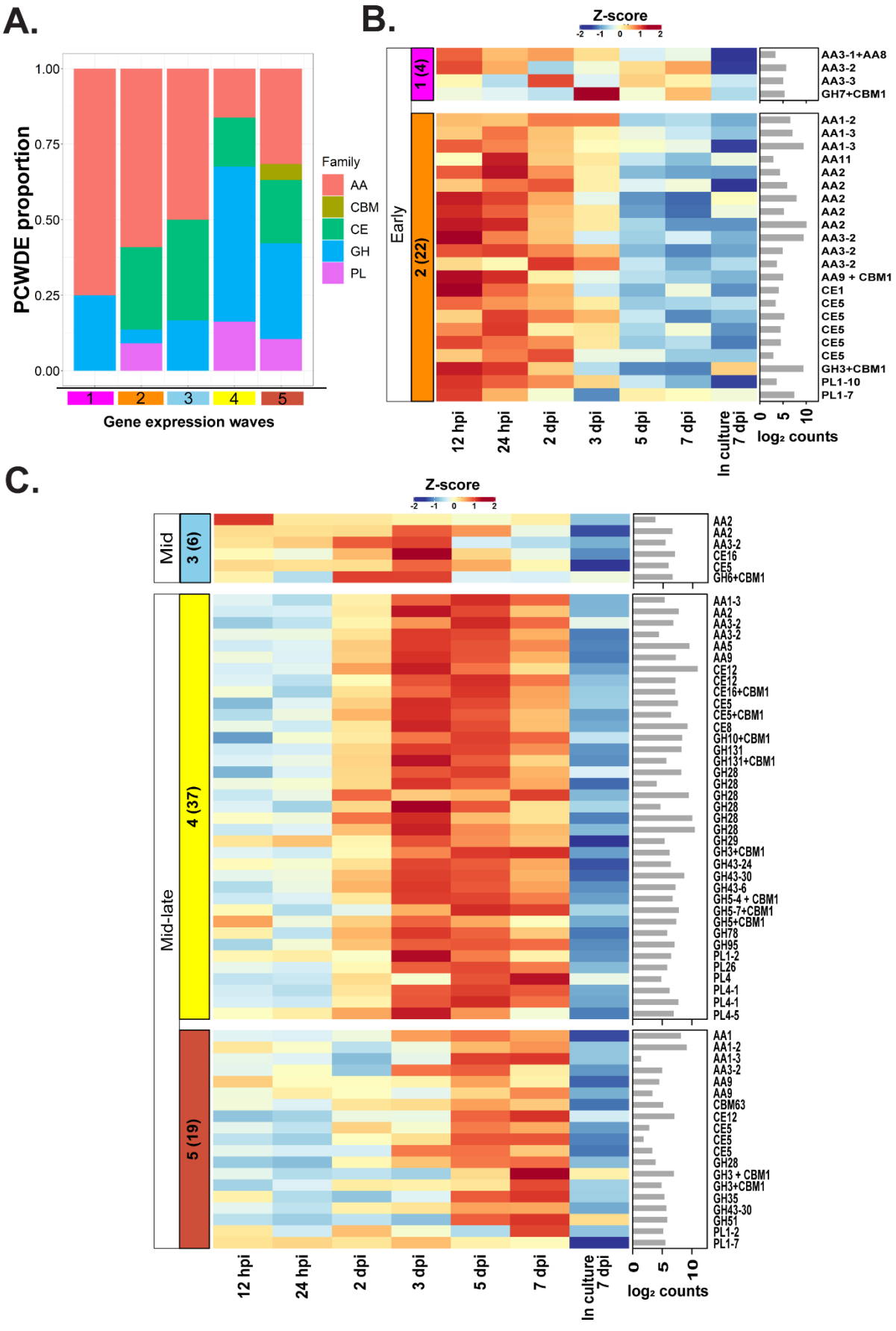
A.
PCWDE proportion
1.00
0.75
0.50
0.25
0.00
Family
AA
CBM
CE
GH
PL
1
2
3
4
5
Gene expression waves
B.
Z-score
-2 -1 0 1 2
Early
1 (4)
2 (22)
AA3-1+AA8
AA3-2
AA3-3
GH7+CBM1
AA1-2
AA1-3
AA1-3
AA11
AA2
AA2
AA2
AA2
AA2
AA3-2
AA3-2
AA3-2
AA9 + CBM1
CE1
CE5
CE5
CE5
CE5
CE5
GH3+CBM1
PL1-10
PL1-7
12 hpi
24 hpi
2 dpi
3 dpi
5 dpi
7 dpi
In culture 7 dpi
0 5 10
log2 counts
C.
Z-score
-2 -1 0 1 2
Mid
3 (6)
AA2
AA2
AA3-2
CE16
CE5
GH6+CBM1
Mid-late
4 (37)
AA1-3
AA2
AA3-2
AA3-2
AA5
AA9
CE12
CE12
CE16+CBM1
CE5
CE5+CBM1
CE8
GH10+CBM1
GH131
GH131+CBM1
GH28
GH28
GH28
GH28
GH28
GH28
GH29
GH3+CBM1
GH43-24
GH43-30
GH43-6
GH5-4 + CBM1
GH5-7+CBM1
GH5+CBM1
GH78
GH95
PL1-2
PL26
PL4
PL4-1
PL4-1
PL4-5
5 (19)
AA1
AA1-2
AA1-3
AA3-2
AA9
AA9
CBM63
CE12
CE5
CE5
CE5
GH28
GH3 + CBM1
GH3+CBM1
GH35
GH43-30
GH51
PL1-2
PL1-7
12 hpi
24 hpi
2 dpi
3 dpi
5 dpi
7 dpi
In culture 7 dpi
0 5 10
log2 counts

Additional file 5: Figure A 3-2. Plant cell wall-degrading enzyme (PCWDE)-encoding genes of *Venturia inaequalis* up-regulated during infection of susceptible apple cultivar 'Royal Gala', relative to growth of the fungus in culture on the surface of cellophane membranes overlying potato dextrose agar. **A.** Proportion of *in planta* up-regulated PCWDE-encoding genes in each host infection-specific temporal expression wave. **B.** Heatmap of PCWDE-encoding genes up-regulated *in planta* that demonstrate a peak level of expression during waves 1 and 2 of the early infection stage at 12 and 24 hours post-inoculation (hpi). **C.** Heatmap of PCWDE-encoding genes up-regulated *in planta* that demonstrate a peak level of expression during wave 3 of the mid infection stage at 2 and 3 days post-inoculation (dpi) and waves 4 and 5 of the mid-late infection stage at 5 and 7 dpi. Block labels on the left indicate gene expression wave. Numbers in brackets indicate number of genes per wave. Gene expression data are scaled rlog-normalized counts across all samples (Z-score), averaged from four biological replicates. Labels on the right indicate carbohydrate-active enzyme (CAZyme) classification. Bar plots depict the maximum $\log_2$ DESeq2-normalized count value across all *in planta* time points. AA: auxiliary activity; GH: glycoside hydrolase; CE: carbohydrate esterase; PL: polysaccharide lyase; CBM: carbohydrate-binding module.

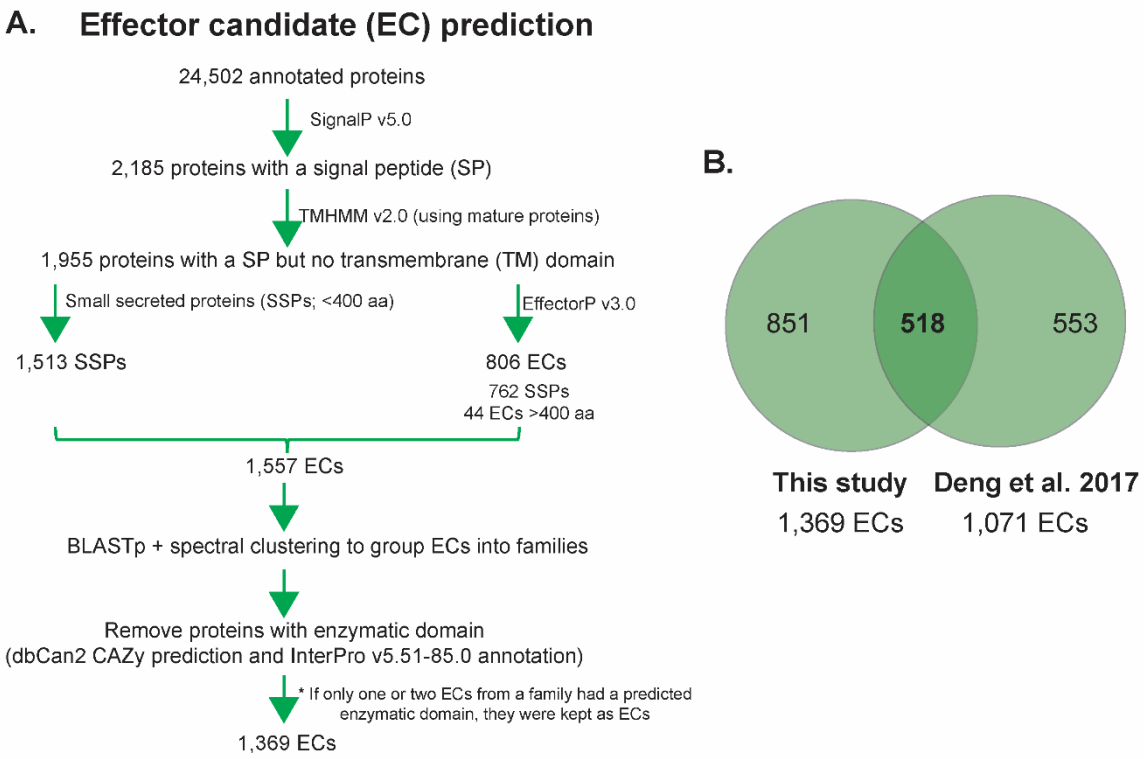

Additional file 6: Figure A 3-3. Effector candidates (ECs) prediction. A. Pipeline for the identification of ECs from *Venturia inaequalis.* **B.** Comparison of the number of ECs predicted from *V. inaequalis* isolate MNH120 in this study and a previous study [19]. The comparison is based on an exact protein sequence match. The previous study by Deng et al. [19] defined ECs as small proteins of <500 amino acid residues in length with a signal peptide and no similarity to lytic enzymes.

Additional file 7: List of effector candidates (ECs) identified from *Venturia inaequalis*, their family classification, and indication of whether *EC* family members cluster in the genome.

https://www.biorxiv.org/content/biorxiv/early/2022/09/22/2022.03.22.482717/DC4/embed/media-4.xlsx?download=true

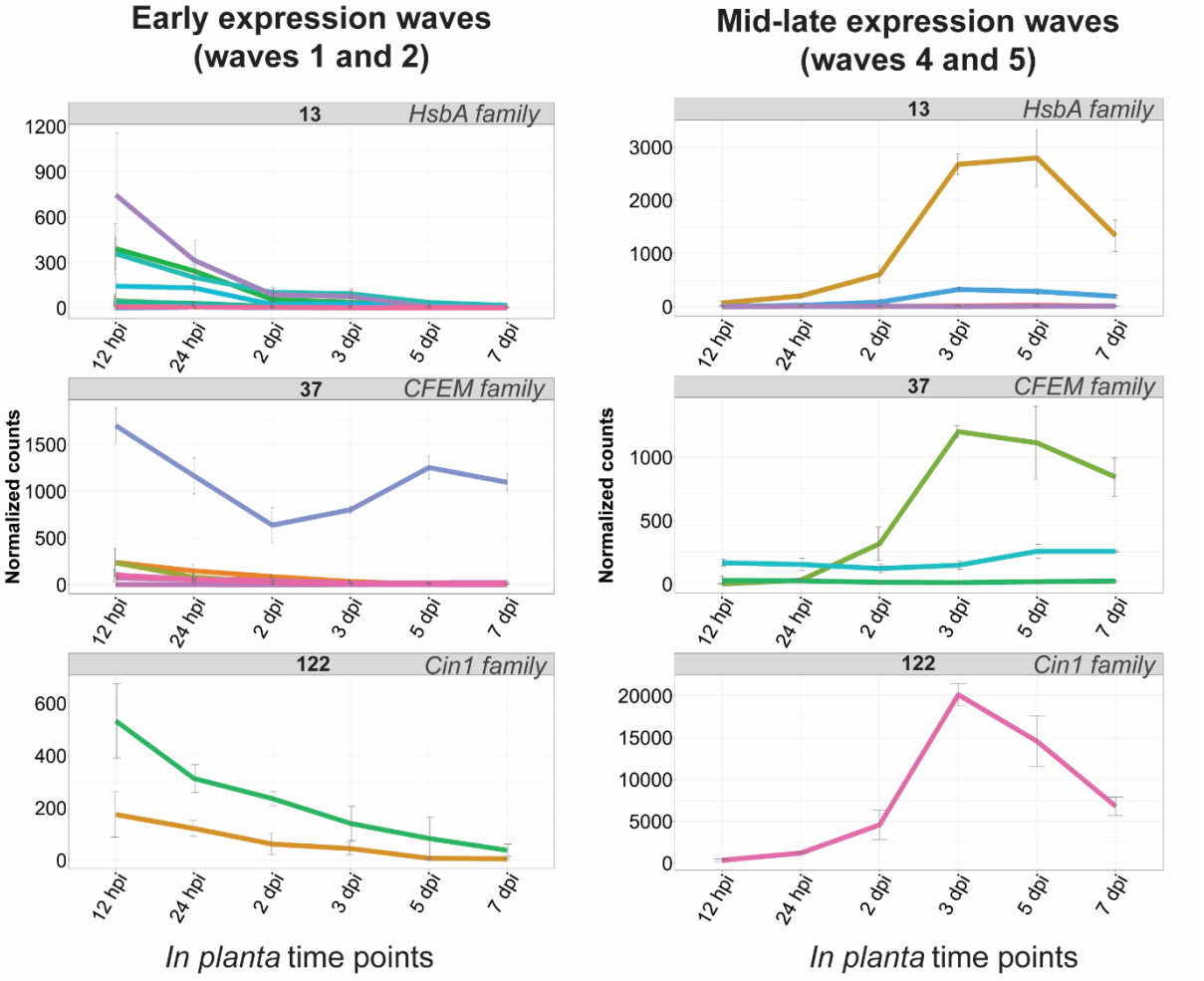

Additional file 8: Figure A 3-4. Gene families encoding proteinaceous effector candidates (ECs) of *Venturia inaequalis* that have members demonstrating different expression profiles during early and mid-late colonization of susceptible apple cultivar 'Royal Gala'. Expression data during host-colonization are DESeq2-normalized counts, averaged from four biological replicates, with error bars representing standard deviation (hpi: hours post-inoculation; dpi: days post-inoculation). *HsbA*: Hydrophobic surface-binding protein A; *CFEM*: common fold in several fungal extracellular membrane proteins; *Cin1*: Cellophane-induced 1.

Additional file 9: Table A 3-2. Effector candidate (EC) protein families or singletons from *Venturia inaequalis* that have sequence similarity to EC or avirulence (Avr) effector proteins from other plant-pathogenic fungi.

EC protein family	Number of family members	Similar EC/Avr and host pathogen	Maximum amino acid identity to similar EC/Avr	Temporal gene expression wave
Gas1-like family	2	*Magnaporthe oryzae* Gas1	24.6%	Wave 2 (early infection)
Ave1-like family	11	*Verticillium dahliae* Ave1	36.5%	Waves 4 and 5 (mid-late infection)
Ecp39-like family	6	*Fulvia fulva* Ecp39	46.9%	Waves 4 and 5 (mid-late infection)
Ecp10-like family	61	*F. fulva* Ecp10	23.2%	Waves 4 and 5 (mid-late infection)
AvrLm6-like family	31	*Leptosphaeria maculans* AvrLm6	22.7%	Waves 4 and 5 (mid-late infection)
Ecp6-like singleton	NA	*F. fulva* Ecp6	43%	Wave 4 (mid-late infection)

NA: Not applicable, as the protein is a singleton.

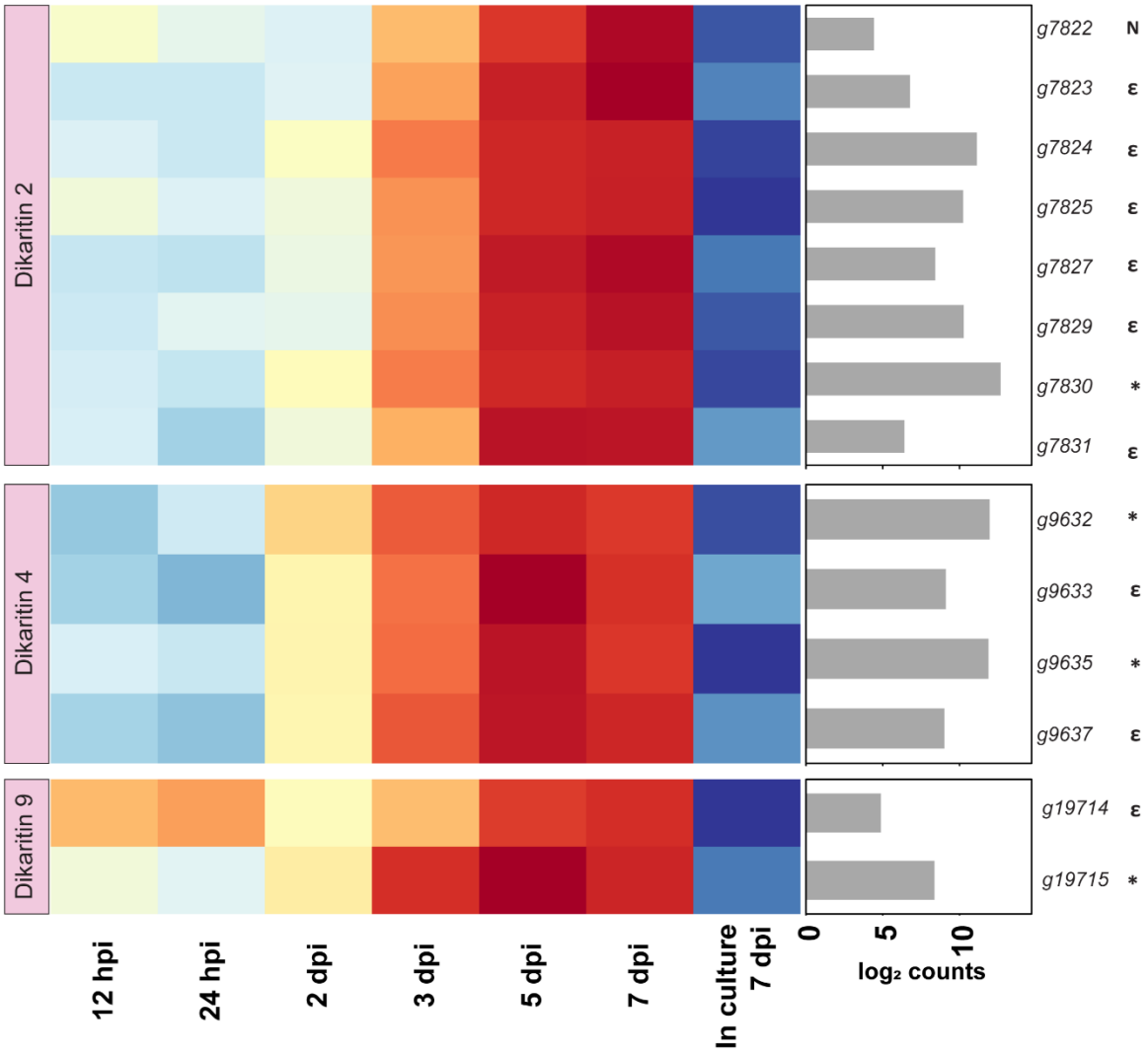

Additional file 10: Figure A 3-5. Expression of ribosomally-synthesized and post-translationally modified peptide (*RiPP*) *dikaritin* gene clusters from *Venturia inaequalis* that are up-regulated during colonization of susceptible apple cultivar 'Royal Gala', relative to growth of the fungus in culture on the surface of cellophane membranes overlying potato dextrose agar. Heatmap gene expression data are scaled rlog-normalized counts across all samples (Z-score), averaged from four biological replicates. hpi: hours post-inoculation; dpi: days post-inoculation. Bar plot annotation depicts the maximum $\log_2$ DESeq2-normalized count value across all *in planta* time points. Genes marked as ε putatively encode a protein with a DUF3382 domain or were annotated as a major-facilitator superfamily protein. Genes marked with * putatively encode a dikaritin precursor peptide. The gene marked with N encodes a protein with no characterized functional domain.

Additional file 11: List of protein tertiary structures from *Venturia inaequalis* with a confident AlphaFold2 prediction and list of predicted SCOPe folds.

https://www.biorxiv.org/content/biorxiv/early/2022/09/22/2022.03.22.482717/DC5/embed/media-5.xlsx?download=true

Additional file 12: Table A 3-3. Effector candidates (ECs) of *Venturia inaequalis* (*Vi*) with predicted structural similarity to EC or avirulence (Avr) effector proteins from other plant-pathogenic fungi that have a characterized tertiary structure present in the RCSB PDB.

***Vi* protein ID**	**EC family**	**Number of family members**	**pLDDT score[1]**	**Structural similarity (RCSB PDB ID)**	**Dali Z-score[2]**	**RMSD**
g13386	Family 1	75	84.34	*Magnaporthe oryzae* MAX effector (6R5J);	4.9;	3.81;
				M. oryzae AvrPiz-t (2LW6);	3.7;	2.72;
				Pyrenophora tritici-repentis ToxB (2MM2);	3.4;	2.98;
				M. oryzae Avr-Pia (2N37);	3.3;	3.14;
				M. oryzae Avr-Pib (5Z1V);	3.3;	4.71;
				M. oryzae Avr1-CO39 (2MYV);	2.9;	4.31;
				M. oryzae Avr-Pik (6FUB)	2.4	3.95
g11711	Family 2	32	97.77	*Zymoseptoria tritici* Zt-KP6-1 (6QPK)	5.8	2.02
g18375	Family 5	36	89.01	*Z. tritici* Zt-KP6-1 (6QPK)	5.7	2.34
g20030	AvrLm6-like[3]	31	89.96	*Z. tritici* Zt-KP6-1 (6QPK)	4.2	2.79
g4577	Family 23	5	80.18	*Z. tritici* Zt-KP6-1 (6QPK)	5.9	3.03
g12079	Family 26	4	88.49	*Z. tritici* Zt-KP6-1 (6QPK)	4.9	3.15
g18322	Singleton	NA	73.8	*Z. tritici* Zt-KP6-1 (6QPK)	4.4	3.28
g4356	Singleton	NA	78.02	*Z. tritici* Zt-KP6-1 (6QPK)	5.8	2.57
g4781	Family 7	22	89.89	*P. tritici-repentis* ToxA (1ZLE);	5.3;	2.95;
				Fusarium oxysporum Avr2/Six3 (5OD4);	3.2;	3.63;
				Melampsora lini AvrL567-A (2OPC)	2.7	3.48
g13172	Family 28	6	59.95[4]	*P. tritici-repentis* ToxA (1ZLE);	7.4;	2.47;
				F. oxysporum Avr2/Six3 (5OD4);	6.5;	3.36;
				M. lini AvrL567-D (2QVT);	5.3;	3.39;
				M. lini AvrL567-A (2OPC)	4.9	3.78
g9034	Family 38	3	49.75	*P. tritici-repentis* ToxA (1ZLE);	5.8;	3.01;
				F. oxysporum Avr2/Six3 (5OD4);	5.0;	3.28;
				M. lini AvrL567-D (2QVT);	3.1;	3.39;
				M. lini AvrL567-A (2OPC)	2.9	3.67

***Vi* protein ID**	**EC family**	**Number of family members**	**pLDDT score[1]**	**Structural similarity (RCSB PDB ID)**	**Dali Z-score[2]**	**RMSD**
g4288	Singleton	NA	55.02[4]	*F. oxysporum* Avr2/Six3 (5OD4); *P. tritici-repentis* ToxA (1ZLE); *M. lini* AvrL567-A (2OPC)	4.5; 3.6; 2.8	3.42; 3.38; 3.05
g11097	Family 15	12	89.58	*Leptosphaeria maculans* AvrLm5-9 (7AD5); *L. maculans* AvrLm4-7 (4FPR); *Fulvia fulva* Ecp11-1 (6ZUQ)	6.5; 5.9; 5.4	3.50; 3.98; 3.63
g24490	Family 47	2	75.85	*L. maculans* AvrLm4-7 (4FPR); *L. maculans* AvrLm5-9 (7AD5); *F. fulva* Ecp11-1 (6ZUQ)	4.1; 3.6; 3.5	3.86; 3.61; 3.69
g3787	Family 49	3	78.15	*F. oxysporum* Avr1/Six4 (7T6A); *F. oxysporum* Avr3/Six2 (7T69)	NA; NA	5.10; 4.00

[1]pLDDT: AlphaFold2 predicted Local Distance Difference Test score (0–100). A score of 70–100 is indicative of medium to high confidence. RCSB PDB: Research Collaboratory for Structural Bioinformatics Protein Data Bank.

[2]Z-score: A Dali Z-score above 2 indicates 'significant similarities' between proteins. RMSD: root-mean-square deviation (a measure of similarity between protein structures). The smaller the RMSD, the more similar the proteins structures are. NA: Not applicable, structures not available on Dali server database.

[3]: Effector candidate family has similarity to the AvrLm6 protein from *L. maculans.*

[4]: Indicates that the protein is predicted to have an intrinsically disordered region, which reduces the overall pLDDT score.

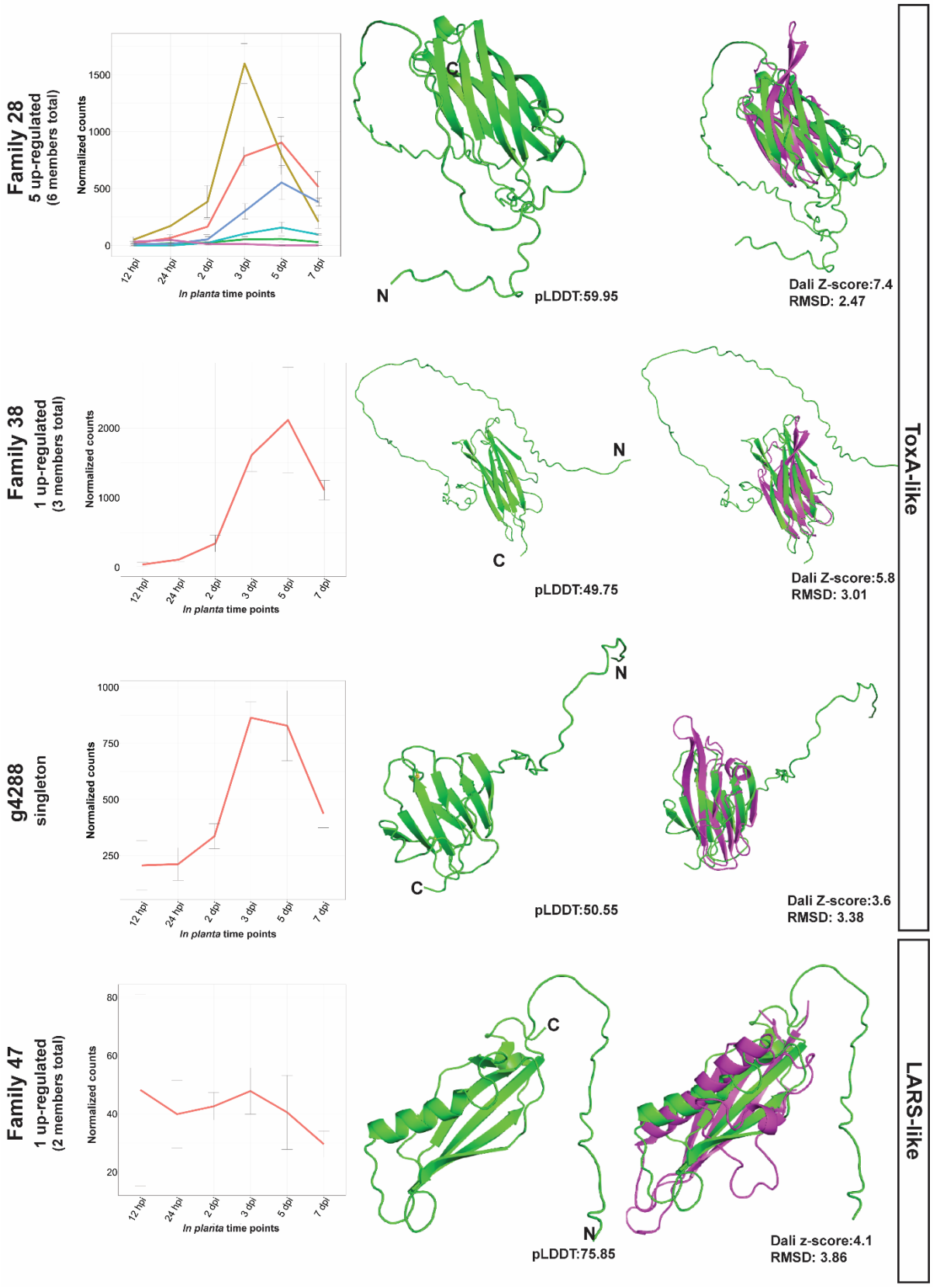
Family 28
5 up-regulated
(6 members total)
Normalized counts
1500
1000
500
0
12 hpi
24 hpi
2 dpi
3 dpi
5 dpi
7 dpi
In planta time points
C
N
pLDDT:59.95
Dali Z-score:7.4
RMSD: 2.47
Family 38
1 up-regulated
(3 members total)
Normalized counts
2000
1000
0
12 hpi
24 hpi
2 dpi
3 dpi
5 dpi
7 dpi
In planta time points
N
C
pLDDT:49.75
Dali Z-score:5.8
RMSD: 3.01
g4288
singleton
Normalized counts
1000
750
500
250
12 hpi
24 hpi
2 dpi
3 dpi
5 dpi
7 dpi
In planta time points
N
C
pLDDT:50.55
Dali Z-score:3.6
RMSD: 3.38
ToxA-like
Family 47
1 up-regulated
(2 members total)
Normalized counts
80
60
40
20
12 hpi
24 hpi
2 dpi
3 dpi
5 dpi
7 dpi
In planta time points
C
N
pLDDT:75.85
Dali z-score:4.1
RMSD: 3.86
LARS-like

Additional file 13: Figure A 3-6. Effector candidates (ECs) from *Venturia inaequalis* with structural similarity to known avirulence (Avr) effector proteins from other plant-pathogenic fungi not shown in **Figure 3-4**. Representative *V. inaequalis* protein structures (green; family 28 [g13172], family 38 [g9034], singleton g4288) aligned to ToxA from *Pyrenophora tritici-repentis* (1ZLE) (purple), LARS-like protein structure (green; family 47 [g24490]) aligned to AvrLm4-7 from *Leptosphaeria maculans* (7FPR). Protein tertiary structures predicted by AlphaFold2 are the most highly expressed member from each EC family. Disulfide bonds coloured in yellow. N: amino (N) terminus; C: carboxyl (C) terminus. pLDDT: predicted Local Distance Difference Test score (0–100); a pLDDT score of 70–100 is indicative of medium to high confidence. A Dali Z-score above 2 indicates 'significant similarities' between structures. RMSD: root-mean-square deviation. Gene expression data are from up-regulated *ECs* during host-colonization and are based on DESeq2-normalized counts, averaged from four biological replicates, with error bars representing standard deviation (hpi: hours post-inoculation; dpi: days post-inoculation).

Additional file 14: Matrix amino acid identity of the effector candidate (EC) structural families (MAX, ToxA, LARS, FOLD).

https://www.biorxiv.org/content/biorxiv/early/2022/09/22/2022.03.22.482717/DC6/embed/media-6.xlsx?download=true

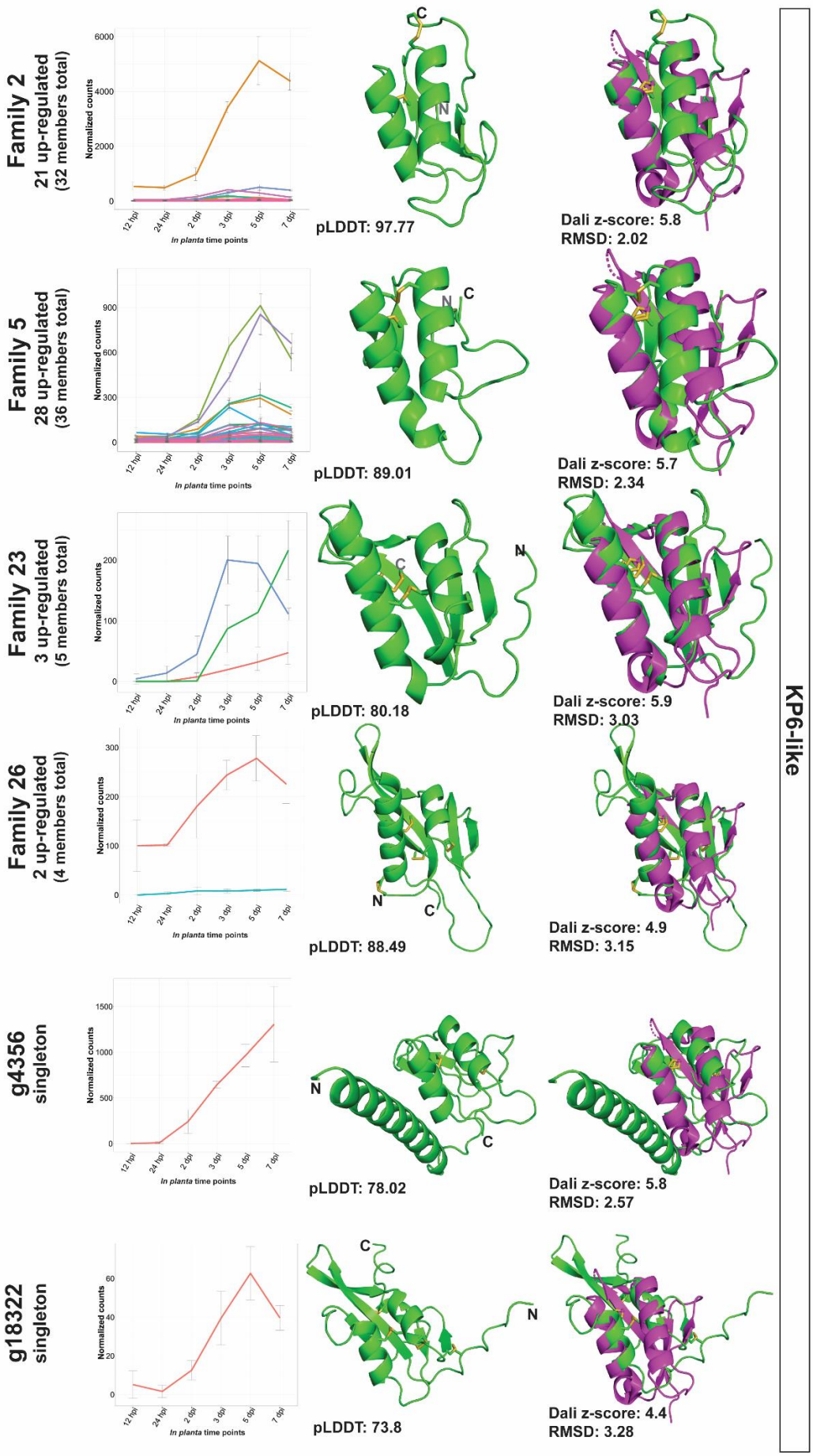
Family 2
21 up-regulated
(32 members total)
Normalized counts
6000
4000
2000
0
12 hpi
24 hpi
2 dpi
3 dpi
5 dpi
7 dpi
In planta time points
C
N
pLDDT: 97.77
Dali z-score: 5.8
RMSD: 2.02
Family 5
28 up-regulated
(36 members total)
900
600
300
0
N
C
pLDDT: 89.01
Dali z-score: 5.7
RMSD: 2.34
Family 23
3 up-regulated
(5 members total)
200
100
0
C
N
pLDDT: 80.18
Dali z-score: 5.9
RMSD: 3.03
Family 26
2 up-regulated
(4 members total)
300
200
100
0
N
C
pLDDT: 88.49
Dali z-score: 4.9
RMSD: 3.15
g4356
singleton
1500
1000
500
0
N
C
pLDDT: 78.02
Dali z-score: 5.8
RMSD: 2.57
g18322
singleton
60
40
20
0
C
N
pLDDT: 73.8
Dali z-score: 4.4
RMSD: 3.28
KP6-like

Additional file 15: Figure A 3-7. Effector candidates (ECs) from *Venturia inaequalis* with structural similarity to killer protein 6 (KP6) from *Ustilago maydis* P6 virus not shown in **Figure 3-4**. Representative *V. inaequalis* protein structures (green; family 2 [g11711], family 5 [g18375], family 23 [g4577], family 26 [g12079], singleton g4356, singleton g18322) aligned to EC Zt-KP6-1 from *Zymoseptoria tritici* (6QPK). Protein structures predicted by AlphaFold2 are the most highly expressed member from each EC family. Disulfide bonds coloured in yellow. N: amino (N) terminus; C: carboxyl (C) terminus. pLDDT: predicted Local Distance Difference Test score (0–100); a pLDDT score of 70–100 is indicative of medium to high confidence. A Dali Z-score above 2 indicates 'significant similarities' between structures. RMSD: root-mean-square deviation. Gene expression data are from up-regulated *ECs* during host-colonization and are based on DESeq2-normalized counts, averaged from four biological replicates, with error bars representing standard deviation (hpi: hours post-inoculation; dpi: days post-inoculation).

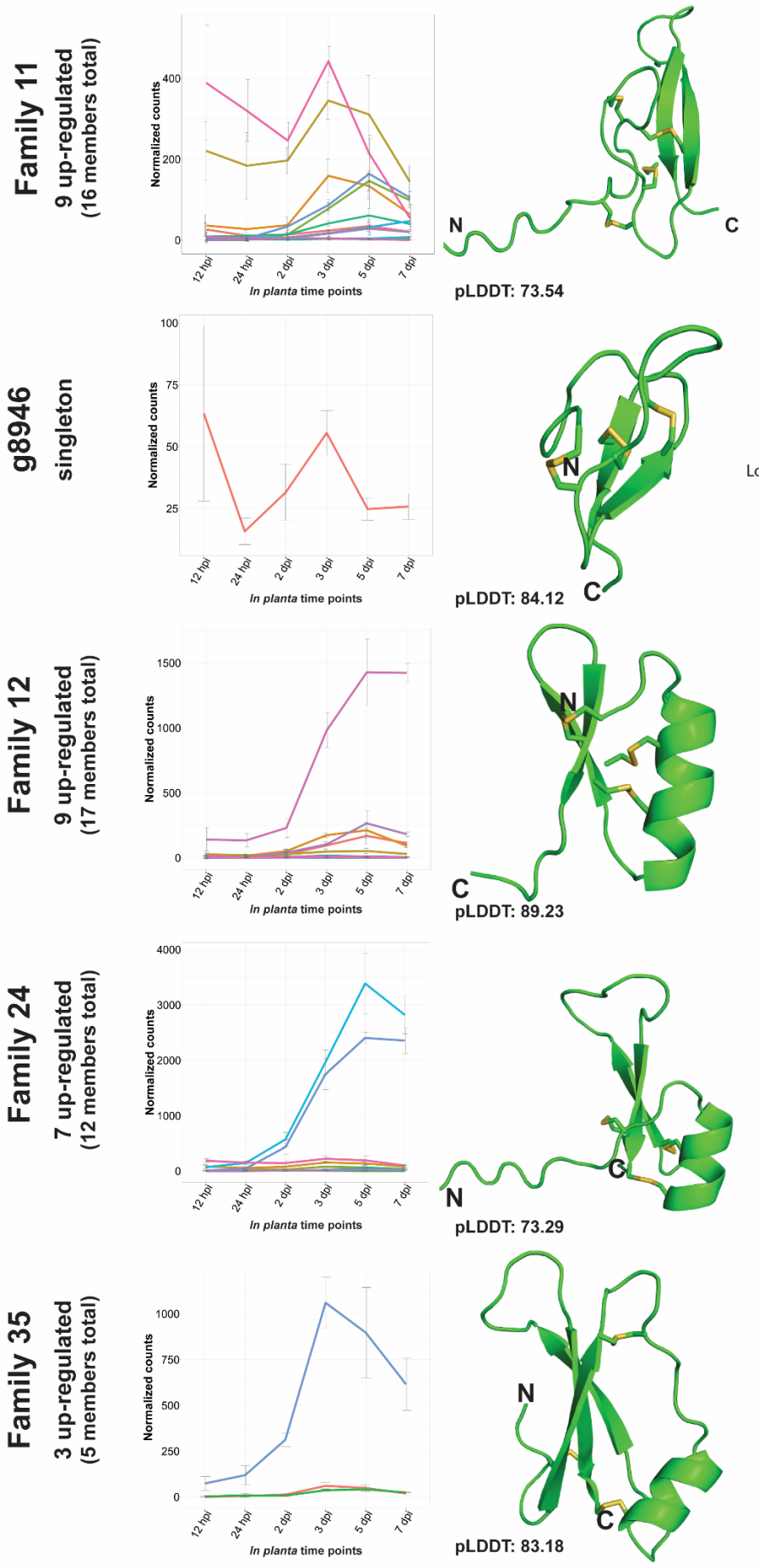
Family 11
9 up-regulated
(16 members total)
Normalized counts
400
200
0
12 hpi
24 hpi
2 dpi
3 dpi
5 dpi
7 dpi
In planta time points
N
C
pLDDT: 73.54
g8946
singleton
Normalized counts
100
75
50
25
12 hpi
24 hpi
2 dpi
3 dpi
5 dpi
7 dpi
In planta time points
N
C
pLDDT: 84.12
Family 12
9 up-regulated
(17 members total)
Normalized counts
1500
1000
500
0
12 hpi
24 hpi
2 dpi
3 dpi
5 dpi
7 dpi
In planta time points
N
C
pLDDT: 89.23
Family 24
7 up-regulated
(12 members total)
Normalized counts
4000
3000
2000
1000
0
12 hpi
24 hpi
2 dpi
3 dpi
5 dpi
7 dpi
In planta time points
C
N
pLDDT: 73.29
Family 35
3 up-regulated
(5 members total)
Normalized counts
1000
750
500
250
0
12 hpi
24 hpi
2 dpi
3 dpi
5 dpi
7 dpi
In planta time points
N
C
pLDDT: 83.18

Additional file 16: Figure A 3-8. Effector candidates (ECs) from *Venturia inaequalis* with a predicted knottin-like fold. Representative *V. inaequalis* structures (green; family 11 [g8686], family 12 [g10808], family 24 [g22936], family 35 [g22623], singleton g8946). Protein structures predicted by AlphaFold2 are the most highly expressed member from each EC family. pLDDT: predicted Local Distance Difference Test score (0–100); a pLDDT score of 70–100 is indicative of medium to high confidence. A Dali Z-score above 2 indicates 'significant similarities' between structures. Gene expression data are from up-regulated *ECs* during host-colonization are based on DESeq2-normalized counts, averaged from four biological replicates, with error bars representing standard deviation (hpi: hours post-inoculation; dpi: days post-inoculation). Disulfide bonds coloured in yellow. N: amino (N) terminus; C: carboxyl (C) terminus.

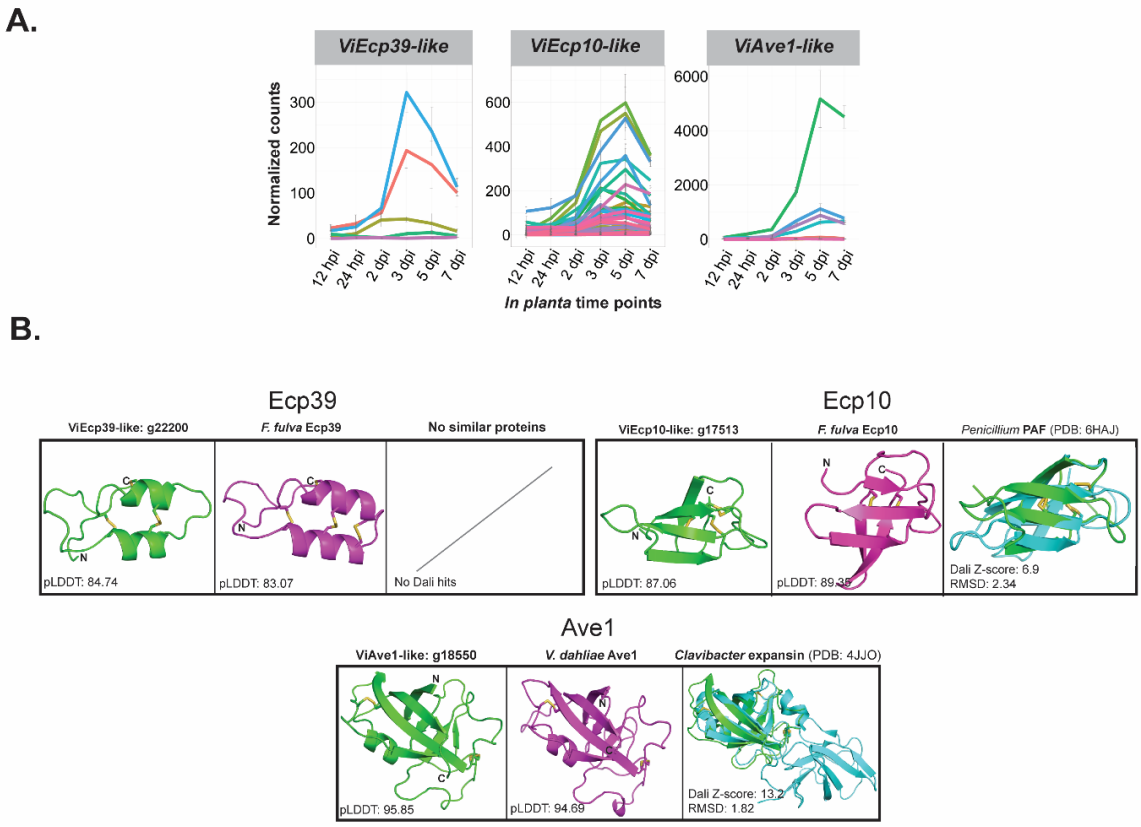

Additional file 17: Figure A 3-9. Effector candidate (EC) families from *Venturia inaequalis* (*Vi*) with sequence similarity to effectors and characterized or candidate avirulence (Avr) effector proteins from other plant-pathogenic fungi. **A.** Expression data of *EC* genes during host-colonization are DESeq2-normalized counts, averaged from four biological replicates, with error bars representing standard deviation (hpi: hours post-inoculation; dpi: days post-inoculation). **B.** Protein tertiary structures of candidate virulence and avirulence (Avr) effector proteins predicted by AlphaFold2. Disulfide bonds coloured in yellow. *F. fulva* is *Fulvia fulva* and *V. dahliae* is *Verticillium dahliae*. Green tertiary structures represent the *V. inaequalis* protein; purple structures represent the EC/Avr from the other fungal pathogen; cyan, represents closest analogous structure in the RCSB PDB database. Sequence similarity was identified by reciprocal protein searches based on BLASTp (E-value <0.05). pLDDT: predicted Local Distance Difference Test score (0–100). A pLDDT score of 70–100 is indicative of medium to high confidence. A Dali Z-score above 2 indicates 'significant similarities' between proteins. RMSD: root-mean-square deviation.

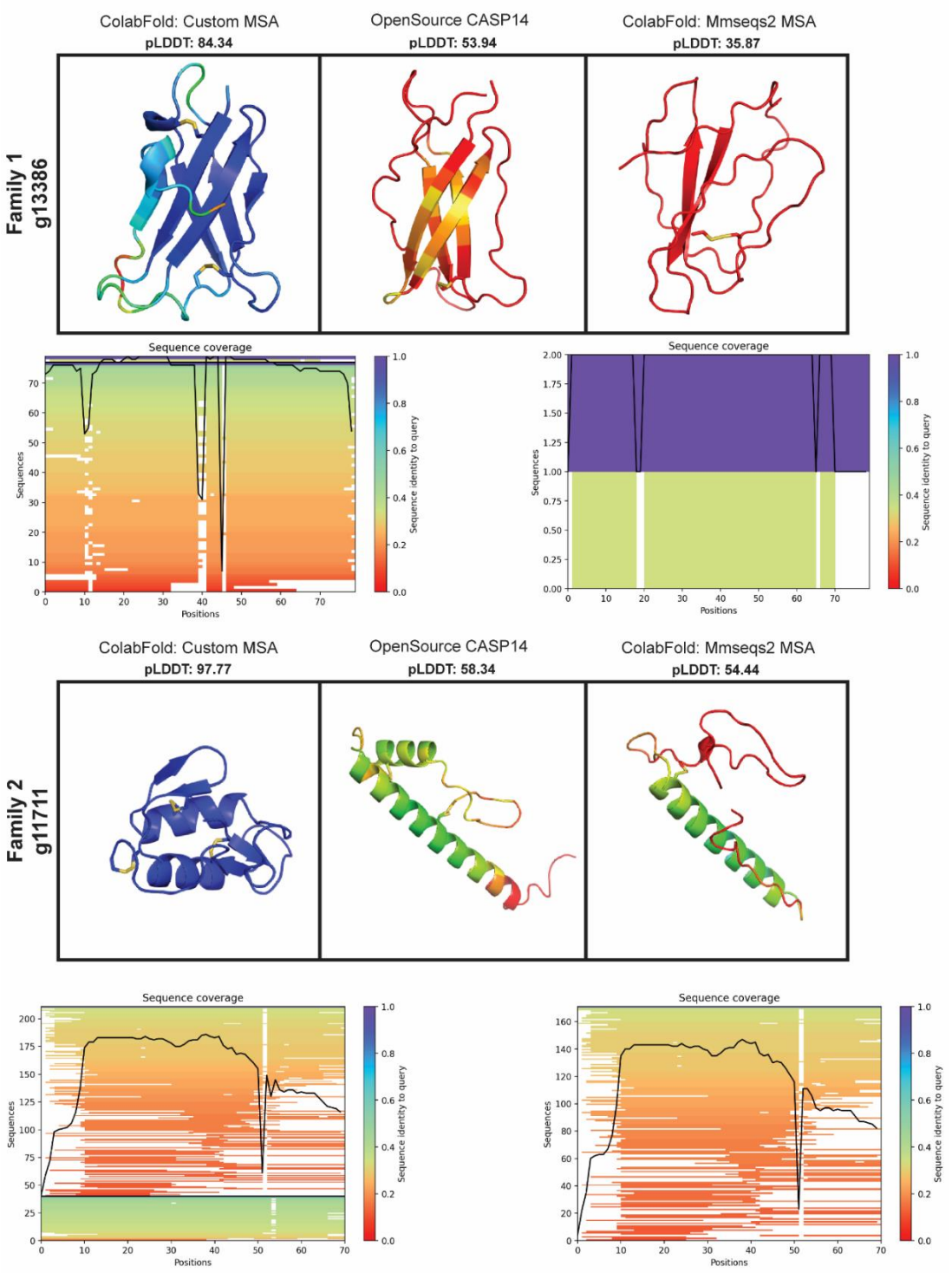

Additional file 18: Figure A 3-10. Comparison of protein tertiary structures predicted for two effector candidates (ECs) of *Venturia inaequalis* using different AlphaFold2 methods. EC protein tertiary structures are coloured by amino acid pLDDT (predicted Local Distance Difference Test) score, with a high pLDDT score coloured in blue and a low pLDDT score coloured in red. ColabFold multiple sequence alignments (MSAs) were generated with Mmseqs2 [172] and MSAs generated by AlphaFold2 open source CASP14 were assembled using HHBlits and HMMER [173,174]. Sequence coverage graphs of the MSAs used for the structural predictions were automatically generated by ColabFold [160].

Additional file 19: A1 Text. Supplementary methods for the identification of *dikaritin RiPP* gene clusters in *Venturia inaequalis*. As a starting point for the identification of *dikaritin RiPP* gene clusters in *V. inaequalis*, genes encoding DUF3328 proteins were identified through a tBLASTn analysis of the MNH120 genome in Geneious v9.1.8, using the g7827 DUF3328 protein of *V. inaequalis* (Dikaritin cluster 2) as a query. This was followed by exhaustive reciprocal tBLASTn analyses of the identified sequences against the *V. inaequalis* genome until no new sequences were identified. The resulting protein sequences were then analysed using InterproScan v5.51-85.0 to identify those that carried a putative DUF3328 domain [141]. Notably, some proteins were not predicted to contain a DUF3328 domain or were instead predicted to belong to the Major facilitator superfamily (MFS). These proteins were manually investigated and proteins with a characteristic DUF3328 domain structure, consisting of a short amino (N)-terminal tail (34–58 aa), a transmembrane (TM) domain (19–24 aa) and a domain containing the tandem HxxCH DUF3328 active site motif, were manually annotated as putative DUF3328 proteins. Up to 10 genes up- and down-stream of the putative DUF3328-encoding gene in the MNH120 genome were then assessed for signatures of a classical dikaritin RiPP precursor-encoding gene (i.e. a gene that encodes a precursor peptide with an N-terminal signal peptide, followed by one or more perfect or imperfect tandem sequence repeats of at least 10 amino acids in length that are separated by putative kexin protease cleavage sites), and analysed for functional domains using InterproScan v5.51-85.0. Finally, to define the borders of *dikaritin RiPP* gene clusters, transcriptome data from this study were used to investigate the expression of genes encoding the DUF3328 domain-containing protein and putative precursor protein, as well as the surrounding genes. Only those genes with a similar *in planta* expression profile to the genes encoding the DUF3328 domain-containing protein and putative precursor peptide were considered to form part of the *dikaritin RiPP* gene cluster in question.

8. Appendix B: Beyond proteinaceous effectors - the role of fungal nutrition and secondary metabolism during host-infection

This appendix contains additional information relating to subcuticular host-colonization by *V. inaequalis* that was not included in the manuscript due to size constraints. Here, the results and discussion are condensed in a combined format. All results presented in this appendix are discussed in the context of Chapter 3.

8.1. Results and discussion

8.1.1. Genes encoding nutrient transporters peak in expression during mid-late infection

To better understand the general biology and nutritional requirements of *V. inaequalis* during colonization of the subcuticular environment, I investigated the expression profile of genes encoding fungal transporters, with a focus on nitrogen-associated transporters, adenosine triphosphate (ATP)-binding cassette (ABC) transporters, and major facilitator superfamily (MFS) transporters. Among the MFS transporters, the sugar transport family (PF0083) is the largest. As this family is likely associated with sugar nutrition, I refer to its members as sugar transporters from this point forward.

Early infection is divided into wave 1, which contains genes that peak in expression at 12 hpi, and wave 2, which contains genes that peak in expression at 12–24 hpi. During wave 1, only one transporter-encoding gene associated with nutrition (specifically, a nitrogen-associated transporter) was upregulated. The low number of upregulated genes encoding nutrient transporters during wave 1 indicates that, at 12 hpi, amino acid or sugar uptake is not a significant process. This is in line with a transcriptomic study in *M. oryzae* that reported that the number of genes encoding nitrogen transporters was low during early infection [175]. In addition, in *V. inaequalis*, four genes encoding non-nutritional transporters peaked on expression during wave 1, two genes

encoding MFS transporters and two genes encoding ABC transporters. The expression profile of these genes, together with the enriched GO-terms 'RNA-binding' and 'branched amino acids synthesis' during wave 1, suggests, that this wave represents a pre-infection stage, where the fungus is gearing up for infection, and genes associated with nutrition and detoxification of the host are not expressed yet.

During wave 2, the expression of genes encoding transporters associated with nutrition was still low, with only two sugar transporter genes expressed. However, six genes encoding nitrogen-associated transporters peaked in expression during wave 2. Most of these transporters belonged to the oligopeptide transporter (OPT) family (**Additional file 20: Figure B 3-1**), which transport different substrates such as small peptides, amino acids, and glutathione [176]. Additionally, these transporters can mediate sulfur uptake by taking up glutathione and they have been reported to be associated with stress tolerance [176,177]. Therefore, the transporters encoded by these genes could facilitate detoxification of the hostile subcuticular environment during early infection. No ABC transporter-encoding genes and only eight genes encoding MFS transporters were expressed during wave 2. The MFS transporters could play a role in detoxification of the host, as observed with an MFS-transporter from *M. oryzae* that detoxifies host-derived phytoalexins during early host-infection [178]. Interestingly, one of the expressed MFS transporters from *V. inaequalis* belonged to the multidrug and toxic compound extrusion (MATE) family. In bacteria, MATE transporters are associated with protection against ROS [179], and in *M. oryzae*, a MATE transporter has been found to regulate carbon metabolism [180].

During mid infection (wave 3), only two genes encoding sugar transporters and six genes encoding nitrogen-associated transporters peaked in expression. These genes encoding the nitrogen-associated transporters were mostly ammonium and nitrite transporters. Up-regulation of these genes likely reflects the scarcity of nitrogen available in the subcuticular environment and suggests the nitrogen starvation during host-colonization has started. Additionally, during wave 3,

there was an increase in the number of MFS transporter-encoding genes that peaked in expression and of these, two were annotated as trichothecene efflux pump proteins. Trichothecene is a mycotoxin produced by different fungal species and its synthesis has been well-studied in *Fusarium* spp. [181,182]. There is no evidence that *V. inaequalis* can produce trichothecene and the genes encoding these transporters did not locate in any of the identified secondary metabolite clusters (**Additional file 21: Figure B 3-2**). Of note, trichothecene efflux pump genes are abundant in the genomes of plant-pathogenic fungi and, intriguingly, many species with an expansion in trichothecene efflux pump-encoding genes do not have the biosynthetic machinery to produce this mycotoxin [181]. Therefore, these transporters could play a role during infection that is not associated with trichothecene biosynthesis, for example in protection against plant-derived toxins or mycotoxins produced by antagonistic microbes [181].

Later, at the start of mid-late infection, wave 4, there was a drastic increase in the number of genes encoding sugar and nitrogen-associated transporters that peaked in expression, suggesting a change in nutrition. The main nitrogen transporters encoded by genes with a peak of expression during wave 4 were OPT transporters, proton-dependent oligopeptide (POT) transporters, ammonium transporters and amino acid (aa) permeases (**Additional file 20: Figure B 3-1**). Interestingly, genes encoding aa permeases were almost exclusively expressed during mid-late infection (**Additional file 20: Figure B 3-1**). In *M. oryzae*, up-regulation of aa permease-encoding genes was observed under nitrogen starvation conditions [183], suggesting that during this stage of colonization by *V. inaequalis*, nitrogen is scarce. Additionally, the up-regulated genes encoding nitrogen transporters were co-expressed with six genes encoding aspartyl proteases; these proteases may degrade extracellular apple proteins to obtain oligopeptides that are then taken up by OPT transporters to be used as a nitrogen source. Co-regulation of genes encoding OPT transporters and aspartyl proteases has been reported in the human pathogen *Candida albicans* and the plant pathogen *U. maydis* [34,184].

Finally, during the late infection stage, wave 5, the high level of expression of genes encoding sugar and nitrogen-associated transporters observed in wave 4, was maintained. Additionally, during this infection stage, there was an increase in the number of genes encoding MFS and ABC transporters that peaked in expression (**Additional file 20: Figure B 3-1**). The large number of genes encoding MFS and ABC transporters with a peak in expression during wave 5 could be associated with the increased expression of genes associated with secondary metabolism (**Additional file 21: Figure B 3-2)**. Indeed, wave 5 corresponded to the last stage of biotrophic host-colonization, as apple leaves infected with *V. inaequalis* started to decay after 7 dpi. In line with this, *PCWDE* genes expressed during this late infection stage mainly encoded auxiliary activity (AA) enzymes. These AA enzymes may facilitate the maceration of the plant cell wall at the end of the biotrophic stage, following leaf senescence as a means of nutrition. A subset of cutinase-encoding genes were also expressed during late infection, which I anticipate may help *V. inaequalis* to rupture through the plant cuticle to enable the release of conidiospores from infection structures.

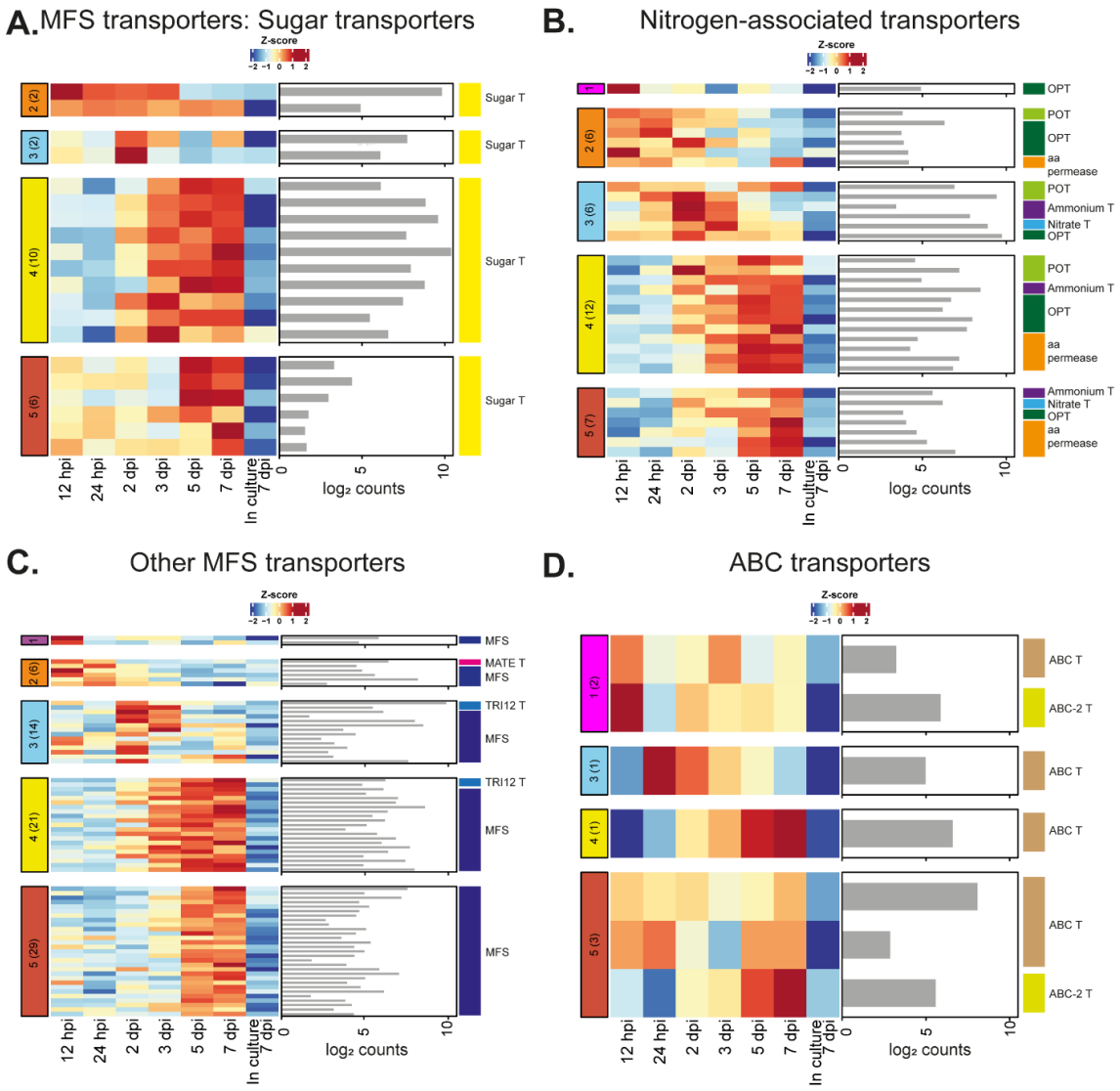

Additional file 20: Figure B 3-1. Expression profile of transporter-encoding genes from *Venturia inaequalis* during colonization of the apple cultivar 'Royal Gala', relative to the growth of the fungus in culture on the surface of cellophane membranes (CMs) overlying potato dextrose agar. A. Major facilitator superfamily (MFS) transporter belonging to the sugar transporter family (PF0083)**. B.** Nitrogen-associated transporters (PF13520: amino acid [aa] permease; PF03169: oligopeptide transporter [OPT]; PF01226: formate/nitrite transporter; PF00909: ammonium transporter; PF00854: proton-dependent oligopeptide transporter [POT]). **C.** MFS transporters not associated with sugar transport (PF07690: MFS; PF06609: fungal trichothecene efflux pump [TRI12]; PF01554: Multi Antimicrobial Extrusion/Multidrug and Toxin Extrusion [MATE] transporter). **D.** Adenosine triphosphate (ATP)-binding cassette (ABC) transporters (PF00005: ABC transporter; PF00664: ABC transporter type 1; PF01061: ABC-2 type transporter; PF19055: ABC-2 type transporter). Gene expression data are scaled rlog-normalized counts across all samples (Z-score), averaged from four biological replicates. Bar plots depict the maximum $\log_2$ DESeq2-normalized count value across all *in planta* time points. Coloured block labels on the left indicate gene expression waves and numbers in brackets indicate number of genes per wave. Labels on the right indicate transporter classification. dpi: days post-inoculation, hpi: hours post-inoculation.

Next, I performed an analysis of genes putatively associated with secondary metabolism. To identify putative secondary metabolite gene clusters in the *V. inaequalis* genome, antiSMASH v6.0.1 [185-190] was used. A total of 26 putative secondary metabolite gene clusters were identified and, of these, only seven were up-regulated during host-colonization. Remarkably, most of these genes peaked in expression during late infection (**Additional file 21: Figure B 3-2**). The up-regulated genes belonged to two NRPS-like clusters, two T1PKS clusters, two indole clusters, and one siderophore cluster (**Additional file 21: Figure B 3-2**). The core biosynthetic gene from the NRPS-like cluster (*g17828*) was the most highly expressed secondary metabolite gene during host infection, with a peak of expression during wave 5 (**Additional file 21: Figure B 3-2**). This gene encodes a protein with an N-terminal 'adenosine monophosphate (AMP)-binding' domain and a carboxyl (C)-terminal 'phosphopantetheine (PP)-binding' domain that is likely an acetyl-CoA synthase based on BLASTp similarity searches. Given that acetyl-CoA is an important precursor for secondary metabolism, this enzyme is likely crucial for *V. inaequalis* infection. Interestingly, in *Gibberella zeae*, deletion of an acetyl-CoA-like synthetase gene affected sexual reproduction [191], suggesting that this enzyme could be necessary to produce secondary metabolites required for the start of sexual reproduction by *V. inaequalis* at the end of its biotrophic phase. The second most highly expressed core biosynthetic gene was *g5336*, which forms part of a T1PKS secondary metabolite gene cluster. This gene is highly expressed during late infection (**Additional file 21: Figure B 3-2**) and, based on a BLASTp analysis, likely encodes a polyketide synthase.

The low expression of genes putatively associated with secondary metabolites during early and mid host-colonization is in line with the biotrophic nature of *V. inaequalis*. In contrast with necrotrophic fungi that produce secondary metabolites to induce cell death and obtain nutrients [192,193], *V. inaequalis* appear to only express secondary metabolites towards the end of the biotrophic infection stage. Indeed, many biotrophic fungal pathogens, such as *F. fulva*, have been

observed to express genes associated with secondary metabolites to a low level during host-colonization [194]. Potentially, many of the *V. inaequalis* genes associated with secondary metabolism expressed during late infection could play a role in shaping microbial communities in preparation for saprobic growth inside fallen leaf litter, as hypothesized for RIPPs in Chapter 3 [195].

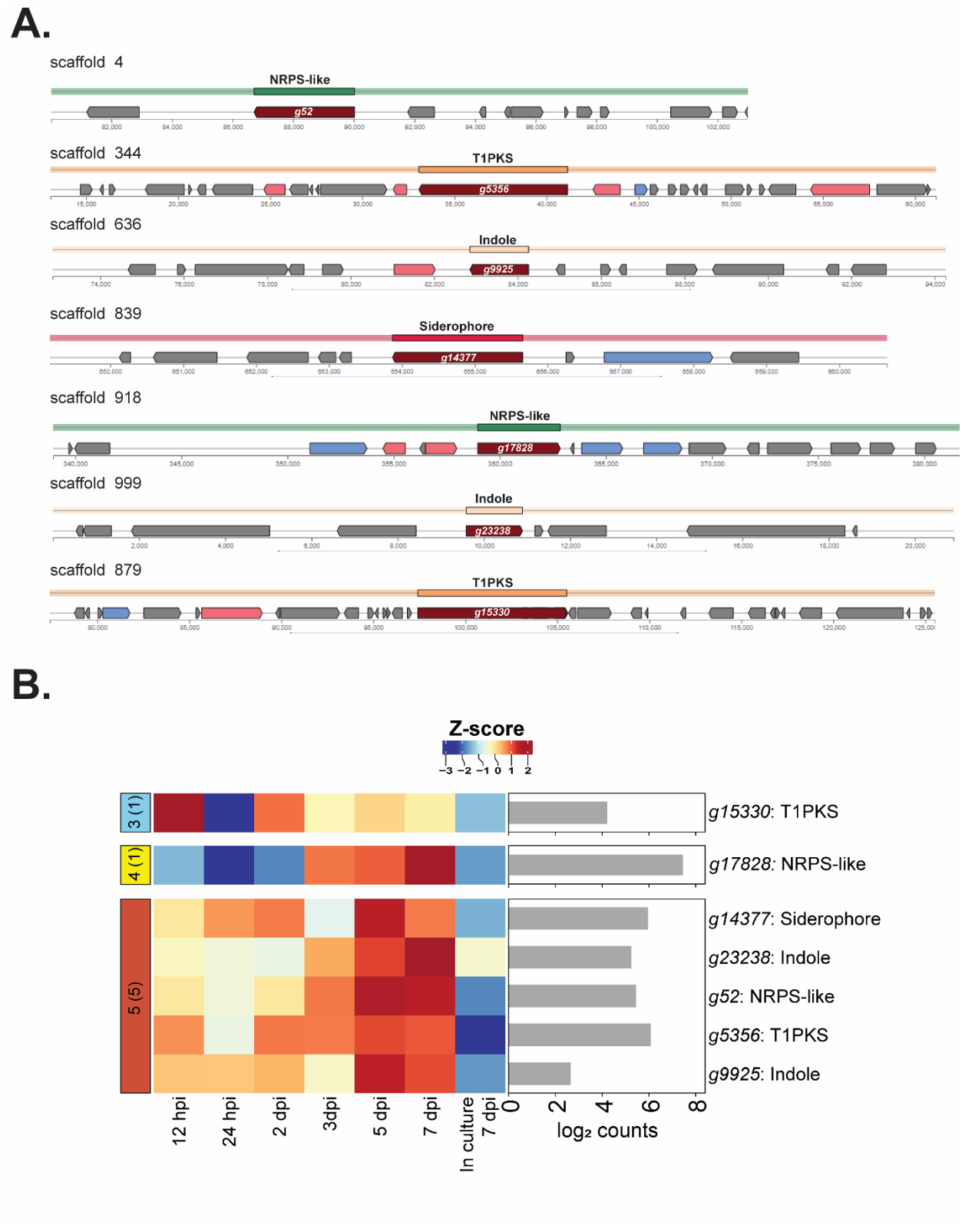

Additional file 21: Figure B 3-2. Secondary metabolite clusters of *Venturia inaequalis* that are up-regulated during colonization of apple cultivar 'Royal Gala', relative to the growth of the fungus in culture on the surface of cellophane membranes (CMs) overlying potato dextrose agar. A. Genome location of the up-regulated secondary metabolite gene clusters in the *V. inaequalis* MNH120 genome [19]. Dark red: biosynthetic gene; pink:

secondary biosynthetic gene; blue: transporter gene; grey: other genes (no annotation). Secondary metabolite clusters were predicted by antiSMASH v6.0.1 for fungi. **B.** Expression of the core secondary metabolite biosynthetic genes from *V. inaequalis* that are up-regulated during colonization. Heatmap gene expression data are scaled rlog-normalized counts across all samples (Z-score), averaged from four biological replicates. Bar plot annotation depicts the maximum $\log_2$ DESeq2-normalized count value across all *in planta* time points. NRPS-like: non-ribosomal peptide-synthetase; T1PKS: Type I polyketide synthase. dpi: hours post-inoculation; hpi: hours post-inoculation. Coloured block labels on the left indicate gene expression waves and numbers in brackets indicate number of genes per wave.

9. Appendix C: Towards the functional characterization of the *V. inaequalis* Nod19 EC family

This appendix contains preliminary data towards the functional characterization of the Nod19 EC family from *V. inaequalis*.

9.1. Results and discussion

9.1.1. The potential role of the Nod19 EC family modulating ROS during host-colonization

The *Nod19* family, identified in Chapter 3, is an EC family expanded in *V. inaequalis.* Members of this EC family had an annotated 'Stress-up regulated Nod19' domain of unknown function. Proteins with a Nod19 domain are commonly found and widely distributed in plants [77] and oomycetes (**Additional file 22: Figure C 3-1. A, C**). However, in fungi, these proteins are only found in selected species of the phylum Ascomycota, mostly from the Dothideomycetes class. Interestingly, genes with an annotated Nod19 domain appear to be exclusively expanded in *Venturia* spp. and these genes are not found in other well-known fungal pathogens (**Additional file 22: Figure C 3-1. B**). The phylogenetic distribution of the genes encoding these proteins in phylum Ascomycota does not suggest that they were acquired by horizontal gene transfer (**Additional file 22: Figure C 3-1. A**). In *V. inaequalis*, the Nod19 family had 39 annotated members and of those, 21 were encoded by genes that peaked in expression during early host-colonization (waves 1 and 2) (**Additional file 23: Figure C 3-2**). The observation that this EC family was almost exclusively expressed during early host-colonization, suggests that it could play an important role during early infection.

Alignment of Nod19 EC family members from *V. inaequalis* with Nod19 domain-containing proteins from apple (*M. x domestica*) and the potato late blight oomycete *Phytophthora*

infestans revealed that, although these proteins were quite diverse at the amino acid level, they all contained the conserved H-X-H-X-GG-X motif (**Additional file 24: Figure C 3-3. A).**

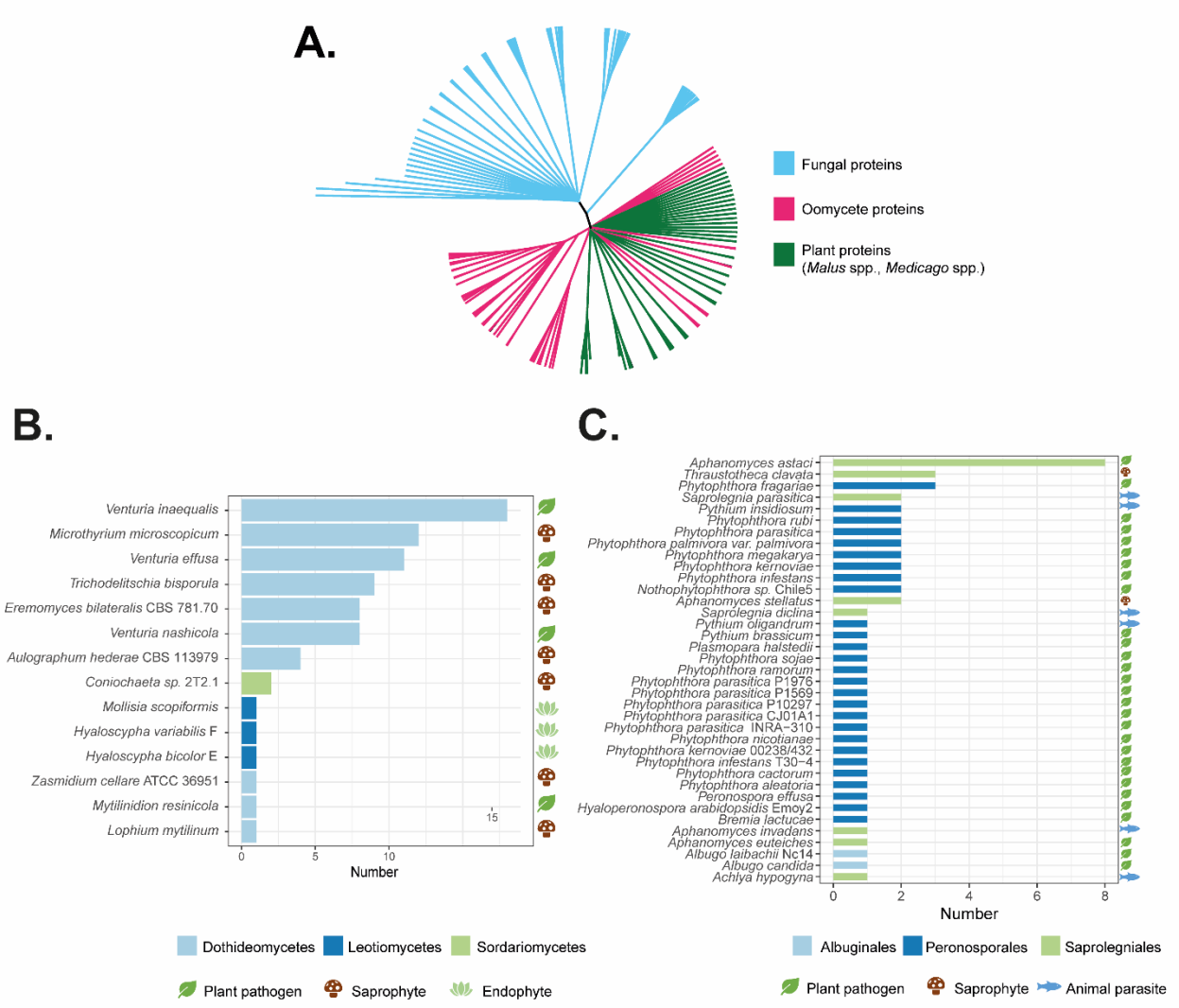

Additional file 22: Figure C 3-1. Phylogenetic distribution of Nod19 protein with a 'Stress-upregulated Nod19' domain. A. Phylogenetic tree of Nod19 proteins from fungi (phylum Ascomycota), oomycetes and plants from the *Malus* and *Medicago* genera. Phylogenetic tree generated using the Geneious tree builder software from Geneious v.9.1.8 with clustering method: neighbor-joining, resampling method: bootstrap**.** Number of proteins with an annotated 'Stress-upregulated Nod19' domain (Pfam: PF07712, InterPro: IPR011692) in **B.** Ascomycetes and **C.** Oomycetes. Domain distributions based on the InterPro database [196]. Lifestyle classification based on current literature. Note that some species are not well studied, and some species classified as saprophyte here, have an unclear lifestyle.

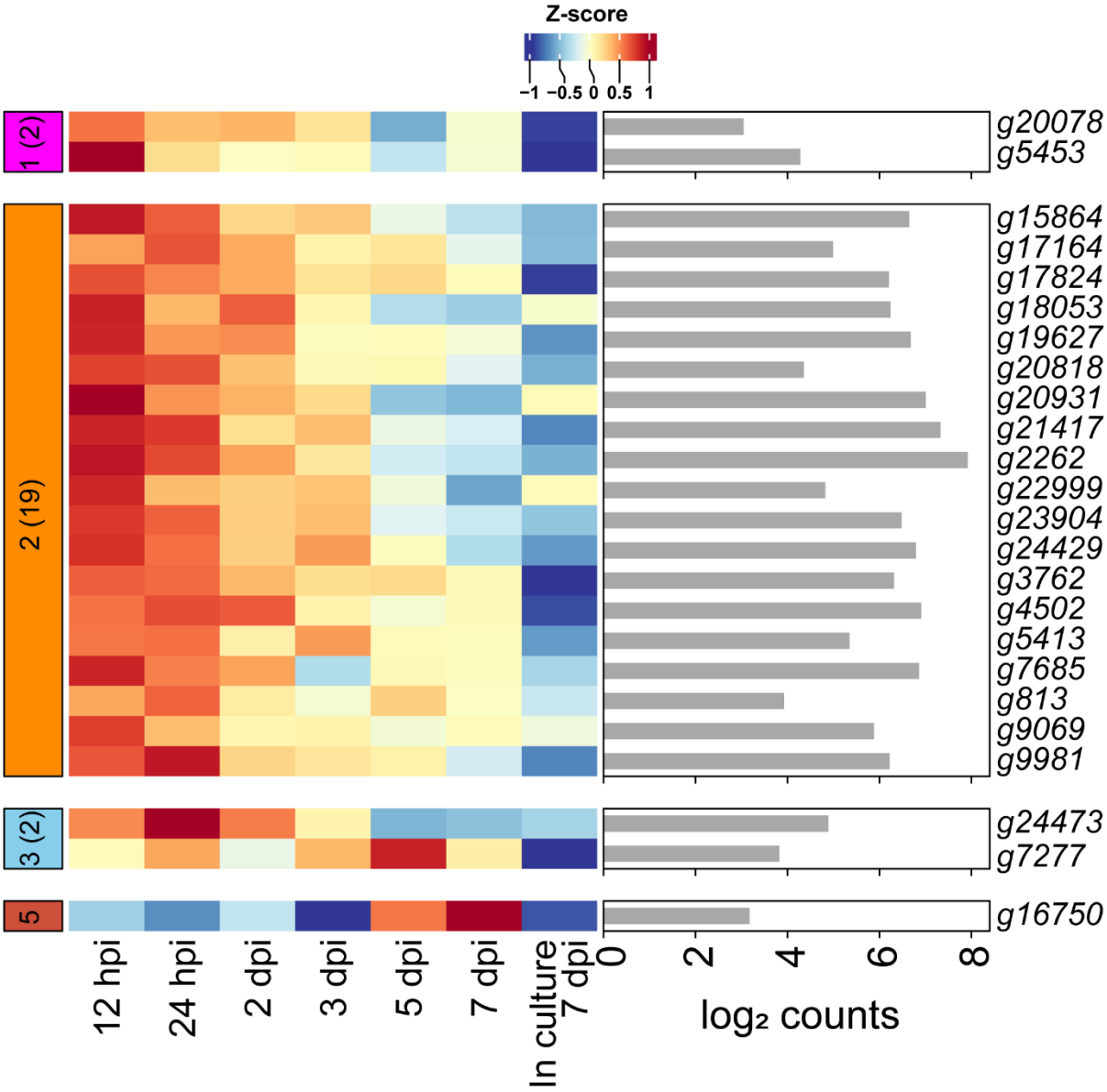

Additional file 23: Figure C 3-2. Heatmap of *Nod19 EC* genes up-regulated during colonization of susceptible apple cultivar 'Royal Gala', relative to growth of the fungus in culture on the surface of cellophane membranes (CMs) overlying potato dextrose agar. Heatmap gene expression data are scaled rlog-normalized counts across all samples (Z-score), averaged from four biological replicates. Bar plot annotation depicts the maximum $\log_2$ DESeq2-normalized count value across all *in planta* time points. dpi: days post-inoculation; hpi: hours post-inoculation.

Tertiary structure predictions of the representative Nod19 member from *V. inaequalis*, as well as a representative protein from *M. x domestica* and *P. infestans*, showed that all proteins had a predicted dual domain structure composed of two β-barrels (**Additional file 24: Figure C 3-3. B**). To shed light on the putative function of these proteins, I searched for proteins with a similar

structure in the public protein database using the Dali server. The predicted structures of the Nod19 proteins were found to be analogous to different peptidyl-glycine α-amidating monooxygenases from animal and bacterial species. Monoxygenase enzymes are metalloproteins that catalyse reactions using redox-active metals [197]. Interestingly, cytochrome P450 monooxygenases have been shown to be associated with ROS scavenging [198] and in *V. dahliae*, a cytochrome P450 monooxygenase was shown to promote host-colonization by scavenging ROS [199]. Altogether, these findings suggest that members of the *V. inaequalis* Nod19 EC family could be metalloenzymes that promote host-colonization by directly or indirectly manipulating ROS to suppress the oxidative burst associated with plant defence.

To test whether *V. inaequalis* Nod19 proteins could manipulate ROS, the three most highly expressed members of the *V. inaequalis Nod19* family were overexpressed in *Nicotiana benthamiana* using *Agrobacterium tumefaciens*-mediated transient transformation. The *V. inaequalis* Nod19 proteins have a predicted signal peptide, and thus are expected to function in the apoplast. Therefore, for expression in *N. benthamiana*, the *Nod19* proteins were fused to the *Nicotiana tabacum* PR1α signal peptide for delivery into the plant apoplast, and an N-terminal 3xFLAG tag for detection of the proteins via Western blot. The GFP-labelled Avr3a effector from *P. infestans*, which is a protein that has been shown to inhibit the oxidative burst during host infection [200] was used as a positive control,while the PR1α-3xFLAG-green fluorescent protein (GFP) was used as a negative control. Constructs were transformed into *N. benthamiana* by infiltration of *A. tumefaciens*, and after 48 h, plant defence responses were elicited by infiltration of PR1α-3xFLAG-INF1, as INF1 from *P. infestans* is a well-known elicitor of plant defences [201]. To detect ROS generated by INF1 elicitation, leaves were stained using 3, 3'-diaminobenzidine (DAB). As a starting point, DAB staining revealed that none of the PR1α-3xFLAG-Nod19 proteins, the negative PR1α-3xFLAG-GFP control, or the GFP-Avr3a positive control elicited a ROS burst alone (**Additional file 25: Figure C 3-4. A**). However, after infiltration with INF1, an oxidative

burst (ROS production) associated with plant defences was observed. In 38% of the samples elicited with INF1, the positive control GFP-Avr3a, gave only weak DAB staining, indicative of ROS inhibition (**Additional file 25: Figure C 3-4. A**). This low percentage of ROS inhibition by the positive control highlights the variability an unreliability of this assay. On some occasions where the positive control worked, the most highly expressed Nod19 member (Nod19#1) also displayed a weaker DAB staining, suggestive of oxidative burst inhibition (**Additional file 25: Figure C 3-4. A**). However, the ROS inhibition percentage observed for Nod19#1 ranged from 60–15% across biological replicates. Therefore, the putative ROS inhibition by Nod19#1 was not consistent (**Additional file 25: Figure C 3-4. A**). All proteins, except the positive control GFP-Avr3a, could be detected by Western blot (**Additional file 25: Figure C 3-4. B**). It is important to note that the GFP-Avr3a protein has been observed to be functional and was detected by Western Blot in a previous study [207]. Therefore, the lack of detection of the GFP-Avr3a positive control here is likely due to antibody problems, as the anti-GFP antibody used has low binding affinity. Remarkably, Nod19#1 appeared to be the most stable protein, as only one band of the expected size (41 kDa) was observed (**Additional file 25: Figure C 3-4. B**). In contrast, multiple bands for Nod19#2 protein were observed, and one band of the expected size (46 KDa) was observed for Nod19#3 in addition to a slightly bigger band. In all cases, the INF1 elicitor protein was detected (**Additional file 25: Figure C 3-4. B**).

Given that the DAB staining results were inconsistent, and that this assay is not quantitative, I next quantified ROS using luminol-based chemiluminescence after plant defence elicitation with chitin fragments. In this assay, I only investigated Nod19#1, as it was the only Nod19 protein displaying putative ROS inhibition based on the DAB staining. As a positive control, I attempted to use Ecp6 from *F. fulva* overexpressed in *N. benthamiana*, as this effector has been shown to inhibit chitin-triggered immunity [202]. The PR1α-3xFLAG-Nod19#1 construct, the positive control PR1α-3xFLAG-Ecp6 and the negative control PR1α-3xFLAG-GFP

were overexpressed in *N. benthamiana* by *A. tumefaciens* transient expression transformation. After 48h, *N. benthamiana* leaf discs overexpressing each construct of interest were harvested and plant defences were elicited by the addition of chitin to induce an oxidative burst. Surprisingly, I did not observe any ROS inhibition by the Ecp6 or Nod19#1 proteins (**Additional file 25: Figure C 3-4. C**). It should be noted that previous studies used purified protein to assess suppression of chitin-triggered immunity by Ecp6, instead of overexpressing the gene in *N. benthamiana* [202]. Therefore, the lack of ROS inhibition by Ecp6 in this assay could be due to insufficient protein production. Additionally, I attempted to use the Pep1 effector from *U. maydis* as an alternative positive control, as this effector is known to inhibit host peroxidases [203]. However, ROS inhibition assays by Pep1 do not work when the gene is overexpressed in *N. benthamiana* (personal communication, Prof. Gunther Doehlemann). Therefore, this luminol-based assay was inconclusive due to the lack of an appropriate positive control. Therefore, it is suggested that purified protein needs to be used to perform luminol-based ROS inhibition assays in any future Nod19-based experiments. Additionally, it is also possible that the target of Nod19 proteins required for the manipulation of ROS in apple is not present in *N. benthamiana.* Therefore, it would be beneficial to perform a ROS inhibition assay in apple, for instance by using apple leaf discs. Another important step towards the characterization of the Nod19 EC family is to study its contribution to virulence during host-colonization. Deletion of some of the most highly expressed members could be performed with the recently developed CRISPR-Cas9 technology for *V. inaequalis* (see **Chapter 5**). However, given the large number of family members in the Nod19 EC family, functional redundancy among members is expected. Another alternative could be to overexpress some of the *Nod19* EC genes in *V. inaequalis* and investigate if there is an impact on the virulence of this fungus during host-colonization.

In conclusion, more experimental work is needed to unravel the function of the Nod19 EC family from *V. inaequalis*. Once the function is elucidated, it would be interesting to determine if

this function is conserved across the oomycete and the plant Nod19 proteins. Potentially, these Nod19 proteins could share a conserved function and some plant pathogens could be mimicking the function of the plant Nod19 proteins to contribute to virulence.

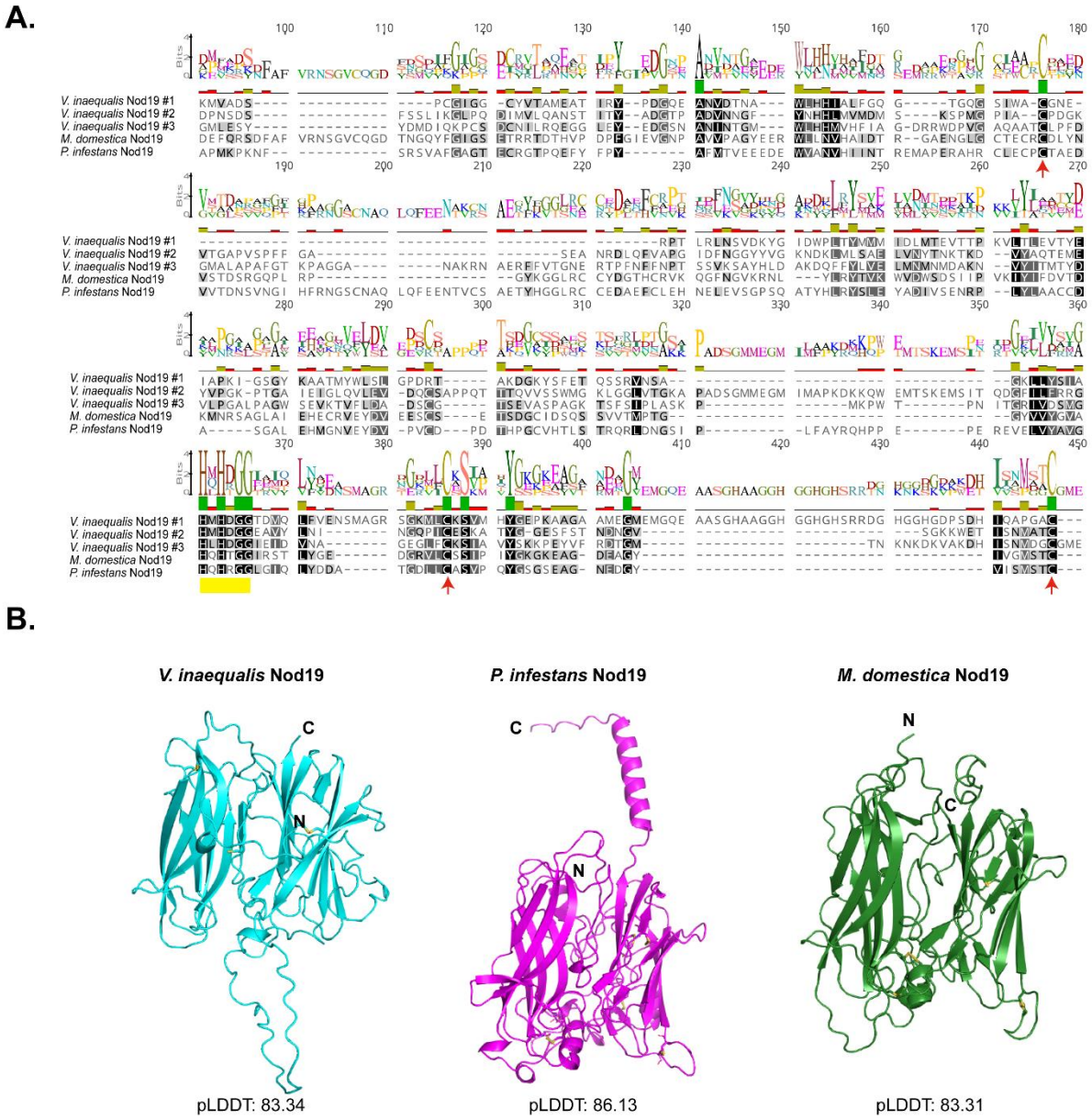

Additional file 24: Figure C 3-3. Proteins with a 'Stress-upregulated Nod19' domain are present in oomycetes, plants and fungi from the phylum Ascomycota. A. Alignment of three Nod19 proteins from *Venturia inaequalis* (Nod19#1: g2262, Nod19#2: g4502, Nod19#3: g7685; encoded by the most highly expressed *Nod19* genes during infection of apple), *Malus x domestica* (Mdg_14A013850) and *Phytophthora infestans* (rna12209). Identical amino acids are coloured in black and similar amino acids are coloured in grey. **B.** Nod19 protein structures of Nod19#1, *M. x domestica* and *P. infestans* Nod19s from A. were predicted by Alphafold2. In both A. and B. mature protein sequences (i.e. without their amino [N]-terminal signal peptide) were used.

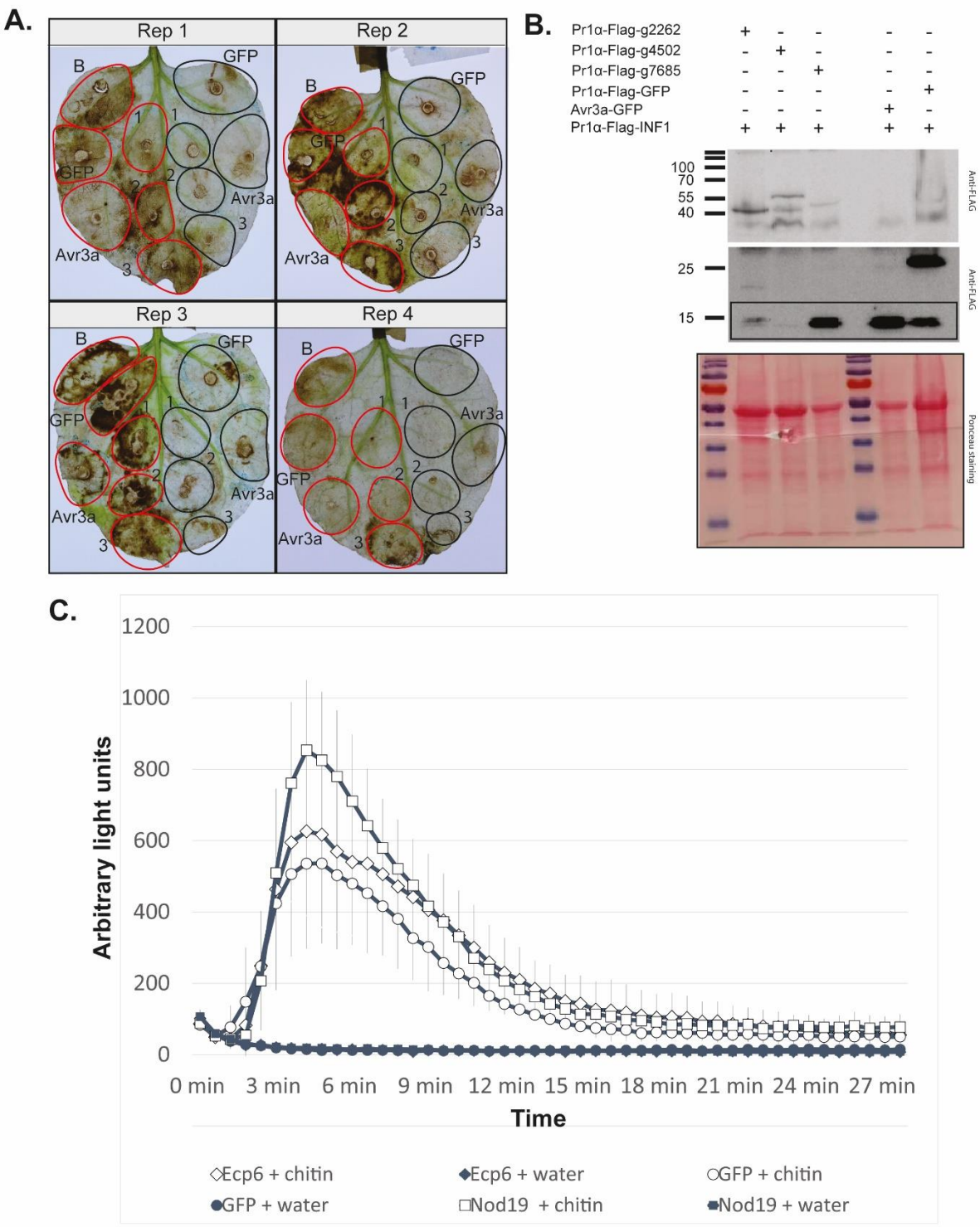

Additional file 25: Figure C 3-4. The putative role of the Nod19 EC proteins in scavenging ROS remains elusive. **A.** *Nicotiana benthamiana* leaves expressing the PR1α-3xFLAG-g2262 (Nod19 #1) (1), PR1α-3xFLAG-g4502 (Nod19 #2) (2), PR1α-3xFLAG-g7685 (Nod19 #3) (3), PR1α-3xFLAG-GFP (GFP), GFP-Avr3a (Avr3a) protein constructs using *Agrobacterium tumefaciens*-mediated transient transformation assays. Right side of the leaf shows expression of the protein constructs of interest (black circles) alone (i.e. as a control to show that the protein constructs alone do not induce reactive oxygen species [ROS] production). Left side of the leaf shows expression of the protein

constructs of interest in conjunction with PR1α-3xFLAG-INF1 (i.e. the elicitor of ROS production) 48 hours post-infiltration (red circles). Detection of ROS (H_2O_2) accumulation in *N. benthamiana* was performed by 3,3'-diaminobenzidine (DAB) staining at 72 hours post-infiltration of the constructs of interest and 24 hours post-infiltration of the INF1 elicitor. Pictures are representative of each biological replicate; total number of technical replicates (n): 84. **B.** Western blot (WB) with anti-Flag antibody showing production of the proteins of interest and the elicitor INF1 in *N. benthamiana*. The protein GFP-Avr3a could not be detected by WB with the α-GFP antibody (not shown). The total protein load in the WB is shown by ponceau staining. Expected size of PR1α-3xFLAG-g2262: 41.45 KDa, PR1α-3xFLAG-g4502: 45.05 KDa, PR1α-3xFLAG-g7685: 46.35 KDa, PR1α-3xFLAG-GFP: 32 KDa, PR1α-3xFLAG-INF1: 16 KDa, GFP-Avr3a: 44 KDa. **C.** ROS production quantified using luminol-based chemiluminescence for 60 minutes (only 30 minutes shown) following elicitation of *N. benthamiana* leaf discs expressing the constructs of interest (PR1α-3xFLAG-g2262 (□), PR1α-3xFLAG-Ecp6 (◇), PR1α-3xFLAG-GFP (○)) with 10 nM chitin (white fill) or water (grey fill). Data plotted from three independent biological replicates with eight leaf discs each; n: 24. Error bars display standard deviation. Note that the PR1α-3xFLAG-g2262 protein construct appears to display a higher amount of ROS after elicitation of plant defences; however, this was not significant given the large standard deviation.

9.2. Material and methods

9.2.1. Phylogenetic analysis of the Nod19 domain

To investigate the phylogenetic distribution of proteins with a 'Stress-upregulated Nod19' domain, amino acid sequences of proteins annotated with this domain in the InterPro database were downloaded (August, 2022) [196]. Specifically, all sequences from oomycetes and members of the fungal kingdom were downloaded. Given the large number of proteins with an annotated 'Stress-upregulated Nod19' domain in plants, only proteins from the *Medicago* (where the initial Nod19 studies have been performed) and *Malus* genera, were downloaded. All protein sequences were aligned using the MUSCLE plug in from Geneious v.9.1.8 and a phylogenetic tree was generated using the Geneious tree builder software in conjunction with the clustering neighbor-joining and resampling bootstrap methods. A figure with the frequency of Nod19 proteins across fungal, oomycete and plant species was generated using the annotated proteins identified in the InterPro database with ggplots2 v3.3.5 [156].

9.2.2. cDNA synthesis

RNA of *V. inaequalis* colonizing susceptible apple leaves at 12 hpi and 24 hpi was extracted as described in section 6.4 of this chapter. RNA was mixed in a 1:1 ratio and used for cDNA synthesis. cDNA synthesis was performed using 10 µg RNA as template and the QuantiTect Reverse Transcription Kit (Qiagen, Hilden, Germany) following manufacturer's instructions. Genomic DNA (gDNA) was removed using the gDNA Wipeout Buffer from the same QuantiTect kit.

9.2.3. Agrobacterium tumefaciens-*mediated transient transformation assays*

The three most highly expressed *V. inaequalis Nod19* genes (*g2262*, *g4502*, *g7685*) were amplified from cDNA generated in section 9.2.2, using primers listed in **Table C 3-1**. Then, the *Nod19* genes and a *PR1α -FLAG* fragment (synthesized by Integrated DNA Technologies, IDT) were used as fragments for Golden Gate assembly [204] for cloning into the *Agrobacterium* expression vector pICH86988 [205]. Constructs were verified by sequencing using the Massey Genome Service (Massey University, Palmerston North, New Zealand) and were transformed into *A. tumefaciens* GV3101 [206]. For the ROS inhibition assays, overnight cultures of *A. tumefaciens* GV3101 carrying the construct of interest were grown in lysogeny broth (LB) with the appropriate antibiotics at 28 ºC. Then, cells were resuspended in infiltration buffer (10 mM MgCl2:6H_2O, 10 mM MES-KOH pH 5.6, 100 µM acetosyringone) to a final OD_{600} of 0.4 and were infiltrated into fully expanded leaves of 5 week-old *N. benthamiana* plants. For DAB staining, *N. benthamiana* leaves expressing the genes of interest (48 h) were infiltrated with an *A. tumefaciens* strain carrying pICH86988: *PR1α-FLAG-INF1* construct [207], to express the well-known elicitor gene *INF1* [201]. The pICH86988: *PR1α -FLAG-GFP* construct [208] was used as a negative control, while the pICH86988*:GFP-Avr3a* construct was used as a positive control, as Avr3a has been shown to inhibit the oxidative burst during host infection [200].

Table C 3-1. Oligonucleotides used in this study. Bold sequence corresponds to the Bsa*I* restriction site and underlined sequence corresponds to the Golden Gate overhangs for cloning into pICH86988 plasmid.

Oligonucleotide name	Oligonucleotide name (5'-3')	Construct name
MR260	**GGTCTC**CCAAGCCTCTCGCTGAGGTGGCC	*PR1α -FLAG-g2262*
MR261	**GGTCTC**AAAGCTTAAGTAGGACCGACGTA	*PR1α -FLAG-g2262*
MR262	**GGTCTC**CCAAGGCACCAGCAGCAAATGAG	*PR1α -FLAG-4502*
MR263	**GGTCTC**AAAGCTTACATCTTAGGCTGAGG	*PR1α -FLAG-g4502*
MR266	**GGTCTC**CCAAGGCGCCGGCAAACGAGAAG	*PR1α -FLAG-g7685*
MR267	**GGTCTC**AAAGCCTAGGCTCCGGGATATTT	*PR1α -FLAG-g7685*

9.2.4. DAB staining and luminol-based ROS assay

A 1 mg/ml DAB (Sigma-Aldrich) solution in 10 mM Na_2HPO_4 was prepared as previously described [209]. For each biological replicate, the DAB staining solution was prepared fresh and kept on the dark. For staining, *N. benthamiana* leaves infiltrated with the *A. tumefaciens* strains carrying the construct of interest were harvested at 72 hours post-infiltration, submerged in DAB staining solution, and vacuum-infiltrated for 20 minutes in the dark, two times. Then, leaves were incubated overnight in the DAB staining solution with slow shaking at room temperature. The next morning, leaves were de-stained by boiling in 95% ethanol until the chlorophyll was removed.

For the luminol-based chemiluminescence assay, leaf discs (~4 mm) were carefully harvested from *N. benthamiana* leaves 48 hours post-infiltration carefully, so as not to damage the plant tissue. Importantly, to avoid variation in ROS production between leaves, leaf discs for all samples and technical controls were harvested from the same leaf. Leaf discs were soaked in 100 µl distilled water overnight in a white OptiPlate-96 well plate (PerkinElmer, Waltham, United States). The next morning, the water was carefully removed, and samples were elicited by the addition of a 100 µl of elicitor master mix: 10 mM chitohexose $(GlcNAc)_6$ (IsoSep AB, Tullingen, Sweden), 100 µM luminol (Sigma-Aldrich) and 20 µg/ml horseradish peroxidase (HRP) (Sigma-

Aldrich). For the blank controls, 100 µl of control master mix: 100 µM luminol and 20 µg/ml HRP, without the elicitor was added. Immediately, following this step, luminol signal was measured using a POLARstar Omega plate reader (BMGLabtech, Ortenberg, Germany), with signal measured every 36 seconds for 60 minutes.

9.2.5. Crude protein extraction

To extract total protein from *N. benthamiana* leaves, half leaves were frozen in liquid nitrogen and ground to a fine powder. Then, GTEN extraction buffer (10% v/v glycerol, 0.1 M (v/v) Tris-HCl (pH 7.5), 1 mM (v/v) EDTA, 150 mM (w/v) NaCl) plus 10 mM (v/v) dithiothreitol (DTT) (Sigma-Aldrich), 0.1% (v/v) Tween20 (Ajax Fine Chemicals)) was added to a 1:1 ratio with plant tissue as well as 10 µl/ml protease inhibitory cocktail (Sigma-Aldrich), and 2% (w/v) polyvinylpolypyrrolidone (PVPP) (Sigma-Aldrich). Samples were incubated at 4°C rotating at 60 rpm for 30 min and centrifuged at 5,000 *g* for 20 min to remove plant debris. Finally, the supernatant was filtered through miracloth (Merck) and transferred to a fresh tube. The protein extraction was concentrated to an approximate final volume of 200 µl using a SpeedVac concentrator (Thermo Fisher Scientific).

9.2.6. SDS page and Western blot

Proteins samples were mixed in a 2:1 ratio with 3 x SDS loading dye (30% v/v glycerol, 3% w/v SDS, 94 mM v/v Tris (pH 7.5), 0.05% w/v bromophenol blue, 24 mM v/v DTT) and proteins were resolved in a 10% resolution gel (10.2% (v/v) acrylamide (Bio-Rad), 390 mM Tris (v/v) (pH8.8), 0.1% SDS (v/v), 0.1% (v/v) ammonium persulfate, 0.04% (v/v) tetramethylethylenediamine TEMED (Sigma-Aldrich) and a 5% stacking gel (5.1% (v/v) acrylamide, 130 mM (v/v) Tris (pH 6.8), 0.1% (v/v) SDS, 0.1% (v/v) ammonium persulfate, 0.001% (v/v) TEMED).

After the SDS-PAGE, proteins were electrophoretically transferred (30 V, 4°C, overnight) to a polyvinylidene fluoride (PVDF) membrane (Bio-Rad) that was previously activated in 100% (v/v) methanol. The next day, the membrane was blocked using 5% blocking solution (20 mM (v/v) Tris, 136 mM (v/v) NaCl, 10% (v/v) Tween, 5% (w/v) skim milk) for 1.5 h at room temperature. For FLAG detection, membranes were immunolabelled with 1:5,000 dilution of the monoclonal anti-FLAG® M antibody (Sigma-Aldrich) for 1 h at room temperature. The secondary antibody (chicken anti-mouse, produced by Santa Cruz Biotechnology, Texas, USA) was added to the membrane at a 1:20,000 ratio and incubated for 1 h at room temperature. For GFP detection, the membrane was incubated with 1:1,000 dilution anti-GFP antibody (Santa Cruz Biotechnology) for 1.5 h at room temperature and incubated with the secondary antibody (chicken anti-mouse; Santa Cruz Biotechnology) with a 1:10,000 dilution for 1 h at room temperature. Finally, the membrane was washed and it was incubated 5 minutes with 0.8 mL of SuperSignal® West Dura Extended Duration substrate (Thermo Fisher Scientific). Western blot was visualised using an Azure Biosystems c600 Bioanalytical Imaging system (Azure Biosystems, CA, USA).

10. Appendix D: Statement of contribution doctorate with publications/manuscripts (DRC16)

We, the candidate and the candidate's Primary Supervisor, certify that all co-authors have consented to their work being included in the thesis and they have accepted the candidate's contribution as indicated below in the *Statement of Originality*.

Name of candidate:	Mercedes Rocafort Ferrer
Name/title of Primary Supervisor:	Carl H. Mesarich
Name of Research Output and full reference:	
The Venturia inaequalis effector repertoire is expressed in waves and is dominated by expanded families with predicted structural similarity to avirulence proteins from other plant-pathogenic fungi	
In which Chapter is the Manuscript /Published work:	Chapter 3
Please indicate:	
• The percentage of the manuscript/Published Work that was contributed by the candidate:	70
and	
• Describe the contribution that the candidate has made to the Manuscript/Published Work:	
The candidate performed all bioinformatic analyses, generated all figures and tables, and wrote the manuscript draft (which was subsequently edited by co-authors). The candidate did not perform the sample preparation and RNA extractions required for the RNA-seq experiment. Likewise, the candidate did not perform the bright-field microscopy.	
For manuscripts intended for publication please indicate target journal:	
BMC Biology	
Candidate's Signature:	Mercedes Rocafort Ferrer Firmado digitalmente por Mercedes Rocafort Ferrer Fecha: 2022.09.23 09:26:18 +02'00'
Date:	23/09/2022
Primary Supervisor's Signature:	Carl Mesarich Digitally signed by Carl Mesarich Date: 2022.09.23 19:44:48 +12'00'
Date:	23/09/2022

Chapter 3_ DRC 16 - V3 Online Statement (

11. References

1. Ristaino JB, Anderson PK, Bebber DP, Brauman KA, Cunniffe NJ, Fedoroff NV, Finegold C, Garrett KA, Gilligan CA, Jones CM, et al.: **The persistent threat of emerging plant disease pandemics to global food security**. *Proceedings of the National Academy of Sciences* 2021, **118**:e2022239118.
2. Cook DE, Mesarich CH, Thomma BPHJ: **Understanding plant immunity as a surveillance system to detect invasion**. *Annual Review of Phytopathology* 2015, **53**:541-563.
3. Saijo Y, Loo EPi, Yasuda S: **Pattern recognition receptors and signaling in plant–microbe interactions**. *The Plant Journal* 2018, **93**:592-613.
4. Lo Presti L, Lanver D, Schweizer G, Tanaka S, Liang L, Tollot M, Zuccaro A, Reissmann S, Kahmann R: **Fungal effectors and plant susceptibility**. *Annual Review of Plant Biology* 2015, **66**:513-545.
5. Rovenich H, Boshoven JC, Thomma BPHJ: **Filamentous pathogen effector functions: of pathogens, hosts and microbiomes**. *Current Opinion in Plant Biology* 2014, **20**:96-103.
6. Bolton MD: **Primary metabolism and plant defense—Fuel for the fire**. *Molecular Plant-Microbe Interactions* 2009, **22**:487-497.
7. Bradley EL, Ökmen B, Doehlemann G, Henrissat B, Bradshaw RE, Mesarich CH: **Secreted glycoside hydrolase proteins as effectors and invasion patterns of plant-associated fungi and oomycetes**. *Frontiers in Plant Science* 2022, **13**.
8. Lolle S, Stevens D, Coaker G: **Plant NLR-triggered immunity: from receptor activation to downstream signaling**. *Current Opinion in Immunology* 2020, **62**:99-105.
9. Bowen JK, Mesarich CH, Bus VG, Beresford RM, Plummer KM, Templeton MD: ***Venturia inaequalis*: the causal agent of apple scab**. *Molecular Plant Pathology* 2011, **12**:105-122.
10. Jha G, Thakur K, Thakur P: **The *Venturia* apple pathosystem: pathogenicity mechanisms and plant defense responses**. *Journal of Biomedicine and Biotechnology* 2009, **2009**:680160.
11. Kucheryava N, Bowen JK, Sutherland PW, Conolly JJ, Mesarich CH, Rikkerink EH, Kemen E, Plummer KM, Hahn M, Templeton MD: **Two novel *Venturia inaequalis* genes induced upon morphogenetic differentiation during infection and *in vitro* growth on cellophane**. *Fungal Genetics and Biology* 2008, **45**:1329-1339.
12. Nusbaum CJ, Keitt GW: **A cytological study of host-parasite relations of *Venturia inaequalis* on apple leaves**. *Journal of Agricultural Research* 1938, **56**:595-618.
13. Shiller J, Van de Wouw AP, Taranto AP, Bowen JK, Dubois D, Robinson A, Deng CH, Plummer KM: **A large family of *AvrLm6-like* genes in the apple and pear scab pathogens, *Venturia inaequalis* and *Venturia pirina***. *Frontiers in Plant Science* 2015, **6**.
14. Manktelow D, Beresford R, Batchelor T, Walker J: **Use patterns and economics of fungicides for disease control in New Zealand apples**. In *International Conference on Integrated Fruit Production*: 1995:187-192.
15. Cox KD: **Fungicide resistance in *Venturia inaequalis*, the causal agent of apple scab, in the United States**. In *Fungicide resistance in plant pathogens: principles and a guide to practical management*. Edited by Ishii H, Hollomon DW: Springer Japan; 2015:433-447.
16. Khajuria YP, Kaul S, Wani AA, Dhar MK: **Genetics of resistance in apple against *Venturia inaequalis* (Wint.) Cke**. *Tree Genetics & Genomes* 2018, **14**:16.
17. Patocchi A, Wehrli A, Dubuis PH, Auwerkerken A, Leida C, Cipriani G, Passey T, Staples M, Didelot F, Philion V, et al.: **Ten years of VINQUEST: first insight for breeding new apple cultivars with durable apple scab resistance**. *Plant Disease* 2020, **104**:2074-2081.

18. Papp D, Singh J, Gadoury D, Khan A: **New North American isolates of *Venturia inaequalis* can overcome apple scab resistance of *Malus floribunda* 821**. *Plant Disease* 2020, **104**:649-655.
19. Deng CH, Plummer KM, Jones DAB, Mesarich CH, Shiller J, Taranto AP, Robinson AJ, Kastner P, Hall NE, Templeton MD, et al.: **Comparative analysis of the predicted secretomes of Rosaceae scab pathogens *Venturia inaequalis* and *V. pirina* reveals expanded effector families and putative determinants of host range**. *BMC Genomics* 2017, **18**:339.
20. Passey TAJ, Armitage AD, Sobczyk MK, Shaw MW, Xu X: **Genomic sequencing indicates non-random mating of *Venturia inaequalis* in a mixed cultivar orchard**. *Plant Pathology* 2020, **69**:669-676.
21. Passey TAJ, Armitage AD, Xu X: **Annotated draft genome sequence of the apple scab pathogen *Venturia inaequalis***. *Microbiology Resource Announcements* 2018, **7**:e01062-01018.
22. Le Cam B, Sargent D, Gouzy J, Amselem J, Bellanger M-N, Bouchez O, Brown S, Caffier V, De Gracia M, Debuchy R, et al.: **Population genome gequencing of the scab fungal species *Venturia inaequalis, Venturia pirina, Venturia aucupariae* and *Venturia asperata***. *G3: Genes, Genomes, Genetics* 2019, **9**:2405-2414.
23. Lichtner FJ, Jurick WM, Ayer KM, Gaskins VL, Villani SM, Cox KD: **A genome resource for several North American *Venturia inaequalis* isolates with multiple fungicide resistance phenotypes**. *Phytopathology* 2020, **110**:544-546.
24. Fudal I, Ross S, Gout L, Blaise F, Kuhn ML, Eckert MR, Cattolico L, Bernard-Samain S, Balesdent MH, Rouxel T: **Heterochromatin-like regions as ecological niches for avirulence genes in the *Leptosphaeria maculans* genome: map-based cloning of *AvrLm6***. *Molecular Plant-Microbe Interactions* 2007, **20**:459-470.
25. de Jonge R, Peter van Esse H, Maruthachalam K, Bolton MD, Santhanam P, Saber MK, Zhang Z, Usami T, Lievens B, Subbarao KV, et al.: **Tomato immune receptor Ve1 recognizes effector of multiple fungal pathogens uncovered by genome and RNA sequencing**. *Proceedings of the National Academy of Sciences* 2012, **109**:5110.
26. Snelders NC, Rovenich H, Petti GC, Rocafort M, van den Berg GCM, Vorholt JA, Mesters JR, Seidl MF, Nijland R, Thomma BPHJ: **Microbiome manipulation by a soil-borne fungal plant pathogen using effector proteins**. *Nature Plants* 2020, **6**:1365-1374.
27. Caffier V, Le Cam B, Expert P, Tellier M, Devaux M, Giraud M, Chevalier M: **A new scab-like disease on apple caused by the formerly saprotrophic fungus *Venturia asperata***. *Plant Pathology* 2012, **61**:915-924.
28. Latham AJR, A. E.: **Development of *Cladosporium caryigenum* in pecan leaves**. *Phytopathology* 1988, **78**:1104-1108.
29. Lanza B, Ragnelli AM, Priore M, Aimola P: **Morphological and histochemical investigation of the response of *Olea europaea* leaves to fungal attack by *Spilocaea oleagina***. *Plant Pathology* 2017, **66**:1239-1247.
30. Avrova A, Knogge W: ***Rhynchosporium commune*: a persistent threat to barley cultivation**. *Molecular Plant Pathology* 2012, **13**:986-997.
31. Jones P, Ayres PG: ***Rhynchosporium* leaf blotch of barley studied during the subcuticular phase by electron microscopy**. *Physiological Plant Pathology* 1974, **4**:229-233.
32. Blechert O, Debener T: **Morphological characterization of the interaction between *Diplocarpon rosae* and various rose species**. *Plant Pathology* 2005, **54**:82-90.
33. Zhao H, Han Q, Wang J, Gao X, Xiao C-L, Liu J, Huang L: **Cytology of infection of apple leaves by *Diplocarpon mali***. *European Journal of Plant Pathology* 2013, **136**:41-49.

34. Lanver D, Müller AN, Happel P, Schweizer G, Haas FB, Franitza M, Pellegrin C, Reissmann S, Altmüller J, Rensing SA, et al.: **The biotrophic development of *Ustilago maydis* studied by RNA-Seq analysis**. *The Plant Cell* 2018, **30**:300.
35. Gervais J, Plissonneau C, Linglin J, Meyer M, Labadie K, Cruaud C, Fudal I, Rouxel T, Balesdent M-H: **Different waves of effector genes with contrasted genomic location are expressed by *Leptosphaeria maculans* during cotyledon and stem colonization of oilseed rape**. *Molecular Plant Pathology* 2017, **18**:1113-1126.
36. Bradshaw RE, Guo Y, Sim AD, Kabir MS, Chettri P, Ozturk IK, Hunziker L, Ganley RJ, Cox MP: **Genome-wide gene expression dynamics of the fungal pathogen *Dothistroma septosporum* throughout its infection cycle of the gymnosperm host *Pinus radiata***. *Molecular Plant Pathology* 2016, **17**:210-224.
37. Thakur K, Chawla V, Bhatti S, Swarnkar MK, Kaur J, Shankar R, Jha G: ***De novo* transcriptome sequencing and analysis for *Venturia inaequalis*, the devastating apple scab pathogen**. *PLoS ONE* 2013, **8**:e53937.
38. Xue C, Park G, Choi W, Zheng L, Dean RA, Xu J-R: **Two novel fungal virulence genes specifically expressed in appressoria of the rice blast fungus**. *The Plant Cell* 2002, **14**:2107-2119.
39. Kulkarni RD, Kelkar HS, Dean RA: **An eight-cysteine-containing CFEM domain unique to a group of fungal membrane proteins**. *Trends in Biochemical Sciences* 2003, **28**:118-121.
40. Garrido SM, Kitamoto N, Watanabe A, Shintani T, Gomi K: **Functional analysis of FarA transcription factor in the regulation of the genes encoding lipolytic enzymes and hydrophobic surface binding protein for the degradation of biodegradable plastics in *Aspergillus oryzae***. *Journal of Bioscience and Bioengineering* 2012, **113**:549-555.
41. Ohtaki S, Maeda H, Takahashi T, Yamagata Y, Hasegawa F, Gomi K, Nakajima T, Abe K: **Novel hydrophobic surface binding protein, HsbA, produced by *Aspergillus oryzae***. *Applied and Environmental Microbiology* 2006, **72**:2407-2413.
42. Mesarich CH, Schmitz M, Tremouilhac P, McGillivray DJ, Templeton MD, Dingley AJ: **Structure, dynamics and domain organization of the repeat protein Cin1 from the apple scab fungus**. *Biochimica et Biophysica Acta* 2012, **1824**:1118-1128.
43. Mesarich CH, Ökmen B, Rovenich H, Griffiths SA, Wang C, Karimi Jashni M, Mihajlovski A, Collemare J, Hunziker L, Deng CH, et al.: **Specific hypersensitive response-associated recognition of new apoplastic effectors from *Cladosporium fulvum* in wild tomato**. *Molecular Plant-Microbe Interactions* 2018, **31**:145-162.
44. Bolton MD, Van Esse HP, Vossen JH, De Jonge R, Stergiopoulos I, Stulemeijer IJE, Van Den Berg GCM, Borrás-Hidalgo O, Dekker HL, De Koster CG, et al.: **The novel *Cladosporium fulvum* lysin motif effector Ecp6 is a virulence factor with orthologues in other fungal species**. *Molecular Microbiology* 2008, **69**:119-136.
45. Kessler SC, Zhang X, McDonald MC, Gilchrist CLM, Lin Z, Rightmyer A, Solomon PS, Turgeon BG, Chooi Y-H: **Victorin, the host-selective cyclic peptide toxin from the oat pathogen *Cochliobolus victoriae* is ribosomally encoded**. *Proceedings of the National Academy of Sciences* 2020, **117**:24243.
46. Kessler SC, Chooi Y-H: **Out for a RiPP: challenges and advances in genome mining of ribosomal peptides from fungi**. *Natural Product Reports* 2022, **39**:222-230.
47. Jumper J, Evans R, Pritzel A, Green T, Figurnov M, Ronneberger O, Tunyasuvunakool K, Bates R, Žídek A, Potapenko A, et al.: **Highly accurate protein structure prediction with AlphaFold**. *Nature* 2021, **596**:583-589.
48. Holm L: **Using dali for protein structure comparison**. *Methods in Molecular Biology* 2020, **2112**:29-42.

49. Hoh F, Padilla, A., De Guillen, K.: **New MAX effector from *Magnaporthe oryzae***. 2019.
50. Li W, Wang B, Wu J, Lu G, Hu Y, Zhang X, Zhang Z, Zhao Q, Feng Q, Zhang H, et al.: **The *Magnaporthe oryzae* avirulence gene *AvrPiz-t* encodes a predicted secreted protein that triggers the immunity in rice mediated by the blast resistance gene *Piz-t***. *Molecular Plant-Microbe Interactions* 2009, **22**:411-420.
51. de Guillen K, Ortiz-Vallejo D, Gracy J, Fournier E, Kroj T, Padilla A: **Structure analysis uncovers a highly diverse but structurally conserved effector family in phytopathogenic fungi**. *PLoS Pathogens* 2015, **11**:e1005228.
52. Ose T, Oikawa A, Nakamura Y, Maenaka K, Higuchi Y, Satoh Y, Fujiwara S, Demura M, Sone T, Kamiya M: **Solution structure of an avirulence protein, AVR-Pia, from *Magnaporthe oryzae***. *Journal of Biomolecular NMR* 2015, **63**:229-235.
53. Zhang X, He D, Zhao Y, Cheng X, Zhao W, Taylor IA, Yang J, Liu J, Peng YL: **A positive-charged patch and stabilized hydrophobic core are essential for avirulence function of AvrPib in the rice blast fungus**. *The Plant Journal* 2018, **96**:133-146.
54. De la Concepcion JC, Franceschetti M, Maqbool A, Saitoh H, Terauchi R, Kamoun S, Banfield MJ: **Polymorphic residues in rice NLRs expand binding and response to effectors of the blast pathogen**. *Nature Plants* 2018, **4**:576-585.
55. Nyarko A, Singarapu KK, Figueroa M, Manning VA, Pandelova I, Wolpert TJ, Ciuffetti LM, Barbar E: **Solution NMR structures of *Pyrenophora tritici-repentis* ToxB and its inactive homolog reveal potential determinants of toxin activity**. *The Journal of Biological Chemistry* 2014, **289**:25946-25956.
56. Sarma GN, Manning VA, Ciuffetti LM, Karplus PA: **Structure of Ptr ToxA: An RGD-containing host-selective toxin from *Pyrenophora tritici-repentis*** *The Plant Cell* 2005, **17**:3190-3202.
57. Ma L, Cornelissen BJC, Takken FLW: **A nuclear localization for Avr2 from *Fusarium oxysporum* is required to activate the tomato resistance protein I-2**. *Frontiers in Plant Science* 2013, **4**:94-94.
58. Di X, Cao L, Hughes RK, Tintor N, Banfield MJ, Takken FLW: **Structure-function analysis of the *Fusarium oxysporum* Avr2 effector allows uncoupling of its immune-suppressing activity from recognition**. *New Phytologist* 2017, **216**:897-914.
59. Guncar G, Wang C-IA, Forwood JK, Teh T, Catanzariti A-M, Ellis JG, Dodds PN, Kobe B: **The use of Co2+ for crystallization and structure determination, using a conventional monochromatic X-ray source, of flax rust avirulence protein**. *Crystallization Communications* 2007, **63**:209-213.
60. Wang C-IA, Gunčar G, Forwood JK, Teh T, Catanzariti A-M, Lawrence GJ, Loughlin FE, Mackay JP, Schirra HJ, Anderson PA, et al.: **Crystal structures of flax rust avirulence proteins AvrL567-A and -D reveal details of the structural basis for flax disease resistance specificity**. *The Plant Cell* 2007, **19**:2898-2912.
61. Blondeau K, Blaise F, Graille M, Kale SD, Linglin J, Ollivier B, Labarde A, Lazar N, Daverdin G, Balesdent MH, et al.: **Crystal structure of the effector AvrLm4-7 of *Leptosphaeria maculans* reveals insights into its translocation into plant cells and recognition by resistance proteins**. *The Plant Journal* 2015, **83**:610-624.
62. Lazar N, Mesarich CH, Petit-Houdenot Y, Talbi N, Li de la Sierra-Gallay I, Zélie E, Blondeau K, Gracy J, Ollivier B, Blaise F, et al.: **A new family of structurally conserved fungal effectors displays epistatic interactions with plant resistance proteins**. *PLoS Pathogens* 2022, **18**:e1010664.
63. Yu DS, Outram MA, Smith A, McCombe CL, Khambalkar PB, Rima SA, Sun X, Ma L, Ericsson DJ, Jones DA, et al.: **The structural repertoire of *Fusarium oxysporum* f. sp.**

***lycopersici* effectors revealed by experimental and computational studies**. *bioRxiv* 2021: 472499.

64. Li N, Erman M, Pangborn W, Duax WL, Park C-M, Bruenn J, Ghosh D: **Structure of *Ustilago maydis* killer toxin KP6 α-subunit: A multimeric assembly with a central pore**. *The Journal of Biological Chemistry* 1999, **274**:20425-20431.
65. Allen A, Chatt E, Smith TJ: **The atomic structure of the virally encoded antifungal protein, KP6**. *Journal of Molecular Biology* 2013, **425**:609-621.
66. Padilla A, Hoh, F., De guillen, K.: **Zt-KP6-1: an effector from *Zymoseptoria tritici***. 2019.
67. Fox NK, Brenner SE, Chandonia J-M: **SCOPe: Structural classification of proteins-extended, integrating SCOP and ASTRAL data and classification of new structures**. *Nucleic Acids Research* 2014, **42**:D304-D309.
68. Huber A, Hajdu D, Bratschun-Khan D, Gáspári Z, Varbanov M, Philippot S, Fizil Á, Czajlik A, Kele Z, Sonderegger C, et al.: **New antimicrobial potential and structural properties of PAFB: a cationic, cysteine-rich protein from *Penicillium chrysogenum* Q176**. *Scientific Reports* 2018, **8**:1751.
69. Marx F, Binder U, Leiter E, Pócsi I: **The *Penicillium chrysogenum* antifungal protein PAF, a promising tool for the development of new antifungal therapies and fungal cell biology studies**. *Cellular Molecular Life Sciences* 2008, **65**:445-454.
70. Sonderegger C, Fizil Á, Burtscher L, Hajdu D, Muñoz A, Gáspári Z, Read ND, Batta G, Marx F: **D19S mutation of the cationic, cysteine-rich protein PAF: Novel insights into its structural dynamics, thermal unfolding and antifungal function**. *PLoS ONE* 2017, **12**:e0169920.
71. Rocafort M, Fudal I, Mesarich CH: **Apoplastic effector proteins of plant-associated fungi and oomycetes**. *Current Opinion in Plant Biology* 2020, **56**:9-19.
72. Takahashi T, Maeda H, Yoneda S, Ohtaki S, Yamagata Y, Hasegawa F, Gomi K, Nakajima T, Abe K: **The fungal hydrophobin RolA recruits polyesterase and laterally moves on hydrophobic surfaces**. *Molecular Microbiology* 2005, **57**:1780-1796.
73. Koller W, Parker DM, Becker CM: **Role of cutinase in the penetration of apple leaves by *Venturia inaequalis.*** *Phytopathology* 1991, **81**:1375-1379.
74. Martínez-Cruz J, Romero D, Hierrezuelo J, Thon M, de Vicente A, Pérez-García A: **Effectors with chitinase activity (EWCAs), a family of conserved, secreted fungal chitinases that suppress chitin-triggered immunity**. *The Plant Cell* 2021, **33**:1319-1340.
75. Gamas P, Niebel Fde C, Lescure N, Cullimore J: **Use of a subtractive hybridization approach to identify new *Medicago truncatula* genes induced during root nodule development**. *Molecular Plant-Microbe Interactions* 1996, **9**:233-242.
76. Kimura M, Yamamoto YY, Seki M, Sakurai T, Sato M, Abe T, Yoshida S, Manabe K, Shinozaki K, Matsui M: **Identification of *Arabidopsis* genes regulated by high light-stress using cDNA microarray**. *Photochemistry and Photobiology* 2003, **77**:226-233.
77. Doss RP: **Treatment of pea pods with bruchin B results in up-regulation of a gene similar to *MtN19***. *Plant Physiology Biochemistry* 2005, **43**:225-231.
78. Naya L, Paul S, Valdés-López O, Mendoza-Soto AB, Nova-Franco B, Sosa-Valencia G, Reyes JL, Hernández G: **Regulation of copper homeostasis and biotic interactions by MicroRNA 398b in common bean**. *PLoS ONE* 2014, **9**:e84416.
79. Zhang Z-N, Wu Q-Y, Zhang G-Z, Zhu Y-Y, Murphy RW, Liu Z, Zou C-G: **Systematic analyses reveal uniqueness and origin of the CFEM domain in fungi**. *Scientific Reports* 2015, **5**:13032.
80. Zhao S, Shang X, Bi W, Yu X, Liu D, Kang Z, Wang X, Wang X: **Genome-wide identification of effector candidates with conserved motifs from the wheat leaf rust fungus *Puccinia triticina***. *Frontiers in Microbiology* 2020, **11**.

81. Zhu W, Wei W, Wu Y, Zhou Y, Peng F, Zhang S, Chen P, Xu X: **BcCFEM1, a CFEM domain-containing protein with putative GPI-anchored site, is involved in pathogenicity, conidial production, and stress tolerance in *Botrytis cinerea***. *Frontiers in Microbiology* 2017, **8**.
82. Wang J-x, Long F, Zhu H, Zhang Y, Wu J-y, Shen S, Dong J-g, Hao Z-m: **Bioinformatic analysis and functional characterization of CFEM proteins in *Setosphaeria turcica***. *Journal of Integrative Agriculture* 2021, **20**:2438-2449.
83. Choi W, Dean RA: **The adenylate cyclase gene *MAC1* of *Magnaporthe grisea* controls appressorium formation and other aspects of growth and development**. *The Plant Cell* 1997, **9**:1973-1983.
84. Skrzydeł J, Borowska-Wykręt D, Kwiatkowska D: **Structure, assembly and function of cuticle from mechanical perspective with special focus on perianth**. *International Journal of Molecular Sciences* 2021, **22**:4160.
85. Sacristán S, Vigouroux M, Pedersen C, Skamnioti P, Thordal-Christensen H, Micali C, Brown JKM, Ridout CJ: **Coevolution between a family of parasite virulence effectors and a class of LINE-1 retrotransposons**. *PLoS ONE* 2009, **4**:e7463.
86. Spanu PD, Abbott JC, Amselem J, Burgis TA, Soanes DM, Stüber K, Ver Loren van Themaat E, Brown JK, Butcher SA, Gurr SJ, et al.: **Genome expansion and gene loss in powdery mildew fungi reveal tradeoffs in extreme parasitism**. *Science* 2010, **330**:1543-1546.
87. Dutheil JY, Mannhaupt G, Schweizer G, C MKS, Münsterkötter M, Güldener U, Schirawski J, Kahmann R: **A tale of genome compartmentalization: the evolution of virulence clusters in smut fungi**. *Genome Biology Evolution* 2016, **8**:681-704.
88. Fouché S, Plissonneau C, Croll D: **The birth and death of effectors in rapidly evolving filamentous pathogen genomes**. *Current Opinion in Microbiology* 2018, **46**:34-42.
89. Amoozadeh S, Johnston J, Meisrimler C-N: **Exploiting structural modelling tools to explore host-translocated effector proteins**. *International Journal of Molecular Sciences* 2021, **22**:12962.
90. Seong K, Krasileva KV: **Computational structural genomics unravels common folds and novel families in the secretome of fungal phytopathogen *Magnaporthe oryzae***. *Molecular Plant-Microbe Interactions* 2021:MPMI-03-21-0071-R.
91. Seong K, Krasileva KV: **Comparative computational structural genomics highlights divergent evolution of fungal effectors**. *bioRxiv* 2022: 490317.
92. Cesari S, Thilliez G, Ribot C, Chalvon V, Michel C, Jauneau A, Rivas S, Alaux L, Kanzaki H, Okuyama Y, et al.: **The rice resistance protein pair RGA4/RGA5 recognizes the *Magnaporthe oryzae* effectors AVR-Pia and AVR1-CO39 by direct binding**. *The Plant Cell* 2013, **25**:1463-1481.
93. Yoshida K, Saitoh H, Fujisawa S, Kanzaki H, Matsumura H, Yoshida K, Tosa Y, Chuma I, Takano Y, Win J, et al.: **Association genetics reveals three novel avirulence genes from the rice blast fungal pathogen *Magnaporthe oryzae*.** *The Plant Cell* 2009, **21**:1573-1591.
94. Ashikawa I, Hayashi N, Yamane H, Kanamori H, Wu J, Matsumoto T, Ono K, Yano M: **Two adjacent nucleotide-binding site–leucine-rich repeat class genes are required to confer *Pikm*-specific rice blast resistance**. *Genetics* 2008, **180**:2267.
95. Zhang S, Wang L, Wu W, He L, Yang X, Pan Q: **Function and evolution of *Magnaporthe oryzae* avirulence gene *AvrPib* responding to the rice blast resistance gene *Pib***. *Scientific Reports* 2015, **5**:11642.
96. Oikawa K, Fujisaki K, Shimizu M, Takeda T, Saitoh H, Hirabuchi A, Hiraka Y, Białas A, Langner T, Kellner R, et al.: **The blast pathogen effector AVR-Pik binds and stabilizes rice heavy metal-associated (HMA) proteins to co-opt their function in immunity**. *bioRxiv* 2020: 406389.

97. Guo L, Cesari S, de Guillen K, Chalvon V, Mammri L, Ma M, Meusnier I, Bonnot F, Padilla A, Peng Y-L, et al.: **Specific recognition of two MAX effectors by integrated HMA domains in plant immune receptors involves distinct binding surfaces**. *Proceedings of the National Academy of Sciences* 2018, **115**:11637.
98. Franceschetti M, Maqbool A, Jiménez-Dalmaroni Maximiliano J, Pennington Helen G, Kamoun S, Banfield Mark J: **Effectors of filamentous plant pathogens: commonalities amid diversity**. *Microbiology and Molecular Biology Reviews* 2017, **81**:e00066-00016.
99. Schouten HJ, Brinkhuis J, Burgh AMvd, Schaart JG, Groenwold R, Broggini GAL, Gessler C: **Cloning and functional characterization of the *Rvi15* (*Vr2*) gene for apple scab resistance**. *Tree Genetics & Genomes* 2013, **10**:251-260.
100. Rafiqi M, Gan PH, Ravensdale M, Lawrence GJ, Ellis JG, Jones DA, Hardham AR, Dodds PN: **Internalization of flax rust avirulence proteins into flax and tobacco cells can occur in the absence of the pathogen**. *The Plant Cell* 2010, **22**:2017-2032.
101. Manning VA, Hamilton SM, Karplus PA, Ciuffetti LM: **The Arg-Gly-Asp-containing, solvent-exposed loop of Ptr ToxA is required for internalization**. *Molecular Plant-Microbe Interactions* 2008, **21**:315-325.
102. Cao L, Blekemolen MC, Tintor N, Cornelissen BJC, Takken FLW: **The *Fusarium oxysporum* Avr2-Six5 effector pair alters plasmodesmatal exclusion selectivity to facilitate cell-to-cell movement of Avr2**. *Molecular Plant* 2018, **11**:691-705.
103. Dagvadorj B, Outram MA, Williams SJ, Solomon PS: **The necrotrophic effector ToxA from *Parastagonospora nodorum* interacts with wheat NHL proteins to facilitate Tsn1-mediated necrosis**. *The Plant Journal* 2022,**110**: 407-418.
104. Belfanti E, Silfverberg-Dilworth E, Tartarini S, Patocchi A, Barbieri M, Zhu J, Vinatzer BA, Gianfranceschi L, Gessler C, Sansavini S: **The *HcrVf2* gene from a wild apple confers scab resistance to a transgenic cultivated variety**. *Proceedings of the National Academy of Sciences of the United States of America* 2004, **101**:886-890.
105. Ghanbarnia K, Ma L, Larkan NJ, Haddadi P, Fernando WGD, Borhan MH: ***Leptosphaeria maculans* AvrLm9: a new player in the game of hide and seek with AvrLm4-7**. *Molecular Plant Pathology* 2018, **19**:1754-1764.
106. Plissonneau C, Daverdin G, Ollivier B, Blaise F, Degrave A, Fudal I, Rouxel T, Balesdent M-H: **A game of hide and seek between avirulence genes *AvrLm4-7* and *AvrLm3* in *Leptosphaeria maculans***. *New Phytologist* 2016, **209**:1613-1624.
107. Houterman PM, Cornelissen BJC, Rep M: **Suppression of plant resistance gene-based immunity by a fungal effector**. *PLoS Pathogens* 2008, **4**:e1000061.
108. Outram MA, Figueroa M, Sperschneider J, Williams SJ, Dodds PN: **Seeing is believing: Exploiting advances in structural biology to understand and engineer plant immunity**. *Current Opinion in Plant Biology* 2022, **67**: 102210.
109. Petit-Houdenot Y, Degrave A, Meyer M, Blaise F, Ollivier B, Marais CL, Jauneau A, Audran C, Rivas S, Veneault-Fourrey C, et al.: **A two genes - for - one gene interaction between *Leptosphaeria maculans* and *Brassica napus***. *New Phytologist* 2019, **223**:397-411.
110. Mosquera G, Giraldo MC, Khang CH, Coughlan S, Valent B: **Interaction transcriptome analysis identifies *Magnaporthe oryzae* BAS1-4 as biotrophy-associated secreted proteins in rice blast disease**. *Plant Cell* 2009, **21**:1273-1290.
111. Ebert MK, Rangel LI, Spanner RE, Taliadoros D, Wang X, Friesen TL, de Jonge R, Neubauer JD, Secor GA, Thomma BPHJ, et al.: **Identification and characterization of *Cercospora beticola* necrosis-inducing effector CbNip1**. *Molecular Plant Pathology* 2021, **22**:301-316.

112. Postic G, Gracy J, Périn C, Chiche L, Gelly J-C: **KNOTTIN: the database of inhibitor cystine knot scaffold after 10 years, toward a systematic structure modeling**. *Nucleic Acids Research* 2018, **46**:D454-D458.
113. Vervoort J, van den Hooven HW, Berg A, Vossen P, Vogelsang R, Joosten MHAJ, de Wit PJGM: **The race-specific elicitor AVR9 of the tomato pathogen *Cladosporium fulvum*: a cystine knot protein: Sequence-specific 1H NMR assignments, secondary structure and global fold of the protein**. *FEBS Letters* 1997, **404**:153-158.
114. van den Hooven HW, van den Burg HA, Vossen P, Boeren S, de Wit PJGM, Vervoort J: **Disulfide bond structure of the AVR9 elicitor of the fungal tomato pathogen *Cladosporium fulvum*: Evidence for a cystine knot**. *Biochemistry* 2001, **40**:3458-3466.
115. de Guillen K, Lorrain C, Tsan P, Barthe P, Petre B, Saveleva N, Rouhier N, Duplessis S, Padilla A, Hecker A: **Structural genomics applied to the rust fungus *Melampsora larici-populina* reveals two candidate effector proteins adopting cystine knot and NTF2-like protein folds**. *Scientific Reports* 2019, **9**:18084.
116. Snelders NC, Petti GC, van den Berg GCM, Seidl MF, Thomma BPHJ: **An ancient antimicrobial protein co-opted by a fungal plant pathogen for *in planta* mycobiome manipulation**. *Proceedings of the National Academy of Sciences* 2021, **118**:e2110968118.
117. Lee H-T, Lee C-C, Yang J-R, Lai JZC, Chang KY: **A large-scale structural classification of antimicrobial peptides**. *BioMed Research International* 2015, **2015**:475062.
118. Vogt E, Künzler M: **Discovery of novel fungal RiPP biosynthetic pathways and their application for the development of peptide therapeutics**. *Applied Microbiology and Biotechnology* 2019, **103**:5567-5581.
119. Slazak B, Kapusta M, Strömstedt AA, Słomka A, Krychowiak M, Shariatgorji M, Andrén PE, Bohdanowicz J, Kuta E, Göransson U: **How does the sweet violet (*Viola odorata* L.) fight pathogens and pests – cyclotides as a comprehensive plant host defense system**. *Frontiers in Plant Science* 2018, **9**:1296.
120. Rocafort M, Arshed S, Hudson D, Sidhu JS, Bowen JK, Plummer KM, Bradshaw RE, Johnson RD, Johnson LJ, Mesarich CH: **CRISPR-Cas9 gene editing and rapid detection of gene-edited mutants using high-resolution melting in the apple scab fungus, *Venturia inaequalis***. *Fungal Biology* 2021, **126**:35-46.
121. Chen C, Bock CH, Wood BW: **Draft genome sequence of *Venturia carpophila*, the causal agent of peach scab**. *Standards in genomic sciences* 2017, **12**:68-68.
122. Jaber MY, Bao J, Gao X, Zhang L, He D, Wang X, Wang A, Wang Z, Wang B: **Genome sequence of *Venturia oleaginea*, the causal agent of olive leaf scab**. *Molecular Plant-Microbe Interactions* 2020, **33**:1095-1097.
123. Johnson S, Jones D, Thrimawithana AH, Deng CH, Bowen JK, Mesarich CH, Ishii H, Won K, Bus VGM, Plummer KM: **Whole genome sequence resource of the Asian pear scab pathogen *Venturia nashicola***. *Molecular Plant-Microbe Interactions* 2019, **32**:1463-1467.
124. Prokchorchik M, Won K, Lee Y, Choi ED, Segonzac C, Sohn KH: **High contiguity whole genome sequence and gene annotation resource for two *Venturia nashicola* isolates**. *Molecular Plant-Microbe Interactions* 2019, **32**:1091-1094.
125. Winter DJ, Charlton ND, Krom N, Shiller J, Bock CH, Cox MP, Young CA: **Chromosome-level reference genome of *Venturia effusa*, causative agent of pecan scab**. *Molecular Plant-Microbe Interactions* 2020, **33**:149-152.
126. Zhou Y, Zhang L, Fan F, Wang ZQ, Huang Y, Yin LF, Yin WX, Luo CX: **Genome sequence of *Venturia carpophila*, the causal agent of peach scab**. *Molecular Plant-Microbe Interactions* 2021, **34**:852-856.
127. Hamelin R: **The *Venturia populina* CBS256.38 v1.0 genome**. 2022.

128. Stehmann C, Pennycook S, Plummer KM: **Molecular identification of a sexual interloper: The pear pathogen, *Venturia pirina*, has sex on apple**. *Phytopathology* 2001, **91**:633-641.
129. Caffier V, Patocchi A, Expert P, Bellanger M-N, Durel C-E, Hilber-Bodmer M, Broggini GAL, Groenwold R, Bus VGM: **Virulence characterization of *Venturia inaequalis* reference isolates on the differential set of *Malus* hosts**. *Plant Disease* 2014, **99**:370-375.
130. Xu X, Harvey A, Barbara DJ: **Population variation of apple scab (*Venturia inaequalis*) within mixed orchards in the UK**. *European Journal of Plant Pathology* 2013, **135**:97-104.
131. Parker D, Hilber U, Bodmer M, Smith F, Yao C, Köller W: **Production and transformation of conidia of *Venturia inaequalis***. *Phytopathology* 1995, **85**:87-91.
132. Win J, Greenwood DR, Plummer KM: **Characterisation of a protein from *Venturia inaequalis* that induces necrosis in *Malus* carrying the *Vm* resistance gene**. *Physiological and Molecular Plant Pathology* 2003, **62**:193-202.
133. Bruzzese E, Hasan S: **A whole leaf clearing and staining technique for host specificity studies of rust fungi**. *Plant Pathology* 1983, **32**:335-338.
134. Atkinson RG, Johnston SL, Yauk Y-K, Sharma NN, Schröder R: **Analysis of *xyloglucan endotransglucosylase/hydrolase* (*XTH*) gene families in kiwifruit and apple**. *Postharvest Biology and Technology* 2009, **51**:149-157.
135. Wu TD, Watanabe CK: **GMAP: a genomic mapping and alignment program for mRNA and EST sequences**. *Bioinformatics* 2005, **21**:1859-1875.
136. Kim D, Langmead B, Salzberg SL: **HISAT: a fast spliced aligner with low memory requirements**. *Nature Methods* 2015, **12**:357-360.
137. Kim D, Paggi JM, Park C, Bennett C, Salzberg SL: **Graph-based genome alignment and genotyping with HISAT2 and HISAT-genotype**. *Nature Biotechnology* 2019, **37**:907-915.
138. Danecek P, Bonfield JK, Liddle J, Marshall J, Ohan V, Pollard MO, Whitwham A, Keane T, McCarthy SA, Davies RM, et al.: **Twelve years of SAMtools and BCFtools**. *Gigascience* 2021, **10**.
139. Grabherr MG, Haas BJ, Yassour M, Levin JZ, Thompson DA, Amit I, Adiconis X, Fan L, Raychowdhury R, Zeng Q, et al.: **Full-length transcriptome assembly from RNA-Seq data without a reference genome**. *Nature Biotechnology* 2011, **29**:644-652.
140. Kearse M, Moir R, Wilson A, Stones-Havas S, Cheung M, Sturrock S, Buxton S, Cooper A, Markowitz S, Duran C, et al.: **Geneious Basic: an integrated and extendable desktop software platform for the organization and analysis of sequence data**. *Bioinformatics* 2012, **28**:1647-1649.
141. Jones P, Binns D, Chang H-Y, Fraser M, Li W, McAnulla C, McWilliam H, Maslen J, Mitchell A, Nuka G, et al.: **InterProScan 5: genome-scale protein function classification**. *Bioinformatics* 2014, **30**:1236-1240.
142. Törönen P, Medlar A, Holm L: **PANNZER2: a rapid functional annotation web server**. *Nucleic Acids Research* 2018, **46**:W84-W88.
143. Almagro Armenteros JJ, Tsirigos KD, Sønderby CK, Petersen TN, Winther O, Brunak S, von Heijne G, Nielsen H: **SignalP 5.0 improves signal peptide predictions using deep neural networks**. *Nature Biotechnology* 2019, **37**:420-423.
144. Krogh A, Larsson B, von Heijne G, Sonnhammer EL: **Predicting transmembrane protein topology with a hidden Markov model: application to complete genomes**. *Journal of Molecular Biology* 2001, **305**:567-580.

145. Zhang H, Yohe T, Huang L, Entwistle S, Wu P, Yang Z, Busk PK, Xu Y, Yin Y: **dbCAN2: a meta server for automated carbohydrate-active enzyme annotation**. *Nucleic Acids Research* 2018, **46**:W95-W101.
146. Drula E, Garron ML, Dogan S, Lombard V, Henrissat B, Terrapon N: **The carbohydrate-active enzyme database: functions and literature**. *Nucleic Acids Research* 2022, **50**:D571-d577.
147. Sperschneider J, Dodds PN: **EffectorP 3.0: prediction of apoplastic and cytoplasmic effectors in fungi and oomycetes**. *bioRxiv* 2021:454080.
148. Nepusz T, Sasidharan R, Paccanaro A: **SCPS: a fast implementation of a spectral method for detecting protein families on a genome-wide scale**. *BMC Bioinformatics* 2010, **11**:120.
149. Jacques Dainat DH, Ed Davis, Kathryn Crouch, LucileSol, pascal-git, & tayyrov: **AGAT: Another gff analysis toolkit to handle annotations in any gtf/gff format**. *Zenodo* 2022.
150. Quinlan AR, Hall IM: **BEDTools: a flexible suite of utilities for comparing genomic features**. *Bioinformatics* 2010, **26**:841-842.
151. Li H, Durbin R: **Fast and accurate long-read alignment with Burrows–Wheeler transform**. *Bioinformatics* 2010, **26**:589-595.
152. Wingett SW, Andrews S: **FastQ Screen: A tool for multi-genome mapping and quality control**. *F1000Research* 2018, **7**:1338.
153. Liao Y, Smyth GK, Shi W: **featureCounts: an efficient general purpose program for assigning sequence reads to genomic features**. *Bioinformatics* 2014, **30**:923-930.
154. Ewels P, Magnusson M, Lundin S, Käller M: **MultiQC: summarize analysis results for multiple tools and samples in a single report**. *Bioinformatics* 2016, **32**:3047-3048.
155. Love MI, Huber W, Anders S: **Moderated estimation of fold change and dispersion for RNA-seq data with DESeq2**. *Genome Biology* 2014, **15**:550.
156. Wickham H: **ggplot2: Elegant graphics for data analysis**. *Springer-Verlag New York* 2016.
157. Gu Z, Eils R, Schlesner M: **Complex heatmaps reveal patterns and correlations in multidimensional genomic data**. *Bioinformatics* 2016, **32**:2847-2849.
158. Alexa A, Rahnenführer J, Lengauer T: **Improved scoring of functional groups from gene expression data by decorrelating GO graph structure**. *Bioinformatics* 2006, **22**:1600-1607.
159. Ruff KM, Pappu RV: **AlphaFold and implications for intrinsically disordered proteins**. *Journal of Molecular Biology* 2021, **433**:167208.
160. Mirdita M, Schütze K, Moriwaki Y, Heo L, Ovchinnikov S, Steinegger M: **ColabFold: making protein folding accessible to all**. *Nature Methods* 2022, **19**:679-682.
161. Sievers F, Wilm A, Dineen D, Gibson TJ, Karplus K, Li W, Lopez R, McWilliam H, Remmert M, Söding J, et al.: **Fast, scalable generation of high-quality protein multiple sequence alignments using Clustal Omega**. *Molecular Systems Biology* 2011, **7**:539.
162. Goujon M, McWilliam H, Li W, Valentin F, Squizzato S, Paern J, Lopez R: **A new bioinformatics analysis tools framework at EMBL–EBI**. *Nucleic Acids Research* 2010, **38**:W695-W699.
163. Zimmermann L, Stephens A, Nam SZ, Rau D, Kübler J, Lozajic M, Gabler F, Söding J, Lupas AN, Alva V: **A completely reimplemented MPI bioinformatics toolkit with a new HHpred server at its core**. *Journal of Molecular Biology* 2018, **430**:2237-2243.
164. Gabler F, Nam SZ, Till S, Mirdita M, Steinegger M, Söding J, Lupas AN, Alva V: **Protein sequence analysis using the MPI bioinformatics toolkit**. *Current Protocols in Bioinformatics* 2020, **72**:e108.

165. Necci M, Piovesan D, Dosztányi Z, Tosatto SCE: **MobiDB-lite: fast and highly specific consensus prediction of intrinsic disorder in proteins**. *Bioinformatics* 2017, **33**:1402-1404.
166. Ishida T, Kinoshita K: **PrDOS: prediction of disordered protein regions from amino acid sequence**. *Nucleic Acids Research* 2007, **35**:W460-464.
167. Shindyalov IN, Bourne PE: **Protein structure alignment by incremental combinatorial extension (CE) of the optimal path**. *Protein Engineering* 1998, **11**:739-747.
168. Zhang Y, Skolnick J: **TM-align: a protein structure alignment algorithm based on the TM-score**. *Nucleic Acids Research* 2005, **33**:2302-2309.
169. Ayoub R, Lee Y: **RUPEE: A fast and accurate purely geometric protein structure search**. *PLoS ONE* 2019, **14**:e0213712.
170. Ayoub R, Lee Y: **Protein structure search to support the development of protein structure prediction methods**. *Proteins: Structure, Function, and Bioinformatics* 2021, **89**:648-658.
171. Chandonia J-M, Fox NK, Brenner SE: **SCOPe: classification of large macromolecular structures in the structural classification of proteins—extended database**. *Nucleic Acids Research* 2019, **47**:D475-D481.
172. Steinegger M, Söding J: **MMseqs2 enables sensitive protein sequence searching for the analysis of massive data sets**. *Nature Biotechnology* 2017, **35**:1026-1028.
173. Remmert M, Biegert A, Hauser A, Söding J: **HHblits: lightning-fast iterative protein sequence searching by HMM-HMM alignment**. *Nature Methods* 2011, **9**:173-175.
174. Johnson LS, Eddy SR, Portugaly E: **Hidden Markov model speed heuristic and iterative HMM search procedure**. *BMC Bioinformatics* 2010, **11**:431.
175. Soanes DM, Chakrabarti A, Paszkiewicz KH, Dawe AL, Talbot NJ: **Genome-wide transcriptional profiling of appressorium development by the rice blast fungus *Magnaporthe oryzae***. *PLoS Pathogens* 2012, **8**:e1002514.
176. Lubkowitz M: **The oligopeptide transporters: a small gene family with a diverse group of substrates and functions?** *Molecular Plant* 2011, **4**:407-415.
177. Bourbouloux A, Shahi P, Chakladar A, Delrot S, Bachhawat AK: **Hgt1p, a high affinity glutathione transporter from the yeast *Saccharomyces cerevisiae***. *Journal of Biology and Chemistry* 2000, **275**:13259-13265.
178. Vela-Corcía D, Aditya Srivastava D, Dafa-Berger A, Rotem N, Barda O, Levy M: **MFS transporter from *Botrytis cinerea* provides tolerance to glucosinolate-breakdown products and is required for pathogenicity**. *Nature Communications* 2019, **10**:2886.
179. Guelfo JR, Rodríguez-Rojas A, Matic I, Blázquez J: **A MATE-family efflux pump rescues the *Escherichia coli* 8-oxoguanine-repair-deficient mutator phenotype and protects against H2O2 killing**. *PLoS Genetics* 2010, **6**:e1000931.
180. Fernandez J, Wright JD, Hartline D, Quispe CF, Madayiputhiya N, Wilson RA: **Principles of carbon catabolite repression in the rice blast fungus: Tps1, Nmr1-3, and a MATE-family pump regulate glucose metabolism during infection**. *PLoS Genetics* 2012, **8**:e1002673.
181. Perlin MH, Andrews J, San Toh S: **Chapter Four - Essential letters in the fungal alphabet: ABC and MFS transporters and their roles in survival and pathogenicity**. In *Advances in Genetics*. Edited by Friedmann T, Dunlap JC, Goodwin SF: Academic Press; 2014:201-253. vol 85.]
182. Li Y, Wang Z, Beier RC, Shen J, Smet DD, De Saeger S, Zhang S: **T-2 toxin, a trichothecene mycotoxin: review of toxicity, metabolism, and analytical Methods**. *Journal of Agricultural and Food Chemistry* 2011, **59**:3441-3453.

183. Donofrio NM, Oh Y, Lundy R, Pan H, Brown DE, Jeong JS, Coughlan S, Mitchell TK, Dean RA: **Global gene expression during nitrogen starvation in the rice blast fungus, *Magnaporthe grisea***. *Fungal Genetics and Biology* 2006, **43**:605-617.
184. Martínez P, Ljungdahl PO: **Divergence of Stp1 and Stp2 transcription factors in *Candida albicans* places virulence factors required for proper nutrient acquisition under amino acid control**. *Molecular Cell Biology* 2005, **25**:9435-9446.
185. Medema MH, Blin K, Cimermancic P, de Jager V, Zakrzewski P, Fischbach MA, Weber T, Takano E, Breitling R: **antiSMASH: rapid identification, annotation and analysis of secondary metabolite biosynthesis gene clusters in bacterial and fungal genome sequences**. *Nucleic Acids Research* 2011, **39**:W339-346.
186. Blin K, Shaw S, Kloosterman AM, Charlop-Powers Z, van Wezel GP, Medema MH, Weber T: **antiSMASH 6.0: improving cluster detection and comparison capabilities**. *Nucleic Acids Research* 2021, **49**:W29-w35.
187. Blin K, Shaw S, Steinke K, Villebro R, Ziemert N, Lee SY, Medema MH, Weber T: **antiSMASH 5.0: updates to the secondary metabolite genome mining pipeline**. *Nucleic Acids Research* 2019, **47**:W81-W87.
188. Blin K, Wolf T, Chevrette MG, Lu X, Schwalen CJ, Kautsar SA, Suarez Duran HG, de Los Santos ELC, Kim HU, Nave M, et al.: **antiSMASH 4.0-improvements in chemistry prediction and gene cluster boundary identification**. *Nucleic Acids Research* 2017, **45**:W36-w41.
189. Weber T, Blin K, Duddela S, Krug D, Kim HU, Bruccoleri R, Lee SY, Fischbach MA, Müller R, Wohlleben W, et al.: **antiSMASH 3.0-a comprehensive resource for the genome mining of biosynthetic gene clusters**. *Nucleic Acids Research* 2015, **43**:W237-243.
190. Blin K, Medema MH, Kazempour D, Fischbach MA, Breitling R, Takano E, Weber T: **antiSMASH 2.0--a versatile platform for genome mining of secondary metabolite producers**. *Nucleic Acids Research* 2013, **41**:W204-212.
191. Lee S, Son H, Lee J, Min K, Choi GJ, Kim JC, Lee YW: **Functional analyses of two acetyl coenzyme A synthetases in the ascomycete *Gibberella zeae***. *Eukaryotic Cell* 2011, **10**:1043-1052.
192. Howlett BJ: **Secondary metabolite toxins and nutrition of plant pathogenic fungi**. *Current Opinion in Plant Biology* 2006, **9**:371-375.
193. Stergiopoulos I, Collemare J, Mehrabi R, De Wit PJGM: **Phytotoxic secondary metabolites and peptides produced by plant pathogenic Dothideomycete fungi**. *FEMS Microbiology Reviews* 2013, **37**:67-93.
194. Collemare J, Griffiths S, Iida Y, Karimi Jashni M, Battaglia E, Cox RJ, de Wit PJGM: **Secondary metabolism and biotrophic lifestyle in the tomato pathogen *Cladosporium fulvum***. *PLoS ONE* 2014, **9**:e85877.
195. Rangel LI, Hamilton O, de Jonge R, Bolton MD: **Fungal social influencers: secondary metabolites as a platform for shaping the plant-associated community**. *The Plant Journal* 2021, **108**:632-645.
196. Blum M, Chang H-Y, Chuguransky S, Grego T, Kandasaamy S, Mitchell A, Nuka G, Paysan-Lafosse T, Qureshi M, Raj S, et al.: **The InterPro protein families and domains database: 20 years on**. *Nucleic Acids Research* 2021, **49**:D344-D354.
197. Torres Pazmiño DE, Winkler M, Glieder A, Fraaije MW: **Monooxygenases as biocatalysts: Classification, mechanistic aspects and biotechnological applications**. *Journal of Biotechnology* 2010, **146**:9-24.
198. Wang M, Yuan J, Qin L, Shi W, Xia G, Liu S: ***TaCYP81D5*, one member in a wheat cytochrome P450 gene cluster, confers salinity tolerance via reactive oxygen species scavenging**. *Plant Biotechnology Journal* 2020, **18**:791-804.

199. Zhang J, Jin X, Wang Y, Zhang B, Liu T: **A cytochrome P450 monooxygenase in nondefoliating strain of *Verticillium dahliae* manipulates virulence via scavenging reactive oxygen species**. *Phytopathology* 2022, **112**:1723-1729.
200. Chaparro-Garcia A, Schwizer S, Sklenar J, Yoshida K, Petre B, Bos JIB, Schornack S, Jones AME, Bozkurt TO, Kamoun S: ***Phytophthora infestans* RXLR-WY effector AVR3a associates with dynamin-related protein 2 required for endocytosis of the plant pattern recognition receptor FLS2**. *PLoS ONE* 2015, **10**:e0137071.
201. Kamoun S, van West P, Vleeshouwers VGAA, de Groot KE, Govers F: **Resistance of *Nicotiana benthamiana* to *Phytophthora infestans* is mediated by the recognition of the elicitor protein INF1**. *The Plant Cell* 1998, **10**:1413-1425.
202. de Jonge R, Peter van Esse H, Kombrink A, Shinya T, Desaki Y, Bours R, van der Krol S, Shibuya N, Joosten Matthieu HAJ, Thomma Bart PHJ: **Conserved fungal LysM effector Ecp6 Prevents chitin-triggered immunity in plants**. *Science* 2010, **329**:953-955.
203. Hemetsberger C, Herrberger C, Zechmann B, Hillmer M, Doehlemann G: **The *Ustilago maydis* effector Pep1 suppresses plant immunity by inhibition of host peroxidase activity**. *PLoS Pathogens* 2012, **8**:e1002684.
204. Engler C, Kandzia R, Marillonnet S: **A one pot, one step, precision cloning method with high throughput capability**. *PLoS ONE* 2008, **3**:e3647.
205. Weber E, Engler C, Gruetzner R, Werner S, Marillonnet S: **A modular cloning system for standardized assembly of multigene constructs**. *PLoS ONE* 2011, **6**:e16765.
206. Holsters M, Silva B, Van Vliet F, Genetello C, De Block M, Dhaese P, Depicker A, Inzé D, Engler G, Villarroel R, et al.: **The functional organization of the nopaline *A. tumefaciens* plasmid pTiC58**. *Plasmid* 1980, **3**:212-230.
207. Guo Y, Dupont PY, Mesarich CH, Yang B, McDougal RL, Panda P, Dijkwel P, Studholme DJ, Sambles C, Win J, et al.: **Functional analysis of RXLR effectors from the New Zealand kauri dieback pathogen *Phytophthora agathidicida***. *Molecular Plant Pathology* 2020, **21**:1131-1148.
208. Rosa Sdl: **Identification of novel avirulence effectors in the Dothideomycete plant pathogens, *Venturia inaequalis* and *Cladosporium fulvum***. In *School of Agriculture and Environment*. Edited by: Massey University; 2022.
209. Daudi A, O'Brien JA: **Detection of hydrogen peroxide by DAB staining in *Arabidopsis* leaves**. *Bio Protocols* 2012, **2**.

Chapter 4:

Cell wall carbohydrate dynamics during the differentiation of infection structures by the apple scab fungus, *Venturia inaequalis*

Mercedes Rocafort[1], Vaibhav Srivastava[2], Joanna K. Bowen[3], Sara M. Díaz-Moreno[2], Vincent Bulone[2,4],§, Kim M. Plummer[5], Paul W. Sutherland[3], Marilyn A. Anderson[6], Rosie E. Bradshaw[7] and Carl H. Mesarich[1,*]

[1]Laboratory of Molecular Plant Pathology/Bioprotection Aotearoa, School of Agriculture and Environment, Massey University, Private Bag 11222, Palmerston North 4442, New Zealand.

[2]Division of Glycoscience, Department of Chemistry, School of Engineering Sciences in Chemistry, Biotechnology and Health, Royal Institute of Technology (KTH), AlbaNova University Centre, Stockholm 10691, Sweden.

[3]The New Zealand Institute for Plant and Food Research Limited, Mount Albert Research Centre, Auckland 1025, New Zealand.

[4]School of Food, Agriculture and Wine, The University of Adelaide, Waite Campus, Adelaide South Australia 5064, Australia.

[5]Department of Animal, Plant and Soil Sciences, La Trobe University, AgriBio, Centre for AgriBiosciences, La Trobe University, Bundoora, Victoria 3086, Australia.

[6]Department of Biochemistry and Genetics, La Trobe Institute for Molecular Science, La Trobe University, Bundoora, Victoria 3086, Australia.

[7]Bioprotection Aotearoa, School of Natural Sciences, Massey University, Private Bag 11222, Palmerston North 4442, New Zealand.

[§]Present address: College of Medicine and Public Health, Flinders University, Bedford Park, South Australia 5042, Australia.

[*]Corresponding author: Carl H. Mesarich

A slightly modified version of this chapter was published in *bioRxiv* (2022).

DOI: 10.1101/2022.09.21.508768

1. Abstract

Scab, caused by the biotrophic fungal pathogen *Venturia inaequalis*, is the most economically important disease of apples. During infection, *V. inaequalis* colonizes the subcuticular host environment, where it develops specialized infection structures called runner hyphae and stromata. These structures are thought to be involved in nutrient acquisition and effector (virulence factor) delivery, but also give rise to conidia that further the infection cycle. Despite their importance, very little is known about how these structures are differentiated. Likewise, nothing is known about how these structures are protected from host defences or recognition by the host immune system. To better understand these processes, we first performed a glycosidic linkage analysis of sporulating tubular hyphae from *V. inaequalis* developed in culture. This analysis revealed that the *V. inaequalis* cell wall is mostly composed of glucans (44%) and mannans (37%), whereas chitin represents a much smaller proportion (4%). Next, we used transcriptomics and confocal laser scanning microscopy to provide insights into the cell wall carbohydrate composition of runner hyphae and stromata. These analyses revealed that, during subcuticular host-colonization, genes of *V. inaequalis* putatively associated with the biosynthesis of immunogenic carbohydrates, such as chitin and β-1,6-glucan, are down-regulated relative to growth in culture, while on the surface of runner hyphae and stromata, chitin is deacetylated to the less immunogenic carbohydrate, chitosan. These changes are anticipated to enable the subcuticular differentiation of runner hyphae and stromata by *V. inaequalis*, as well as to protect these structures from host defences and recognition by the host immune system.

2. Importance

Plant-pathogenic fungi are a major threat to food security. Among these are subcuticular pathogens, which often cause latent asymptomatic infections, making them difficult to control. A key feature of these pathogens is their ability to differentiate specialized subcuticular infection structures that, to date, remain largely understudied. This is typified by *Venturia inaequalis*, which causes scab, the most economically important disease of apples. In this study, we show that, during subcuticular host-colonization, *V. inaequalis* down-regulates genes associated with the biosynthesis of two immunogenic cell wall carbohydrates, chitin and β-1,6-glucan, and coats its infection structures with a less-immunogenic carbohydrate, chitosan. These changes are anticipated to enable subcuticular host-colonization by *V. inaequalis* and provide a foundation for understanding subcuticular host-colonization by other plant-pathogenic fungi. Such an understanding is important, as it may inform the development of novel control strategies against subcuticular plant-pathogenic fungi.

Keywords

Venturia inaequalis, apple scab, cell wall, morphological differentiation, subcuticular infection structures.

3. Introduction

Scab, caused by the fungus *Venturia inaequalis*, is one of the most devastating diseases of apples worldwide [1,2]. Under favourable conditions, disease symptoms emerge as brown-green lesions on leaves, buds and fruit, rendering the fruit unmarketable and reducing crop yield by up to 70% [3,4]. Scab is also the most expensive disease of apples to control, with up to 20 fungicide treatments required each year [4,5]. This intensive fungicide use has accelerated the development of fungicide resistance in *V. inaequalis* and has increased production costs for growers [6]. While some disease-resistant apple cultivars have been developed, their use has been limited due to the rapid emergence of resistance-breaking strains of *V. inaequalis* in the field [7]. Thus, there is an urgent need to develop durable control strategies against scab.

V. inaequalis is a biotrophic pathogen that colonizes the subcuticular (apoplastic) host environment located between the cuticle and underlying epidermal cells of apple tissues [1,4]. During colonization, *V. inaequalis* develops specialized subcuticular infection structures called runner hyphae and stromata [8-10]. These structures are non-melanized and are different from regular tubular hyphae developed on the host surface [9]. Indeed, runner hyphae are wider and flatter than regular tubular hyphae and are often fused along their length to form ‘hyphal superhighways’ [9], while stromata are multi-layered pseudoparenchymatous structures that are the result of a switch from polar tip extension to non-polar lateral division [9]. In terms of functionality, stromata give rise to asexual conidia that further the infection cycle but are also thought to be involved in nutrient acquisition and effector (virulence factor) delivery. Runner hyphae, on the other hand, enable the fungus to radiate out from the initial site of host penetration, acting as a base from which additional stromata can be differentiated [9].

Notably, subcuticular infection structures are also produced by other crop-infecting members of the *Venturia* genus [11-14], as well as several other species of plant-pathogenic fungi.

The latter include *Diplocarpon rosae*, which causes black spot disease of roses [15], and *Rhynchosporium secalis*, which causes barley and rye scald [16,17]. Despite these observations, very little is known about how these structures are differentiated or how the fungal cell wall is remodelled during this process. Strikingly, *V. inaequalis* can develop infection-like structures inside cellophane membranes (CMs) that are reminiscent of those formed *in planta* [9]. This contrasts with growth on the CM surface, where the fungus develops tubular hyphae like those formed on the surface of apple tissues [9]. This finding suggests that CMs can be used as an in culture model for studying the differentiation of subcuticular infection structures and the dynamics of cell wall remodelling.

The fungal cell wall is an external barrier that plays an essential role in fungal growth and morphogenesis [18,19]. For plant-pathogenic fungi, the cell wall also has an important role in protection, as it is the first structure to encounter the hostile apoplastic environment of the host [20]. Despite this importance, its composition and biosynthesis are still poorly understood, especially for non-model filamentous pathogens [19]. While the structure and composition of the fungal cell wall differs between species, it is typically comprised of a polysaccharide and protein matrix, with glucans, chitin and mannans the main components [18]. Crucially, some of these carbohydrates, such as chitin and β-glucan, are strong elicitors of the plant immune system, with defence responses initiated upon their recognition as microbe-associated molecular patterns (MAMPs) by cell surface-localized plant immune receptors [21,22].

Chitin, a linear polymer of β-1,4-linked N-acetylglucosaminyl residues, is synthesized by membrane-bound glycosyltransferase (GT) family 2 enzymes called chitin synthases (CHSs) [18,23]. In terms of glucans, the majority is of the β-1,3-linked type, which in some instances is cross-linked with chitin to form the core structure of the fungal cell wall. Additionally, different proportions of branched β-1,6-glucan can be found in some fungi, usually

extending to the cell wall surface where it forms connections to mannoproteins [19,24,25]. β-1,3-glucan is synthesized by a membrane-bound enzyme from GT family 48 (GT48) [25,26]. The enzymes required for β-1,6-glucan biosynthesis have not been described in any filamentous fungal species [27]. However, multiple enzymes associated with β-1,6-glucan biosynthesis and β-1,3-glucan modification have been described in the yeast *Saccharomyces cerevisiae* [18,27,28].

Given the immunogenic nature of some cell wall carbohydrates, plant-associated fungi must modify their cell wall during host-colonization to avoid detection [29,30]. Likewise, as the apoplast is rich in plant-derived glucanases and chitinases [29], fungi must also actively prevent the hydrolytic release of chitin and β-glucan oligomers from their cell walls [31]. One proposed strategy used by fungi is to deacetylate chitin to chitosan [32-35], which is a poor elicitor of plant defences [36-38] and a weak substrate of plant chitinases [39,40]. Another strategy is to accumulate α-1,3-glucan on the cell surface, which shields it from the action of plant hydrolases and, in doing so, prevents the release of carbohydrate-based MAMPs [41-44].

In line with the importance of the fungal cell wall, its structure and the enzymes required for its biosynthesis are common targets for antifungal compounds [24,45]. As such, knowledge of fungal cell wall carbohydrate composition is important for the development of novel fungicides and, therefore, control strategies. To date, a detailed analysis of the cell wall carbohydrate composition in a *Venturia* species has not been published, with only one study in 1965 reporting that the cell wall of *V. inaequalis* grown in culture is made up of 28% hemicellulose, 13% β(γ)-cellulose, 20% α-cellulose and 7% chitin [46]. As cellulose is generally accepted to be absent from fungal cell walls [47], a more thorough investigation of the cell wall carbohydrate composition in *V. inaequalis* using state-of-the-art techniques is now needed. Here, using a glycosidic linkage analysis, with support from gene expression and proteomic data, we report the cell wall carbohydrate composition of sporulating tubular hyphae from *V. inaequalis*

developed on the surface of CMs. Then, using confocal laser scanning microscopy (CLSM), again in conjunction with gene expression data, we provide insights into the cell wall carbohydrate composition of infection structures developed by *V. inaequalis in planta* and compare these to the infection-like structures developed in CMs.

4. Results

4.1. The major cell wall polysaccharides of sporulating tubular hyphae formed by *V. inaequalis* in culture are glucans and mannans

To investigate the carbohydrate composition of the *V. inaequalis* cell wall during growth in culture, a glycosidic linkage analysis was performed on cell walls harvested from sporulating tubular hyphae developed on CMs overlaying potato dextrose agar (PDA) (**Figure 4-1**). The fungal material was extensively washed to avoid contamination from the underlying PDA. The glycosidic linkage analysis revealed that most polysaccharides present in the *V. inaequalis* cell wall were composed of glucosyl (Glc) (~44%) and mannosyl (Man) (~37%) residues, followed by unidentified hexopyranosyl (Hxp) (~10%), galactosyl (Gal) (~8 %) and N-acetylglucosaminosyl (GlcNAc) (~4%) residues (**Figure 4-2**). This analysis also revealed that the most dominant Glc linkage was 1,3-Glc (41.7%), followed by 1,4-Glc (26%), terminal (t)-Glc (9.63%), 1,3,6-Glc (8.03%), 1,6-Glc (3.8%) and 1,4,6-Glc (3.5%) (**Figure 4-2**). The entire GlcNAc fraction consisted of 1,4-GlcNAc residues, while the most dominant Man linkage was t-Man (50.4%), followed by 1,2-Man (33.1%). Finally, the Hxp fraction consisted of only two linkages, 2,6-Hxp (78.3%) and 4,6-Hxp (21.7%), while the Gal fraction was mostly t-Gal (87.2%) and 1,4-Gal (12.8%) (**Figure 4-2**).

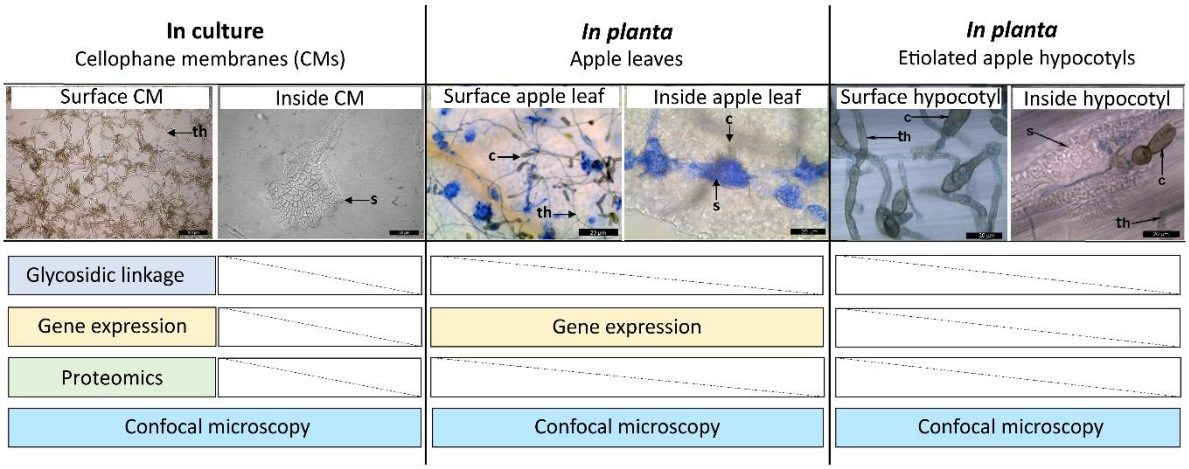

Figure 4-1. Summary of *Venturia inaequalis* samples used in this study. Tubular hyphae growing on the surface of cellophane membranes (CMs) overlaying potato dextrose agar were used for the glycosidic linkage analysis, proteomic analysis, gene expression (RNA-seq) analysis, as well as confocal laser scanning microscopy (CLSM). Infection-like structures formed inside CMs were used for CLSM. Infected apple leaves were used for the gene expression analysis and CLSM. Infected etiolated apple hypocotyls (a model *in planta* infection system) were used for CLSM. All scale bars: 20 µm. c, conidium; s, stroma; th, tubular hypha.

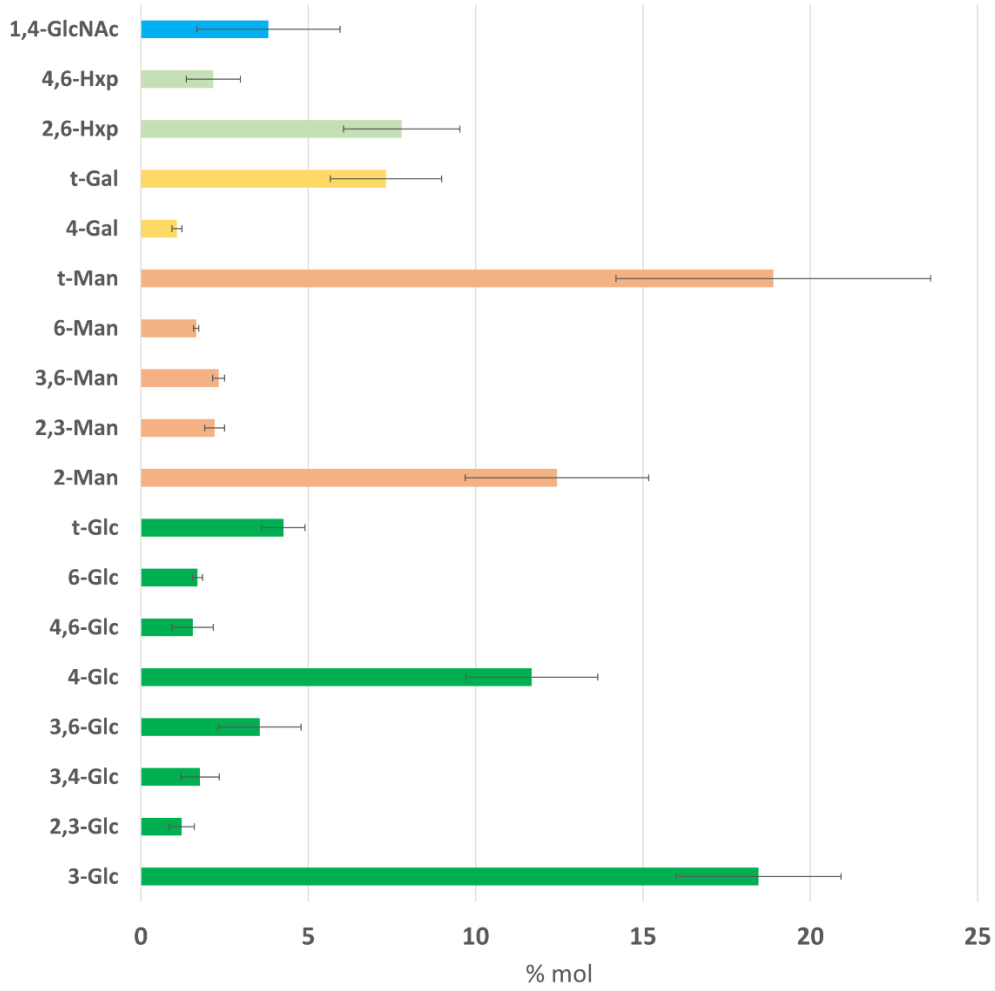

Figure 4-2. Glycosidic linkage analysis (mole percentage, % mol) of the cell wall carbohydrate fraction from sporulating tubular hyphae of *Venturia inaequalis* developed on the surface of cellophane membranes (CMs) overlaying potato dextrose agar at 5 days post-inoculation. Man, mannose; Glc, glucose; Gal, galactose; Hxp, hexopyranose; GlcNAc, N-acetylglucosamine. Error bars represent standard deviation across three technical replicates.

4.2. Identification and expression of genes putatively associated with cell wall polysaccharide biosynthesis in sporulating tubular hyphae of *V. inaequalis*

To determine which cell wall carbohydrate biosynthetic genes are expressed during growth of *V. inaequalis* on the surface of CMs, we used a combination of bioinformatic, proteomic and transcriptomics approaches (**Figure 4-1**). As a starting point, the most recently predicted gene catalogue for *V. inaequalis* [48] was inspected to identify genes putatively associated with cell wall biosynthesis (**Appendix A: Table A 4-1, Appendix A: Supplementary file 1**). Based on this analysis, 231 genes were identified (**Appendix A: Supplementary file 1**). Next, the expression of

these genes was investigated using pre-existing RNA-seq data from sporulating tubular hyphae of *V. inaequalis* grown on CMs at 7 dpi [48]. This analysis revealed that, of the 231 predicted cell wall biogenesis genes, 135 were expressed with a transcripts per million (TPM) value >10 (**Figure 4-3, Supplementary file 2**). Finally, a proteomic analysis of total protein from sporulating tubular hyphae of *V. inaequalis* grown on CMs at 5 dpi was performed. Based on this analysis, 24 of the 231 putative cell wall biosynthetic genes were found to encode proteins with proteomic support (**Appendix A: Supplementary file 3** and **4**), confirming that they were indeed produced. Of these, 17 had a TPM expression value >10 (**Figure 4-3**).

Among the glycosyltransferases (GTs) identified, 13 were putative family 2 enzymes and, of these, eight were annotated as CHSs. These were named ViCHS1–7 according to the previously established CHS classification scheme [49], based on both their CHS domain (**Figure 4-4. A**) and phylogenetic distribution (**Figure 4-4. B**). *V. inaequalis* had at least one representative from each CHS class (class I–VI), and two CHSs from class III (**Figure 4-4. A**). Four CHSs were from division I, having a simple 'amino (N)-terminus CHS domain 1' plus 'CHS domain 1' structure (**Figure 4-4. A**). All division I CHSs, except ViCHS1, were encoded by genes that had a TPM expression value >10, with *ViCHS3b* being the most highly expressed and the only CHS with proteomic support (**Figure 4-3**). Three CHSs were from division II and, of these, ViCHS4 only had a single 'CHS domain 2' module (**Figure 4-4. A**). In contrast, ViCHS5 and ViCHS7 both had a 'cytochrome b5-binding domain' and a 'Dek domain' at their carboxyl (C)-terminus, while ViCHS5 also had an N-terminal 'myosin motor-like' domain (**Figure 4-4. A**). Finally, ViCHS6 was from division III and had a single C-terminal 'CHS domain 2' module (**Figure 4-4. A**). The gene encoding this CHS, however, was not highly expressed in culture (<10 TPM). All CHSs contained both a QxxRW motif required for catalytic activity, as well as QxxEY and EDRxL domains of unknown function (**Appendix A: Figure A 4-1**) [23].

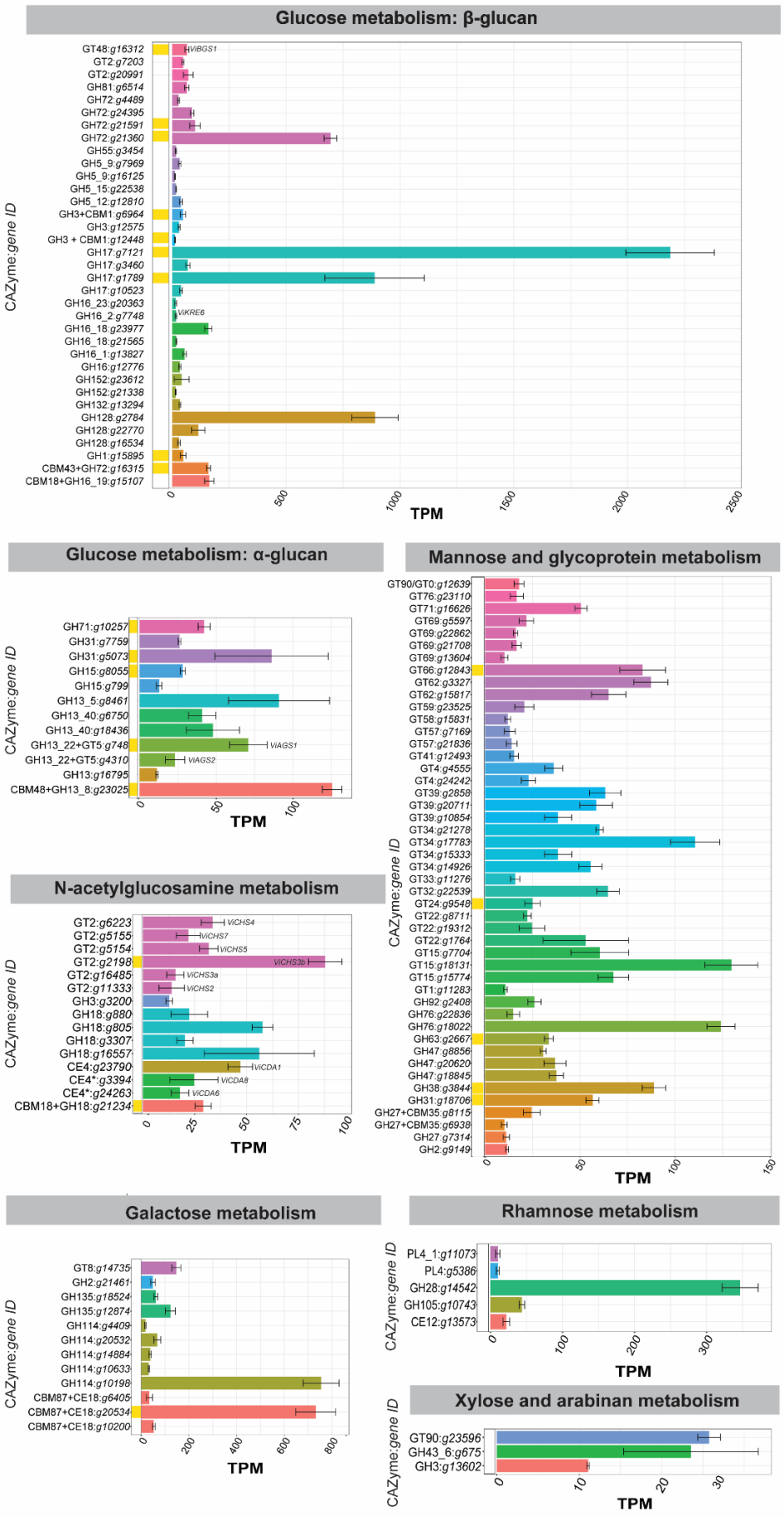
Glucose metabolism: β-glucan
GT48:g16312
GT2:g7203
GT2:g20991
GH81:g6514
GH72:g4489
GH72:g24395
GH72:g21591
GH72:g21360
GH55:g3454
GH5_9:g7969
GH5_9:g16125
GH5_15:g22538
GH5_12:g12810
GH3+CBM1:g6964
GH3:g12575
GH3 + CBM1:g12448
GH17:g7121
GH17:g3460
GH17:g1789
GH17:g10523
GH16_23:g20363
GH16_2:g7748
GH16_18:g23977
GH16_18:g21565
GH16_1:g13827
GH16:g12776
GH152:g23612
GH152:g21338
GH132:g13294
GH128:g2784
GH128:g22770
GH128:g16534
GH1:g15895
CBM43+GH72:g16315
CBM18+GH16_19:g15107
ViBGS1
ViKRE6
CAZyme:gene ID
0
500
1000
1500
2000
2500
TPM
Glucose metabolism: α-glucan
GH71:g10257
GH31:g7759
GH31:g5073
GH15:g8055
GH15:g799
GH13_5:g8461
GH13_40:g6750
GH13_40:g18436
GH13_22+GT5:g748
GH13_22+GT5:g4310
GH13:g16795
CBM48+GH13_8:g23025
ViAGS1
ViAGS2
CAZyme:gene ID
0
50
100
TPM
Mannose and glycoprotein metabolism
GT90/GT0:g12639
GT76:g23110
GT71:g16626
GT69:g5597
GT69:g22862
GT69:g21708
GT69:g13604
GT66:g12843
GT62:g3327
GT62:g15817
GT59:g23525
GT58:g15831
GT57:g7169
GT57:g21836
GT41:g12493
GT4:g4555
GT4:g24242
GT39:g2859
GT39:g20711
GT39:g10854
GT34:g21278
GT34:g17783
GT34:g15333
GT34:g14926
GT33:g11276
GT32:g22539
GT24:g9548
GT22:g8711
GT22:g19312
GT22:g1764
GT15:g7704
GT15:g18131
GT15:g15774
GT1:g11283
GH92:g2408
GH76:g22836
GH76:g18022
GH63:g2667
GH47:g8856
GH47:g20620
GH47:g18845
GH38:g3844
GH31:g18706
GH27+CBM35:g8115
GH27+CBM35:g6938
GH27:g7314
GH2:g9149
CAZyme:gene ID
0
50
100
150
TPM
N-acetylglucosamine metabolism
GT2:g6223
GT2:g5155
GT2:g5154
GT2:g2198
GT2:g16485
GT2:g11333
GH3:g3200
GH18:g880
GH18:g805
GH18:g3307
GH18:g16557
CE4:g23790
CE4*:g3394
CE4*:g24263
CBM18+GH18:g21234
ViCHS4
ViCHS7
ViCHS5
ViCHS3b
ViCHS3a
ViCHS2
ViCDA1
ViCDA8
ViCDA6
CAZyme:gene ID
0
25
50
75
100
TPM
Galactose metabolism
GT8:g14735
GH2:g21461
GH135:g18524
GH135:g12874
GH114:g4409
GH114:g20532
GH114:g14884
GH114:g10633
GH114:g10198
CBM87+CE18:g6405
CBM87+CE18:g20534
CBM87+CE18:g10200
CAZyme:gene ID
0
200
400
600
800
TPM
Rhamnose metabolism
PL4_1:g11073
PL4:g5386
GH28:g14542
GH105:g10743
CE12:g13573
CAZyme:gene ID
0
100
200
300
TPM
Xylose and arabinan metabolism
GT90:g23596
GH43_6:g675
GH3:g13602
CAZyme:gene ID
0
10
20
30
TPM

Figure 4-3. Expression of carbohydrate-active enzyme (CAZyme)-encoding genes from *Venturia inaequalis* putatively associated with cell wall biosynthesis during growth as sporulating tubular hyphae on the surface of cellophane membranes overlying potato dextrose agar at 7 days post-inoculation. Gene expression data are transcripts per million (TPM), averaged from four biological replicates, with error bars representing standard deviation. Only genes with TPM values >10 are shown and are grouped into families by colour. Enzymes labelled with an asterisk (*) were identified by Protein family (Pfam) search. Yellow blocks indicate proteins that have proteomic support by mass spectrometry. AGS, α-1,3-glucan synthase; BGS, β-1,3-glucan synthase; CBM, carbohydrate-binding module; CDA, chitin deacetylase; CE, carbohydrate esterase; CHS, chitin synthase; GH, glycoside hydrolase; GT, glycosyltransferase; PL, polysaccharide lyase.

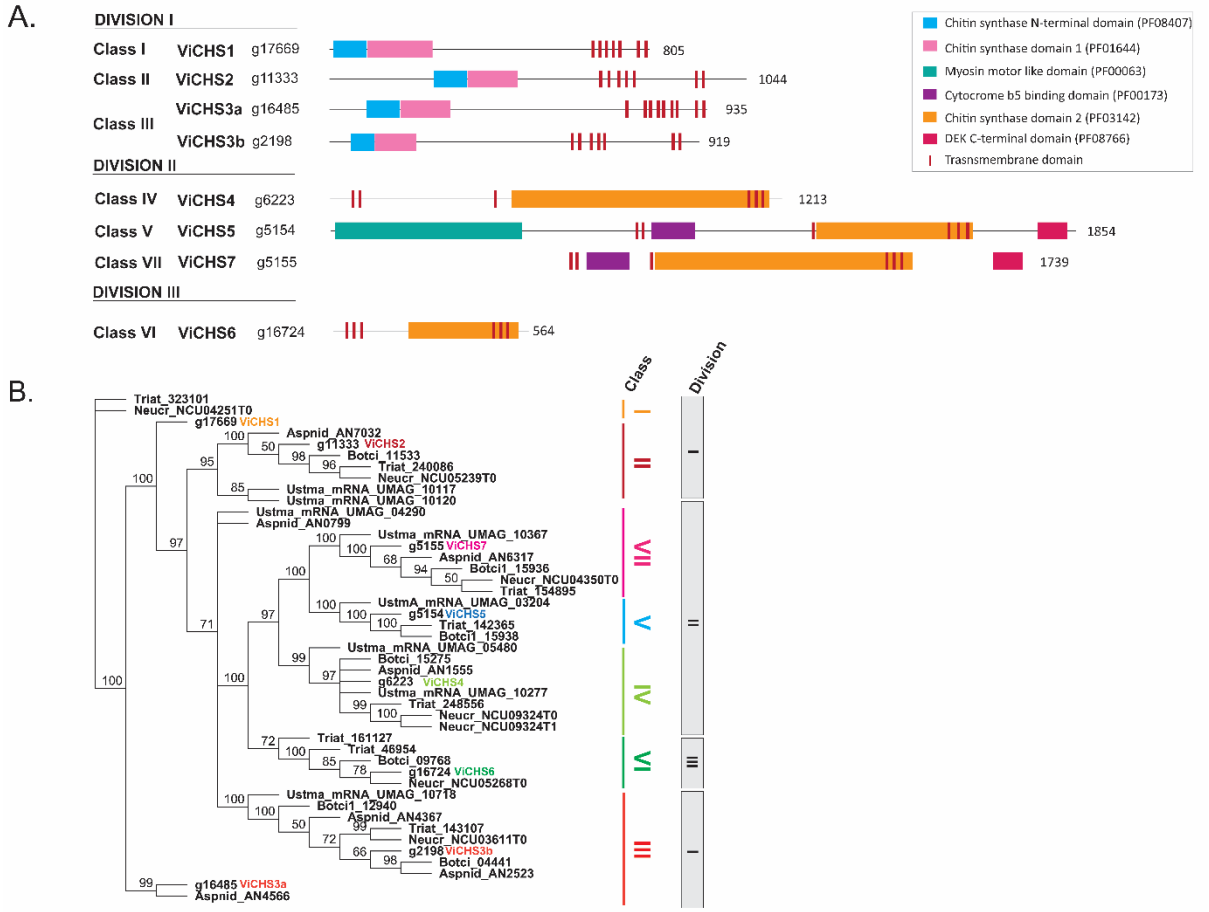

Figure 4-4. Chitin synthase (CHS) proteins of *Venturia inaequalis*. A. Predicted classification and domain organization of CHS proteins. **B.** Phylogenetic classification of the eight predicted CHSs. CHSs from *Aspergillus nidulans* (Aspnid), *Neurospora crassa* (Neucr), *Botrytis cinerea* (Botci) and *Ustilago maydis* (Ustma) were included for reference. *V. inaequalis* CHS proteins are highlighted in bold and coloured letters. Phylogenetic tree was generated from a MUSCLE alignment and end-joining method using Geneious v9.0.5, with node values indicating consensus support (%) from 100 replicates.

Multiple enzymes putatively associated with chitin modification were encoded by genes expressed during growth of *V. inaequalis* in culture, including five glycoside hydrolase (GH) family 18 chitinases, and one β-N-acetyl hexosaminidase of GH family 3 (**Figure 4-3, Appendix A: Supplementary file 1**). However, only one chitinase had proteomic support (**Figure 4-3**). In total, eight putative chitin deacetylase (*CDA*) genes were identified (**Appendix A: Supplementary file 1**). Of those (**Appendix A: Figure A 4-2. A**), a sequence alignment revealed that only ViCDA1 and ViCDA7 possessed all previously described conserved residues for catalytic activity and metal-binding and were likely functional [50,51] (**Appendix A: Figure A 4-2. B**). ViCDA4 had all metal-binding and catalytic site residues, except one, as the second conserved aspartic acid for catalytic activity was substituted by a similar negatively charged amino acid, glutamic acid. Therefore, it is likely that ViCDA4 is functional. ViCDA5 and ViCDA6 had all catalytic site residues, except the last histidine, and an amino substitution in the first metal-binding position (**Appendix A: Figure A 4-2. B**). As such, these two proteins might not be functional. ViCDA3 had two amino acid substitutions at the first and third metal-binding positions which are characteristic of allantoinases; enzymes that hydrolyse allantoin, a nitrogen-rich organic compound [52] (**Appendix A: Figure A 4-2. B**). Therefore, ViCDA3 might function as an allantoinase instead of a CDA. Finally, due to a C-terminal truncation, ViCDA8 was missing the last two catalytic site residues and, therefore, is likely to be non-functional (**Appendix A: Figure A 4-2. B**). None of the CDAs had a predicted transmembrane domain or glycosylphosphatidylinositol (GPI) anchor, while only ViCDA1 and ViCDA4 had a predicted N-terminal signal peptide for secretion (**Appendix A: Figure A 4-2. A**). *ViCDA1* was the only potentially active CDA-encoding gene with a high level of expression during growth of *V. inaequalis* in culture; however, this enzyme did not have proteomic support (**Figure 4-3** and **Appendix A: Figure A 4-2. C**).

Only one gene encoding a putative β-1,3-glucan synthase of GT family 48, *ViBGS1*, was identified in the *V. inaequalis* genome (**Appendix A: Supplementary file 1**). This gene was expressed in culture and the resulting enzyme was detected by the proteomic analysis (**Figure 4-3**). Additionally, many genes encoding β-1,3-glucan-modifying enzymes were identified, such as members of the GH17 and GH72 families (**Appendix A: Supplementary file 1**), which are anticipated to assist in either the elongation or branching of β-1,3-glucans [28,53]. Of these, four *GH17* and four *GH72* genes were expressed during growth of *V. inaequalis* in culture and half of these had proteomic support (**Figure 4-3**). This included the *GH17* gene *g7121*, which was the most highly expressed carbohydrate-active enzyme (CAZyme)-encoding gene.

A further 13 genes encoding putative GH family 16 enzymes were also identified (**Appendix A: Supplementary file 1**), with four of these found to be expressed during growth in culture (**Figure 4-3**). Three of these possibly encode chitin transglycosylases required to cross-link chitin with glucan [54], while the fourth encodes a KRE6-like enzyme (ViKRE6) that is possibly associated with β-1,6-glucan biosynthesis [55,56]. None of the four GH16 enzymes were identified in the proteomic analysis.

The genome of *V. inaequalis* also carried two genes encoding putative α-1,3-glucan synthases, named *ViAGS1* and *ViAGS2* (**Appendix A: Supplementary file 1**). Both were expressed in culture; however, only ViAGS1 had proteomic support (**Figure 4-3**). Finally, the *V. inaequalis* genome possessed 71 genes involved in the biosynthesis of mannan (**Appendix A: Supplementary file 1**). Of these, six encoded mannan polymerases and 25 encoded mannosyltransferases expressed with a TPM value >10 in culture. However, none of these enzymes had proteomic support (**Figure 4-3**).

4.3. Genes putatively associated with the biogenesis of carbohydrate-based MAMPs from *V. inaequalis* are down-regulated during host-colonization

A glycosidic linkage analysis could not be performed to determine the carbohydrate composition of infection structures produced by *V. inaequalis* during infection of apple tissue. This was due to the paucity of fungal material generated during subcuticular growth. Thus, to make inferences about how the *V. inaequalis* cell wall carbohydrate composition changes during host infection, relative to growth in culture, the expression of the 231 putative cell wall biosynthesis genes identified above was investigated using pre-existing *in planta* transcriptomic data [48] (**Figure 4-1**). These data were collected from apple leaves infected with *V. inaequalis* at six time points: 12 and 24 hours post-inoculation, as well as 2, 3, 5 and 7 dpi [48]. Using these data, a total of 68 genes putatively associated with fungal cell wall biosynthesis were found to be up-regulated, and 43 down-regulated, at one or more *in planta* time points compared to growth in culture (**Appendix A: Supplementary file 2**). Interestingly, most differentially expressed genes were associated with β-glucan metabolism (**Figure 4-5. A** and **Appendix A: Figure A 4-3**). More specifically, during early infection (12–24 hpi), the *Gas5/Gel1-like* gene, which encodes a GH72 1,3-β-glucanosyltransferase with sequence similarity to Gas5 enzymes from yeast and Gel1 from *Aspergillus* spp. [57,58], was up-regulated. Later, during mid-late infection (5 and 7 dpi), several β-glucosidase-encoding genes were up-regulated. Only a few genes associated with β-glucan metabolism were down-regulated during host-colonization, such as two genes encoding GH17 proteins and the KRE6-like enzyme (**Figure 4-5. A** and **Appendix A:Figure A 4-3**). Regarding α-1,3-glucan metabolism, *ViAGS2* was up-regulated during early (12 and 24 hpi) host infection (**Figure 4-5. B**).

Genes involved in chitin metabolism were, in general, down-regulated during host-colonization (**Figure 4-5. C** and **Appendix A:Figure A 4-4**). During early infection, two genes encoding putative GH18 chitinases and one gene encoding a GH3 enzyme of unknown function,

were down-regulated. Later, during mid-late infection, the *CHS* genes *ViCHS3b*, *ViCHS4* and *ViCHS7* were down-regulated. Interestingly, from 3 dpi, two chitinase-encoding genes, as well as the gene encoding the putatively inactive ViCDA6 were up-regulated (**Figure 4-5. C** and **Appendix A: Figure A 4-4**). Additionally, *ViCDA1*, which encodes the putatively secreted and active CDA, was constitutively expressed both in culture and *in planta* (**Appendix A: Figure A 4-2 .C**).

Several genes associated with galactose metabolism were down-regulated during mid-late infection. However, others were up-regulated over this infection stage, especially three genes encoding GH114 proteins (**Figure 4-5. D**). Finally, most genes associated with mannose and glycoprotein metabolism were up-regulated, especially those genes encoding putative mannosidases (**Appendix A: Supplementary file 2**).

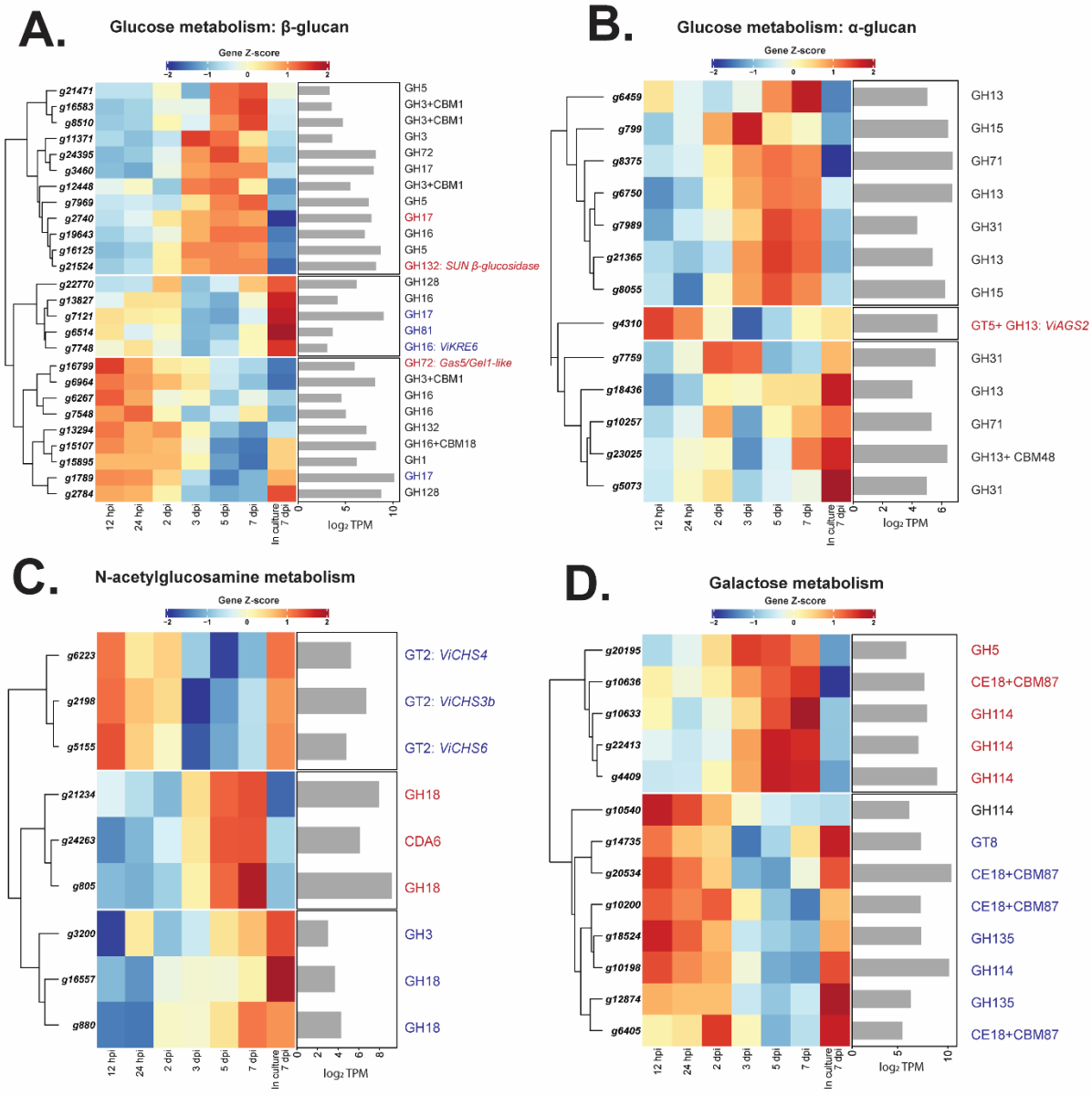

Figure 4-5. Heatmaps showing the expression profiles of genes from *Venturia inaequalis* that are both putatively associated with cell wall biosynthesis and differentially expressed during host-colonization, relative to growth in culture. Only differentially expressed genes putatively associated with **A.** glucose (β-glucan), **B.** glucose (α-glucan), **C.** N-acetylglucosamine, and **D.** galactose metabolism at one or more *in planta* time points when compared to growth on cellophane membranes overlying potato dextrose agar, and with a minimum expression of 10 transcripts per million (TPM) are shown. Heatmaps are rlog-normalized counts across all samples (Z-score), averaged from four biological replicates. Bar plots depict the maximum $\log_2$ TPM count value across all *in planta* time points. hpi, hours post-inoculation; dpi, days post-inoculation; CBM, carbohydrate-binding module; CDA, chitin deacetylase; CE, carbohydrate esterase; CHS, chitin synthase; GH, glycoside hydrolase; GT, glycosyltransferase. Blue colour highlights genes down-regulated and red colour highlights genes up-regulated during host-colonization, relative to growth in culture.

4.4. Chitosan is present on the surface of *V. inaequalis* infection structures formed *in planta*, while chitin is restricted to septa

To further investigate the cell wall carbohydrate composition of the cellular morphotypes formed by *V. inaequalis*, we used CLSM in conjunction with different carbohydrate-specific probes and antibodies to label chitin, chitosan, β-1,3-glucan, and α-1,3-glucan. CLSM was performed on *V. inaequalis* growing in culture on the surface and inside CMs, as well as during host-colonization on the surface and inside living host tissue (**Figure 4-1**). For host-colonization, two approaches were taken, with the first involving detached apple leaves, and the second involving detached etiolated apple hypocotyls (**Figure 4-1**). Here, etiolated apple hypocotyls were included as they have previously been shown to be a good system for visualising infection by *V. inaequalis* due to their reduced tissue thickness, as well as their lower levels of chlorophyll, other pigments and phenolic compounds, when compared to apple leaves [59]. However, it is important to note that hypocotyl infection does not occur in orchards, as these apples are cultivated from clonal bud wood, not seed. Hypocotyl infection may, though, occur in natural apple forests.

To monitor the distribution of chitin on the surface of the fungal cell wall, all samples were labelled with wheat germ agglutinin (WGA) conjugated to the fluorophore AlexaFluor (AF) 488 (WGA^{488}) (**Figure 4-6** and **Appendix A: Figure A 4-6**). Tubular hyphae formed on the surface of CMs (**Figure 4-6. A**), infected apple leaves (**Figure 4-6. D**) and etiolated hypocotyls (**Appendix A: Figure A 4-6**) presented limited amounts of surface-exposed chitin, with labelling mainly restricted to hyphal breakage points and, sometimes, septa. The maximum fluorescence intensity occurred at the cell periphery, indicating that the labelling signal was derived from the cell wall (**Figure 4-6. B**). To label the total chitin present in the cell wall, fungal material was first permeabilized with NaOH and then labelled with the chitin stain calcofluor white. By doing so, faint labelling was observed around the periphery of tubular hyphae, with stronger labelling found at septa (**Figure 4-6. C, E**). On the infection-like structures developed

inside CMs, chitin labelling was observed around the periphery of runner hyphae, as well as at the septa of runner hyphae and stromata (**Figure 4-6. A**). In contrast, following host penetration, chitin was exclusively restricted to septa (**Figure 4-6. D** and **Appendix A: Figure A 4-6**).

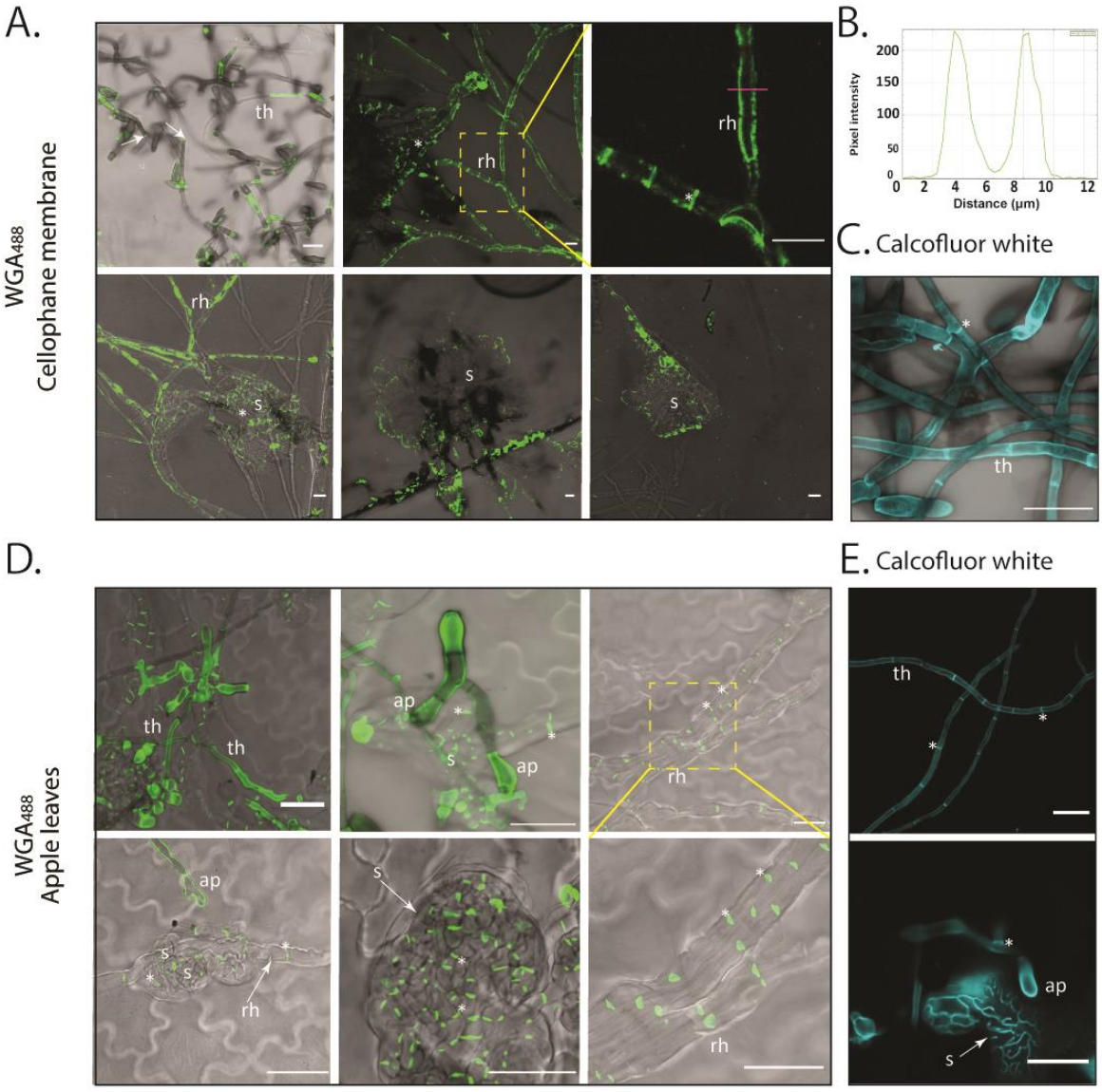

Figure 4-6. Labelling of chitin on *Venturia inaequalis* cellular morphotypes developed in culture and *in planta*. **A.** Cellular morphotypes developed in culture in and on cellophane membranes (CMs) overlaying potato dextrose agar labelled with wheat germ agglutinin-AlexaFluor 488 (WGA^{488}) (green pseudocolour). **B.** Plot profile of pixel intensity along a line (magenta) in A (top right-hand image) made with ImageJ 1.x. **C.** Tubular hyphae developed on a CM labelled with calcofluor white (cyan pseudocolour) after permeabilization with NaOH. **D.** Cellular morphotypes developed in and on 'Royal Gala' apple leaves labelled with WGA^{488} (green pseudocolour). **E.** Tubular hyphae developed on 'Royal Gala' apple leaves labelled with calcofluor white (cyan pseudocolour) after permeabilization with NaOH. Dashed yellow squares indicate zoomed-in areas. ap, appressorium; rh, runner hyphae; s, stroma; th, tubular hypha; arrow, hyphal breakage; *, septum. All scale bars: 20 µm.

Next, as *V. inaequalis* has eight putative *CDA* genes (**Appendix A: Figure A 4-2**) and, of these, *ViCDA6* is up-regulated during infection, while *ViCDA1* is constitutively expressed in culture and *in planta*, it was hypothesized that *V. inaequalis* deacetylates chitin to chitosan during host-colonization. Therefore, the tubular hyphae and infection structures of *V. inaequalis* developed in culture and *in planta* were probed using the oligogalacturonate (OGA) probe conjugated with AF488 (OGA^{488}) [60].

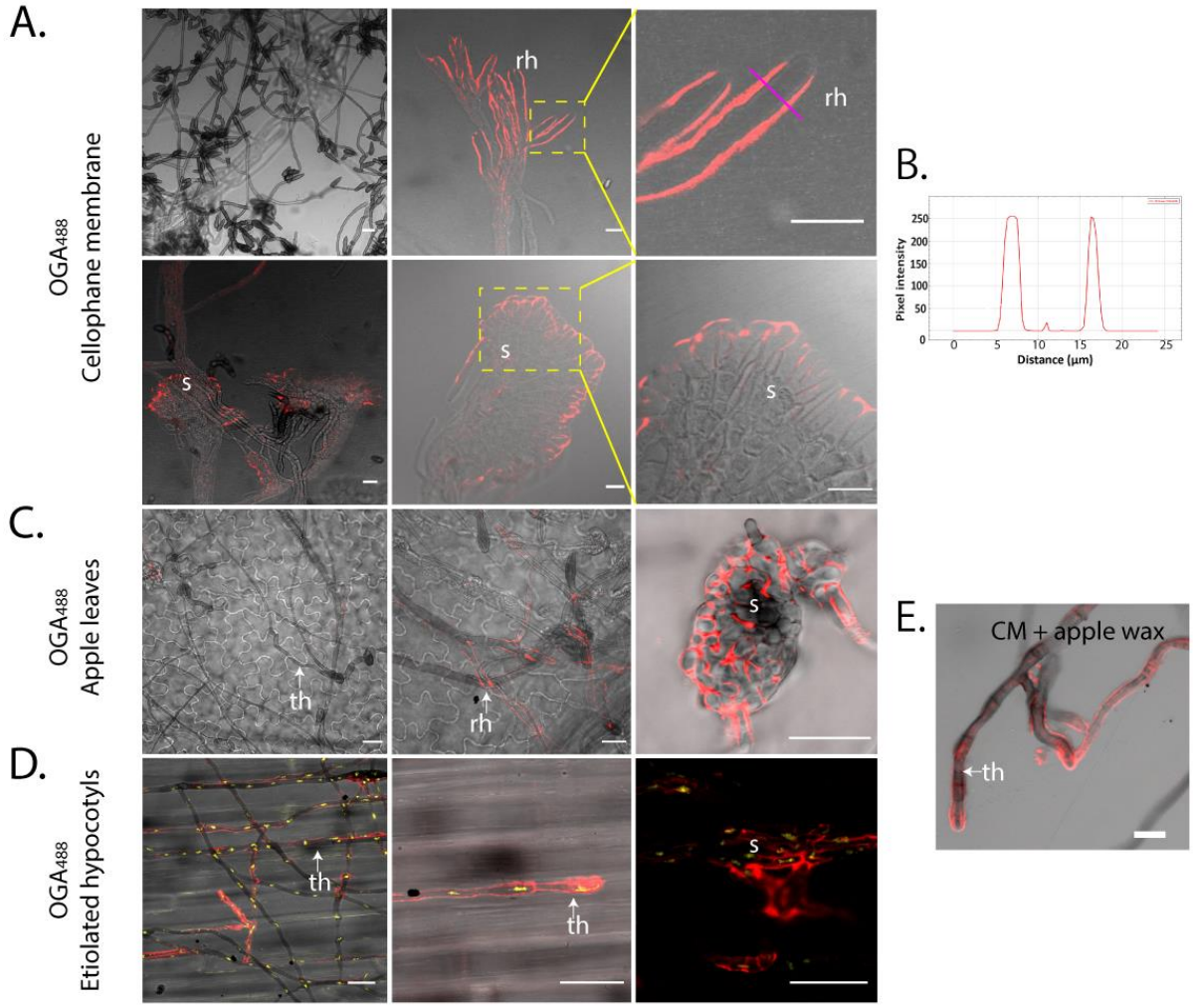

Figure 4-7. Label-accessible chitosan on the surface of *Venturia inaequalis* cellular morphotypes developed in culture and *in planta*. The fluorophore-labelled oligosaccharide OGA^{488} was used to visualize chitosan (red pseudocolour). **A.** *V. inaequalis* cellular morphotypes developed in culture in and on cellophane membranes (CMs) overlying potato dextrose agar. **B.** Plot profile of pixel intensity along a line (magenta) in A (top right-hand image) made with ImageJ 1.x. **C.** Cellular morphotypes developed in and on apple leaves. **D.** Cellular morphotypes developed in and on etiolated hypocotyls, fungal nuclei labelled with propidium iodide (PI, yellow pseudocolour). **E.** Surface hyphae developed on a CM covered with apple wax. All scale bars: 20 µm. ap, appressorium; rh, runner hyphae; th, tubular hypha; s, stroma. Dashed yellow squares indicate zoomed-in areas.

Chitosan labelling was not detected on tubular hyphae developed on the surface of CMs or apple leaves (**Figure 4-7. A, C**). In contrast, tubular hyphae developed on etiolated hypocotyls had surface-exposed chitosan (**Figure 4-7. D**), highlighting a key difference among these host infection systems. The reason behind chitosan induction on the surface of etiolated hypocotyls is not clear, but we hypothesize that *V. inaequalis* may grow more intimately with the cutin layer and, as part of this, there might be some plant-derived trigger (e.g. cutin monomers) inducing chitosan production. With this in mind, we tested if chitosan production could be induced in culture. For this purpose, wax was extracted from apple fruit and added to the surface of CMs before inoculation with *V. inaequalis* conidia. Remarkably, following germination, apple wax triggered chitosan production on tubular hyphae developed in culture (**Figure 4-7. E**). The maximum fluorescence intensity from chitosan labelling occurred at the cell periphery, indicating that the labelling signal was derived from the cell wall (**Figure 4-7. B**). Regarding the infection structures developed *in planta*, as well as the infection-like structures developed in CMs, chitosan labelling was also observed at the periphery (**Figure 4-7. C, D**).

Next, we investigated the distribution of β-1,3-glucan during growth of *V. inaequalis* in culture and *in planta*, as β-1,3-glucan is known to be an elicitor of plant defences [61]. For this purpose, β-1,3-glucan localization was investigated with a primary mouse antibody specific to β-1,3-glucan in conjunction with the anti-mouse secondary antibody CF^{488}. β-1,3-glucan-specific labelling was rarely observed around tubular hyphae developed on the surface of CMs, with labelling mostly observed at hyphal breakage points (**Figure 4-8. A**). To label β-1,3-glucan present on the surface of infection-like structures formed inside CMs, sandpaper had to be used to create antibody entry points. In doing so, we observed an intense but patchy labelling at the periphery of the infection-like structures (**Figure 4-8. A**). A similar patchy distribution was observed on tubular hyphae developed on the surface of apple leaves and etiolated hypocotyls (**Figure 4-8. B** and **Appendix A: Figure A 4-6. B**). Interestingly, labelling of β-1,3-glucan was

not observed on young infection structures developed in leaves (**Figure 4-8. B**) or hypocotyls (**Appendix A: Figure A 4-6. B**). Instead, labelling of β-1,3-glucan could only be observed on mature stromata that had ruptured the apple cuticle upon sporulation (**Figure 4-8. B**).

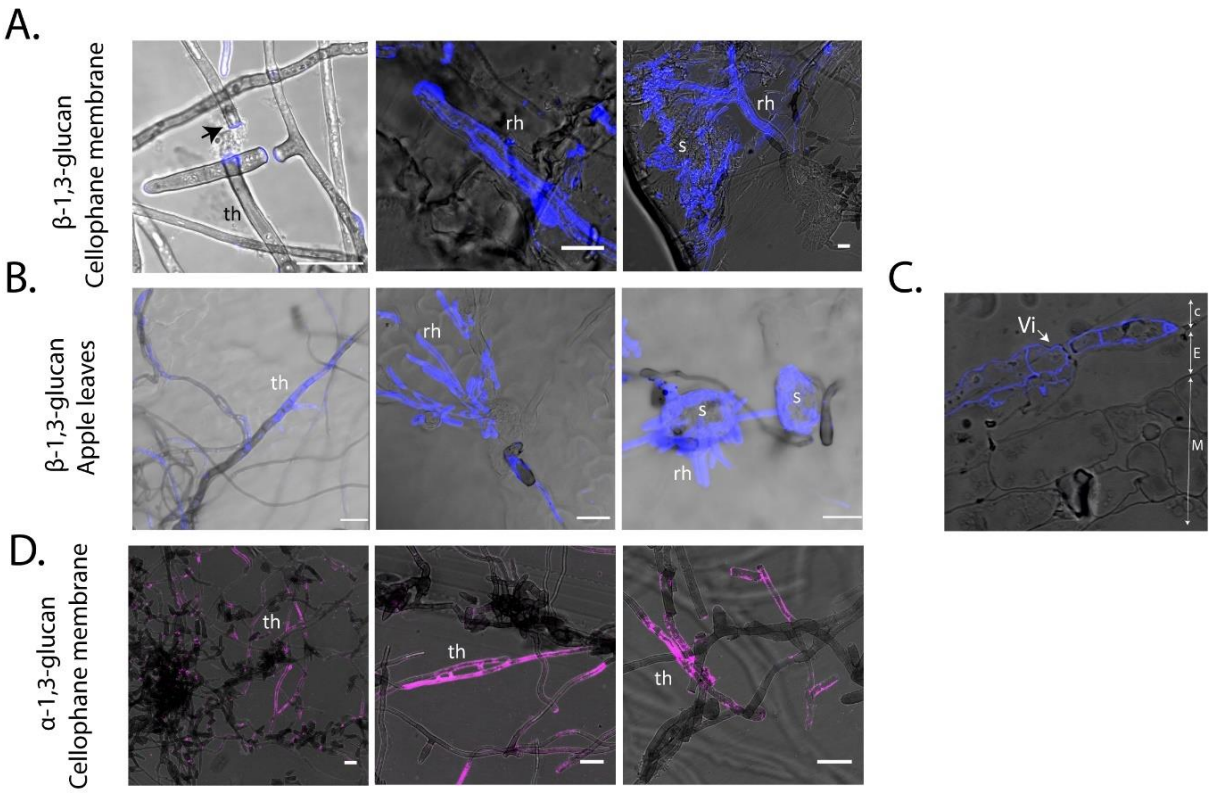

Figure 4-8. Label-accessible β-1,3-glucan and α-1,3-glucan of *Venturia inaequalis* (Vi) cellular morphotypes developed in culture and *in planta*. The monoclonal anti β-1,3-glucan primary antibody and CF^{488} secondary antibody were used to label β-1,3-glucan (blue pseudocolour), while the monoclonal MOPC-104E primary antibody and CF^{488} secondary antibody were used to label α-1,3-glucan (pink pseudocolour). **A.** β-1,3-glucan labelling of *V. inaequalis* cellular morphotypes developed in culture in and on cellophane membranes (CMs). **B.** β-1,3-glucan labelling of *V. inaequalis* cellular morphotypes developed in and on detached apple leaves. **C.** β-1,3-glucan labelling of a cross-section of a detached leaf infected with *V. inaequalis*. C: apple cuticle, E: apple epidermal cells, M: apple mesophyll cells. **D.** α-1,3-glucan labelling of *V. inaequalis* cellular morphotypes developed in culture in and on CMs. All scale bars: 20 μm. rh, runner hyphae; s, stroma; th, tubular hyphae; arrow: hyphal breakage points.

As *V. inaequalis* has two putative α-1,3-glucan synthase genes and, of these, *ViAGS2* is up-regulated during early host-colonization (**Figure 4-5**), we attempted to label α-1,3-glucan using the primary antibody MOPC-104E in conjunction with the secondary antibody anti-mouse CF^{488}. Labelling of α-1,3-glucan was observed on tubular hyphae developed on the surface

of CMs (**Figure 4-8. D**), but not on tubular hyphae developed on the surface of apple tissue (data not shown). Likewise, no labelling of α-1,3-glucan was observed on the surface of infection-like structures formed in culture or on the infection structures developed *in planta* (data not shown).

5. Discussion

Even though the cell wall plays a crucial role in viability and pathogenesis [20,30,62], few studies have focused on the cell wall of plant-pathogenic fungi. Here, we examined the cell wall carbohydrate composition of sporulating tubular hyphae from *V. inaequalis* developed on the surface of CMs using glycosidic linkage analysis. As observed in other fungi, the most abundant glucosyl linkages found in *V. inaequalis* were 1,3-Glc, with the proportion identified similar to that found in the subcuticular plant pathogen, *R. secalis* (**Table 4-1**) [63]. Glycosidic linkage analysis does not allow discrimination between α- and β-linkages. However, using CLSM, we were able to show that α-1,3-glucan was present on surface hyphae developed in culture. Therefore, a fraction of the identified 1,3-Glc could be from α-1,3-glucan, which coats the surface of the *V. inaequalis* cell wall.

Surprisingly, α-1,3-glucan could not be detected on the surface of *V. inaequalis* infection-like structures developed inside CMs or on the infection structures developed *in planta*, even though the α-1,3-glucan synthase gene, *ViAGS2*, was up-regulated during early host-colonization. The lack of α-1,3-glucan labelling *in planta* could indicate that this carbohydrate is not label-accessible on the cell wall surface during host-colonization. However, it is more plausible that this is due to the problem we encountered with antibody penetration inside host tissue. Interestingly, in some human fungal pathogens, such as *Histoplasma capsulatum* and *Aspergillus fumigatus*, as well as the fungal plant pathogen *Magnaporthe oryzae*, α-1,3-glucan accumulates on the surface of the fungal cell wall to conceal cell wall-derived MAMPs and, thus, prevents the induction of host defence responses during host infection [41-44,64]. Additionally, in *A. fumigatus*, α-1,3-glucan is important for hyphal and conidial aggregation [65,66]. With this research in mind, additional experiments are now needed to investigate whether α-1,3-glucan is present on the surface of *V. inaequalis* infection structures.

Another abundant glucosyl linkage identified as part of our glycosidic linkage analysis was 1,4-Glc. It cannot be ruled out that a portion of this 1,4-Glc arose from cellulose contamination from the CM itself, or an intracellular form of a glycogen/starch-like polysaccharide that co-purifies with the cell wall during sample preparation. Nevertheless, the low amount of 1,4,6-Glc identified suggests that not all of the 1,4-Glc originated from glycogen/starch-like polymers. Notably, there is very little evidence for the presence of β-1,4-linked glucosyl residues in fungal cell walls although, interestingly, these residues were recently reported in the cell wall of *A. fumigatus* by solid-state nuclear magnetic resonance [47,67]. Hence, it cannot be ruled out that a small fraction of the reported 1,4-Glc from *V. inaequalis* originates from β-1,4-glucan. Another more likely possibility is that a portion of the identified 1,4-Glc forms part of nigeran, a polymer commonly found in Ascomycota fungal cell walls that are composed of α-1,3- and α-1,4-glucans [68].

The presence of 1,3,6-Glc suggests that a fraction of the identified 1,3-Glc is branched. A set of *GH17* and *GH72* genes found to be highly expressed in culture likely encode the enzymes responsible for the presence of 1,3,6-linked glucosyl residues in the *V. inaequalis* cell wall, as these enzymes are putative β-1,3-glucan transglycosylases involved in cross-linking β-1,3-glucans through β-1,6-linkages [28,53,54,69]. Interestingly, during mid-late infection, *V. inaequalis* was observed to down-regulate a gene encoding a KRE6 enzyme, *ViKRE6*, which is putatively associated with β-1,6-glucan biosynthesis [55,56,70]. We suggest that, as reported in *Colletotrichum graminicola* [70], *V. inaequalis* down-regulates *ViKRE6* to reduce surface-exposed β-1,3-6-glucans that would otherwise elicit plant immune responses.

The glycosidic linkage analysis also revealed a relatively large proportion of Man (~37%) and Gal (~8%) residues in the cell wall of *V. inaequalis*, with the majority being terminal. Due to this terminal nature, we cannot conclude from which polymer these residues are derived.

The large amount of t-Man (18.9%), however, is similar to the amount of t-Man reported in *S. cerevisiae* (15.7%) [71] and drastically more than other filamentous fungi (1–3%) [63,72,73].

Table 4-1. Carbohydrate composition (%) of the *Venturia inaequalis* cell wall, determined in this study using glycosidic linkage analysis, compared to other fungal species for which carbohydrate composition is known.

[1]	***V. inaequalis***	***B. graminis* f.sp. *hordei***	***R. secalis***	***N. crassa***	***A. fumigatus***	***S. cerevisiae***
t-Man	18.9	1.7	3.1	1.5	0.1	15.7
t-Glc	4.3	5.7	13.9	13	0.3	5.5
t-Gal	7.3	2.2	0	1	2.2	0
3-Glc	18.5	35.6	11.6	54	43.3	26.9
2-Man	12.4	4.3	4.3	3	2.4	7.9
6-Man	1.7	3.8	4.4	0	1.2	1.2
6-Glc	1.7	2	0.5	0	0.3	0.7
4-Gal	1.1	6.8	0	0	0	0
4-Glc	11.7	6.3	17.2	4	14.2	0
2,3-Man	2.2	0	0.9	0	0	0
3,4-Glc	1.8	2.1	0.5	0	0.3	0.7
2,3-Glc	1.2	7.5	1.5	0	0	7
3,6-Glc	3.5	1.6	2.7	5	1.6	2
3,6-Man	2.3	0.6	0.6	0	0	0.4
2,6-Hxp	7.8	0	0	0	0	0
4,6-Glc	1.5	2.3	0.5	0	0	0
4,6-Hxp	2.2	0	0	0	0	0
1,4-GlcNAc	3.8	8.7	6.3	10	17.65	0.6
3,6-Gal	0.0	0	0	0	0	0

[1] This comparison was made for the filamentous fungi *Blumeria graminis* f. sp. *hordei* [73], *Rhynchosporium secalis* [63], *Neurospora crassa* [72], *Aspergillus fumigatus* [74] (alkali-insoluble fraction of the cell wall), and the yeast *Saccharomyces cerevisiae* [71]. This table was extracted and modified from [73]. Gal, galactose; Glc, glucose; GlcNAc, N-acetylglucosamine; Man, mannose; Hxp, hexopyranose.

Following glycosidic linkage analysis, we attempted to investigate the presence and location of β-1,3- and branched β-1,3-6-glucans on the fungal cell wall surface using a specific antibody that labels β-1,3-glucan. Regarding the infection structures developed inside the host, we only observed strong labelling on the surface of mature stromata that were rupturing through the apple cuticle as part of the sporulation process. It is unclear whether these infection structures were labelled because the mature stromata were more accessible to the β-1,3-glucan antibody, or because the β-1,3-glucan is masked during early host-colonization and is only surface-exposed upon sporulation.

The glycosidic linkage analysis also revealed that the cell wall of sporulating tubular hyphae from *V. inaequalis* is comprised of 3.8% chitin, which is relatively low for a filamentous fungus. Indeed, chitin usually makes up around 10–15% of the fungal cell wall [18,25,27] (**Table 4-1**). This result is in line with the labelling profile of chitin present on the surface of tubular hyphae formed on CMs using the WGA^{488} probe and calcofluor white, where chitin was mostly restricted to septa. Transcriptomic and proteomic data obtained in our study suggest that ViCHS3b, a class III CHS enzyme, might be responsible for the bulk of chitin biosynthesis in *V. inaequalis* tubular hyphae.

Interestingly, on the plant surface, chitin was exclusively observed on tubular hyphae and appressoria, while on the infection structures produced after host penetration, chitin was found to be restricted to the septa. Furthermore, genes encoding CHSs and some chitinases were down-regulated during early host-colonization. These findings suggest that, in addition to transcriptionally regulating chitin production, *V. inaequalis* also restricts the amount of chitin it exposes on its surface to prevent activation of chitin-triggered host defences. Another possibility is that *V. inaequalis* masks chitin on the cell wall surface through the secretion of chitin-binding effectors, similar to that shown for the Avr4 effector protein of *Fulvia fulva* [75]. Alternatively, *V. inaequalis* may produce chitin-binding effectors that sequester chitin oligomers during the process of cell wall remodelling to prevent their detection by the apple immune system. Notably, during *in planta* host-colonization, the lysin motif (LysM) domain-containing effector candidate, ViEcp6, which has sequence similarity to the chitin-binding Ecp6 effector of *F. fulva* [76,77], was found to be up-regulated [48] and had proteomic support in culture (**Appendix A: Supplementary file 3** and **4**). Although Ecp6 from *F. fulva* is known to sequester chitin oligomers to evade host defence responses in tomato [78], other LysM domain-containing effectors, such as Mg3LysM from *Zymoseptoria tritici*, have been shown to protect the hyphal cell wall from hydrolysis by plant

chitinases [79]. It is therefore possible that ViEcp6 plays a role in chitin protection and/or sequestration during subcuticular host-colonization.

Another possibility could be that *V. inaequalis* deacetylates chitin to chitosan during host-colonization to avoid activation of plant defences, as reported for other plant-associated fungal pathogens [33,35,80,81] and endophytes [34]. In line with this, we observed that runner hyphae and stromata developed in culture and *in planta* were completely covered with chitosan. This indicates that chitosan is the main surface-exposed carbohydrate present on these structures. Interestingly, chitosan was also observed on tubular hyphae developed on the surface of hypocotyls and chitosan production could be induced during growth on the surface of CMs coated with apple wax. These results suggest that chitosan induction is triggered by a plant-derived cue present in the apple wax. Additionally, chitosan labelling was observed at the periphery of infection-like structures developed inside CMs, indicating that another trigger, such as pressure, might be involved. It is important to note here, however, that although the OGA^{488} probe is specific for chitosan [60], binding to the positively charged groups of the carbohydrate, it cannot be ruled out that it also binds to positively charged proteins present on the surface of infection structures.

In addition to preventing activation of the plant immune system, chitosan has also been reported to be important for cell adhesion and morphogenesis in fungi [81-84]. Therefore, chitosan may play other functions in *V. inaequalis*. The deacetylation of chitin to chitosan is catalysed by CDAs, and an inspection of the *V. inaequalis* genome revealed that this fungus has eight predicted CDA-encoding genes, three of which (*ViCDA1*, *ViCDA4*, *ViCDA7*) are predicted to be functional. One of these, *ViCDA1*, encodes a protein with a predicted N-terminal signal peptide, and is constitutively expressed in culture and during host-colonization. Secreted CDAs are usually assumed to deacetylate chitin to chitosan to prevent activation of the plant immune system [50,85]. Therefore, it seems plausible that ViCDA1 is the main enzyme responsible for

deacetylating chitin to chitosan on the surface of *V. inaequalis* infection structures. In any case, the recently developed CRISPR-Cas9 method for reverse genetics in this fungus [86] will serve to investigate the putative role of ViCDA1 and other CDAs in *V. inaequalis*.

In conclusion, we have detailed, for the first time, the cell wall carbohydrate composition of *V. inaequalis* during growth in culture. Furthermore, by assessing the expression profile of genes putatively associated with cell wall biogenesis, as well as by monitoring the localization of cell surface-associated carbohydrates using CLSM, we have also provided new insights into how this fungus differentiates and protects its infection structures during host-colonization. Importantly, as the first study of its kind for a subcuticular pathogen, our research provides a foundation for understanding not only how this class of plant-pathogenic fungi causes disease, but also how they can potentially be controlled.

6. Materials and methods

6.1. *V. inaequalis* isolate

V. inaequalis isolate MNH120, also known as ICMP 13258 and Vi1 [77,87], derived from a monospore culture, was used in this study.

6.2. Preparation of fungal material for glycosidic linkage analysis and proteomics

Fungal material for glycosidic linkage analysis and proteomics was prepared by inoculating 100 µl of 10^5–10^6 conidia from *V. inaequalis* on CMs (Waugh Rubber Bands; Wellington, New Zealand) overlaying PDA (*Scharlab*, S.L; Senmanat, Spain) and culturing for 5 days at 22°C under a 16 h light/8 h dark cycle. Following culturing, fungal biomass, comprising a mix of tubular hyphae and asexual conidia was harvested from the surface of the CMs using an L-shaped spreader, washed three times by centrifugation at 4,000 g for 15 min, frozen at –20°C, freeze-dried, and then ground to a fine powder using liquid nitrogen.

6.3. Glycosidic linkage analysis

Cell wall material from *V. inaequalis* grown in culture on the surface of CMs overlaying PDA at 5 dpi was prepared in triplicate (i.e. as three technical replicates) using a previously described protocol [88]. The cell wall preparations were subjected to permethylation and GC/EI-MS analysis [88]. Partially methylated alditol acetate (PMAA) derivatives were separated and analysed by gas chromatography (GC) on a SP-2380 capillary column (30 m x 0.25 mm [inner diameter]; Supelco) using an HP-6890 GC system with an HP-5973 electron-impact mass spectrometer (EI-MS) as a detector (Agilent Technologies; CA, US). The temperature was programmed to increase from 180°C to 230°C at a rate of 1.5°C/min. The mass spectra of the fragments obtained from the PMAA derivatives were compared with reference derivatives.

6.4. Proteomic analysis

Approximately 10 mg of powdered fungal material from *V. inaequalis* grown in culture on the surface of CMs overlaying PDA at 5 dpi in triplicate (i.e. as three technical replicates) was boiled in SDS buffer (75 mM Tris-HCl buffer pH 6.8 containing 3% [w/v] SDS, 100 mM DTT, 15% [w/v] glycerol and 0.002% bromophenol blue) for 5 min at 95°C. Insoluble material was then removed by centrifugation at 14,000 *x g* for 10 min and the supernatant was loaded on a 12% Mini-Protean TGX SDS-PAGE system (Bio-Rad; CA, USA). After staining with Coomassie Blue (Thermo Fisher Scientific, MA, USA), the gel lane was cut into 10 bands and the proteins were subjected to in-gel digestion with trypsin (Promega, Madison, WI, United States) as previously described [89].

Peptide analysis was performed with reverse-phase liquid chromatography electrospray ionization–tandem mass spectrometry (LC–ESI–MS/MS) using a nanoACQUITY Ultra Performance Liquid Chromatography system coupled to a Q-TOF mass spectrometer (Xevo Q-TOF, Waters; MA, USA). The in-gel tryptic peptides were resuspended in 0.1% trifluoroacetic acid (TFA) and loaded on a C18 trap column (Symmetry 180 µm × 20 mm, 5 µm, Waters) that was then washed with 0.1% (v/v) formic acid at 10 µl/min for 5 min. The samples eluted from the trap column were separated on a C18 analytical column (75 µm × 150 mm, 1.7 µm, Waters) at 250 nl/min using 0.1% formic acid as solvent A and 0.1% formic acid in acetonitrile as solvent B in a stepwise gradient: 0–10% B (0–5 min), 10–30% B (5–70 min), 30–40% B (70–72 min), 40–90% B (72–75 min), 90% B (75–80 min), and 90–0.1% B (80–85 min). The eluting peptides were sprayed in the mass spectrometer (capillary and cone voltages set to 2.1 kV and 45 V, respectively), and MS/MS spectra were acquired using automated data-directed switching between the MS and MS/MS modes using the instrument software (MassLynx v4.0 SP4). The five most abundant signals of a survey scan (400–1300 m/z range, 1 sec scan time) were selected by charge state, and

collision energy was applied accordingly for sequential MS/MS fragmentation scanning (100–1800 m/z range, 1 sec scan time).

The resulting MS raw data files were processed using Mascot Distiller (v2.4.3.2, Matrix Science, London, UK), and the resulting files were submitted to a local Mascot (Matrix Science, v2.3.1) server using the *Venturia* protein database (25,153 sequences) [48]. The following settings were used for database search: trypsin-specific digestion with two missed cleavages, ethanolated cysteine as fixed and oxidized methionine as variable modifications, peptide tolerance of 200 ppm and fragment tolerance of 0.2 Da. Only those peptides with mascot scores exceeding the threshold for statistical significance (p <0.05) were retained. The peak list files generated from the mass spectrometry raw data have been deposited to the MassIVE database (accession number MSV000090342, doi:10.25345/C56M3379F).

6.5. Plant growth conditions and infection of apple material

Open-pollinated *Malus* x *domestica* cultivar 'Royal Gala' apple seeds (Hawke's Bay, New Zealand) were germinated at 4°C in moist vermiculite containing 100 mg/ml Thiram fungicide (Kiwicare Corporation Limited; Christchurch, New Zealand) for approximately two months in the dark. Once germinated, apple seedlings were planted in potting mix (Daltons^{TM} premium potting mix; Daltons, Matamata, New Zealand) and grown under a 16 h light/8 h dark cycle with a Philips SON-T AGRO 400 Sodium lamp, at 20°C with ambient humidity for 4-to-6 weeks.

For the growth of etiolated hypocotyls, a fast-germination method was used. Seeds were sterilized with 5% ethanol for 5 min, rinsed five times with sterile MilliQ water, and soaked in MilliQ water overnight. The next morning, the testa of the apple seeds were peeled away with sterile forceps until the underlying white embryo was uncovered. Then, the white embryo was placed in Murashige and Skoog (MS) agar medium (2. 25 g/L MS [Sigma-Aldrich; Castle Hill, Australia], 10 g/L agar, pH 5.8 [KOH]) inside 50 ml Falcon^{TM} tubes, with the tip of the radical

submerged in the agar. Once the apple seeds had germinated and the cotyledons were fully expanded, the seedlings were transferred to potting mix soil and grown at 20°C with ambient humidity in the dark for two weeks. *V. inaequalis* infection of detached apple leaves and hypocotyls was performed as described by Rocafort et al. [48] and Shiller et al. [90], respectively.

6.6. Extraction of apple wax and coating of cellophane membranes

Approximately ten fruit from apple cultivar 'Royal Gala', acquired from a local supermarket in New Zealand, were used for wax extraction. To extract the wax, each apple was dipped a total of five times, each for 10 sec, in 200 ml chloroform contained within a glass beaker. Following this step, the chloroform in the beaker was evaporated off at room temperature (RT) until the extracted wax had completely dried out. To coat the CMs with apple wax, a Kimwipe (Kimtech; Milsons Point, Australia) was dipped in chloroform, wiped over the surface of the wax in the beaker, and then transferred by wiping onto the surface of CMs until an homogeneous white coating was observed. Coating of the CMs with apple wax was performed under sterile conditions as much as possible, with coated CMs subsequently subjected to 15 min of UV exposure to ensure sterility.

6.7. Confocal laser scanning microscopy

Cross-sections of detached apple leaves infected with *V. inaequalis* at 7 dpi were prepared for labelling as described previously [9]. Briefly, leaf tissue was fixed in paraformaldehyde and 2.5% (v/v) glutaraldehyde in 0.1 M phosphate buffer (pH 7.2) and then embedded in LR White resin (London Resin, Reading, UK), with samples subsequently cross-sectioned from the resin-embedded material.

All the other samples (non-cross-sectioned), CMs associated with *V. inaequalis* at 6-7 dpi, as well as detached apple leaves and etiolated hypocotyls infected with *V. inaequalis* at 7 dpi, were fixed in 95% ethanol and stored at 4°C until required. Additionally, to enhance the

penetrability of the carbohydrate-specific probes and antibodies used for labelling (see below), *in planta* samples were macerated with 10% KOH at RT for 4 h. For α-1,3-glucan and β-1,3-glucan labelling, non-cross section CM samples were gently scratched with sandpaper (200 grit) to generate entry points for the antibody. All samples were washed 3 times with 1 ml phosphate-buffered saline (PBS) buffer (pH 7.4) prior to labelling.

To facilitate the visualization of *V. inaequalis* infection structures in apple hypocotyls, fungal nuclei were stained with 0.002% (w/v) propidium iodide (PI) in PBS buffer (pH 7.4) containing 0.02% Tween 20. For the labelling of chitin and chitosan, carbohydrate-specific probes were used. More specifically, for WGA^{488} labelling of chitin, samples were vacuum-infiltrated in the dark for 30 min in a solution containing 0.1 mg/ml of WGA^{488} probe and 0.02% Tween 20 in PBS buffer (pH 7.4). For calcofluor white labelling of chitin, samples were incubated in 300 mM sodium hydroxide (NaOH) for 1 h prior to incubation with 0.01% calcofluor white (Sigma-Aldrich) in PBS (pH 7.4). For OGA^{488} labelling of chitosan, samples were vacuum-infiltrated in the dark for 30 min with a solution of 0.1% (w/v) OGA^{488} and 0.02% Tween 20 in PBS buffer (pH 7.4). For this purpose, a 1 mg/ml stock solution of OGA^{488} in 0.1 M sodium acetate buffer (pH 4.9) was kindly provided by Jozef Mravec from the University of Copenhagen [60]. In all cases, the probe used for labelling was vacuum-infiltrated into samples for 20 min, twice, in the dark.

For the labelling of β-1,3-glucan in cross-sectioned and non-cross-sectioned samples, and α-1,3-glucan in non-cross-sectioned samples, carbohydrate-specific antibodies were used. More specifically, samples were first washed three times with 1 ml PBS buffer (pH 7.4) and blocked with 3% bovine serum albumin (BSA, Gibco; Maryland, USA) in PBS buffer for 1 h at RT in a rotatory shaker (John Morris Scientific; Palmerston North, New Zealand). Then, samples were washed with 1 ml PBS buffer three times and vacuum-infiltrated for 20 min with 0.1 mg/ml

of primary mouse anti-1,3-β-glucan antibody (Biosupplies; Sydney, Australia) for β-1,3-glucan labelling or 0.1 mg/ml mouse MOPC-104E primary antibody (Sigma-Aldrich) for α-1,3-glucan labelling, and then incubated overnight with shaking (30 rpm) at 4°C. The next day, samples were washed three times with 1 ml PBS buffer (pH 7.4) and vacuum-infiltrated for 20 min with 0.1 mg/ml anti-mouse CF^{488} secondary antibody (Biotum; California, USA) in PBS buffer (pH 7.4) and incubated with shaking at 30 rpm, at RT in the dark. Finally, samples were washed three times with 1ml PBS buffer.

CLSM was performed on labelled samples using a Leica SP5 DM6000B confocal microscope (488 nm argon and 405 nm UV laser) (Leica Microsystems, Manheim, Germany), with images produced using ImageJ 1.x software (NIH) [91]. Here, multiple optical sections (z-stacks) were projected into a single image as maximum or average intensity projections. PI was excited at 561 nm using a DPSS laser with an emission spectrum of 561–600 nm. WGA^{488}, OGA^{488} and CF^{488} were excited using a 488 nm Argon laser (power ~30%) with an emission spectrum of 498–551 nm. Calcofluor white was excited using a 405 nm UV laser with an emission spectrum of 445–455 nm. For all samples, an appropiate non-stained control was performed (**Appendix A: Figure A 4-5**).

6.8. Annotation of fungal cell wall enzymes

The predicted *V. inaequalis* isolate MNH120 protein catalogue from Rocafort et al. [48] (10.5281/zenodo.6233646) was used in this study. Proteins that were putatively associated with fungal cell wall biogenesis were identified based on CAZyme annotation and KEGG classification, and decisions about the potential classification of enzymes involved in cell wall biosynthesis were further assessed by InterProscan scan annotation (in conjunction with the Pfam, HAMAP, MOBIDB, PIRSF, PROSITE and SUPERFAMILY tools). Here, all InterProScan and CAZyme annotations, as well as KEGG classifications, were provided by Rocafort et al. [48].

To identify CDAs, proteins with a CE4 CAZyme annotation or with 'polysaccharide deacetylase domain' (PF01522) were annotated as CDAs. To further investigate other putative CDAs in the genome a BLASTp [92] search was performed against the *V. inaequalis* MNH120 genome [77] using the protein sequence of CDAs from pathogens whose activity has been experimentally shown: *P. graminis* (GMQ_17027) [93], *Colletotrichum lindemuthianum* (ClCDA) (AAT68493) [50], *Pestalotiopsis* sp. (PesCDA) (KY024221) [85] and *M. oryzae* (MGG_12939, 14966, 09159, 04172, 08774, 01868, 08356, 05023, 04704 and 03461) [81]. Although the enzymatic activity of the *M. oryzae* CDAs has not been experimentally shown, their function as potential CDAs has been reported by gene deletion studies [31,33,81]. The E- value cut-off used for all BLASTp searches was 1E-02. To investigate whether the putative CDAs had the conserved amino acid residues required for catalytic activity and metal binding, an alignment was performed between all of the predicted *V. inaequalis* CDAs and the functionally characterized CDAs from above, ClCDA and PesCDA [94], using the MUSCLE plugin of Geneious v9.0.5.

To classify CHSs, the InterProScan domain annotation from Rocafort et al. [48] was used and an alignment of all *V. inaequalis* CHSs was performed using the MUSCLE plugin of Geneious v9.0.5 [94]. The CHSs from the *Aspergillus nidulans* [95], *Neurospora crassa* [96], *Botrytis cinerea* [97] and *Ustilago maydis* were included in this alignment as a reference. To determine if the predicted CHSs of *V. inaequalis* had the conserved motifs required for CHS activity, a protein sequence alignment was performed with the functionally characterized CHS from *N. crassa* [96] as a reference.

6.9. Gene expression analysis

Pre-existing *V. inaequalis* gene expression data from Rocafort et al. [48] (GEO Series accession: GSE198244) were used for the gene expression analysis, and differentially expressed genes were identified using DESeq2 package v1.32.0 [98]. Genes up- or down-regulated at one or more *in*

planta infection time points, relative to growth in culture, with a $\log_2$ fold change of +/-1.5 and a *p* value of 0.01 were considered differentially expressed. Volcano plots were generated using ggplots2 v3.3.5 [99], while gene expression heatmaps were generated using Complexheatmap v2.9.1 [100].

Funding

MRF and CHM were supported by the Marsden Fund Council from Government funding (project ID 17-MAU-100), managed by Royal Society Te Apārangi.

Author Contributions Statement

CM, MR, JB, VB, MA and KP conceived the project. MR, VS, SM and PS conducted the experiments. MR performed the bioinformatic analyses. MR, CM, VS, VB, JB, KP and RB provided critical input in experimental design or data analysis. MR, CM, VS and VB wrote the manuscript. All authors read, revised, and approved the final manuscript.

Conflicts of Interest Statement

The authors declare no conflicts of interest.

7. Appendix A: Supplementary information

Supplementary file 1: *Venturia inaequalis* genes that encode enzymes putatively associated with fungal cell wall biogenesis. Enzymes were classified according to their predicted roles in cell wall biogenesis, as based on predicted 'Kyoto Encyclopedia of Genes and Genomes' (KEGG) and InterProScan annotations. CBM, carbohydrate-binding module; CDA, chitin deacetylase; CE, carbohydrate esterase; CHS, chitin synthase; GH, glycoside hydrolase; GT, glycosyl transferase; PL, polysaccharide lyase. * Only three CE4 proteins were predicted to be a carbohydrate-active enzyme (CAZYme) using dbCan2.

https://www.biorxiv.org/content/biorxiv/early/2022/09/21/2022.09.21.508768/DC2/embed/media-2.xlsx?download=true

Table A 4-1. *Venturia inaequalis* carbohydrate-active enzymes (CAZymes) putatively involved in fungal cell wall biogenesis and modification.

Enzyme [1]	CAZyme family [2]	Copy number
CHITIN METABOLISM		
Chitin synthase	GT2	8
Chitinase	GH18	5
Hexosaminadase	GH20	1
β-N-acetylhexosaminidase	GH3	1
Chitin deacetylase	CE4	8[3]
GLUCAN METABOLISM		
β-1,3-glucan synthase	GT48	1
α-1,3-glucan synthase	GH13+GT15	2
1,3-β-glucanosyltransferase	GH72	6
β-glycanase	GH16	13
1,3-β-glucanase	GH128, GH152, GH64, GH81	8
β-glucosidase	GH1, GH132, GH17, GH3, GH5, GH55	29
1,4-α-glucan branching enzyme	CBM48+GH13_8	1
α-amylase	GH13	7
alpha-1,6-glucohydrolase	GH13	2
glucan 1,4-alpha-glucosidase	GH15	2
α-glucosidase	GH31, GH71	6
MANNOSE METABOLISM		
α-1,2-mannosyltransferase	GT15, GT4, GT71	7
α-1,3-mannosyltransferase	GT69	7
α-1,6-mannosyltransferase	GT22, GT34	6
α-1,3/α-1,6-mannosyltransferase	GT4	1

Enzyme [1]	CAZyme family [2]	Copy number
GPI-mannosyltransferase	GT22, GT50, GT76	4
β-1,4-mannosyltransferase	GT33	1
Dolichyl-phosphate-mannose-protein mannosyltransferase	GT39	3
Mannan polymerase complex MNN9/ANP1	GT62	2
α-1,2-mannosidase	GH92, GH47	13
Mannan endo-1,6-α-mannosidase	GH76	8
Mannosyl-oligosaccharide glucosidase	GH63, GH31	3
α-mannosidase	GH38	1
β-mannosidase	GH2	1
Mannosyl-glycoprotein endo- β -N-acetylglucosaminidase	GH85	1
GALACTOSE METABOLISM		
Inositol 3-alpha-Galactosyltransferase	GT8	1
α-galactosidase	GH27	6
β-galactosidase	GH2	1
α-1,4-galactosaminogalactan hydrolase	GH135	4
α-1,4-polygalactosaminidase	GH114	9
N-acetylgalactosamine deacetylase	CE18+CBM87	4
Endo- β -1,6-galactanase	GH5	1
UDP-glucose 4-epimerase	-	3

[1] Enzymes were classified according to their predicted roles in cell wall biogenesis, as based on predicted 'Kyoto Encyclopedia of Genes and Genomes' (KEGG) and InterProScan annotations.

[2]CBM, carbohydrate-binding molecule; CE, carbohydrate esterase; GH, glycoside hydrolase; GT, glycosyl transferase; PL, polysaccharide lyase.

[3] Only three CE4 proteins were predicted to be a carbohydrate-active enzyme (CAZYme) using dbCan2.

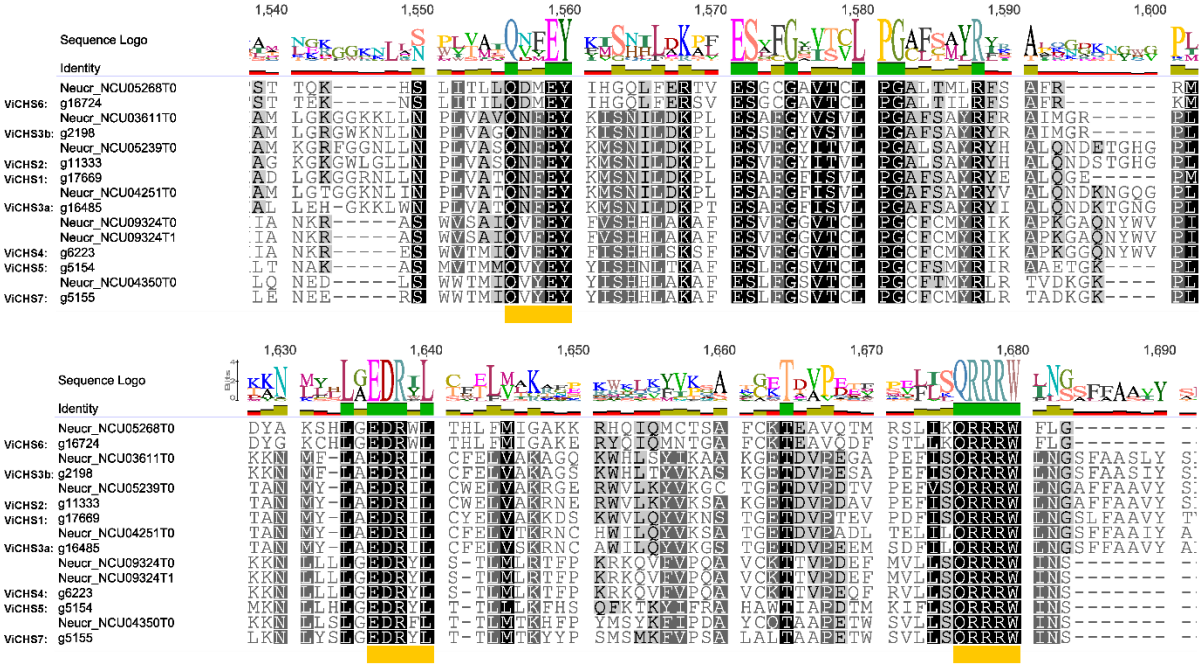

Figure A 4-1. Multiple sequence alignment of putative chitin synthase (CHS) proteins from *Venturia inaequalis*. The CHS proteins from *Neurospora crassa* (Neucr) were used as reference for alignment. Alignment generated using the MUSCLE plugin of Geneious v9.0.5 in conjunction with full-length protein sequences. The conserved motifs for catalytic activity are highlighted under the alignment with orange boxes. Amino acids are coloured based on similarity, with the most similar amino acids coloured black.

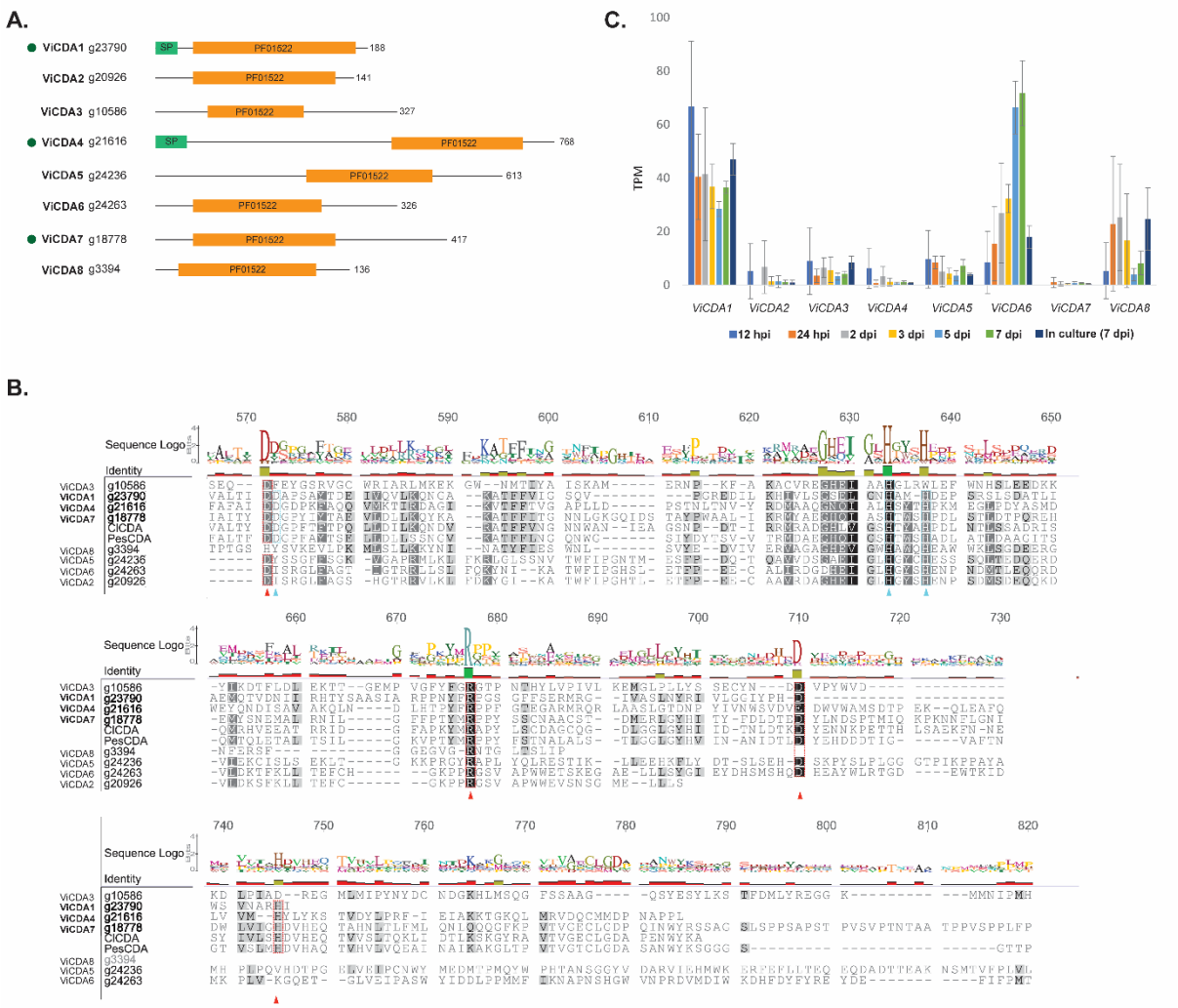

Figure A 4-2. Predicted chitin deacetylases (CDAs) of *Venturia inaequalis*. A. Domain organization of putative CDA proteins from *V. inaequalis*. Only ViCDA1, ViCDA4 and ViCDA7 display all conserved amino acid residues required for catalytic activity and metal binding and, therefore, are likely to be functional (labelled with green circles). Protein lengths are shown. SP, Signal peptide; PF01522, Protein family (Pfam) polysaccharide deacetylase domain. **B.** Multiple sequence alignment of putative CDA proteins from *V. inaequalis*. CDA proteins from *Colletotrichum lindemuthianum* (ClCDA) and *Pestalotiopsis sp.* (PesCDA) were used as references for alignment. Alignment generated using the MUSCLE plugin of Geneious v9.0.5 in conjunction with full-length protein sequences. The conserved amino acids for catalytic activity are highlighted with red triangles under the alignment and with dashed red boxes. Conserved amino acids for metal binding are highlighted with cyan triangles under the alignment and with dashed cyan boxes. Amino acids are coloured based on similarity, with the most similar amino acids coloured black. **C.** Expression of the eight predicted *V. inaequalis* CDA genes during growth of the fungus *in planta* (12 hours post-inoculation [hpi] to 7 days post-inoculation [dpi]) and in culture on the surface of cellophane membranes (CMs) (7 dpi). Gene expression is shown as transcripts per million (TPM). Error bars represent standard deviation across four biological replicates.

Supplementary file 2: List of genes encoding putative cell wall biogenesis proteins from *Venturia inaequalis* that are up- or down-regulated at one or more *in planta* time points during infection of apple leaves (12 hours post-inoculation [hpi] to 7 days post-inoculation [dpi]), relative to growth of the fungus in culture on the surface of cellophane membranes (CMs) overlaying potato dextrose agar (7 dpi).

https://www.biorxiv.org/content/biorxiv/early/2022/09/21/2022.09.21.508768/DC3/embed/media-3.xlsx?download=true

Supplementary file 3: List of proteins identified by mass spectrometry from *Venturia inaequalis* grown on the surface of cellophane membranes overlaying potato dextrose agar at 5 days post-inoculation, and short-list of proteins putatively associated with fungal cell wall biogenesis from this list. Only peptides exceeding the threshold for statistical significance ($p < 0.05$) were selected.

https://www.biorxiv.org/content/biorxiv/early/2022/09/21/2022.09.21.508768/DC4/embed/media-4.xlsx?download=true

Supplementary file 4: Peptide coverage of proteins identified by mass spectrometry from *Venturia inaequalis* grown on the surface of cellophane membranes overlaying potato dextrose agar at 5 days post-inoculation that are putatively associated with fungal cell wall biogenesis.

https://www.biorxiv.org/content/biorxiv/early/2022/09/21/2022.09.21.508768/DC5/embed/media-5.pdf?download=true

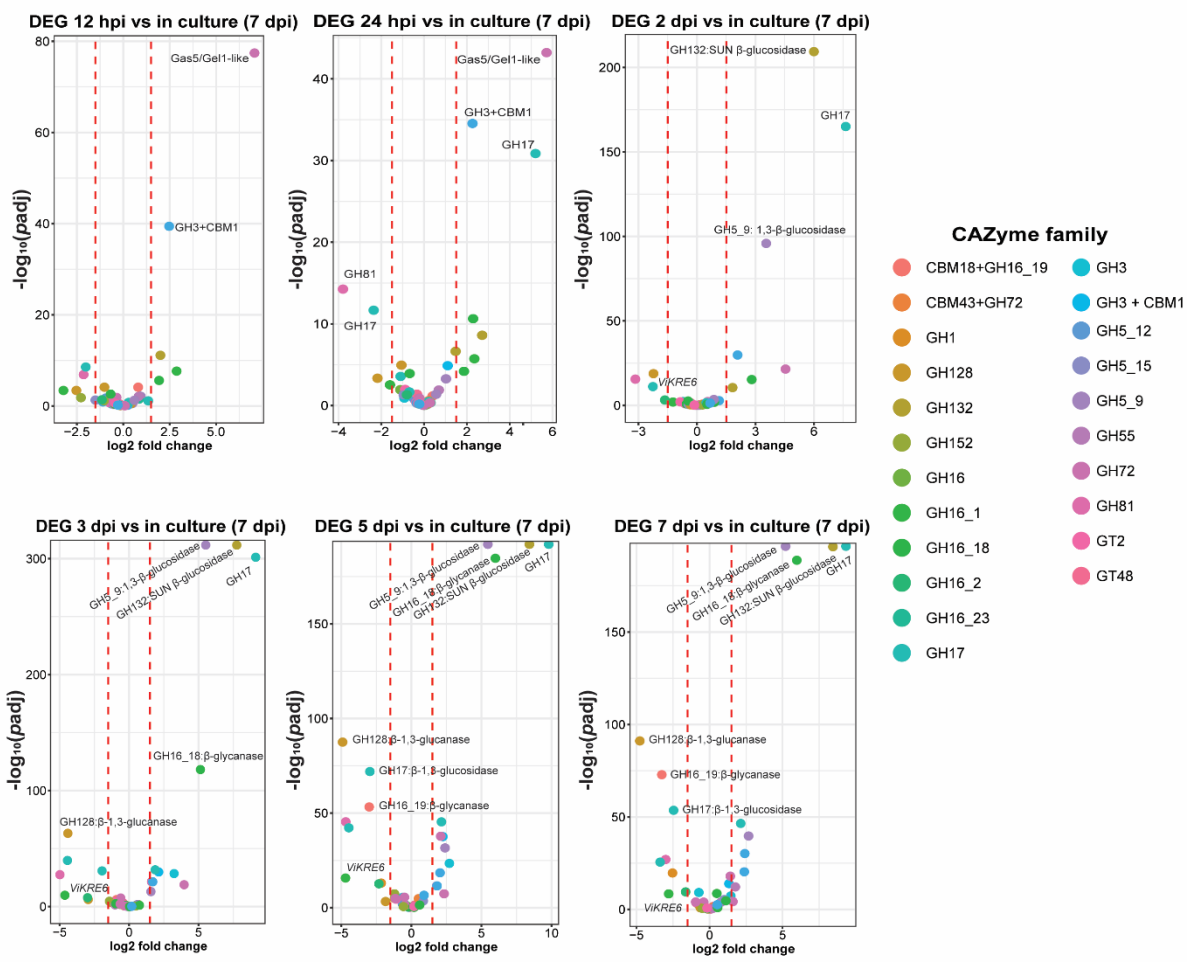

Figure A 4-3. Volcano plots illustrating genes of *Venturia inaequalis* that are both putatively associated with β-glucan metabolism and are up- or down-regulated during one or more *in planta* time points compared with growth in culture on the surface of cellophane membranes (CMs) overlaying potato dextrose agar. *In planta* time points were at 12 and 24 hours post-inoculation (hpi), as well as 2, 3, 5 and 7 days post-inoculation (dpi), while growth in culture was at 7 dpi. Dashed red lines indicate the 1.5 $\log_2$-fold change used in this study to identify significant (*p*-adjusted, *p*adj) differentially expressed genes (DEGs). Each dot represents one gene, coloured by carbohydrate-active enzyme (CAZyme) classification. Only genes with a minimum expression of 10 transcripts per million (TPM) at one or more *in planta* time point are shown. CBM, carbohydrate-binding module; GH, glycoside hydrolase; GT, glycosyl transferase.

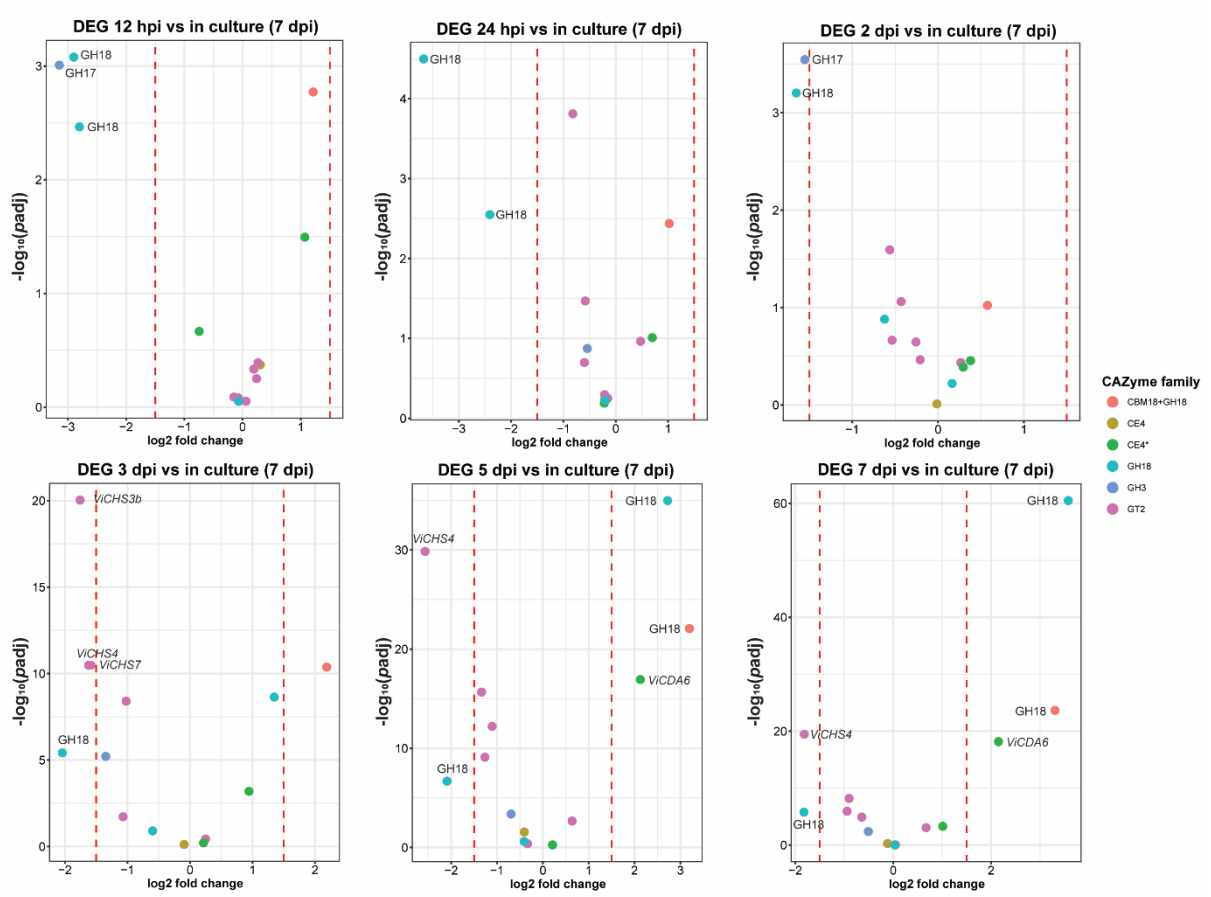

Figure A 4-4. Volcano plots illustrating genes of *Venturia inaequalis* that are both putatively associated with chitin (N-acetylglucosamine) metabolism and are up- or down-regulated during one or more *in planta* time points compared with growth in culture on the surface of cellophane membranes CMs overlaying potato dextrose agar. *In planta* time points were at 12 and 24 hours post-inoculation (hpi), as well as 2, 3, 5 and 7 days post-inoculation (dpi), while growth in culture was at 7 dpi. Dashed red lines indicate the 1.5 $\log_2$-fold change used in this study to identify significant (*p*-adjusted, *p*adj) differentially expressed genes (DEGs). Each dot represents one gene, coloured by carbohydrate-active enzyme (CAZyme) classification. Only genes with a minimum expression of 10 transcripts per million (TPM) at one or more *in planta* time point are shown. CBM, carbohydrate-binding module; CE, carbohydrate esterase; GH, glycoside hydrolase; GT, glycosyl transferase. Asterisk (*) indicates CE family 4 (CE4) proteins were only predicted using a protein family (Pfam) domain search.

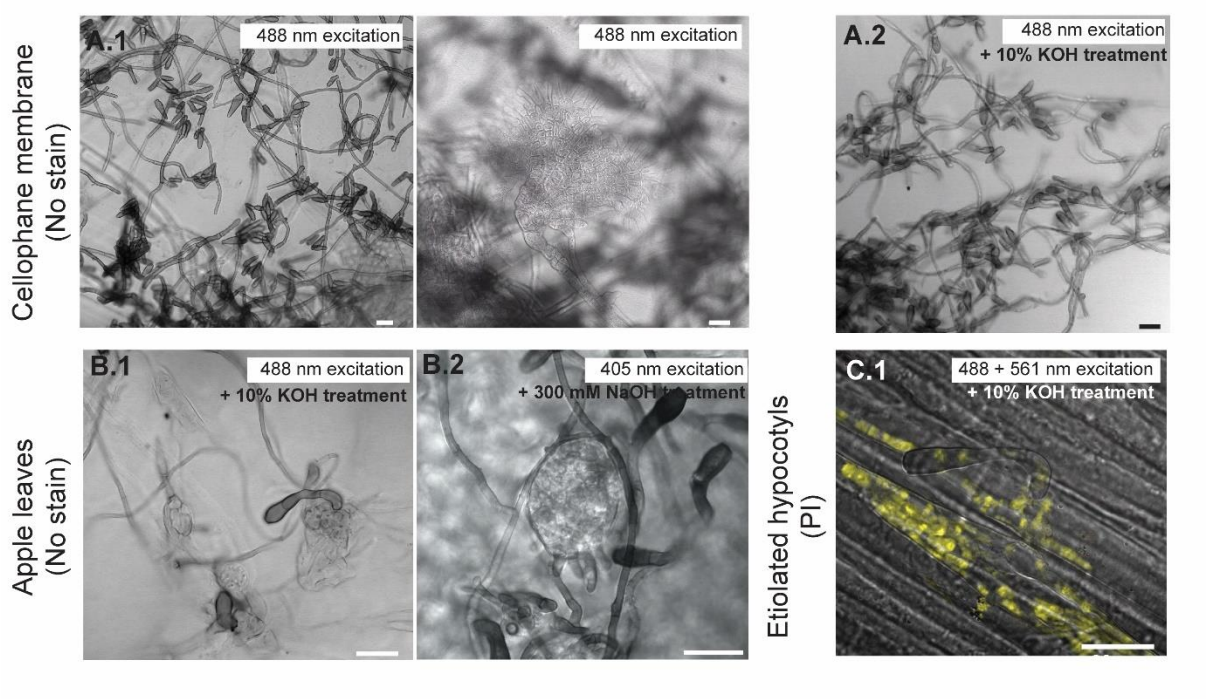

Figure A 4-5. Representative negative controls to ensure that the emission signals observed during confocal laser scanning microscopy (CLSM) were derived from specific labelling and not autofluorescence. Samples of non-labelled cellophane membranes (CMs) (**A. 1**) associated with *V. inaequalis* or treated with 10% KOH (**A. 2**) did not emit any signal when excited at 488 or 405 nm by CLSM. Likewise, non-labelled *V. inaequalis*-infected apple leaf (**B.1**) treated with 10% KOH or *V. inaequalis*-infected apple leaf treated with 300 mM NaOH (**B. 2**) did not emit any autofluorescence signal. Finally, etiolated apple hypocotyls treated with 10% KOH (**C. 1**) were only stained with propidium iodide (PI) to label fungal nuclei, and only PI-derived signal was observed after excitation at 561 nm. No emission was observed after excitation at 488 nm. All scale bars: 20 μm.

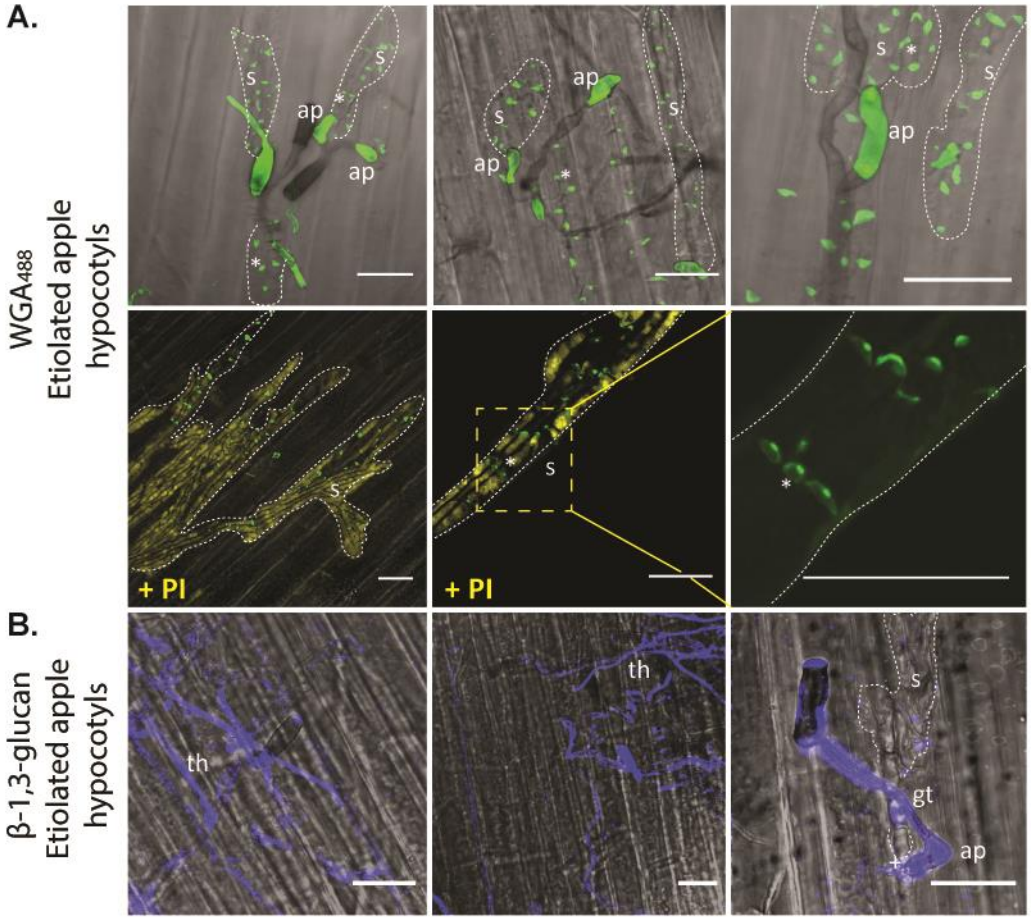

Figure A 4-6. Label-accessible chitin and β-1,3-glucan on the surface of infection structures developed by *Venturia inaequalis* in and on etiolated apple hypocotyls. A. The fluorophore-labelled lectin WGA_{488} was used to visualize chitin (green pseudocolour), and propidium iodide (PI, yellow pseudocolour) was used to stain fungal nuclei, in conjunction with confocal laser scanning microscopy. Dashed yellow squares indicate zoomed-in areas. **B.** The monoclonal anti-β-1,3-glucan primary antibody and CF^{488} secondary antibody were used to label β-1,3-glucan (blue pseudocolour). All scale bars: 20 µm. ap, appressorium; s, stroma; th, tubular hyphae; *: septa; dashed white lines highlight stromata.

8. Appendix B: Statement of contribution doctorate with publications/manuscripts (DRC16)

We, the candidate and the candidate's Primary Supervisor, certify that all co-authors have consented to their work being included in the thesis and they have accepted the candidate's contribution as indicated below in the *Statement of Originality*.

Name of candidate:	Mercedes Rocafort Ferrer
Name/title of Primary Supervisor:	Carl H. Mesarich
Name of Research Output and full reference:	
Cell wall carbohydrate dynamics during the differentiation of infection structures by the apple scab fungus, *Venturia inaequalis*	
In which Chapter is the Manuscript /Published work:	Chapter 4
Please indicate:	
• The percentage of the manuscript/Published Work that was contributed by the candidate:	70
and	
• Describe the contribution that the candidate has made to the Manuscript/Published Work:	
The candidate carried out the sample preparation for the glycosidic linkage and proteomic analyses, performed all bioinformatic analyses and confocal microscopy, generated all figures and tables, and wrote the manuscript draft (which was subsequently edited by co-authors). The candidate did not perform the proteomic and glycosidic linkage analyses.	
For manuscripts intended for publication please indicate target journal:	
mSystems	
Candidate's Signature:	Mercedes Rocafort Ferrer Firmado digitalmente por Mercedes Rocafort Ferrer Fecha: 2022.09.23 09:27:17 +02'00'
Date:	23/09/2022
Primary Supervisor's Signature:	Carl Mesarich Digitally signed by Carl Mesarich Date: 2022.09.23 19:45:53 +12'00'
Date:	23/09/2022

Chapter 4_ DRC 16 - V3 Online Statement

9. References

1. Bowen JK, Mesarich CH, Bus VG, Beresford RM, Plummer KM, Templeton MD: ***Venturia inaequalis*: the causal agent of apple scab**. *Molecular Plant Pathology* 2011, **12**:105-122.
2. Carisse O, Bernier J: **Effect of environmental factors on growth, pycnidial production and spore germination of *Microsphaeropsis* isolates with biocontrol potential against apple scab**. *Mycological Research* 2002, **106**:1455-1462.
3. Jha G, Thakur K, Thakur P: **The *Venturia* apple pathosystem: pathogenicity mechanisms and plant defense responses**. *Journal of Biomedicine and Biotechnology* 2009, **2009**:680160.
4. MacHardy WE: *Apple Scab, Biology, Epidemiology, and Management*, vol 33: The Amercian Phytopathological Society 1996.
5. Le Cam B, Sargent D, Gouzy J, Amselem J, Bellanger M-N, Bouchez O, Brown S, Caffier V, De Gracia M, Debuchy R, et al.: **Population genome gequencing of the scab fungal species *Venturia inaequalis*, *Venturia pirina*, *Venturia aucupariae* and *Venturia asperata***. *G3: Genes, Genomes, Genetics* 2019, **9**:2405-2414.
6. Manktelow D, Beresford R, Batchelor T, Walker J: **Use patterns and economics of fungicides for disease control in New Zealand apples**. In *International Conference on Integrated Fruit Production*: 1995:187-192.
7. Patocchi A, Wehrli A, Dubuis PH, Auwerkerken A, Leida C, Cipriani G, Passey T, Staples M, Didelot F, Philion V, et al.: **Ten years of VINQUEST: first insight for breeding new apple cultivars with durable apple scab resistance**. *Plant Disease* 2020, **104**:2074-2081.
8. Gessler C, Stumm D: **Infection and stroma formation by *Venturia inaequalis* on apple leaves with different degrees of susceptibility to scab**. *Journal of Phytopathology* 1984, **110**:119-126.
9. Kucheryava N, Bowen JK, Sutherland PW, Conolly JJ, Mesarich CH, Rikkerink EH, Kemen E, Plummer KM, Hahn M, Templeton MD: **Two novel *Venturia inaequalis* genes induced upon morphogenetic differentiation during infection and *in vitro* growth on cellophane**. *Fungal Genetics and Biology* 2008, **45**:1329-1339.
10. Nusbaum CJ, Keitt GW: **A cytological study of host-parasite relations of *Venturia inaequalis* on apple leaves**. *Journal of Agricultural Research* 1938, **56**:595-618.
11. Caffier V, Le Cam B, Expert P, Tellier M, Devaux M, Giraud M, Chevalier M: **A new scab-like disease on apple caused by the formerly saprotrophic fungus *Venturia asperata***. *Plant Pathology* 2012, **61**:915-924.
12. Latham AJR, A. E.: **Development of *Cladosporium caryigenum* in pecan leaves**. *Phytopathology* 1988, **78**:1104-1108.
13. Lanza B, Ragnelli AM, Priore M, Aimola P: **Morphological and histochemical investigation of the response of *Olea europaea* leaves to fungal attack by *Spilocaea oleagina***. *Plant Pathology* 2017, **66**:1239-1247.
14. Hunter GC, Zeil-Rolfe I, Jourdan M, Morin L: **Exploring the host range and infection process of *Venturia paralias* isolated from *Euphorbia paralias* in France**. *European Journal of Plant Pathology* 2021, **159**:811-823.
15. Blechert O, Debener T: **Morphological characterization of the interaction between *Diplocarpon rosae* and various rose species**. *Plant Pathology* 2005, **54**:82-90.
16. Zhan J, Fitt BDL, Pinnschmidt HO, Oxley SJP, Newton AC: **Resistance, epidemiology and sustainable management of *Rhynchosporium secalis* populations on barley**. *Plant Pathology* 2008, **57**:1-14.

17. Linsell KJ, Keiper FJ, Forgan A, Oldach KH: **New insights into the infection process of *Rhynchosporium secalis* in barley using GFP**. *Fungal Genetics and Biology* 2011, **48**:124-131.
18. Free SJ: **Chapter two - Fungal cell wall organization and biosynthesis**. In *Advances in Genetics*. Edited by Friedmann T, Dunlap JC, Goodwin SF: Academic Press; 2013:33-82. vol 81.]
19. Latgé J-P: **The cell wall: a carbohydrate armour for the fungal cell**. *Molecular Microbiology* 2007, **66**:279-290.
20. Sánchez-Vallet A, Mesters JR, Thomma BP: **The battle for chitin recognition in plant-microbe interactions**. *FEMS Microbiology Reviews* 2015, **39**:171-183.
21. Zhang J, Zhou J-M: **Plant immunity triggered by microbial molecular signatures**. *Molecular Plant* 2010, **3**:783-793.
22. Saijo Y, Loo EPi, Yasuda S: **Pattern recognition receptors and signaling in plant–microbe interactions**. *The Plant Journal* 2018, **93**:592-613.
23. Gonçalves IR, Brouillet S, Soulié M-C, Gribaldo S, Sirven C, Charron N, Boccara M, Choquer M: **Genome-wide analyses of chitin synthases identify horizontal gene transfers towards bacteria and allow a robust and unifying classification into fungi**. *BMC Evolutionary Biology* 2016, **16**:252.
24. Gow NAR, Latge JP, Munro CA: **The fungal cell wall: structure, biosynthesis, and function**. *Microbiology Spectrum* 2017, **5**.
25. Osherov N, Yarden O: **The cell wall of filamentous fungi**. *Cellular and Molecular Biology of Filamentous Fungi* 2010:224-237.
26. Mouyna I, Henry C, Doering TL, Latgé J-P: **Gene silencing with RNA interference in the human pathogenic fungus *Aspergillus fumigatus***. *FEMS Microbiology Letters* 2004, **237**:317-324.
27. Garcia-Rubio R, de Oliveira HC, Rivera J, Trevijano-Contador N: **The fungal cell wall: *Candida, Cryptococcus,* and *Aspergillus* species**. *Frontiers in Microbiology* 2020, **10**.
28. Mouyna I, Hartl L, Latgé J: **β-1,3-glucan modifying enzymes in *Aspergillus fumigatus***. *Frontiers in Microbiology* 2013, **4**.
29. Rovenich H, Zuccaro A, Thomma BPHJ: **Convergent evolution of filamentous microbes towards evasion of glycan-triggered immunity**. *New Phytologist* 2016, **212**:896-901.
30. Oliveira Silva A-SL, Wirsel Stefan, Deising Holger: **Pathogenesis-related cell wall biogenesis with emphasis on the maize anthracnose fungus *Colletotrichum graminicola***. In *Plants*. Edited by; 2022. vol 11.]
31. Geoghegan I, Steinberg G, Gurr S: **The role of the fungal cell wall in the infection of plants**. *Trends in Microbiology* 2017, **25**:957-967.
32. Gao F, Zhang B-S, Zhao J-H, Huang J-F, Jia P-S, Wang S, Zhang J, Zhou J-M, Guo H-S: **Deacetylation of chitin oligomers increases virulence in soil-borne fungal pathogens**. *Nature Plants* 2019, **5**:1167-1176.
33. Geoghegan IA, Gurr SJ: **Investigating chitin deacetylation and chitosan hydrolysis during vegetative growth in *Magnaporthe oryzae***. *Cellular Microbiology* 2017, **19**:e12743.
34. Noorifar N, Savoian MS, Ram A, Lukito Y, Hassing B, Weikert TW, Moerschbacher BM, Scott B: **Chitin deacetylases are required for *Epichloë festucae* endophytic cell wall remodeling during establishment of a mutualistic symbiotic interaction with *Lolium perenne***. *Molecular Plant-Microbe Interactions* 2021:MPMI-12-20-0347-R.
35. Rizzi Y S, Happel P, Lenz S, Urs M J, Bonin M, Cord-Landwehr S, Singh R, Moerschbacher B M, Kahmann R: **Chitosan and chitin deacetylase activity are necessary for development and virulence of *Ustilago maydis***. *mBio* 2021, **12**:e03419-03420.

36. Iriti M, Faoro F: **Chitosan as a MAMP, searching for a PRR**. *Plant Signaling & Behavior* 2009, **4**:66-68.
37. Gubaeva E, Gubaev A, Melcher RLJ, Cord-Landwehr S, Singh R, El Gueddari NE, Moerschbacher BM: **'Slipped Sandwich' model for chitin and chitosan perception in *Arabidopsis***. *Molecular Plant-Microbe Interactions* 2018, **31**:1145-1153.
38. Vander P, KM Vr, Domard A, Eddine El Gueddari N, Moerschbacher BM: **Comparison of the ability of partially N-acetylated chitosans and chitooligosaccharides to elicit resistance reactions in wheat leaves**. *Plant Physiology* 1998, **118**:1353-1359.
39. Ride JP, Barber MS: **Purification and characterization of multiple forms of endochitinase from wheat leaves**. *Plant Science* 1990, **71**:185-197.
40. Lopez-Moya F, Suarez-Fernandez M, Lopez-Llorca LV: **Molecular mechanisms of chitosan interactions with fungi and plants**. *International Journal of Molecular Sciences* 2019, **20**:332.
41. Rappleye CA, Engle JT, Goldman WE: **RNA interference in *Histoplasma capsulatum* demonstrates a role for α-(1,3)-glucan in virulence**. *Molecular Microbiology* 2004, **53**:153-165.
42. Rappleye CA, Eissenberg LG, Goldman WE: ***Histoplasma capsulatum* alpha-(1,3)-glucan blocks innate immune recognition by the beta-glucan receptor**. *Proceedings of the National Academy of Sciences* 2007, **104**:1366-1370.
43. Fujikawa T, Sakaguchi A, Nishizawa Y, Kouzai Y, Minami E, Yano S, Koga H, Meshi T, Nishimura M: **Surface α-1,3-glucan facilitates fungal stealth infection by interfering with innate immunity in plants**. *PLoS Pathogens* 2012, **8**:e1002882.
44. Fujikawa T, Kuga Y, Yano S, Yoshimi A, Tachiki T, Abe K, Nishimura M: **Dynamics of cell wall components of *Magnaporthe grisea* during infectious structure development**. *Molecular Microbiology* 2009, **73**:553-570.
45. Ibe C, Munro CA: **Fungal cell wall: An underexploited target for antifungal therapies**. *PLoS Pathogens* 2021, **17**:e1009470.
46. Jaworski C, Wang L: **Gross cell wall composition of *V. inaequalis* cell wall**. *Phytopathology* 1965, **55**:401-403.
47. Ruiz-Herrera J, Ortiz-Castellanos L: **Cell wall glucans of fungi. A review**. *The Cell Surface* 2019, **5**:100022.
48. Rocafort M, Bowen JK, Hassing B, Cox MP, McGreal B, de la Rosa S, Plummer KM, Bradshaw RE, Mesarich CH: **The *Venturia inaequalis* effector repertoire is expressed in waves, and is dominated by expanded families with predicted structural similarity to avirulence proteins from other fungi**. *bioRxiv* 2022:482717.
49. Mandel AM, Galgiani JN, Scott K, Orbach MJ: ***Coccidioides posadasii* contains single chitin synthase genes corresponding to classes I to VII**. *Fungal Genetics and Biology* 2006, **43**:775-788.
50. Blair DE, Hekmat O, Schüttelkopf AW, Shrestha B, Tokuyasu K, Withers SG, van Aalten DM: **Structure and mechanism of chitin deacetylase from the fungal pathogen *Colletotrichum lindemuthianum***. *Biochemistry* 2006, **45**:9416-9426.
51. Hekmat O, Tokuyasu K, Withers SG: **Subsite structure of the endo-type chitin deacetylase from a deuteromycete, *Colletotrichum lindemuthianum*: an investigation using steady-state kinetic analysis and MS**. *Biochemistry Journal* 2003, **374**:369-380.
52. Ramazzina I, Cendron, L., Folli, C., Berni, R., Monteverdi, D., Zanotti, G., & Percudani, R.: **Logical identification of an allantoinase analog (*puuE*) recruited from polysaccharide deacetylases**. *Journal of Biological Chemistry* 2008, **283**:23295-23304.

53. Mouyna I, Hartland RP, Fontaine T, Diaquin M, Simenel C, Delepierre M, Henrissat B, Latgé J: **A 1,3-beta-glucanosyltransferase isolated from the cell wall of *Aspergillus fumigatus* is a homologue of the yeast *Bgl2p***. *Microbiology* 1998, **144 (Pt 11)**:3171-3180.
54. Patel P, Free SJ: **Characterization of *Neurospora crassa GH16, GH17,* and *GH72* gene families of cell wall crosslinking enzymes**. *The Cell Surface* 2022, **8**:100073.
55. Gilbert NM, Donlin MJ, Gerik KJ, Specht CA, Djordjevic JT, Wilson CF, Sorrell TC, Lodge JK: ***KRE* genes are required for beta-1,6-glucan synthesis, maintenance of capsule architecture and cell wall protein anchoring in *Cryptococcus neoformans***. *Molecular Microbiology* 2010, **76**:517-534.
56. Levinson JN, Shahinian S, Sdicu A-M, Tessier DC, Bussey H: **Functional, comparative and cell biological analysis of *Saccharomyces cerevisiae Kre5p***. *Yeast* 2002, **19**:1243-1259.
57. Mouyna I, Monod M, Fontaine T, Henrissat B, Léchenne B, Latgé JP: **Identification of the catalytic residues of the first family of beta(1-3)glucanosyltransferases identified in fungi**. *The Biochemical journal* 2000, **347 Pt 3**:741-747.
58. Ragni E, Fontaine T, Gissi C, Latgè JP, Popolo L: **The Gas family of proteins of *Saccharomyces cerevisiae*: characterization and evolutionary analysis**. *Yeast* 2007, **24**:297-308.
59. Nicholson RL, Van Scoyoc S, Williams EB, Kuc J: **Etiolated apple hypocotyls: a useful host tissue in apple scab research**. *Phytopathology* 1972, **63**:363-366.
60. Mravec J, Kračun SK, Rydahl MG, Westereng B, Miart F, Clausen MH, Fangel JU, Daugaard M, Van Cutsem P, De Fine Licht HH, et al.: **Tracking developmentally regulated post-synthetic processing of homogalacturonan and chitin using reciprocal oligosaccharide probes**. *Development* 2014, **141**:4841-4850.
61. Fesel PH, Zuccaro A: **β-glucan: crucial component of the fungal cell wall and elusive MAMP in plants**. *Fungal Genetics and Biology* 2016, **90**:53-60.
62. Verdín J, Sánchez-León E, Rico-Ramírez AM, Martínez-Núñez L, Fajardo-Somera RA, Riquelme M: **Off the wall: The rhyme and reason of *Neurospora crassa* hyphal morphogenesis**. *The Cell Surface* 2019, **5**:100020.
63. Pettolino F, Sasaki I, Turbic A, Wilson SM, Bacic A, Hrmova M, Fincher GB: **Hyphal cell walls from the plant pathogen *Rhynchosporium secalis* contain (1,3/1,6)-β-d-glucans, galacto- and rhamnomannans, (1,3;1,4)-β-d-glucans and chitin**. *The FEBS Journal* 2009, **276**:3698-3709.
64. Beauvais A, Bozza S, Kniemeyer O, Formosa C, Balloy V, Henry C, Roberson RW, Dague E, Chignard M, Brakhage AA, et al.: **Deletion of the α-(1,3)-glucan synthase genes induces a restructuring of the conidial cell wall responsible for the avirulence of *Aspergillus fumigatus***. *PLoS Pathogens* 2013, **9**:e1003716.
65. Yoshimi A, Miyazawa K, Abe K: **Function and biosynthesis of cell wall α-1,3-glucan in fungi**. *Journal of Fungi* 2017, **3**:63.
66. Fontaine T, Beauvais A, Loussert C, Thevenard B, Fulgsang CC, Ohno N, Clavaud C, Prevost M-C, Latgé J-P: **Cell wall α1-3glucans induce the aggregation of germinating conidia of Aspergillus fumigatus**. *Fungal Genetics and Biology* 2010, **47**:707-712.
67. Kang X, Kirui A, Muszyński A, Widanage MCD, Chen A, Azadi P, Wang P, Mentink-Vigier F, Wang T: **Molecular architecture of fungal cell walls revealed by solid-state NMR**. *Nature Communications* 2018, **9**:2747.
68. Ruiz-Herrera J: *Fungal cell wall: structure, synthesis, and assembly*: CRC press; 1991.
69. Gastebois A, Mouyna I, Simenel C, Clavaud C, Coddeville B, Delepierre M, Latgé J-P, Fontaine T: **Characterization of a new β(1–3)-glucan branching activity of *Aspergillus fumigatus***. *Journal of Biological Chemistry* 2010, **285**:2386-2396.

70. Oliveira-Garcia E, Deising HB: **Attenuation of PAMP-triggered immunity in maize requires down-regulation of the key β-1,6-glucan synthesis genes *KRE5* and *KRE6* in biotrophic hyphae of *Colletotrichum graminicola***. *The Plant Journal* 2016, **87**:355-375.
71. Fleet GH: **Composition and structure of yeast cell walls**. In *Current Topics in Medical Mycology*. Edited by McGinnis MR: Springer New York; 1985:24-56.
72. Mélida H, Sain D, Stajich JE, Bulone V: **Deciphering the uniqueness of Mucoromycotina cell walls by combining biochemical and phylogenomic approaches**. *Environmental Microbiology* 2015, **17**:1649-1662.
73. Pham TAT, Kyriacou BA, Schwerdt JG, Shirley NJ, Xing X, Bulone V, Little A: **Composition and biosynthetic machinery of the *Blumeria graminis* f. sp. *hordei* conidia cell wall**. *The Cell Surface* 2019, **5**:100029.
74. Fontaine T, Simenel C, Dubreucq G, Adam O, Delepierre M, Lemoine J, Vorgias CE, Diaquin M, Latgé J-P: **Molecular organization of the alkali-insoluble fraction of *Aspergillus fumigatus* cell wall**. *Journal of Biological Chemistry* 2000, **275**:27594-27607.
75. van den Burg HA, Harrison SJ, Joosten MH, Vervoort J, de Wit PJ: ***Cladosporium fulvum* Avr4 protects fungal cell walls against hydrolysis by plant chitinases accumulating during infection**. *Molecular Plant-Microbe Interactions* 2006, **19**:1420-1430.
76. Bolton MD, Van Esse HP, Vossen JH, De Jonge R, Stergiopoulos I, Stulemeijer IJE, Van Den Berg GCM, Borrás-Hidalgo O, Dekker HL, De Koster CG, et al.: **The novel *Cladosporium fulvum* lysin motif effector Ecp6 is a virulence factor with orthologues in other fungal species**. *Molecular Microbiology* 2008, **69**:119-136.
77. Deng CH, Plummer KM, Jones DAB, Mesarich CH, Shiller J, Taranto AP, Robinson AJ, Kastner P, Hall NE, Templeton MD, et al.: **Comparative analysis of the predicted secretomes of Rosaceae scab pathogens *Venturia inaequalis* and *V. pirina* reveals expanded effector families and putative determinants of host range**. *BMC Genomics* 2017, **18**:339.
78. de Jonge R, Peter van Esse H, Kombrink A, Shinya T, Desaki Y, Bours R, van der Krol S, Shibuya N, Joosten Matthieu HAJ, Thomma Bart PHJ: **Conserved fungal LysM effector Ecp6 prevents chitin-triggered immunity in plants**. *Science* 2010, **329**:953-955.
79. Marshall R, Kombrink A, Motteram J, Loza-Reyes E, Lucas J, Hammond-Kosack KE, Thomma BPHJ, Rudd JJ: **Analysis of two *in planta* expressed LysM effector homologs from the fungus *Mycosphaerella graminicola* reveals novel functional properties and varying contributions to virulence on wheat.** *Plant Physiology* 2011, **156**:756-769.
80. El Gueddari NE, Rauchhaus U, Moerschbacher BM, Deising HB: **Developmentally regulated conversion of surface-exposed chitin to chitosan in cell walls of plant pathogenic fungi**. *New Phytologist* 2002, **156**:103-112.
81. Geoghegan IA, Gurr SJ: **Chitosan mediates germling adhesion in *Magnaporthe oryzae* and is required for surface sensing and germling morphogenesis**. *PLoS Pathogens* 2016, **12**:e1005703-e1005703.
82. Kamakura T, Yamaguchi S, Saitoh K, Teraoka T, Yamaguchi I: **A novel gene, *CBP1*, encoding a putative extracellular chitin-binding protein, may play an important role in the hydrophobic surface sensing of *Magnaporthe grisea* during appressorium differentiation**. *Molecular Plant-Microbe Interactions* 2002, **15**:437-444.
83. Kuroki M, Okauchi K, Yoshida S, Ohno Y, Murata S, Nakajima Y, Nozaka A, Tanaka N, Nakajima M, Taguchi H, et al.: **Chitin-deacetylase activity induces appressorium differentiation in the rice blast fungus *Magnaporthe oryzae***. *Scientific Reports* 2017, **7**:9697-9697.

84. Banks IR, Specht CA, Donlin MJ, Gerik KJ, Levitz SM, Lodge JK: **A chitin synthase and its regulator protein are critical for chitosan production and growth of the fungal pathogen *Cryptococcus neoformans***. *Eukaryotic Cell* 2005, **4**:1902-1912.
85. Cord-Landwehr S, Melcher RLJ, Kolkenbrock S, Moerschbacher BM: **A chitin deacetylase from the endophytic fungus *Pestalotiopsis* sp. efficiently inactivates the elicitor activity of chitin oligomers in rice cells**. *Scientific Reports* 2016, **6**:38018.
86. Rocafort M, Arshed S, Hudson D, Sidhu JS, Bowen JK, Plummer KM, Bradshaw RE, Johnson RD, Johnson LJ, Mesarich CH: **CRISPR-Cas9 gene editing and rapid detection of gene-edited mutants using high-resolution melting in the apple scab fungus, *Venturia inaequalis***. *Fungal Biology* 2021, **126**:35-46.
87. Stehmann C, Pennycook S, Plummer KM: **Molecular identification of a sexual interloper: The pear pathogen, *Venturia pirina*, has sex on apple**. *Phytopathology* 2001, **91**:633-641.
88. Mélida H, Sandoval-Sierra JV, Diéguez-Uribeondo J, Bulone V: **Analyses of extracellular carbohydrates in oomycetes unveil the existence of three different cell wall types**. *Eukaryotic Cell* 2013, **12**:194-203.
89. Leijon F, Melzer M, Zhou Q, Srivastava V, Bulone V: **Proteomic analysis of plasmodesmata from populus cell suspension cultures in relation with callose biosynthesis**. *Frontiers in Plant Science* 2018, **9**:1681.
90. Shiller J, Van de Wouw AP, Taranto AP, Bowen JK, Dubois D, Robinson A, Deng CH, Plummer KM: **A large family of *AvrLm6-like* genes in the apple and pear scab pathogens, *Venturia inaequalis* and *Venturia pirina***. *Frontiers in Plant Science* 2015, **6**.
91. Schneider CA, Rasband WS, Eliceiri KW: **NIH Image to ImageJ: 25 years of image analysis**. *Nature Methods* 2012, **9**:671-675.
92. Altschul SF, Madden TL, Schäffer AA, Zhang J, Zhang Z, Miller W, Lipman DJ: **Gapped BLAST and PSI-BLAST: a new generation of protein database search programs**. *Nucleic Acids Research* 1997, **25**:3389-3402.
93. Naqvi S, Cord-Landwehr S, Singh R, Bernard F, Kolkenbrock S, El Gueddari NE, Moerschbacher BM: **A recombinant fungal chitin deacetylase produces fully defined chitosan oligomers with novel patterns of acetylation**. *Applied Environmental Microbiology* 2016, **82**:6645-6655.
94. Kearse M, Moir R, Wilson A, Stones-Havas S, Cheung M, Sturrock S, Buxton S, Cooper A, Markowitz S, Duran C, et al.: **Geneious Basic: an integrated and extendable desktop software platform for the organization and analysis of sequence data**. *Bioinformatics* 2012, **28**:1647-1649.
95. Mouyna I, Dellière S, Beauvais A, Gravelat F, Snarr B, Lehoux M, Zacharias C, Sun Y, de Jesus Carrion S, Pearlman E, et al.: **What are the functions of chitin deacetylases in *Aspergillus fumigatus*?** *Frontiers in Cellular and Infection Microbiology* 2020, **10**.
96. Fajardo-Somera RA, Jöhnk B, Bayram Ö, Valerius O, Braus GH, Riquelme M: **Dissecting the function of the different chitin synthases in vegetative growth and sexual development in *Neurospora crassa***. *Fungal Genetics and Biology* 2015, **75**:30-45.
97. Choquer M, Boccara M, Gonçalves IR, Soulié MC, Vidal-Cros A: **Survey of the *Botrytis cinerea* chitin synthase multigenic family through the analysis of six euascomycetes genomes**. *European Journal of Biochemistry* 2004, **271**:2153-2164.
98. Love MI, Huber W, Anders S: **Moderated estimation of fold change and dispersion for RNA-seq data with DESeq2**. *Genome Biology* 2014, **15**:550.
99. Wickham H: **ggplot2: Elegant graphics for data analysis**. *Springer-Verlag New York* 2016.
100. Gu Z, Eils R, Schlesner M: **Complex heatmaps reveal patterns and correlations in multidimensional genomic data**. *Bioinformatics* 2016, **32**:2847-2849

Chapter 5:

CRISPR-Cas9 gene editing and rapid detection of gene-edited mutants using high-resolution melting in the apple scab fungus, *Venturia inaequalis*

Mercedes Rocafort[1], Saadiah Arshed[2], Debbie Hudson[3], Jaspreet Singh Sidhu[3], Joanna K. Bowen[2], Kim M. Plummer[4], Rosie E. Bradshaw[5,6], Richard D. Johnson[3], Linda J. Johnson[3] and Carl H. Mesarich[1,6,*]

[1]Laboratory of Molecular Plant Pathology, School of Agriculture and Environment, Massey University, Palmerston North 4410, New Zealand.

[2]The New Zealand Institute for Plant and Food Research Limited, Mount Albert Research Centre, Auckland 1025, New Zealand.

[3]Grasslands Research Centre, AgResearch Limited, Palmerston North 4410, New Zealand.

[4]Department of Animal, Plant and Soil Sciences, La Trobe University, AgriBio, Centre for AgriBiosciences, La Trobe University, Bundoora, Victoria 3086, Australia.

[5]Laboratory of Molecular Plant Pathology, School of Fundamental Sciences, Massey University, Palmerston North 4410, New Zealand.

[6]The New Zealand Bio-Protection Research Centre, Massey University, Palmerston North 4410, New Zealand.

[*]Corresponding author: Carl H. Mesarich.

A modified version of this chapter was published in Fungal Biology, **126**, 35-46 (2022)

DOI: 10.1016/j.funbio.2021.10.001

1. Abstract

Apple scab, caused by the fungal pathogen *Venturia inaequalis,* is the most economically important disease of apple (*Malus* x *domestica*) worldwide. To develop durable control strategies against this disease, a better understanding of the genetic mechanisms underlying the growth, reproduction, virulence and pathogenicity of *V. inaequalis* is required. A major bottleneck for the genetic characterization of *V. inaequalis* is the inability to easily delete or disrupt genes of interest using homologous recombination. Indeed, no gene deletions or disruptions in *V. inaequalis* have yet been published. Using the melanin biosynthesis pathway gene *trihydroxynaphthalene reductase* (*THN*) as a target for inactivation, which has previously been shown to result in a light-brown colony phenotype when transcriptionally silenced using RNA interference, we show, for the first time, that the CRISPR-Cas9 gene editing system can be successfully applied to the apple scab fungus. More specifically, using a CRISPR-Cas9 single guide RNA (sgRNA) targeted to the *THN* gene, delivered by a single autonomously replicating Golden Gate-compatible plasmid, we were able to identify six of 36 stable transformants with a light-brown phenotype, indicating an ~16.7% gene inactivation efficiency. Notably, of the six *THN* mutants, five had an independent mutation. As part of our pipeline, we also report a high-resolution melting (HRM) curve protocol for the rapid detection of CRISPR-Cas9 gene-edited mutants of *V. inaequalis*. This protocol identified a single base pair deletion mutation in a sample containing only 5% mutant genomic DNA, indicating high sensitivity for mutant screening. In establishing CRISPR-Cas9 as a tool for gene editing in *V. inaequalis*, we have provided a strong starting point for studies aiming to decipher gene function in this fungus. The associated HRM curve protocol will enable CRISPR-Cas9 transformants to be screened for gene inactivation in a high-throughput and low-cost manner, which will be particularly powerful in cases where the CRISPR-Cas9-mediated gene inactivation efficiency is low.

Keywords

CRISPR-Cas9 gene editing, *Venturia inaequalis*, fungus, apple scab, high-resolution melting, *trihydroxynaphthalene reductase* gene, melanin biosynthesis pathway.

2. Introduction

Fungal species from the *Venturia* genus are devastating plant pathogens of economically important crops that mainly belong to the *Rosaceae* [1-3]. The best researched of these pathogens is *Venturia inaequalis*, which causes scab, or black spot, the most economically important disease of apple (*Malus* x *domestica*) worldwide [3]. Under favourable conditions, this disease can result in 70% or more of the crop being lost, as scab renders the apples unmarketable (i.e. through blemishes and deformation), and reduces both the growth and yield of the plant (i.e. by causing repeated defoliation of trees over several seasons) [2-4]. To develop durable control strategies against scab disease, a better understanding of the genetic mechanisms underlying the growth, reproduction, virulence and pathogenicity of *V. inaequalis* is required.

A key development over recent years has been the availability of several *V. inaequalis* genome sequences and gene catalogues [1,5-9], as well as the development of both polyethylene glycol (PEG)-mediated protoplast and *Agrobacterium tumefaciens*-mediated transformation protocols for use with this fungus [10]. However, while several *V. inaequalis* genes of interest that are putatively involved in the infection process of apple have been identified [5,11-15], none have been functionally characterized to date using traditional gene deletion or disruption techniques. Indeed, no gene deletions or disruptions have yet been reported for *V. inaequalis* in the literature. This suggests that gene deletion or disruption by traditional homologous recombination is extremely inefficient in *V. inaequalis*. It should be noted that transcriptional silencing of multiple genes in *V. inaequalis* has been achieved using RNA interference (RNAi) [16]. However, RNAi does not typically silence a gene to completion and the observed phenotypes can be inconsistent, unclear or absent, making it difficult to determine function [17,18]. Taken together, alternative gene disruption and deletion tools, such as the Clustered Regularly Interspaced Short Palindromic

Repeats-Cas9 (CRISPR-Cas9) system [19], are desperately needed to assess gene function in *V. inaequalis*.

The CRISPR-Cas9 system is a powerful tool for gene editing that has been established in many species of filamentous plant-pathogenic microbes. Indeed, CRISPR-Cas9 has been used to generate gene inactivations in more than 40 species of filamentous fungi and oomycetes [20], including *Phytophthora sojae* [21], *Magnaporthe oryzae* [22], *Ustilago maydis* [23] and a fungus that is closely related to *V. inaequalis*, *Leptosphaeria maculans* [24]. The CRISPR-Cas9 gene editing system requires two components: the Cas9 endonuclease and a single guide RNA (sgRNA). The Cas9 endonuclease is an RNA-guided enzyme that generates a double strand break (DSB) in the genome. The sgRNA often consists of a protospacer sequence of 20 nucleotides at the 5' end that targets specific DNA by base pairing, and an 80-nucleotide scaffold structure that binds to Cas9 [25]. The sgRNA-Cas9 complex only cleaves the target DNA if it is flanked by a protospacer adjacent motif (PAM) [19].

After the Cas9 endonuclease generates a DSB in the target DNA, DNA repair mechanisms of the target organism are activated [19,26]. The DNA can be repaired by a non-homologous end-joining mechanism (NHEJ) or homology-directed repair (HDR), although NHEJ is usually the dominant DNA repair pathway in fungi [27]. DNA repair by NHEJ is error-prone and is likely to introduce small insertions/deletions (indels) or nucleotide substitutions, which can lead to frameshift mutations that cause a gene disruption [26]. Alternatively, a double-stranded DNA template (donor DNA), usually harbouring a selectable marker, can be introduced to use as a repair template for HDR.

Traditionally, screening for the identification of mutants generated by the CRISPR-Cas9 system can be achieved using an enzymatic mismatch cleavage (EMC) method [28] or a polyacrylamide gel electrophoresis (PAGE)-based method [29] that both rely on the detection of DNA heteroduplexes. Both EMC and PAGE detect large indels with a similar efficiency; however,

the sensitivity with which they detect small indels (i.e. the type of indels that are usually generated by CRISPR-Cas9 DSB) is low [28-30]**.** Alternatively, CRISPR-Cas9 mutants can be identified by amplicon sequencing, which is a tedious and expensive process. A high-resolution melting (HRM) curve analysis is a fluorescence-based technique that measures the melting temperature of double-stranded DNA and, in doing so, can discriminate between amplicons with different melting temperatures [31-33]. An HRM curve analysis has been widely used to identify mutations and single nucleotide polymorphisms in various genes [31,34], and has recently been used to reliably identify CRISPR-Cas9-mediated base pair (bp) indels in plants [30,35]. To date, even though HRM curve analyses are largely used for fungal species identification, to our knowledge, an HRM curve analysis has not yet been employed to screen for CRISPR-Cas9-generated mutants in fungi.

In this study, we set out to establish the CRISPR-Cas9 gene editing system in *V. inaequalis*. For this purpose, we first generated the Golden Gate-compatible plasmid Cas9HygAMAccdB by modifying the previously published Cas9 autonomously replicating plasmid ANEp8-Cas9-LIC [36]. Here, Golden Gate-compatibility was chosen as it enabled the introduction of a sgRNA into Cas9HygAMAccdB using a single step, facilitating the creation of a Cas9HygAMA-*sgRNA* plasmid in less than one week. Next, using the melanin biosynthesis pathway gene *trihydroxynaphthalene reductase* (*THN*) as a proof of concept, we showed, in conjunction with the Cas9HygAMA-*sgRNA* plasmid, that the CRISPR-Cas9 gene editing system can be successfully applied to *V. inaequalis*. As part of this process, we also established a method based on an HRM curve analysis for the high-throughput screening of CRISPR-Cas9 gene-edited mutants of *V. inaequalis*.

3. Methods

3.1. Strains used and growth conditions

V. inaequalis isolate MNH120 from New Zealand (ICMP 13258; [37]) was used for CRISPR-Cas9 experiments, and was grown on a cellophane membrane (Waugh Rubber Bands) overlaying potato-dextrose agar (PDA) (Scharlab) at 22°C with a 16 h light/dark cycle. For long-term storage, *V. inaequalis* cellophane membranes were air-dried overnight and stored at –20°C. *Escherichia coli* strain DH5α (Thermo Fisher Scientific) was used for cloning, propagation and maintenance of all plasmids without the *ccdB* gene, and *E. coli* strain TG1 (kindly provided by Jasna Rakonjac, Massey University) for propagation of all plasmids with the *control of cell death B* (*ccdB*) killer gene, in lysogeny broth (LB) at 37°C and 180 rpm, or on LB agar at 37°C.

3.2. Construction of the Cas9HygAMAccdB plasmid

The ANEp8-Cas9-LIC and ANEp8-Cas9-gRNA plasmids were kindly provided by Adrian Tsang from Concordia University. The first plasmid, ANEp8-Cas9-LIC, was previously constructed by Song et al. [36] through the introduction of a 38-bp ligation-independent cloning (LIC) site, centred with a *Swa*I restriction site, into the ANEp8-Cas9 plasmid. The second plasmid, ANEp8-Cas9-gRNA, was previously constructed by Song et al. [36] through the introduction of a sgRNA cassette, via the LIC method, into the ANEp8-Cas9-LIC plasmid (see S5 Fig. of Song et al. [36] for more details). We adapted the ANEp8-Cas9-LIC plasmid to contain a hygromycin resistance cassette in place of the *PyrG* gene for the selection of fungal transformants (summarized in **Appendix A: Figure A 5-4. A**). To achieve this, the ANEp8-Cas9-LIC plasmid was first digested with *Not*I (New England Biolabs) to liberate a 5.3 Kb fragment containing the AMA1 cassette, and a 10.3 Kb fragment containing the *Cas9* and *PyrG* genes, with both fragments purified by gel

extraction using a PureLink Quick Gel Extraction Kit (Thermo Fisher Scientific). Subsequent digestion of the 10.3 Kb fragment with *Kpn*I (New England Biolabs) liberated a 9 Kb Cas9 cassette containing the *Cas9* gene (i.e. through removal of the *PyrG* gene), which was again purified by gel extraction. Next, the 2.9 Kb hygromycin resistance cassette was amplified by PCR from the pDONR221-Hyg plasmid [38] using Phusion DNA polymerase (New England Biolabs), according to the manufacturer's instructions, in conjunction with the restriction enzyme-adapted primers *Not*I P*gpdA Hyg* pDONR Fw and *Kpn*I T*rpC Hyg* DONR Rv (**Table 5-1**), purified by gel extraction, and digested with both *Not*I and *Kpn*I. Following digestion, the *Not*I/*Kpn*I-digested Cas9 cassette and the *Not*I/*Kpn*I-digested hygromycin resistance cassette were ligated together with T4 ligase (Invitrogen) at 16°C overnight to create the Cas9Hyg plasmid, and then purified using a PureLink Quick Plasmid Miniprep Kit (Invitrogen). Finally, the Cas9Hyg plasmid was digested with *Not*I, dephosphorylated with Shrimp Alkaline Phosphatase (rSAP) (New England Biolabs), and purified by gel extraction, before ligation with the *Not*I-digested AMA1 cassette using T4 ligase to create the Cas9HygAMA plasmid.

Next, we set out to create the CasHygAMASapI plasmid by adding the sgRNA cassette, which contains a mock 20-bp sgRNA protospacer flanked by *Sap*I restriction sites, to the Cas9HygAMA plasmid (summarized in **Appendix A: Figure A 5-4. A**). This was achieved through overlap fusion PCR and ligation-independent cloning (LIC) [36]. More specifically, a fragment containing the tRNA promoter and mock protospacer sequences was first amplified from the ANEp8-Cas9-gRNA plasmid by PCR, as above, using the primers Fw LIC2 and *Sap*I site CRISPR Rv (**Table 5-1**). Here, the *Sap*I site CRISPR Rv primer was designed to introduce a *Sap*I restriction site between the tRNA promoter and mock protospacer sequences. At the same time, a second fragment containing the mock protospacer and tRNA terminator sequences was amplified from the ANEp8-Cas9-gRNA plasmid by PCR using the primers *Sap*I site CRISPR Fw and Rv LIC2 (**Table 5-1**). In this case, the *Sap*I site CRISPR Rv primer was designed to introduce a *Sap*I

restriction site between the mock protospacer and tRNA terminator sequences. Following gel extraction, the two purified fragments were then fused by PCR. For this purpose, 1 ng of each of the purified PCR fragments was combined and used as template in a 25 μL PCR with Phusion DNA polymerase in conjunction with the Fw LIC2 and Rv LIC2 primers (**Table 5-1**). The overlap fusion PCR was performed with the following thermocycler program: 30 sec at 98°C, followed by 35 cycles of 98°C for 5 sec, 60°C for 10 sec, 72°C for 30 sec, and then a final step of 72°C for 10 min. Finally, upon gel extraction, the purified PCR product was inserted into the Cas9HygAMA plasmid through LIC via its *Swa*I restriction site [36] to create the Cas9HygAMASapI plasmid.

Lastly, to insert the *ccdB* and *chloramphenicol acetyltransferase* (*cat*) resistance genes into the Cas9HygAMASapI plasmid (i.e. for subsequent cloning and screening), a 2 Kb fragment containing the *ccdB* and *cat* resistance gene cassette was amplified by PCR, as above, from the pSM1 plasmid [39] using the *Sap*I restriction enzyme-adapted primers *Sap*I *ccdB* Fw and *Sap*I *ccdB* Rv (**Table 5-1**). The resulting product was purified by gel extraction, digested by *Sap*I at 37 ℃, and ligated into the *Sap*I-digested Cas9HygAMASapI plasmid using T4 ligase at 16°C for 24 h to create the Cas9HygAMAccdB plasmid (**Figure 5-1** and Supplementary Information 1).

Table 5-1. Oligonucleotides used in this study. Bold sequence corresponds to the *Sap*I restriction site. Italicised sequence corresponds to the *Not*I restriction site. Bold italicized sequence corresponds to the *Kpn*I restriction site.

Oligonucleotide name	Oligonucleotide sequence (5´–3´)
MR135	**GTC**TTTCAAGGACGTCACACCAG
MR136	**AAC**CTGGTGTGACGTCCTTGAAA
MR137	**GTC**GCCCCATCATGGTCTTTGGA
MR138	**AAC**TCCAAAGACCATGATGGGGC
MR139	TTTTCTCTTCCATTTACGC
MR161	GTAGGGAGGTCCATTAGTG
MR162	GGATAACACACTAGAGATA
MR170	TTATAGTCGACCACCGCTCG
MR171	CCACGACCTGTTGATTGCAT
MR172	CCCACTCACTAAACAAACTA

Oligonucleotide name	**Oligonucleotide sequence (5´–3´)**
MR173	TCGATTGACAAGAACATACC
MR182	GCATCTGACGCCCCATCATGGGGTTT
MR183	AAACCCCATGATGGGGCGTCAGATGC
MR184	GCGAGAATGCAGAGAGTTGG
MR185	GTGTGTGTCGCTGGATGATC
MR204	CGCCAGCCTTCAATGCCAAT
MR205	CATTGCGCCATCCCGATCTG
MR252	CGTTGGCCAATCAGACGTCG
MR253	GCCCAGAGCATCATCACCCT
MR258	GAGCGGATTCCTCAGTCTCG
MR259	CTCGGAGGGCGAAGAATCTC
*Kpn*I T*trpC* *Hyg*	
DONR Rv	GCC***GGTACC***GCGCTTACACAGTACACGAG
*Not*I P*gpdA* *Hyg*	
pDONR Fw	AAGGAAAAAA*GCGGCCGC*CTAAAATCCGCCGCCTCCAC
*Sap*I site CRISPR Fw	GTCGGAAGAGCAAAAT**GCTCTTC**AGTTTTAGAGCTAGAAATAGCAAG
*Sap*I site CRISPR Rv	AACTGAAGAGCATTTT**GCTCTTC**CGACGAGCTTACTCGTTTCG
Fw LIC2	CAACCTCCAATCCAATTTGACTCCGCCGAACGTACTGG
Rv LIC2	ACTACTCTACCACTATTTGAAAAGCAAAAAAGGAAGGTACAAAAAAGC
*Sap*I *ccdB* Fw	TCGGCTCGTCGGAAGAGCGACCGACAGCCTTCCAAATG
*Sap*I *ccdB* Rv	TCGCTAAAACTGAAGAGCGTTGGCAGCATCACCCGACG

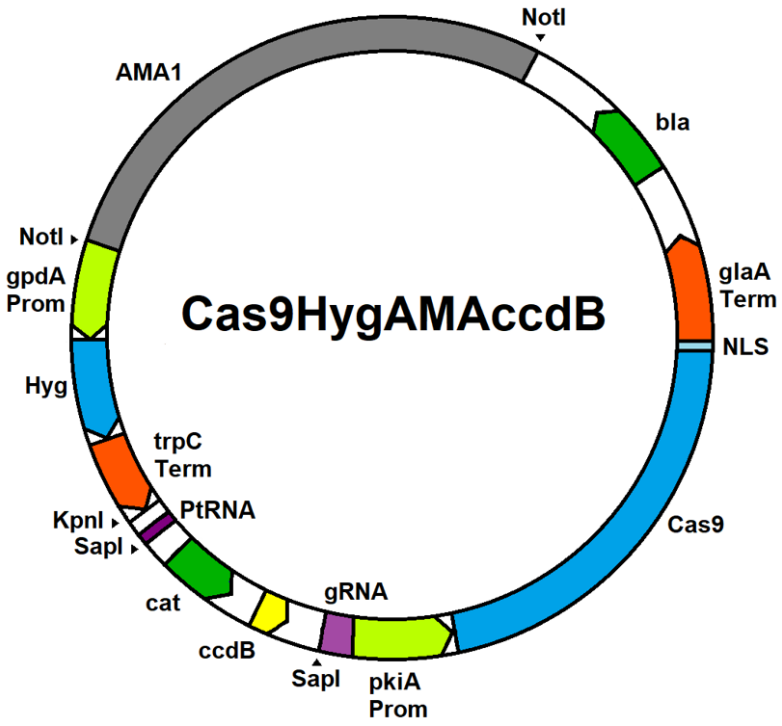

Figure 5-1. Schematic representation of the Cas9HygAMAccdB plasmid. The plasmid, which is 19,273 bp in size, contains the autonomously replicating sequence AMA1 from *Aspergillus nidulans*, as well as the *cas9* gene from *Streptococcus pyogenes* (codon-optimized based on *Asergillus niger*), which is flanked by the *A. niger* pyruvate kinase gene promoter (*pkiA* Prom) and the *A. niger* glucoamylase gene terminator (*glaA* Term) [36]. Fused to the carboxyl (C)-terminus of the *cas9* gene is nucleotide sequence encoding a nuclear localization signal (NLS). The Cas9HygAMAccdB plasmid also contains a hygromycin B resistance casette (Hyg) flanked by the *A. nidulans* glyceraldehyde-3-phosphate dehydrogenase gene promoter (*gpdA* Prom) and the *A. nidulans* tryptophan C gene terminator (*trpC* Term) [38]. *Sap*I restriction sites for introduction of a sgRNA cassette by Golden Gate cloning (i.e. through replacement the control of cell death B [*ccdB*] gene) are shown. *bla*: beta-lactamase gene conferring ampicillin resistance; *cat*: chloramphenicol acetyltransferase gene conferring chloramphenicol resistance.

3.3. Protospacer design and cloning

The *V. inaequalis THN* gene (Joint Genome Institute ID: *atg3631.t1*) was screened for CRISPR-Cas9 target sites with the PAM (NGG) sequence using the 'Find CRISPR Sites' function in Geneious (v.9.0.5) [40]). Only those protospacers with no predicted off-target effects (i.e. a Specificity score of 100%), an on-target (Activity) score of at least 0.4, and no predicted off-target binding sites in the *V. inaequalis* MNH120 PacBio reference genome (unpublished, The New

Zealand Institute for Plant and Food Research Limited) using BLASTn, were considered. Based on these criteria, two protospacer sequences with the best on-target score, targeting the first and second exon of the *THN* gene, respectively, were selected. Each protospacer, with the appropriate *Sap*I overhang for Golden Gate cloning into the destination plasmid Cas9HygAMAccdB, was ordered as a forward and reverse oligonucleotide from Integrated DNA Technologies. The protospacer #20 was generated by pre-annealing 40 ng of the forward (MR135) and reverse (MR136) oligonucleotides (**Table 5-1**), and protospacer #4 by pre-annealing 40 ng of the forward (MR137) and reverse (MR138) oligonucleotides (**Table 5-1**), in annealing buffer (10 mM Tris-HCl pH 8, 50 mM NaCl, 1 mM EDTA, pH 8) with the following thermocycler program: 5 min at 95°C, 20 sec at 92°C, followed by a decrease of 0.5°C each cycle for 140 cycles, and finally, 1 min at 25°C. Pre-annealed oligonucleotides were cloned into the Cas9HygAMAccdB plasmid using Golden Gate in association with the *Sap*I restriction enzyme to generate sgRNA20 and sgRNA4. Golden Gate reactions were performed with the following thermocycler program: 1 min at 37°C, 1 min at 16°C for 30 cycles, followed by 5 min at 55°C and 5 min at 80°C. Transformants positive for each Cas9HygAMA-*sgRNA* plasmid were screened by colony PCR using Taq DNA polymerase (New England Biolabs) with the forward Cas9HygAMAccdB primer (MR139) and reverse sgRNA-specific primer (MR136 or MR138) (**Table 5-1**). Colony PCRs were carried out with the standard manufacturer's protocol. Sequence authenticity of the sgRNAs was confirmed by PCR amplicon sequencing, provided by the Massey Genome Service (Massey University, Palmerston North, New Zealand), using the MR139 forward Cas9HygAMAccdB primer.

3.4. *V. inaequalis* protoplast preparation and transformation

Cas9HygAMA-*sgRNA* plasmids were introduced into *V. inaequalis* using a PEG-mediated protoplast transformation protocol. For this purpose, *V. inaequalis* was first grown on cellophane membranes overlaying PDA for 10–14 days. Fungal mycelia on top and inside cellophane

membranes were then macerated in 1.5 ml microcentrifuge tubes using plastic micropestles, transferred to a 250 ml Erlenmeyer flask containing 30 ml potato-dextrose broth (PDB) (Difco), and cultured without shaking in the dark at 22°C for 48 h. After culturing, fungal material was harvested by centrifugation at 2,800 *g* for 20 min, washed three times with KC buffer (0.60 M KCl, 50 mM $CaCl_2 \cdot 2H_20$), with collection by centrifugation as above after each wash, and incubated in a 250 ml Erlenmeyer flask containing 10 g/L *Trichoderma harzianum* lysing enzymes (Sigma-Aldrich) in 50 ml KC buffer at 24°C and 80 rpm for 4-5 h. Finally, protoplasts were filtered through glass wool, and washed three times with KC buffer as above. Protoplasts were counted using a haemocytometer and re-suspended to a final concentration of 10^4–10^5 protoplasts/ml.

Transformation was performed by mixing 100 µl of *V. inaequalis* protoplasts (10^4-10^5 protoplasts/ml) with 100 µl of 25% PEG4000, 10 µg of circular Cas9HygAMA-*sgRNA* plasmid DNA, and 5 µl of 50 µM sterile spermidine. The protoplast-PEG mixture was then chilled on ice for 20 min and 500 µl of 25% PEG4000 gently added. Each protoplast-PEG mixture was plated across five Sucrose Hepes (SH) plates (0.6 M sucrose, 5 mM HEPES, 0.6% agar) and incubated at 20°C for 48 h. After incubation, protoplasts were overlaid with ½-strength PDA cooled-down to ~50°C and supplemented with 50 mg/ml hygromycin B (Merck). Transformants appearing on the PDA surface, between two and three weeks after transformation, were transferred to 16-well PDA plates supplemented with 50 mg/ml hygromycin B, and grown until abundantly sporulating. After mutant screening, selected transformants were single-spore purified. This was achieved by re-suspending a single colony in 500 µl sterile water and vortexing for 30 sec, with 100 µl streaked onto 4% water agar (WA) plates and the conidia germinated for 24 h. Following germination, one single germinated conidium was transferred to a cellophane membrane overlaying PDA for continued growth.

3.5. *V. inaequalis* genomic DNA extraction

Two-to-four week-old cultures of *V. inaequalis* grown on cellophane membranes were freeze-dried and ground to a fine powder in liquid nitrogen with a pre-cooled mortar and pestle, and approximately 300 mg of powder was transferred to a 1.5 ml microcentrifuge tube. To this, 1 ml of DNA extraction buffer (0.5 M NaCl, 10 mM Tris-HCl, 10 mM EDTA, 1% SDS, pH 7.5) was added, vortexed, and incubated at 65°C for 30 min, followed by 2 min incubation at room temperature (RT). Fungal material was collected by centrifugation at 16,000 *g* for 2 min and 800 µl of supernatant was transferred to a fresh 1.5 ml microcentrifuge tube. Then, 4 µl of RNase A (20 mg/ml) (Invitrogen) was added and samples were incubated at 37°C for 15 min. After incubation, a 0.5 volume of phenol and a 0.5 volume of chloroform:isoamyl alcohol (24:1) were added and samples were centrifuged for 5 min at 16,000 *g*. The aqueous phase was then transferred to a fresh 1.5 ml microcentrifuge tube and 1 volume of phenol:chloroform (1:1) was added. Samples were again centrifuged at 16,000 *g* for 5 min and the supernatant transferred to a new 1.5 ml microcentrifuge tube. The chloroform:isoamyl alcohol (24:1) step was then repeated and the supernatant was transferred to a new 1.5 ml microcentrifuge tube. Genomic DNA was precipitated by the addition of a 0.1 volume of 3 M sodium acetate (pH 5.2) and two volumes of 95% ethanol. Samples were mixed by inversion and incubated overnight at –20°C. Following incubation, the precipitated DNA was collected by centrifugation at 16,000 *g* for 30 min, and the supernatant was decanted. The genomic DNA pellet was then washed with 200 µl of 70% ethanol and collected by centrifugation at 16,000 *g* for 5 min. Finally, the genomic DNA pellet was air-dried for 15-30 min and suspended in 50 µl of MilliQ water.

3.6. High resolution melting curve analysis

A positive control for the HRM curve analysis was created by site-directed mutagenesis. First, primers MR161 and MR162 (**Table 5-1**) were phosphorylated with T4 Polynucleotide Kinase (New England Biolabs) at 37°C for 1 h in a 4.5 µl reaction volume with 10 µM primer, 10x T4 ligase buffer (New England Biolabs) and 0.4 µl of T4 polynucleotide kinase (New England Biolabs). The *THN* gene was amplified with the phosphorylated primers MR161-MR162 using Phusion Flash High-Fidelity PCR Master Mix (Thermo Fisher Scientific) and purified using an OMEGA Gel Extraction kit. The pICH41021 plasmid (kindly provided by Dr Kee Hoon Sohn, formerly of Massey University) was digested with the *Sma*I restriction enzyme in a 50 µl volume for 2 h at 37°C. Digested plasmid was then de-phosphorylated with Shrimp Alkaline Phosphatase (rSAP) for 30 min at 37°C, with the reaction subsequently heat-inactivated at 65°C for 5 min. Finally, the *THN* gene was ligated to pICH41021 in a 3:1 molar ratio using T4 Ligase (New England Biolabs) at 4°C overnight and transformed by heat shock into chemically competent *E. coli* cells. Positive transformants were confirmed by colony PCR. Next, the pICH41021-*THN* plasmid was amplified with overlapping primers MR182 and MR183 to introduce a mutation in the *THN* gene that substituted a thymine and cytosine at nucleotide positions 26 and 27 for two guanines. The resulting re-circularized pICH41021-$THN_{TC(26/27)GG}$ plasmid was confirmed by sequencing.

Two sets of primers (MR170-MR171 and MR172-MR173) were designed with Geneious v.9.0.5 software for use in the HRM curve analysis (**Table 5-1**). These primers were designed to amplify the DNA region in the *THN* gene recognized by the sgRNA (and thus, edited by the Cas9 endonuclease), with an amplicon size of 123 bp (MR172-MR173) and 230 bp (MR170-MR171). Primers were tested to be specific and suitable for HRM by performing an HRM curve analysis

with DNA standards (wild-type and engineered positive control), as described below, with the resulting amplicons resolved by electrophoresis on a 1.5% Tris-acetate-EDTA (TAE) gel.

The HRM curve analysis was performed using a LightCycler 480 Instrument (Roche) with the AccuMelt HRM SuperMix fluorescent dye (DNAture) in a 20 µL reaction with 1x AccuMelt HRM SuperMix, 300 nM forward primers (MR172), 300 nM reverse primer (MR173) and 1.5 ng of genomic DNA template or 0.01 ng of the puc19-$THN_{TC(26/27)GG}$ plasmid. At least two technical replicates were performed for each sample. The qPCR amplification was performed with the following program: initial denaturation of 5 min at 95°C, followed by 40 cycles of 95°C for 8 sec, 60°C for 15 sec, 70°C for 20 sec, with one fluorescence reading per annealing step. The qPCR was followed by a melting program consisting of 95°C for 1 min, 40°C for 1 min and 76°C for 1 sec, at which point the temperature was ramped up to 92°C (with a temperature increase of 0.02°C per second, and a continuous signal acquisition mode made up of 25 acquisitions per degree), followed by a cooling step of 40°C for 30 sec. The HRM curve data were analysed with the LightCycler 480 gene scanning software. To confirm mutants identified by HRM, the *THN* gene was amplified with Phusion Flash High-Fidelity PCR Master Mix using primers MR161 and MR162, with the resultant PCR amplicons gel-purified as above and sequenced using primer MR161.

3.7. Southern blot analysis

For the detection of Cas9HygAMA-*sgRNA* plasmid DNA in genomic DNA samples of *V. inaequalis* by Southern blotting, a probe binding to the hygromycin resistance cassette of the Cas9HygAMAccdB plasmid was generated by PCR using Phusion DNA polymerase in conjunction with primers MR258-MR259 (**Table 5-1**), the PCR product was gel purified and the digoxigenin (DIG) High Prime DNA Labelling and Detection Starter Kit I (Roche) according to manufacturer's instructions. Following synthesis of the probe, genomic DNA was extracted from wild-type *V. inaequalis*, as well as single-spore purified transformants of *V. inaequalis*, using the

method described in section 2.5. A total of 5 µg genomic DNA from each sample, as well as 50 ng of Cas9HygAMAccdB plasmid DNA (positive control DNA), was then digested with the *Eco*RI restriction enzyme (New England Biolabs) overnight at 37°C and resolved by electrophoresis on a 1.5% Tris-borate-EDTA (TBE) gel. DNA was subsequently transferred to a positively charged nylon membrane (Roche) overnight at room temperature. DNA was crosslinked to the membrane by UV irradiation for 2 min using a CEX-800 UV cross-linker (120 mJ/cm2, 254 nm; Ultralum, Inc.), and the probe hybridized to the DNA on the membrane overnight at 50°C. Colorimetric detection of the probe was then performed as per the manufacturer's instructions using the DIG High Prime DNA Labelling and Detection Starter Kit I for 3 h for the Cas9HygAMAccdB plasmid DNA control, and 9 h for *V. inaequalis* genomic DNA samples.

4. Results and discussion

4.1. CRISPR-Cas9 can be used for gene disruption in *V. inaequalis*

We set out to establish the CRISPR-Cas9 gene editing system in *V. inaequalis*, using the melanin biosynthesis pathway gene *THN* (Joint Genome Institute ID: *atg4736.t1*) as a target for inactivation. The *THN* gene was chosen as a proof of concept, as a previous study had shown that *V. inaequalis* displays a distinctive light-brown phenotype when this gene is transcriptionally silenced using RNAi, indicative of reduced melanisation [16]. In this way, transformants of *V. inaequalis* inactivated for the *THN* gene using the CRISPR-Cas9 gene editing system can be rapidly identified through a simple visual screen. For ease of use, we chose to employ a CRISPR-Cas9 gene editing system that, similar to the one previously established in *Aspergillus niger* [36], only requires a single autonomously replicating plasmid derived from Cas9HygAMAccdB and containing both the Cas9 endonuclease and sgRNA, for gene inactivation (**Figure 5-1**).

The Cas9HygAMAccdB plasmid contains an *A. niger* codon-optimized *cas9* gene expressed under the control of the *pkiA* (*pyruvate kinase*) promoter. To ensure expression in the fungal nucleus, the Cas9 endonuclease was tagged at its carboxyl (C) terminus with a nuclear localization signal (NLS). The Cas9HygAMAccdB plasmid also contains an RNA polymerase III promoter to facilitate expression of the sgRNA *in vivo.* Using the chosen CRISPR-Cas9 system, the 20 bp encoding the sgRNA protospacer were synthesized as two pairs of complementary oligonucleotides that were pre-annealed and cloned into the Cas9HygAMAccdB plasmid by a single-step Golden Gate reaction, enabling Polymerase Chain Reaction (PCR)-free cloning that could be completed in less than one week.

An autonomously replicating plasmid was chosen as it has several advantages. Firstly, autonomously replicating plasmids can enhance fungal transformation efficiency, as recombination between the plasmid and chromosome is not required [41]. As such, autonomously

replicating plasmids can be used in fungal species that exhibit low transformation efficiency, such as *V. inaequalis*. Secondly, autonomously replicating plasmids could be lost once selection (e.g., as mediated through hygromycin B) is removed [41]. In doing so, autonomously replicating plasmids can reduce off-target effects by only enabling transient expression of the Cas9 endonuclease in the fungus [42]. As such, autonomously replicating plasmids could be recycled, which would enable the sequential inactivation of genes in CRISPR-Cas9 gene-edited mutants and could also facilitate the subsequent complementation of mutants generated using CRISPR-Cas9 technology.

As a starting point for inactivation, sgRNAs were designed to target the amino (N) terminus (first and second exon) instead of the C terminus of the *THN* gene. This is because mutations at the C terminus of a gene are less likely to cause a frameshift mutation that results in inactivation [43]. As different sgRNAs can display different targeting efficiencies ([43], two different sgRNAs, sgRNA 4 and sgRNA 20, with similar predicted on-target activity, and no predicted off-target activity (**Table 5-2**), were selected for inactivation of the *THN* gene. Special attention was taken to ensure that the sgRNAs did not target any other melanin biosynthesis pathway genes that have a high degree of conservation to *THN*, such as the *1,3,6,8-tetrahydroxynaphthalene reductase* gene (*atg3631.t1*). PEG-mediated protoplast transformation of *V. inaequalis* with sgRNA 4, targeting the first *THN* exon (**Appendix A: Figure 5-2. A**), resulted in 98 independent transformants, of which 62 ceased to grow on hygromycin B selection media after one week, and were therefore considered transient, giving a final number of 36 stable transformants. Transient transformants have been reported in a large number of PEG-mediated protoplast transformations of fungi [44,45], and it has previously been reported that up to 98% of PEG-mediated protoplast transformants of *V. inaequalis* are transient [10]. Of course, it remains possible that the large number of transient transformants generated in our study was the result of premature loss of the autonomously replicating plasmid used to deliver the sgRNA and Cas9.

Notably, of the 36 stable transformants, six had a light-brown phenotype (**Figure 5-2**. **B**). These were transformants THN #9, THN #37, THN #60, THN #66, THN #89 and THN #96. To validate the presence of a mutation in the *THN* gene, it was amplified from each of the six putative mutants by PCR, as well as from three dark-brown transformants without the light-brown phenotype (THN #38, THN #53 and THN #90), and subjected to amplicon sequencing. As expected, all three dark-brown transformants did not contain a mutation in their *THN* gene (**Figure 5-2 .C**). For the putative light-brown mutant THN #9, the *THN* gene could not be amplified by PCR using two different sets of primers (MR161-MR162, MR185-MR186). This was despite the fact that both *THN*-flanking genes could be amplified, suggesting that a large deletion at the *THN* locus might have occurred (**Appendix A: Figure A 5-2**). In contrast to the dark-brown transformants, the remaining light-brown *THN* transformants displayed a range of mutations. More specifically, these were a single bp insertion (T) at the same location in THN #37 and THN #66, a 33-bp deletion (TTTGGAGGGCAAGGTCGCCCTCGTTACCGGTTC) in THN #60, a single bp deletion (T) in THN #89, and a 24-bp deletion (TCATGGTCTTTGGAGGGCAAGGTC) in THN #96. Therefore, from the 36 stable transformants, six had a confirmed mutation, giving a gene inactivation efficiency of ~16.7%.

CRISPR-Cas9 gene inactivation efficiencies in other filamentous fungi, in experiments that rely on NHEJ, range between 10 and 100% [22,23,46-48]. In cases where the CRISPR-Cas9 NHEJ-based gene inactivation efficiency is low, the gene inactivation efficiency could be improved greatly by the incorporation of a donor DNA that is integrated into the genome using HDR [22]. Nevertheless, gene inactivation efficiencies between experiments cannot be compared, as these efficiencies will greatly depend on Cas9 expression, sgRNA design and accessibility of the target gene, among other factors [20]. Therefore, even though the inactivation efficiency of the *V. inaequalis THN* gene with sgRNA 4 is at the low end, it is likely to vary between genes and no conclusions can yet be drawn as to the overall efficiency of the technique.

Remarkably, PEG-mediated protoplast transformation of *V. inaequalis* with sgRNA 20, targeting the second exon of the *THN* gene (**Figure 5-2. A**), resulted in a similar number of stable independent transformants on hygromycin B selection media (31 in total), but none of these transformants had the distinctive light-brown phenotype, indicating that if a Cas9-induced mutation was generated, it was synonymous or did not disrupt THN activity. This stark difference in the number of transformants inactivated for the *THN* gene is interesting, given that both sgRNAs had a similar predicted on-target activity score (**Table 5-2**). However, it is known that different sgRNAs can vary greatly in their efficiency, as previously observed for sgRNAs targeting the *yA* gene of the filamentous fungus *A. nidulans* [49], highlighting the importance of reliable methods to estimate sgRNA efficiency. Thus, while genes will differ in their ability to be inactivated using the CRISPR-Cas9 gene editing system (e.g. due to their location in the genome) [20], it is important that future studies consider multiple sgRNAs for successful gene inactivation in *V. inaequalis*.

Table 5-2. Selected sgRNA protospacers used to target the *Venturia inaequalis* melanin biosynthesis pathway gene *trihydroxynaphthalene reductase* (*THN*).

	Sequence (5'–3´)[1]	Binding site	Direction	Off-targets[2]	Off-target score[3]	On-target score[4]
Protospacer 4	GCCCCATCATGGTCTTTGGAGGG	Exon 1	Forward	0 (0 in CDS)	100%	0.448
Protospacer 20	TTTCAAGGACGTCACACCAGAGG	Exon 2	Forward	0 (0 in CDS)	100%	0.539

[1]NGG: protospacer adjacent motif (PAM) site.

[2]CDS: coding sequence.

[3]Off-target score: prediction of how likely a sgRNA sequence might bind to somewhere else in the genome. Scores are between 0 and 100, with higher scores indicative of less off-target activity.

[4]On-target scores are between 0 and 1, with higher scores indicative of higher expected activity of the sgRNA-Cas9 complex on the target gene, based on Doench et al. [43].

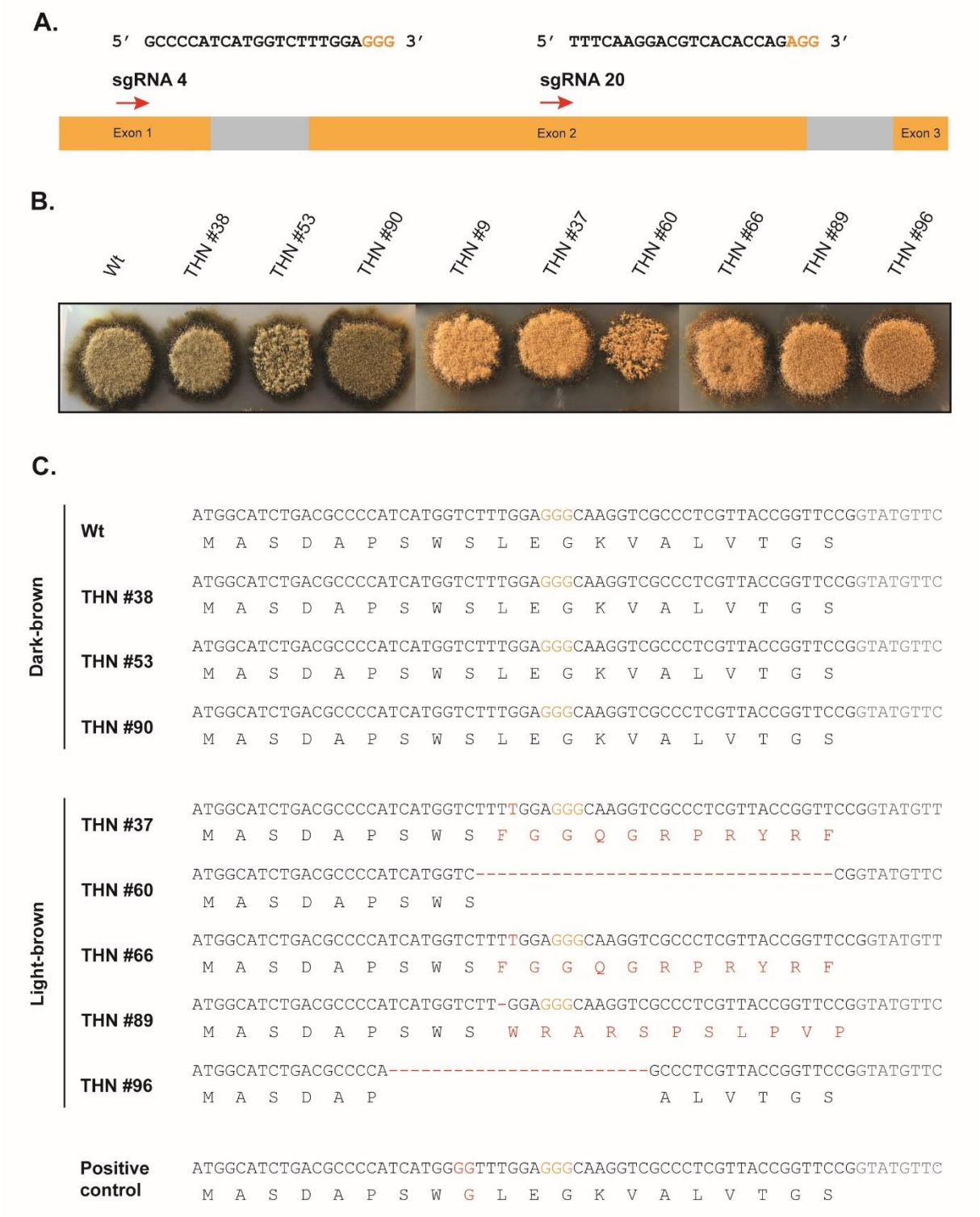

Figure 5-2. Establishment of the CRISPR-Cas9 gene editing system in *Venturia inaequalis*. A. Schematic representation of the *V. inaequalis* melanin biosynthesis pathway gene *trihydroxynaphthalene reductase* (*THN*; 911 bp) with binding sites for the two selected sgRNAs used in CRISPR-Cas9 gene editing experiments shown. Orange: gene exons; Grey: gene introns; Bold nucleotides: expected sgRNA cleavage site; orange nucleotides: PAM site.

Arrows: binding direction of sgRNAs. **B.** Colony phenotype of wild type (wt) *V. inaequalis*, and three dark-brown and six light-brown CRISPR-Cas9 transformants grown on potato-dextrose agar at 22°C for 14 days. **C.** Spectrum of CRISPR-Cas9-generated mutations in the *THN* gene. Black nucleotides: exon; Grey nucleotides: intron; Orange nucleotides: PAM site; Red amino acids/nucleotides: mutations observed. Light-brown mutant THN #9 was not sequenced due to a lack of PCR amplification for the *THN* gene.

4.2. The autonomously replicating CRISPR-Cas9 gene editing plasmid is rapidly lost in most transformants once selection is removed

With the finding that the CRISPR-Cas9 gene editing system could be successfully applied to *V. inaequalis*, we next set out to determine whether this fungus can lose the autonomously replicating plasmid, Cas9HygAMA-*sgRNA*, once the hygromycin B selection is removed. For this purpose, all six light-brown *THN* mutants (THN #9, THN #37, THN #60, THN #66, THN #89 and THN #96), as well as three dark-brown transformants (THN #38, THN #53 and THN #90), all derived from the transformation of *V. inaequalis* with sgRNA 4, were single-spore purified and replica-plated onto both PDA and PDA supplemented with 50 µg/ml hygromycin B. After only one round of single-spore isolation and sub-culturing, four of the *THN* mutants (THN #60, THN #66, THN #89 and THN #96) and two of the transformants without the light-brown phenotype (THN #53 and THN #90) lost the ability to grow on PDA supplemented with hygromycin B, suggesting that they have lost the Cas9HygAMA-*sgRNA* plasmid (**Appendix A: Figure A 5-3**).

To confirm that this is indeed the case, and to assess whether the remaining transformant (THN #38) and *THN* mutants (THN #9 and THN #37) still possess the Cas9HygAMA plasmid in its autonomously replicating form, or whether this plasmid has instead been integrated into their genomes, a Southern blot experiment was performed using a probe binding to the hygromycin B cassette of the Cas9HygAMA plasmid (**Appendix A: Figure A 5-4**). Here, genomic DNA from each of the transformants and *THN* mutants was digested with the restriction enzyme *Eco*RI. Similar amounts of *Eco*RI-digested genomic DNA from each of the transformants and THN mutants was used for Southern blot as observed by gel electrophoresis prior to membrane transfer

and blotting (**Appendix A: Figure A 5-4. A**). For the *THN* mutant THN #37, two bands of approximately 2.7 Kb and 2.4 Kb, respectively, corresponding to the expected banding profile of *Eco*RI-digested Cas9HygAMA plasmid DNA, were observed, indicating that the autonomously replicating plasmid was still present (**Appendix A: Figure A 5-4. B**). However, in addition to these two bands, several bands ranging in size from approximately 3.2 Kb to >10 Kb that do not correspond to the expected banding profile of *Eco*RI-digested Cas9HygAMA plasmid DNA, were also observed (**Appendix A: Figure A 5-4. B**). This suggests that multiple integrations of Cas9HygAMA plasmid DNA into the genome of *THN* mutant THN #37 have also occurred. Unlike THN #37, the *THN* mutants THN #9 and THN #38 were only found to have unique bands that do not correspond to the autonomously replicating Cas9HygAMA plasmid (**Appendix A: Figure A 5-4**). This suggests that these transformants do not possess the plasmid in its autonomously replicating form, but rather, that it has integrated into their genomes. Finally, the Cas9HygAMA plasmid, either in its autonomously replicating form or as a version that has been integrated into the genome, could not be detected in transformants THN #53 and THN #90, as well as *THN* mutants THN #60, THN #66, THN #89 and THN #96 (**Appendix A: Figure A 5-4**. **B**), which collectively lost the ability to grow on PDA supplemented with hygromycin B (**Appendix A: Figure A 5-3**), confirming that they have indeed lost the autonomously replicating Cas9HygAMA plasmid (**Appendix A: Figure A 5-4. B**).

4.3. High-resolution melting analysis is a sensitive and high-throughput method to screen for CRISPR-Cas9 mutants

In our study, mutants of *V. inaequalis* with a CRISPR-Cas9-mediated gene inactivation of the *THN* gene could be rapidly identified based on their light-brown colony phenotype. However, not all genes of *V. inaequalis* will result in an observable phenotype when inactivated or mutated. For this reason, a low-cost, high-throughput method is required to rapidly identify CRISPR-Cas9 gene-

edited mutants of *V. inaequalis* that lack an observable phenotype on a transformation plate facilitating selection. One such method is an HRM curve analysis, which enables the rapid identification of single bp indels in DNA amplicons from transformant genomic DNA (Reed and Wittwer, 2004; Simko, 2016; Wittwer, 2009). We set out to test the efficiency of an HRM curve analysis for the detection of *V. inaequalis THN* mutants generated using CRISPR-Cas9 sgRNA 4. As a starting point for this analysis, we first generated a positive control sequence for detecting indels relative to the wild type (wt) sequence (**Figure 5-2. C**). The positive control was generated by introducing a two-nucleotide substitution into a PCR amplicon of the *THN* gene using site-directed mutagenesis.

According to the literature, an HRM curve analysis can be affected by different parameters such as genomic DNA quality, PCR amplicon size, amplicon GC content and fluorescent dye used [50]. To ensure reliability of the assay, good quality genomic DNA should be extracted. Likewise, the same DNA preparation method should be used across all samples to ensure uniformity in genomic DNA quality. Amplicon size is another crucial parameter that affects the HRM curve analysis. Therefore, two different primer sets were designed to generate amplicons of 230 bp (MR170-MR171) and 123 bp (MR172-MR173) (**Table 5-1**). The HRM curve assay was performed with both primers sets using wt genomic DNA and the engineered positive control as DNA template. Specific DNA amplicons could be amplified using both primers sets (**Figure 5-3. A**); however, the smaller amplicon showed a clearer shift in the melting curve between wt and positive control (**Figure 5-3. B**). Given that smaller amplicons are more suitable for HRM curve analysis [50], and because the smaller amplicon showed a clearer shift in the melting curve, we decided to use the 123 bp amplicon for our screen (primer set MR172-MR173).

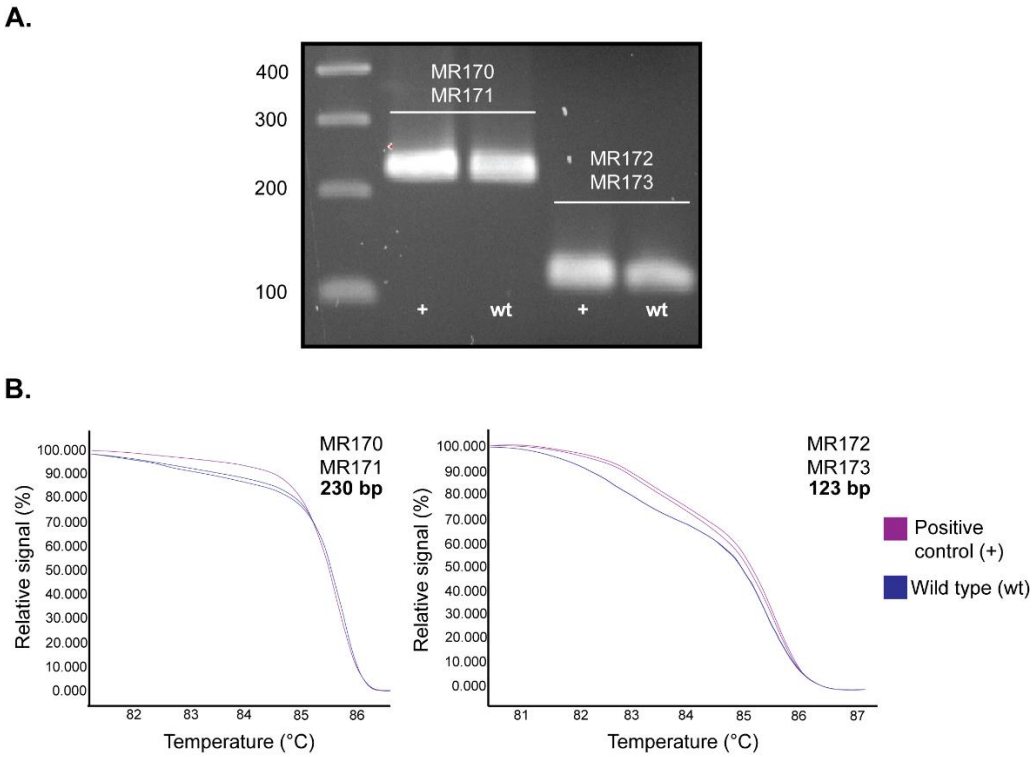

Figure 5-3. Optimization of primers for qPCR-HRM curve analysis of the *trihydroxynaphthalene reductase* (*THN*) gene mutants generated using CRISPR-Cas9 sgRNA 4. **A.** Conventional PCR amplification of the *THN* gene positive control (+) and wild type (wt) sequences with the different primer sets resolved by electrophoresis on a 1.5% TBE agarose gel. Ladder sizes are shown in base pairs (bp)**. B.** Normalized and shifted melting curves of the *THN* gene positive control (+) and wild type (wt) PCR amplicons generated with two different primer sets (MR170-MR171 and MR172-MR173).

The HRM curve analysis was performed using the AccuMelt HRM SuperMix high saturating dye SYTO 9^{TM}, resulting in clear separation of unique melting curves between mutants (**Figure 5-4**). The normalized HRM curves showed that amplicons from wt fungus, as well as dark-brown transformants, clustered together into a group with a similar melting curve profile (blue curves in **Figure 5-4**). In contrast, amplicons from the engineered positive control (green curves in **Figure 5-4**) and the light-brown *THN* mutants showed distinct melting curves (green, red, grey and purple curves in **Figure 5-4**) that correlated with the different mutations seen in **Figure 5-2 .C**. These results indicate that the HRM curve assay can not only efficiently identify CRISPR-Cas9 gene-edited mutants, but can also discriminate between different types of mutations (Reed & Wittwer, 2004). The light-brown mutant THN #9 could not be screened using the HRM

curve analysis due to a lack of PCR amplification for the *THN* gene, suggesting that a large deletion at the *THN* locus has been generated. This highlights one of the main limitations of the HRM curve analysis, in that it is not suitable for the detection of large deletion mutants. However, given that such deletion mutants can be easily assessed using standard PCR, this is not an issue.

One of the main advantages of the HRM curve analysis is that it can detect mutant DNA that is mixed in with wt DNA, even when the amount of mutant DNA is as low as 1–5% [30,35]. To test the efficiency of the HRM curve assay, genomic DNA from one mutant with a single bp insertion (THN #66) was mixed with wt genomic DNA at different mutant:wt ratios (1:99, 5:95, 10:90, 20:80, 30:70 and 50:50), similarly to that performed by [30]. Under our conditions, the assay could not differentiate mutant and wt in 1:99 mutant:wt ratio; however, the mutant DNA could be identified by the HRM curve analysis in all of the other ratios, with a clear shift in the melting curve, indicating an assay sensitivity as high as 5% (**Figure 5-5**). Therefore, mutants do not need to be single-spore purified before performing an HRM curve analysis, and multiple mutants can be pooled together for large-scale screens. The observation that mutant DNA can be detected when mixed with wt DNA further reduces the cost and workload of the assay, and further validates the use of an HRM curve analysis for the high throughput screening of CRISPR-Cas9 fungal transformants.

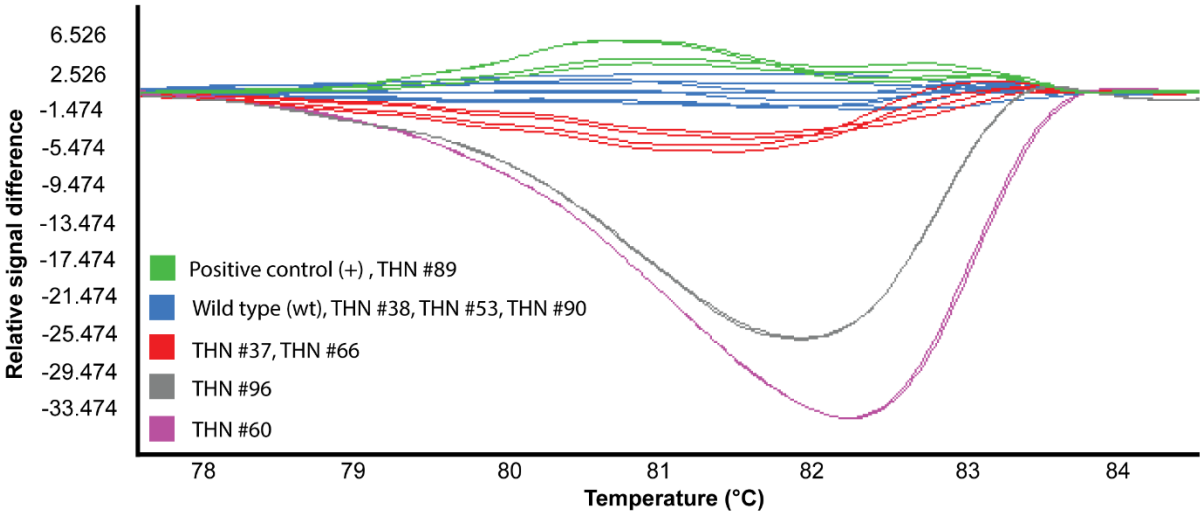

Figure 5-4. Screening of CRISPR-Cas9 transformants of *Venturia inaequalis* using qPCR-HRM curve and PCR amplicon sequencing analyses. Plot showing normalized and temperature-shifted differences in melting curves between *trihydroxynaphthalene reductase* (*THN*) amplicons of transformants. Melting curve groups were generated by LightCycler® 480 gene scanning software with a sensitivity of 0.40 and using AccuMelt HRM SuperMix fluorescent dye (DNAture). The experiment is based on two technical replicates per sample.

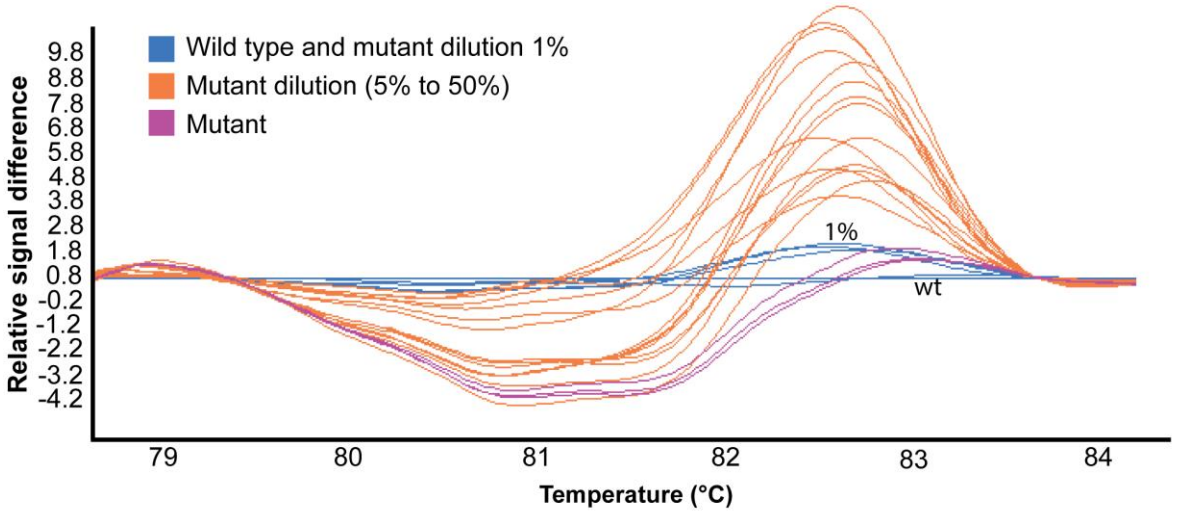

Figure 5-5. qPCR-HRM sensitivity to detect a one base pair deletion in mutant–wild type DNA mixtures. Plot showing normalized and temperature-shifted differences in melting curves between wild type (wt) *trihydroxynaphthalene reductase* (*THN*) DNA samples of *V. inaequalis* wt mixed with mutant *THN* DNA samples to detect the resolution limit of the HRM curve assay. Melting curve groups generated by LightCycler® 480 gene scanning software with a sensitivity of 0.48 and using AccuMelt HRM SuperMix fluorescent dye (DNAture). A minimum of two technical replicates were performed per sample. Wt genomic DNA and mutant THN #66 genomic DNA were diluted in different ratios (mutant:wt): 1:99, 5:95, 10:90, 20:80, 30:70 and 50:50.

4.4. CRISPR-Cas9 editing of the *THN* gene does not alter the phenotype of *V. inaequalis* grown in culture

CRISPR-Cas9-based experiments can sometimes be detrimental to the target organism due to Cas9 toxicity and/or off-target mutations [51], even though CRISPR-Cas9 off-target mutations have been reported to be unlikely in different filamentous fungi [22,23,52]. To test if CRISPR-Cas9-mediated transformation has greatly affected the phenotype of *V. inaequalis* (e.g. through toxicity or off-target effects), we investigated the phenotypes of the wt, three dark-brown transformants (THN #38, THN #53, THN #90) and six light-brown mutants (THN #9, THN#37, THN#60, THN#66, THN#89, THN#96) of *V. inaequalis* on and in cellophane membranes overlaying PDA. During growth in cellophane membranes, *V. inaequalis* undergoes morphological differentiation, similar to that observed under the cuticle *in planta*, where it develops infection structures called runner hyphae and stromata [13]. Therefore, we investigated whether the *THN* mutants maintained their ability to develop runner hyphae and stromata in cellophane membranes after CRISPR-Cas9-mediated transformation (**Figure 5-6**). All mutants showed a similar phenotype to wt, in that they were able to penetrate the cellophane membrane to develop runner hyphae and stromata. Likewise, all mutants maintained their ability to sporulate on the cellophane membrane surface. Taken together, these results suggest that CRISPR-Cas9-mediated transformation has not greatly affected the phenotype of *V. inaequalis*. A more in-depth analysis based on whole genome sequencing is the next step to determine whether this experiment has resulted in any off-target mutations.

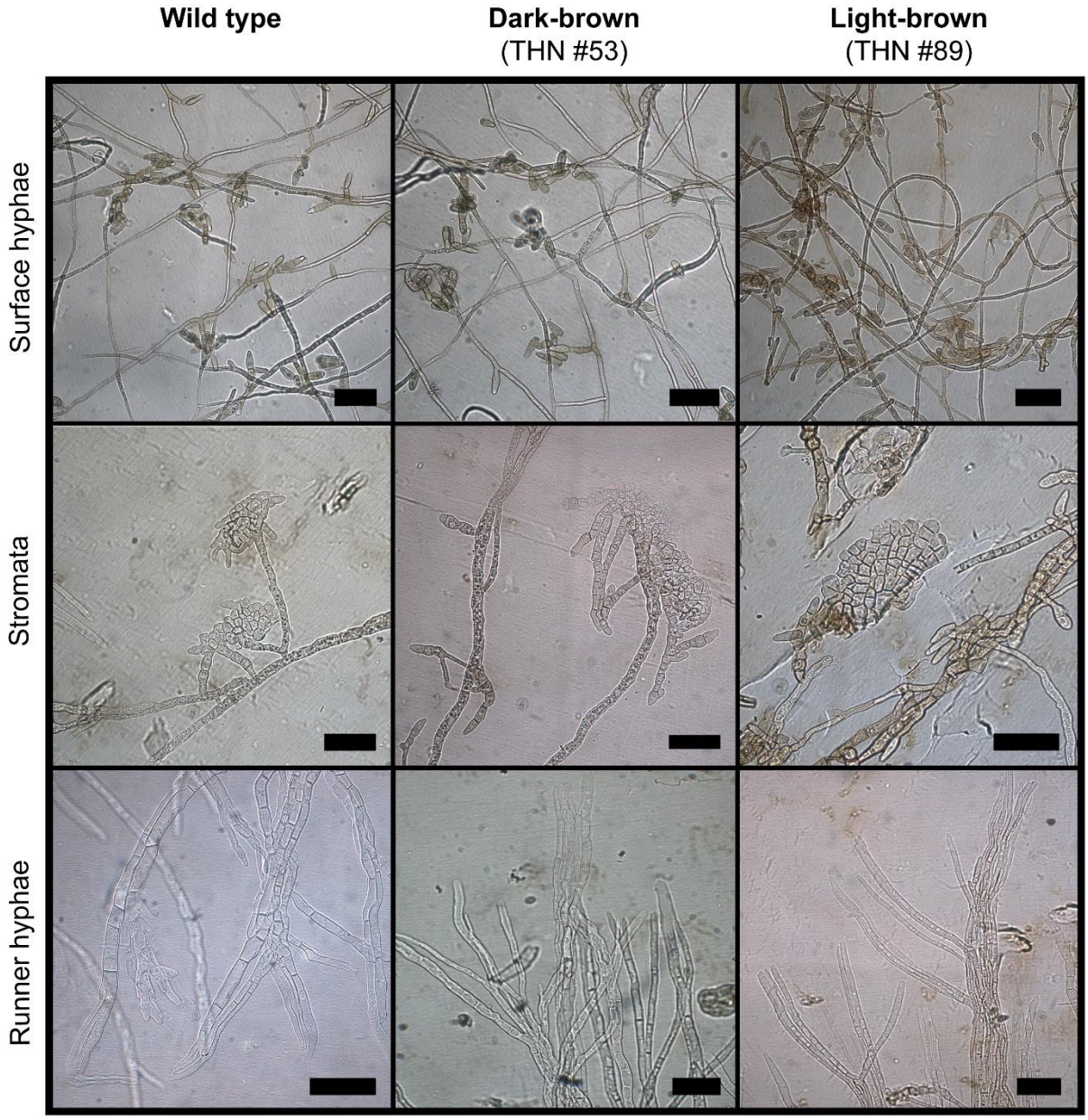

Figure 5-6. In-culture phenotype of wild-type and CRISPR-Cas9 transformants of *Venturia inaequalis* on and in a cellophane membrane. The conidia of each strain were plated on a cellophane membrane overlaying potato-dextrose agar, followed by incubation at 22°C for 10 days. Scale bar 50 µM. Pictures are representative of all *THN* mutants identified.

5. Conclusions

We have successfully applied CRISPR-Cas9 gene editing to the filamentous fungal pathogen, *V. inaequalis*, providing an opportunity for future studies to characterise gene functions associated with the growth, reproduction, virulence and pathogenicity of this fungus. Given that the genomes of several other species from the *Venturia* genus have recently been sequenced [5,53-58], this development will likely be useful for the functional characterization of genes in these species. Notably, genome sequencing has revealed that members of the *Venturia* genus contain large, expanded families of putative effector genes that likely play an important role in host-colonization [5]. As the functional characterization of gene families is often hindered by functional redundancy between family members, and because the sequential deletion of family members using standard homologous recombination is limited by the number of selectable marker genes that are available, our finding that CRISPR-Cas9 technology can be applied to *V. inaequalis* is also expected to greatly facilitate the functional characterization of effector gene families in the *Venturia* genus (i.e. through sequential gene deletion/disruption or simultaneous gene targeting (multiplexing)) [59].

In addition to applying CRISPR-Cas9 gene editing to *V. inaequalis*, we have developed a high-throughput screening protocol based on an HRM curve analysis for the identification of CRISPR-Cas9-generated mutants of this fungus with as little as one bp insertion or deletion. We have observed that this highly sensitive method can detect mutant DNA even when mixed in a 5:95 mutant:wt ratio, making it an excellent method for high-throughput screening, as mutants do not need to be single-spore purified prior to screening. This method will be of great value for the identification of mutants generated by CRISPR-Cas9 technology in different fungal species where the mutation efficiency is low.

Declarations of interest

None.

Funding

MRF and CHM are supported by the Marsden Fund Council from Government funding (project ID 17-MAU-100), managed by Royal Society Te Apārangi. SA and JKB received funding from The New Zealand Institute for Plant and Food Research Limited, Strategic Science Investment Fund, Project number: 12070. DH, JS, RDJ and LJJ are supported by the MBIE partnership programme: Novel variation for a persistent problem (project ID C10X1902). AgResearch work was also supported through a QEII technicians' study award (to JS) and the New Zealand Strategic Science Investment Fund (SSIF) contract A20067.

Author contributions

MR, JKB, KMP, REB, RDJ, LJJ and CHM conceptualization; CHM funding acquisition (Marsden Fund); MR, SA, DH and JS investigation. CHM project administration; JKB, REB and CHM supervision; MR, DH, JKB, KMP, REB, RDJ and CHM roles/writing – original draft; MR, SA, DH, JS, JKB, KMP, REB, RDJ, LJJ and CHM writing – review & editing.

Acknowledgements

We thank Professor Adrian Tsang (Center for Functional and Structural Genomics Biology, Concordia University, Canada) for hosting JS and providing the original CRISPR-Cas9 vectors. We also thank Natasha Forester and Pranav Chettri for useful discussions around vector modification.

6. Appendix A: Supplementary information

This appendix contains all the supplementary information associated with the published manuscript in Fungal Biology.

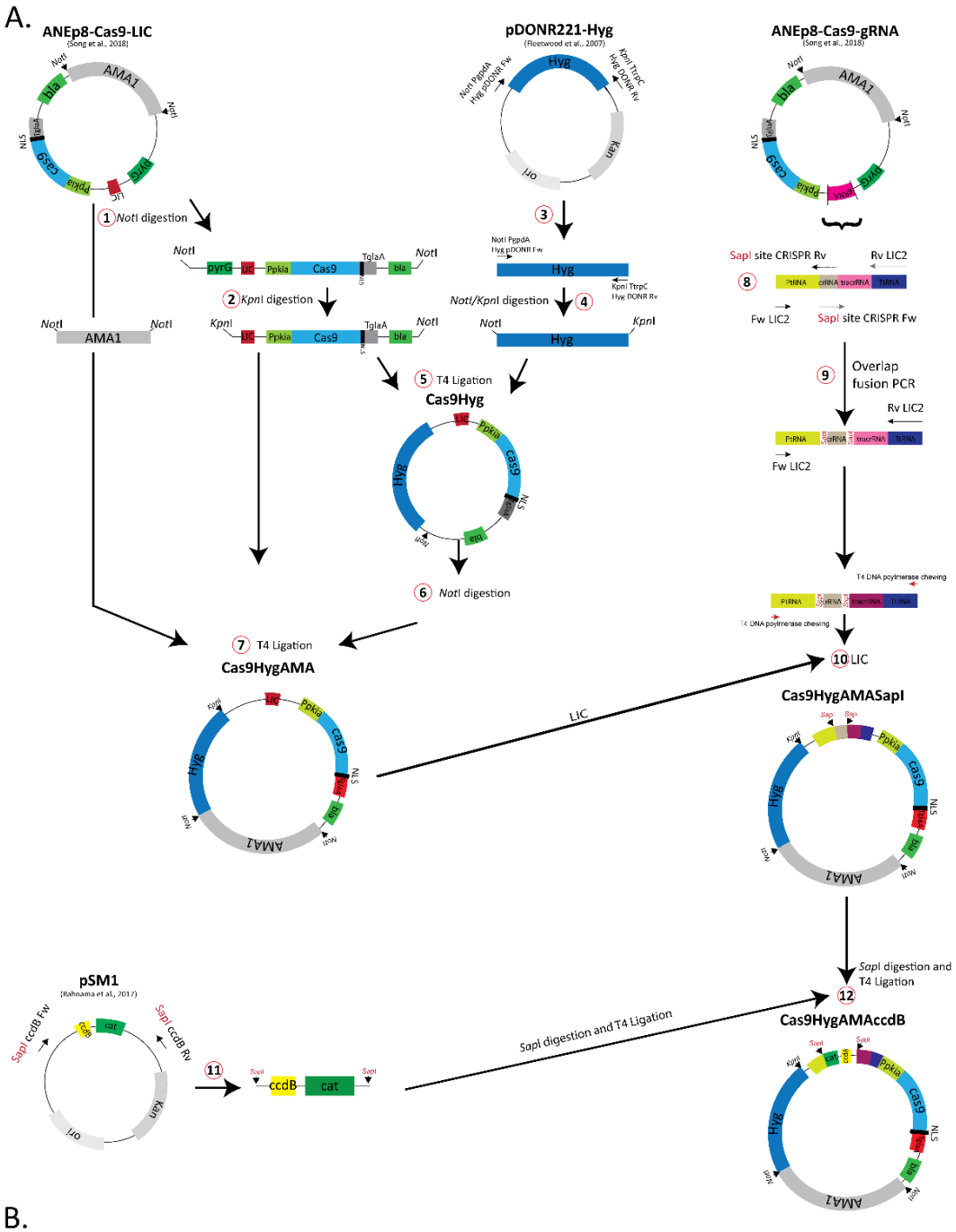
A.
ANEp8-Cas9-LIC
(Song et al., 2018)
pDONR221-Hyg
(Fleetwood et al., 2007)
ANEp8-Cas9-gRNA
(Song et al., 2018)
1 NotI digestion
2 KpnI digestion
3
4 NotI/KpnI digestion
5 T4 Ligation
Cas9Hyg
6 NotI digestion
7 T4 Ligation
Cas9HygAMA
LIC
10 LIC
Cas9HygAMASapI
SapI site CRISPR Rv
Rv LIC2
Fw LIC2
SapI site CRISPR Fw
8
9 Overlap fusion PCR
T4 DNA polymerase chewing
pSM1
(Rahnama et al., 2017)
SapI ccdB Fw
SapI ccdB Rv
11
SapI digestion and T4 Ligation
12
Cas9HygAMAccdB
B.
1)
Primers
MR137: 5' GTCGCCCCATCATGGTCTTTGGA 3'
MR138: 5' AACTCCAAAGACCATGATGGGGC 3'
Primer Annealing
sgRNA
5' GTCGCCCCATCATGGTCTTTGGA 3'
5' CGGGGTAGTACCAGAAACCTCAA 3'
2)
pCas9Hyg AMAccdB
PtRNA
CTCGTCGGAAGAGC .... GCTCTTCAGTTTTA
GAGCAGCCTTCTCG .... CGAGAAGTCAAAAT
tracrRNA
TtRNA
SapI
Golden Gate (SapI)
CTC
GTTTTA
GAGCAG
AAT
GTCGCCCCATCATGGTCTTTGGA
CGGGGTAGTACCAGAAACCTCAA

Figure A 5-1. Flow diagrams illustrating Cas9HygAMAccdB plasmid construction and Golden Gate cloning of the sgRNA. A. Construction of the Cas9HygAMAccdB plasmid. Step 1: the ANEp8-Cas9-LIC plasmid [36] was digested with *Not*I to liberate a 5.3 Kb fragment containing the AMA1 cassette, and a 10.3 Kb fragment containing the *Cas9* and *PyrG* genes; Step 2: the 10.3 Kb fragment containing the *Cas9* and *PyrG* genes from Step 1 was digested with *Kpn*I to liberate a 9 Kb Cas9 cassette containing the *Cas9* gene (i.e. through removal of the *PyrG* gene); Step 3: the 2.9 Kb hygromycin resistance cassette was amplified by PCR from the pDONR221-Hyg plasmid [38] in conjunction with the restriction enzyme-adapted primers *Not*I P*gpdA Hyg* pDONR Fw and *Kpn*I T*trpC Hyg* DONR Rv; Step 4: the PCR amplicon from Step 3 was digested with *Not*I and *Kpn*I; Step 5: the *Not*I/*Kpn*I-digested Cas9 cassette from Step 2 and the *Not*I/*Kpn*I-digested hygromycin resistance cassette from Step 4 were ligated together to create the Cas9Hyg plasmid; Step 6: the Cas9Hyg plasmid from Step 5 was digested with *Not*I; Step 7: the *Not*I-digested Cas9Hyg plasmid from Step 6 and the *Not*I-digested AMA1 cassette from Step 1 were ligated to create the Cas9HygAMA plasmid; Step 8: a fragment containing the tRNA promoter (PtRNA) and mock protospacer (CRISPR RNA; crRNA) sequences was amplified from the ANEp8-Cas9-gRNA plasmid by PCR using the primers Fw LIC2 and *Sap*I site CRISPR Rv. Here, the *Sap*I site CRISPR Rv primer was designed to introduce a *Sap*I restriction site between the tRNA promoter and mock protospacer sequences. At the same time, a second fragment containing the mock protospacer and tRNA terminator (TtRNA) sequences was amplified from the ANEp8-Cas9-gRNA plasmid by PCR using the primers *Sap*I site CRISPR Fw and Rv LIC2 (**Table 5-1**). In this case, the *Sap*I site CRISPR Rv primer was designed to introduce a *Sap*I restriction site between the mock protospacer and tRNA terminator sequences; Step 9: the two PCR amplicons from Step 8 were fused together by overlap PCR using the Fw LIC2 and Rv LIC2 primers; Step 10: the PCR product from Step 9 was inserted into the Cas9HygAMA plasmid from Step 7 through ligation-independent cloning (LIC) via its *Swa*I restriction site [36] to create the Cas9HygAMASapI plasmid; Step 11: a 2 Kb fragment containing the *control of cell death B* (*ccdB*) killer gene and chloramphenicol acetyltransferase (*cat*) resistance gene was amplified by PCR from the pSM1 plasmid [39] using the *Sap*I restriction enzyme-adapted primers *Sap*I *ccdB* F and *Sap*I *ccdB* R; Step 12: the PCR amplicon from Step 11 was digested with *Sap*I and ligated into *Sap*I-digested Cas9HygAMASapI using T4 ligation to create the Cas9HygAMAccdB plasmid. Other abbreviations: *bla*: beta-lactamase gene conferring ampicillin resistance; NLS: Nuclear Localization Signal, Kan: Kanamycin resistance gene; ori: origin of replication; tracrRNA: transactivating crRNA sequence. Black arrowheads depict restriction sites and arrows PCR primer binding sites. Figure not to scale. **B.** Cloning of the sgRNA into the Cas9HygAMAccdB plasmid using a two-step process involving 1) primer-annealing and 2) *Sap*I-dependent Golden Gate assembly. Red line indicates the recognition site of the *Sap*I restriction enzyme, and red triangles indicate the cut site of the *Sap*I restriction enzyme. Yellow and blue boxes show *Sap*I restriction site overhangs.

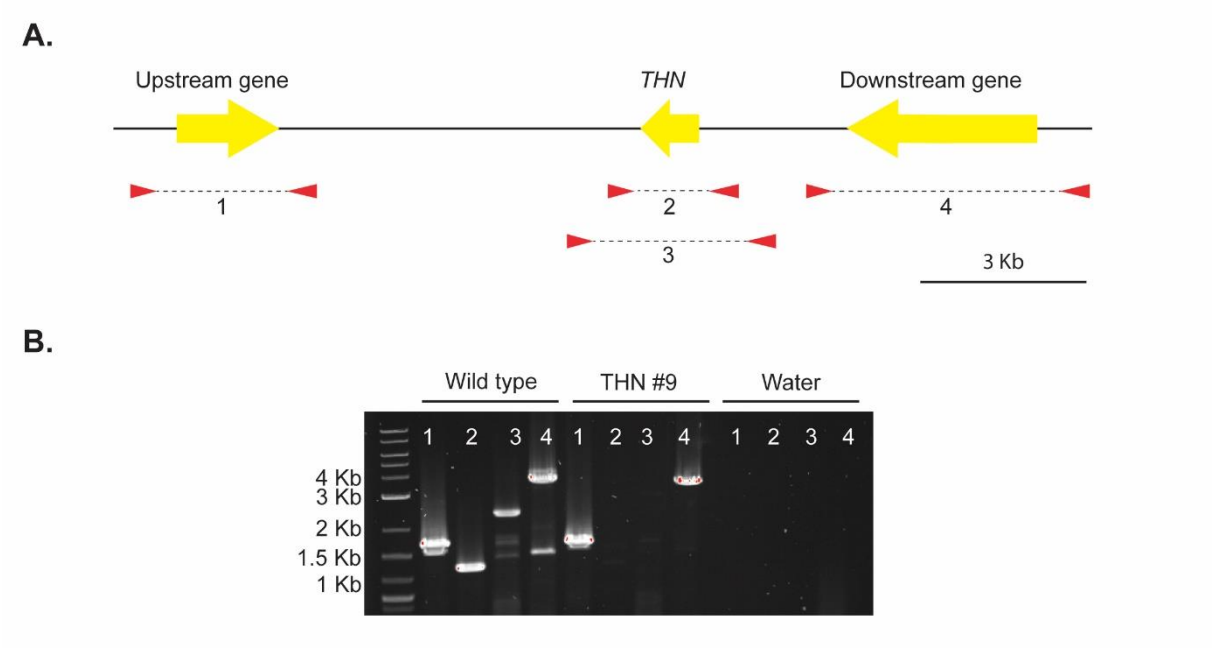

Figure A 5-2. A large deletion event has potentially occurred at the THN locus in mutant THN #9. A. Schematic representation of the *trihydroxynaphthalene reductase* (*THN*) gene locus in the *Venturia inaequalis* MNH120 genome. Arrows: primer binding site, dashed lines: amplicon. **B.** Conventional PCR of *THN* and its neighbouring genes using wild type genomic DNA, *THN* #9 genomic DNA and water as a negative control. PCR amplicons were resolved by electrophoresis on a 1% TBE gel. Marker: 1 Kb plus DNA ladder. 1. MR204-MR205: upstream gene; 2. MR161-MR162: THN; 3. MR184-MR185: THN; 4. MR252-MR253: downstream gene.

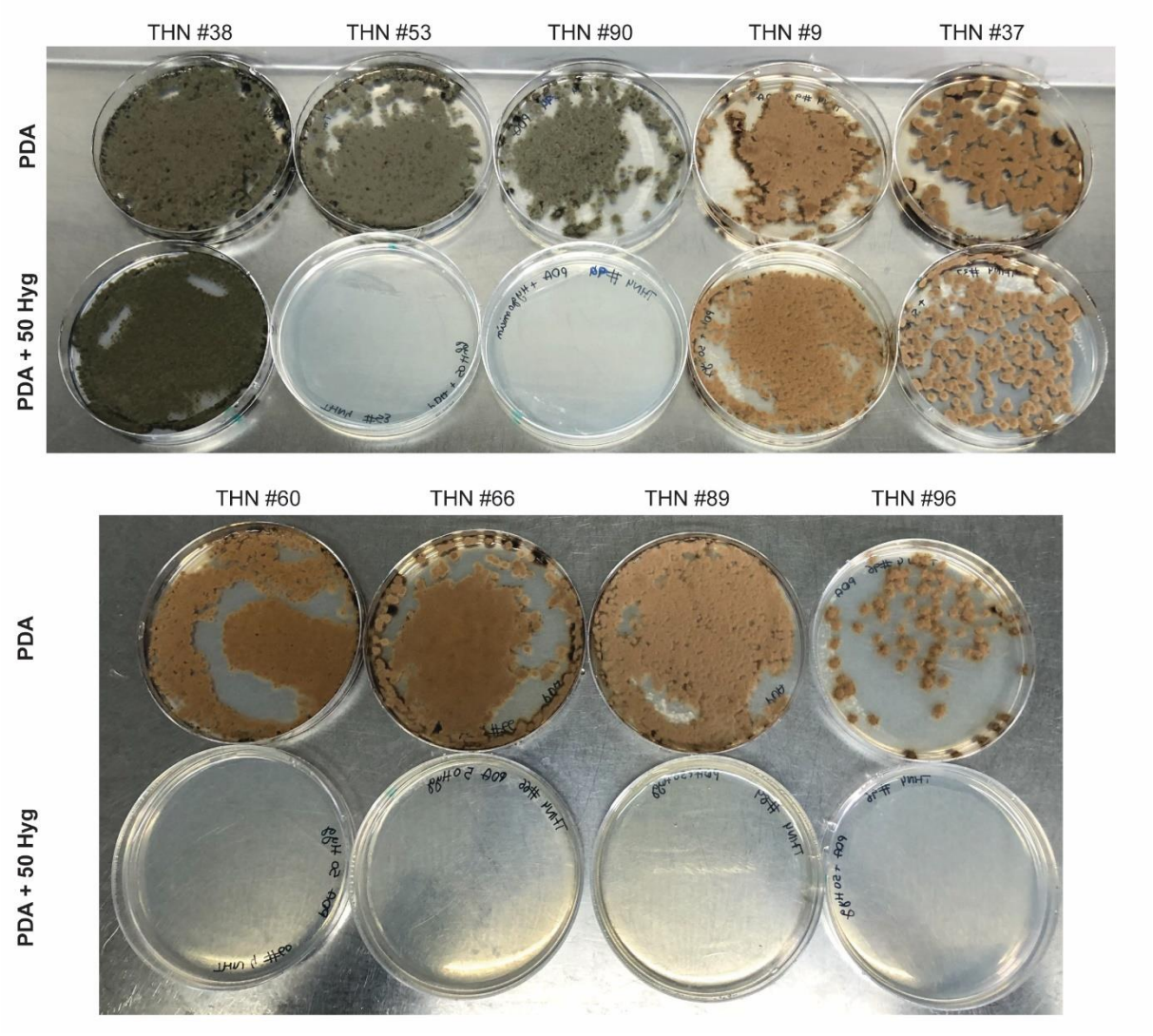

Figure A 5-3. Loss of the autonomously replicating Cas9HygAMA-*sgRNA* plasmid by CRISPR-Cas9 transformants of *Venturia inaequalis*. Conidia of each transformant were plated on a cellophane membrane overlaying potato-dextrose agar (PDA) or a cellophane membrane overlaying PDA supplemented with 50 µg/ml hygromycin B (Hyg), followed by incubation at 22°C for 14 days.

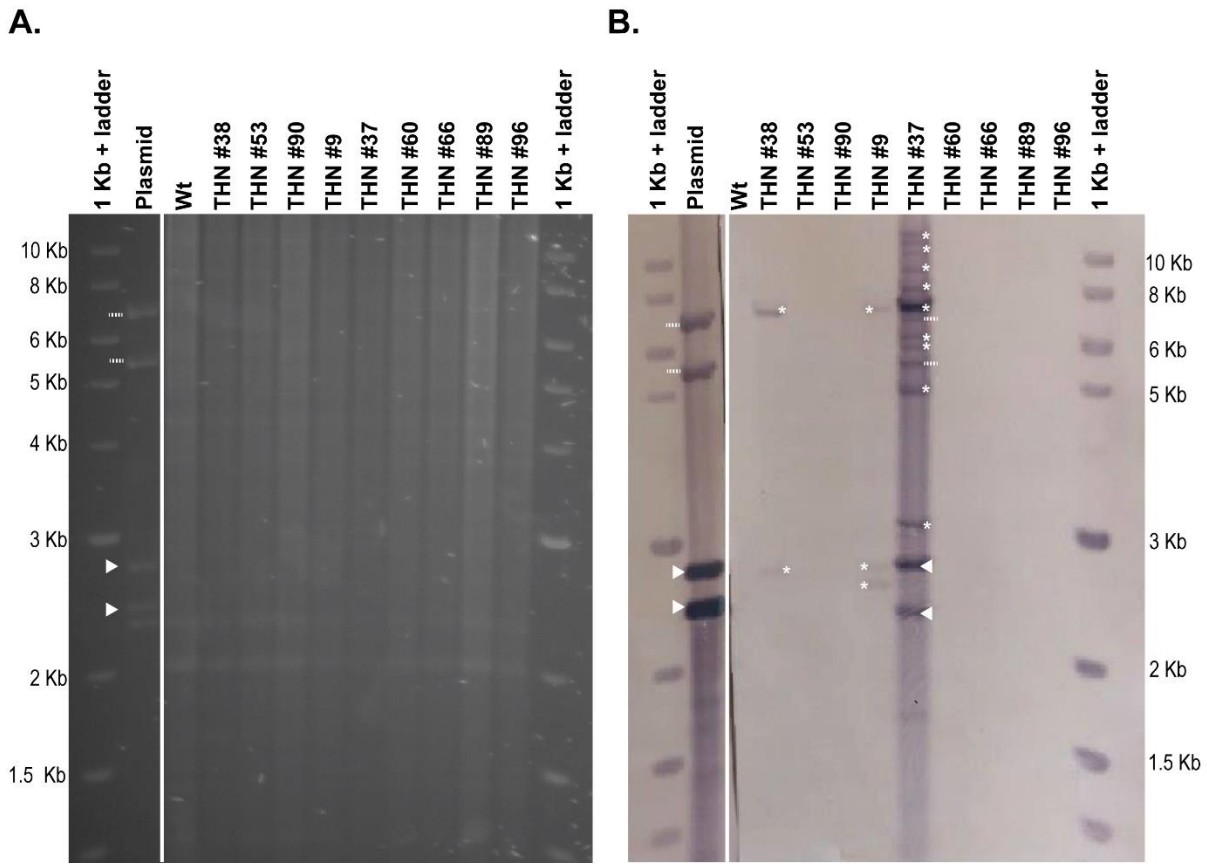

Figure A 5-4. Southern blot analysis of *Venturia inaequalis* CRISPR-Cas9 transformants. **A.** Cas9HygAMA plasmid DNA (50 ng), together with genomic DNA (5 µg) from wild-type *V. inaequalis* (Wt), three transformants of *V. inaequalis* carrying a functional copy of the *THN* gene (THN #38, THN #53 and THN #90), and six mutants of *V. inaequalis* lacking a functional copy of the *THN* gene (THN #9, THN #37, THN #60, THN #66, THN #89 and THN #96), digested with the restriction enzyme *Eco*RI and resolved by 1% TBE gel electrophoresis. Marker: 1 Kb plus DNA ladder. The expected sizes of the five bands following digestion with *Eco*RI are 6,653 bp, 5,310 bp, 2,673 bp, 2,368 bp and 2,281 bp, respectively. **B.** Colorimetric Southern blot based on the gel in A. using a DIG probe specific to the hygromycin resistance cassette in the Cas9HygAMA plasmid. White arrowheads indicate the location of *Eco*RI digestion fragments from the Cas9HygAMA plasmid that are specifically targeted by the probe (2,673 bp and 2,368 bp), while dotted lines indicate the location of *Eco*RI digestion fragments from the Cas9HygAMA plasmid that are not targeted specifically by the probe (6,649 bp and 5,306 bp). These non-specific bands are not present in Wt *V. inaequalis*, and thus do not affect interpretation of the Southern blot. The arrowheads and dotted lines are also shown in A. as a comparison). Asterisks indicate bands derived from the Cas9HygAMA-sgRNA plasmid that have likely integrated to the genome. To enable colorimetric detection of the probe, the section of the blot containing digested Cas9HygAMA plasmid DNA (left side of the vertical white line) was exposed for 3 hours, while the section of the blot containing digested *V. inaequalis* genomic DNA (right side of the vertical white line) was exposed for 9 hours. Marker: 1 Kb plus DNA ladder.

7. Appendix B: Statement of contribution doctorate with publications/manuscripts (DRC16)

We, the candidate and the candidate's Primary Supervisor, certify that all co-authors have consented to their work being included in the thesis and they have accepted the candidate's contribution as indicated below in the *Statement of Originality*.

Name of candidate:	Mercedes Rocafort Ferrer
Name/title of Primary Supervisor:	Carl H. Mesarich
Name of Research Output and full reference:	
CRISPR-Cas9 gene editing and rapid detection of gene-edited mutants using high-resolution melting in the apple scab fungus, *Venturia inaequalis*	
In which Chapter is the Manuscript /Published work:	Chapter 5
Please indicate:	
• The percentage of the manuscript/Published Work that was contributed by the candidate:	70
and	
• Describe the contribution that the candidate has made to the Manuscript/Published Work:	
The candidate performed all experimental work, except for construction of the Cas9HygAMAccdB plasmid. The candidate also designed the high resolution melting analysis for mutant screening and wrote the manuscript draft (which was subsequently edited by co-authors).	
For manuscripts intended for publication please indicate target journal:	
Candidate's Signature:	Mercedes Rocafort Ferrer Firmado digitalmente por Mercedes Rocafort Ferrer Fecha: 2022.09.23 09:28:34 +02'00'
Date:	23/09/2022
Primary Supervisor's Signature:	Carl Mesarich Digitally signed by Carl Mesarich Date: 2022.09.23 19:47:00 +12'00'
Date:	23/09/2022

Chapter 5_ DRC 16 - V3 Online Statement

8. References

1. Le Cam B, Sargent D, Gouzy J, Amselem J, Bellanger M-N, Bouchez O, Brown S, Caffier V, De Gracia M, Debuchy R, et al.: **Population genome sequencing of the scab fungal species *Venturia inaequalis, Venturia pirina, Venturia aucupariae* and *Venturia asperata***. *G3: Genes, Genomes, Genetics* 2019, **9**:2405-2414.
2. González-Domínguez E, Armengol J, Rossi V: **Biology and epidemiology of *Venturia* species affecting fruit crops: a review**. *Frontiers in Plant Science* 2017, **8**.
3. Bowen JK, Mesarich CH, Bus VG, Beresford RM, Plummer KM, Templeton MD: ***Venturia inaequalis*: the causal agent of apple scab**. *Molecular Plant Pathology* 2011, **12**:105-122.
4. Jha G, Thakur K, Thakur P: **The *Venturia* apple pathosystem: pathogenicity mechanisms and plant defense responses**. *Journal of Biomedicine and Biotechnology* 2009, **2009**:680160.
5. Deng CH, Plummer KM, Jones DAB, Mesarich CH, Shiller J, Taranto AP, Robinson AJ, Kastner P, Hall NE, Templeton MD, et al.: **Comparative analysis of the predicted secretomes of Rosaceae scab pathogens *Venturia inaequalis* and *V. pirina* reveals expanded effector families and putative determinants of host range**. *BMC Genomics* 2017, **18**:339.
6. Lichtner FJ, Jurick WM, Ayer KM, Gaskins VL, Villani SM, Cox KD: **A genome resource for several North American *Venturia inaequalis* isolates with multiple fungicide resistance phenotypes**. *Phytopathology* 2020, **110**:544-546.
7. Papp D, Singh J, Gadoury D, Khan A: **New North American isolates of *Venturia inaequalis* can overcome apple scab resistance of *Malus floribunda* 821**. *Plant Disease* 2020, **104**:649-655.
8. Passey TAJ, Armitage AD, Sobczyk MK, Shaw MW, Xu X: **Genomic sequencing indicates non-random mating of *Venturia inaequalis* in a mixed cultivar orchard**. *Plant Pathology* 2020, **69**:669-676.
9. Passey TAJ, Armitage AD, Xu X: **Annotated draft genome sequence of the apple scab pathogen *Venturia inaequalis***. *Microbiology Resource Announcements* 2018, **7**:e01062-01018.
10. Fitzgerald AM, Mudge AM, Gleave AP, Plummer KM: ***Agrobacterium* and PEG-mediated transformation of the phytopathogen *Venturia inaequalis***. *Mycological Research* 2003, **107**:803-810.
11. Bowen JK, Mesarich CH, Rees-George J, Cui W, Fitzgerald A, Win j, Plummer KM, Templeton MD: **Candidate effector gene identification in the ascomycete fungal phytopathogen *Venturia inaequalis* by expressed sequence tag analysis**. *Molecular Plant Pathology* 2009, **10**:431-448.
12. Feurtey A, Guitton E, De Gracia Coquerel M, Duvaux L, Shiller J, Bellanger M-N, Expert P, Sannier M, Caffier V, Giraud T, et al.: **Threat to Asian wild apple trees posed by gene flow from domesticated apple trees and their "pestified" pathogens**. *Molecular Ecology* 2020, **29**:4925-4941.
13. Kucheryava N, Bowen JK, Sutherland PW, Conolly JJ, Mesarich CH, Rikkerink EH, Kemen E, Plummer KM, Hahn M, Templeton MD: **Two novel *Venturia inaequalis* genes induced upon morphogenetic differentiation during infection and *in vitro* growth on cellophane**. *Fungal Genetics and Biology* 2008, **45**:1329-1339.
14. Mesarich CH, Schmitz M, Tremouilhac P, McGillivray DJ, Templeton MD, Dingley AJ: **Structure, dynamics and domain organization of the repeat protein Cin1 from the apple scab fungus**. *Biochimica et Biophysica Acta* 2012, **1824**:1118-1128.

15. Shiller J, Van de Wouw AP, Taranto AP, Bowen JK, Dubois D, Robinson A, Deng CH, Plummer KM: **A large family of *AvrLm6-like* genes in the apple and pear scab pathogens, *Venturia inaequalis* and *Venturia pirina***. *Frontiers in Plant Science* 2015, **6**:980.
16. Fitzgerald A, Van Kan JA, Plummer KM: **Simultaneous silencing of multiple genes in the apple scab fungus, *Venturia inaequalis*, by expression of RNA with chimeric inverted repeats**. *Fungal Genetics and Biology* 2004, **41**:963-971.
17. Nakayashiki H, Nguyen QB: **RNA interference: roles in fungal biology**. *Current Opinion in Microbiology* 2008, **11**:494-502.
18. Salame TM, Ziv C, Hadar Y, Yarden O: **RNAi as a potential tool for biotechnological applications in fungi**. *Applied Microbiology and Biotechnology* 2011, **89**:501-512.
19. Doudna JA, Charpentier E: **The new frontier of genome engineering with CRISPR-Cas9**. *Science* 2014, **346**:1258096.
20. Schuster M, Kahmann R: **CRISPR-Cas9 genome editing approaches in filamentous fungi and oomycetes**. *Fungal Genetics and Biology* 2019, **130**:43-53.
21. Fang Y, Tyler BM: **Efficient disruption and replacement of an effector gene in the oomycete *Phytophthora sojae* using CRISPR/Cas9**. *Molecular Plant Pathology* 2016, **17**:127-139.
22. Foster AJ, Martin-Urdiroz M, Yan X, Wright HS, Soanes DM, Talbot NJ: **CRISPR-Cas9 ribonucleoprotein-mediated co-editing and counterselection in the rice blast fungus**. *Scientific Reports* 2018, **8**:14355.
23. Schuster M, Schweizer G, Reissmann S, Kahmann R: **Genome editing in *Ustilago maydis* using the CRISPR–Cas system**. *Fungal Genetics and Biology* 2016, **89**:3-9.
24. Idnurm A, Urquhart AS, Vummadi DR, Chang S, Van de Wouw AP, López-Ruiz FJ: **Spontaneous and CRISPR/Cas9-induced mutation of the osmosensor histidine kinase of the canola pathogen *Leptosphaeria maculans***. *Fungal Biology and Biotechnology* 2017, **4**:12-12.
25. Krappmann S: **CRISPR-Cas9, the new kid on the block of fungal molecular biology**. *Medical Mycology* 2017, **55**:16-23.
26. Sander JD, Joung JK: **CRISPR-Cas systems for editing, regulating and targeting genomes**. *Nature Biotechnology* 2014, **32**:347-355.
27. Krappmann S: **Gene targeting in filamentous fungi: the benefits of impaired repair**. *Fungal Biology Reviews* 2007, **21**:25-29.
28. Vouillot L, Thélie A, Pollet N: **Comparison of T7E1 and surveyor mismatch cleavage assays to detect mutations triggered by engineered nucleases**. *G3: Genes, Genomes, Genetics* 2015, **5**:407-415.
29. Zhu X, Xu Y, Yu S, Lu L, Ding M, Cheng J, Song G, Gao X, Yao L, Fan D, et al.: **An efficient genotyping method for genome-modified animals and human cells generated with CRISPR/Cas9 system**. *Scientific Reports* 2014, **4**:6420.
30. Denbow CJ, Lapins S, Dietz N, Scherer R, Nimchuk ZL, Okumoto S: **Gateway-compatible CRISPR-Cas9 vectors and a rapid detection by high-resolution melting curve analysis**. *Frontiers in Plant Science* 2017, **8**.
31. Reed GH, Wittwer CT: **Sensitivity and specificity of single-nucleotide polymorphism scanning by high-resolution melting analysis**. *Clinical Chemistry* 2004, **50**:1748-1754.
32. Simko I: **High-resolution DNA melting analysis in plant research**. *Trends in Plant Science* 2016, **21**:528-537.
33. Wittwer CT: **High-resolution DNA melting analysis: advancements and limitations**. *Human Mutation* 2009, **30**:857-859.

34. Dufresne SD, Belloni DR, Wells WA, Tsongalis GJ: ***BRCA1* and *BRCA2* mutation screening using SmartCycler II high-resolution melt curve analysis**. *Archives of Pathology & Laboratory Medicine* 2006, **130**:185-187.
35. Li R, Ba Y, Song Y, Cui J, Zhang X, Zhang D, Yuan Z, Yang L: **Rapid and sensitive screening and identification of CRISPR/Cas9 edited rice plants using quantitative real-time PCR coupled with high resolution melting analysis**. *Food Control* 2020, **112**:107088.
36. Song L, Ouedraogo J-P, Kolbusz M, Nguyen TTM, Tsang A: **Efficient genome editing using tRNA promoter-driven CRISPR/Cas9 gRNA in *Aspergillus niger***. *PLoS one* 2018, **13**:e0202868-e0202868.
37. Stehmann C, Pennycook S, Plummer KM: **Molecular identification of a sexual interloper: The pear pathogen, *Venturia pirina*, has sex on apple**. *Phytopathology* 2001, **91**:633-641.
38. Fleetwood DJ, Scott B, Lane GA, Tanaka A, Johnson RD: **A complex ergovaline gene cluster in Epichloë endophytes of grasses**. *Applied and Environmental Microbiology* 2007, **73**:2571.
39. Rahnama M, Forester N, Ariyawansa KGSU, Voisey CR, Johnson LJ, Johnson RD, Fleetwood DJ: **Efficient targeted mutagenesis in *Epichloë festucae* using a split marker system**. *Journal of Microbiological Methods* 2017, **134**:62-65.
40. Kearse M, Moir R, Wilson A, Stones-Havas S, Cheung M, Sturrock S, Buxton S, Cooper A, Markowitz S, Duran C, et al.: **Geneious Basic: an integrated and extendable desktop software platform for the organization and analysis of sequence data**. *Bioinformatics* 2012, **28**:1647-1649.
41. Aleksenko A, Clutterbuck AJ: **Autonomous plasmid replication in *Aspergillus nidulans*: AMA1 and MATE Elements**. *Fungal Genetics and Biology* 1997, **21**:373-387.
42. Nødvig CS, Nielsen JB, Kogle ME, Mortensen UH: **A CRISPR-Cas9 system for genetic engineering of filamentous fungi**. *PLoS ONE* 2015, **10**:e0133085.
43. Doench JG, Hartenian E, Graham DB, Tothova Z, Hegde M, Smith I, Sullender M, Ebert BL, Xavier RJ, Root DE: **Rational design of highly active sgRNAs for CRISPR-Cas9–mediated gene inactivation**. *Nature Biotechnology* 2014, **32**:1262-1267.
44. Hamada W, Reignault P, Bompeix G, Boccara M: **Transformation of *Botrytis cinerea* with the hygromycin B resistance gene, *hph***. *Current Genetics* 1994, **26**:251-255.
45. Sánchez-Torres P, González R, Pérez-González JA, González-Candelas L, Ramón D: **Development of a transformation system for *Trichoderma longibrachiatum* and its use for constructing multicopy transformants for the *egl1* gene**. *Applied Microbiology and Biotechnology* 1994, **41**:440-446.
46. DiCarlo JE, Norville JE, Mali P, Rios X, Aach J, Church GM: **Genome engineering in *Saccharomyces cerevisiae* using CRISPR-Cas systems**. *Nucleic Acids Research* 2013, **41**:4336-4343.
47. Khan H, McDonald MC, Williams SJ, Solomon PS: **Assessing the efficacy of CRISPR/Cas9 genome editing in the wheat pathogen *Parastagonspora nodorum***. *Fungal Biology and Biotechnology* 2020, **7**:4.
48. Shi TQ, Liu GN, Ji RY, Shi K, Song P, Ren LJ, Huang H, Ji XJ: **CRISPR/Cas9-based genome editing of the filamentous fungi: the state of the art**. *Applied Microbiology and Biotechnology* 2017, **101**:7435-7443.
49. Nødvig CS, Hoof JB, Kogle ME, Jarczynska ZD, Lehmbeck J, Klitgaard DK, Mortensen UH: **Efficient oligo nucleotide mediated CRISPR-Cas9 gene editing in Aspergilli**. *Fungal Genetics and Biology* 2018, **115**:78-89.

50. Słomka M, Sobalska-Kwapis M, Wachulec M, Bartosz G, Strapagiel D: **High Resolution Melting (HRM) for high-throughput genotyping—Limitations and caveats in practical case studies**. *International Journal of Molecular Sciences* 2017, **18**:2316.
51. Morgens DW, Wainberg M, Boyle EA, Ursu O, Araya CL, Tsui CK, Haney MS, Hess GT, Han K, Jeng EE, et al.: **Genome-scale measurement of off-target activity using Cas9 toxicity in high-throughput screens**. *Nature Communications* 2017, **8**:15178.
52. Al Abdallah Q, Souza ACO, Martin-Vicente A, Ge W, Fortwendel JR: **Whole-genome sequencing reveals highly specific gene targeting by *in vitro* assembled Cas9-ribonucleoprotein complexes in *Aspergillus fumigatus***. *Fungal Biology and Biotechnology* 2018, **5**:11.
53. Chen C, Bock CH, Wood BW: **Draft genome sequence of *Venturia carpophila*, the causal agent of peach scab**. *Standards in genomic sciences* 2017, **12**:68-68.
54. Cooke IR, Jones D, Bowen JK, Deng C, Faou P, Hall NE, Jayachandran V, Liem M, Taranto AP, Plummer KM, et al.: **Proteogenomic analysis of the *Venturia pirina* (Pear scab fungus) secretome reveals potential effectors**. *Joutnal of Proteome Research* 2014, **13**:3635-3644.
55. Jaber MY, Bao J, Gao X, Zhang L, He D, Wang X, Wang A, Wang Z, Wang B: **Genome sequence of *Venturia oleaginea*, the causal agent of olive leaf scab**. *Molecular Plant-Microbe Interactions* 2020, **33**:1095-1097.
56. Johnson S, Jones D, Thrimawithana AH, Deng CH, Bowen JK, Mesarich CH, Ishii H, Won K, Bus VGM, Plummer KM: **Whole genome sequence resource of the Asian pear scab pathogen *Venturia nashicola***. *Molecular Plant-Microbe Interactions* 2019, **32**:1463-1467.
57. Prokchorchik M, Won K, Lee Y, Choi ED, Segonzac C, Sohn KH: **High contiguity whole genome sequence and gene annotation resource for two *Venturia nashicola* isolates**. *Molecular Plant-Microbe Interactions* 2019, **32**:1091-1094.
58. Winter DJ, Charlton ND, Krom N, Shiller J, Bock CH, Cox MP, Young CA: **Chromosome-level reference genome of *Venturia effusa*, causative agent of pecan scab**. *Molecular Plant-Microbe Interactions* 2020, **33**:149-152.
59. Schuster M, Schweizer G, Kahmann R: **Comparative analyses of secreted proteins in plant pathogenic smut fungi and related basidiomycetes**. *Fungal Genetics and Biology* 2018, **112**:21-30.

Chapter 6:

General discussion

1. Introduction

Each year, plant pathogens collectively result in up to 30% of the world's crop yield being lost to disease and are therefore considered one of the biggest threats to food security [1,2]. Among these, subcuticular pathogens are a largely understudied group that colonize the subcuticular environment of host plants. A key feature of these pathogens is their ability to develop visibly similar infection structures, called runner hyphae and stromata, that appear to be specialized for subcuticular host-colonization. However, these infection structures have never been studied in detail, and their role in the infection process remains elusive. *Venturia inaequalis* is a model species for studying the process of morphological differentiation during subcuticular host-colonization as this pathogen produces infection-like structures inside cellophane membranes during growth in culture [3].

Even though *V. inaequalis* is a model pathogen for both the *Venturia* genus and the study of subcuticular host-colonization, the reality is that our understanding of the *V. inaequalis*–apple (*Malus*) pathosystem, particularly at the molecular level, is still in its infancy [4-6]. Research on the *V. inaequalis–Malus* pathosystem has progressed slowly due to the nature of the host, as apple is a perennial crop that takes several years to grow. Additionally, *V. inaequalis* is a slow-growing fungal species that is not easily amenable to genetic manipulation, with no gene deletions or disruptions published at the time of starting this thesis. This is despite the fact that protocols for the genetic transformation and manipulation of this fungus have been developed [7,8].

A large gap in our understanding centres around which secreted proteins of *V. inaequalis* are required to promote host-colonization (virulence effectors) or trigger host resistance (avirulence [*Avr*] effectors). Indeed, while previous efforts have been made to identify and characterize effector candidates (ECs) of this fungus [3,9-11], the specific virulence functions of these ECs have not yet been elucidated. Furthermore, no *Avr* effector genes have been published.

However, progress on this front is being made and the *AvrRvi4* and *AvrRvi6 Avr* effector genes of *V. inaequalis* have likely been identified recently (Silvia de la Rosa et al., in preparation; Bruno Le Cam et al., in preparation). The presumed identification of *AvrRvi4* was facilitated through the ease by which *V. inaequalis* isolates can be sexually crossed in culture, which enables genetic dissection of traits.

Given the need to develop novel, durable control strategies against scab, further research on the *V. inaequalis–Malus* pathosystem at the molecular level is desperately needed. In particular, information on *V. inaequalis* effectors and the morphogenesis of infection structures by this fungus is required to help identify targets for control strategies. In addition, as knowledge about subcuticular host-colonization is scarce, it is hoped that any information gained on the infection structures and biology of *V. inaequalis* can be extrapolated to other subcuticular pathogens with the goal of informing disease control programs involving these species.

2. Chapter 2: Apoplastic effector proteins of plant-associated fungi and oomycetes

This chapter represents the most up-to-date review of apoplastic effector proteins from plant-associated fungi and oomycetes performed until the time of its publication. First, in this review, I defined the plant apoplastic environment as a continuum of all spaces and matrices from the plasma membrane to the rhizoplane and cuticle. Next, I highlighted the great diversity of apoplastic environments occupied by plant-associated fungi and oomycetes through the creation of a figure that is the most comprehensive of its kind presented to date. This figure accentuates the complexity of infection lifestyles associated with the apoplast, such as the subcuticular lifestyle used by *V. inaequalis*, which is often overlooked in the literature.

Next, the review described the various functions of apoplastic effector proteins, highlighting that most of those functionally characterized to date are associated with the evasion of glycan-triggered immunity. This is not surprising given that the host apoplast is a hostile environment rich in glucanases and chitinases [12]. Indeed, I suggest that to colonize the subcuticular environment, a large portion of the apoplastic effector protein repertoire in *V. inaequalis* is likely involved in evading glycan-triggered immunity. These effectors can be non-enzymatic proteins (**Chapter 3**) or enzymatic proteins that chemically modify the fungal cell wall to facilitate the morphogenesis and maintenance of infection structures (**Chapter 4**). In general, it is expected that, given the extracellular nature of host-colonization by *V. inaequalis*, many effector proteins secreted by this pathogen perform their functions in the apoplastic environment. However, this does not exclude the possibility that a subset of the effector proteins from *V. inaequalis* function inside host cells, especially given that an intracellular nucleotide-binding domain and leucine-rich repeat (NLR)-type resistance (R) protein against scab has been identified [13].

Finally, I propose that the majority of apoplastic effector proteins functionally characterized to date are associated with glycan-triggered immunity because of the ease by which

these proteins are identified. As described in the review, these effectors usually possess carbohydrate-binding domains, such as the well-studied carbohydrate-binding module family 50 (CBM50)/lysin motif (LysM) originally identified in the Ecp6 effector from the tomato leaf mould fungus *Fulvia fulva* [14,15]. Therefore, mining the genome for carbohydrate-binding domains can quickly facilitate the identification of ECs potentially associated with evading glycan-triggered immunity. Determining the function of apoplastic ECs without carbohydrate-binding domains is not necessarily as straightforward, as these ECs do not usually display an annotated domain or sequence similarity to other proteins. Later, in Chapter 3, I describe a new effector prediction pipeline that could help identify ECs with novel functions beyond evasion of glycan-triggered immunity.

3. Chapter 3: The *Venturia inaequalis* effector repertoire is expressed in waves and is dominated by expanded families with predicted structural similarity to avirulence proteins from other plant-pathogenic fungi

Chapter 3 describes the first comprehensive transcriptome analysis of *V. inaequalis* infecting a susceptible apple host. This chapter aimed to investigate the general biology associated with subcuticular growth (**Chapter 3: Appendix B)** and to generate an enriched list of *V. inaequalis* ECs encoded by genes that are up-regulated during host infection (**Chapter 3**). Over the past few years, many studies have performed transcriptome analysises on plant pathogens to investigate their biology and infection strategies [16-18]. Prior to this thesis, only two gene expression studies of *V. inaequalis* infecting susceptible apple had been published [10,19]. However, these studies were based on a limited number of infection time points with no biological replicates and, thus, were not comprehensive.

3.1. Unravelling the nutritional strategy of a subcuticular pathogen

Little is known about how subcuticular plant-pathogenic fungi acquire nutrients from the subcuticular environment, in which nutrients are scarce [20]. Thus, the first part of the study (**Chapter 3: Appendix B**) focused on unravelling the nutritional strategy of *V. inaequalis* during subcuticular host-colonization. Notably, it had previously been hypothesised that the stromata of *V. inaequalis* are involved in nutrient acquisition during colonization of the subcuticular host environment [21]. In line with this, during the development and expansion of stromata, several genes encoding nutritional transporters were found to peak in expression. In future research, laser microdissection could be used to generate an infection structure-specific transcriptome [22-24], which could help confirm the link between nutrient transporters and the presence of stromata. The use of laser microdissection represents some challenges, mostly in terms of sample preparation, as fungal tissue needs to be effectively separated from plant tissue and in sufficient quantities for RNA extraction [24]. However, this promising technique has been successfully used to study the transcriptome of other infection structures generated by plant pathogens [25,26] and arbuscular mycorrhizal fungi [27]. If a link can be established between nutrient transporters and the presence of stromata, the next step would be to investigate the infection structures of other subcuticular pathogens to assess if these structures display a conserved function for colonization of the subcuticular environment.

In addition to the nutrient transporters, I observed that *V. inaequalis* expresses genes encoding a collection of plant cell wall-degrading enzymes (PCWDEs), especially polygalacturonases that use pectin as a substrate. Therefore, to acquire nutrients for degradation and uptake, *V. inaequalis* may nibble away at the underlying plant cell walls, without killing them, to obtain nutrients during biotrophic infection of apple tissue. The expression and secretion of PCWDEs are generally limited in biotrophic pathogens, when compared with necrotrophic

pathogens that have a more aggressive lifestyle [28,29]. For example, only one polygalacturonase enzyme was observed to be produced by the corn smut fungus *Ustilago maydis* [30] and two by the ergot fungus *Claviceps purpurea* during biotrophic host-colonization [31]. Indeed, the expression of PCWDEs is tightly regulated by biotrophic pathogens, as some PCWDEs, such as polygalacturonases, are well-known elicitors of plant defence [29]. Additionally, degradation of the plant cell wall causes the release of damage-associated molecular patterns (DAMPs) that trigger plant defences by plant cell-surface immune receptors, slowing or halting pathogen infection [29,32,33]. At the same time, as part of the plant defence response, plants produce polygalacturonase inhibitors that stop pathogen infection by hampering pathogen nutrition and promoting the accumulation of DAMPs [33-35]. Therefore, as a counterattack, pathogens secrete effectors to avoid and inhibit plant defences [36,37]. For example, plant-pathogenic fungi might produce effectors that suppress these polygalacturonase inhibitors to promote virulence, as observed recently in the white mould fungus, *Sclerotinia sclerotiorum* [38]. Certainly, in *V. inaequalis*, the expression of PCWDEs is correlated with the peak of expression of most *EC* genes, indicating that to successfully colonize the host while maintaining biotrophy, *V. inaequalis* must deploy a large repertoire of ECs.

3.2. Effector families: an evolutionary playground for effector diversification

V. inaequalis deploys an extensive catalogue of non-enzymatic proteinaceous ECs during infection to facilitate host-colonization (**Chapter 3**). Effectors perform specialized functions during infection and, consequently, the expression of the genes that encode them is tightly regulated during different infection stages and tissues [39]. Indeed, in this study, I determined that *V. inaequalis* expressed *EC* genes in two waves: the early and mid-late *EC* waves. Therefore, this study adds to the growing evidence that effectors are tightly regulated at the transcriptional level.

Remarkably, only a small subset of *EC* genes demonstrated a peak level of expression during early infection, with most *EC* genes found to peak during the mid-late infection stage. This observation was surprising as several biotrophic pathogens have been reported to express a large portion of effectors during early infection [17,40]. This delay in *EC* gene expression highlights the differences in lifestyle of subcuticular pathogens compared with other well-known inter- or intracellular species. I hypothesize that, during early infection, *V. inaequalis* might be restricted to the upper surface of the subcuticular environment and remain largely undetected by the plant immune system until later, when *V. inaequalis* is in close contact with the underlying epidermal cells. Given the lack of transcriptional studies in other subcuticular pathogens, it is unknown if this delay in *EC* gene expression is common among species with this lifestyle. However, this hypothesis might be supported by the observation that many necrotrophic pathogens have a quiescent subcuticular stage, indicating that pathogens can remain undetected in this environment [41].

Interestingly, I also observed that most *EC* genes expressed during mid-late infection belonged to expanded EC families of five or more members. Indeed, as previously reported by Deng et al. [10], many *V. inaequalis* ECs share amino acid similarity and can be grouped into families. Expansion of EC families has been observed in other plant pathogens, such as the powdery mildew fungus *Blumeria graminis* [42,43] and *U. maydis* [44]. This expansion has been suggested to be promoted by gene duplications followed by diversification of the new gene copy towards a novel or altered function [39,45,46]. In many plant pathogens, EC families display a rapid turn-over rate and are close to transposable elements (TEs), which have been proposed to promote genome plasticity to accelerate the evolution of TE-rich genomic compartments [43,45,47-49].

Previous research in *V. inaequalis* determined that many *EC* gene family members were close to TEs and, therefore, TEs could be promoting *EC* family expansion [10,50]. In this study, I observed that in some cases, *EC* genes clustered together in the genome, suggesting that they were created by recent duplication events. Indeed, TEs can induce duplication of genomic material and chromosomal arrangements [47,49]. Additionally, TEs can promote genetic diversification by the induction of repeat-induced mutations (RIPs). RIPs are a type of premeiotic mutation that only occur during sexual reproduction. These mutations target TEs but sometimes they can spread into neighbouring genes [51,52]. Remarkably, RIPs were observed to drive the evolution of effectors towards virulence in the stem canker pathogen, *Leptosphaeria maculans* [53]. Given that *V. inaequalis* has an overwintering sexual stage, and *EC* genes are near TEs, it could be expected that RIP is a mechanism driving EC family diversification. However, even though evidence of RIP was identified in the *V. inaequalis* genome, these mutations did not overlap with TEs near *EC* genes [50], suggesting that RIP is not the main mechanism driving *EC* diversification in this pathogen. Altogether, this thesis has added to the knowledge of *EC* family creation and expansion in plant pathogens. However, deeper analysis to understand the genomic arrangements of these *EC* gene family members in *V. inaequalis* was not possible, as the genome available at the time of this study was largely fragmented. Therefore, future research is now needed to investigate the evolution of *EC* gene families in *V. inaequalis*. once a chromosome-level genome is available.

The EC family expansion in *V. inaequalis* is hypothesized to be the result of selection pressure by the plant immune system [10], as it might facilitate the circumvention of R protein-mediated defence or the improved suppression of host defences. An example of the former could involve, for example, an effector that is directly recognized by a cognate immune receptor. Under this scenario, if the recognized effector belongs to an expanded family of functionally redundant virulence factors, the recognised effector can potentially be lost without an associated

fitness cost to the pathogen. This is because other members of the family, which have diverged enough in sequence to not be recognized directly by the R protein, can step in to perform the virulence role vacated by the lost effector. EC families might also facilitate the evasion of R protein-mediated plant immunity by being tightly transcriptionally regulated. In this thesis, I observed that among an *EC* family, usually only one or a couple of family members were highly expressed while the others remained transcriptionally silent during the *in planta* time points investigated. Indeed, one reported strategy to avoid recognition by the plant immune system is for pathogens to silence the gene encoding a recognized *Avr* effector [54,55]. Therefore, I speculate that some *V. inaequalis* family members could be repressed in specific conditions or tissues to avoid recognition by an apple R protein. Additionally, some *EC* genes might be transcriptionally inactive as these gene copies are in the process of pseudogenization. Finally, in terms of improved suppression of host defences, one possibility could be that members of a given expanded EC family have evolved to target similar or overlapping host targets. For example, different members of an EC family could target different members of a specific pathogenesis-related (PR) protein family to suppress plant defences.

3.2.1. Exploring protein folds to understand effector evolution

Given the strong evolutionary pressure on effectors to diversify their sequence, studying their evolution and function can be difficult, as amino acid similarity to other proteins can be rapidly lost. However, as tertiary structures are usually more conserved than amino acid sequences [56], the tertiary folds that these effector proteins adopt can also be used to provide insights into their function and evolution.

In this study, I took advantage of recent advances in *de novo* protein folding algorithms to predict the tertiary structures of all *V. inaequalis* ECs that were up-regulated during host-colonization. Strikingly, this analysis, which was based on the AlphaFold2 algorithm [57],

revealed that many sequence-unrelated *V. inaequalis* ECs had predicted tertiary structures that were similar to Avr effectors from other phytopathogens, including members of the MAX, LARS, ToxA, and FOLD structural effector families.

The observation that many sequence-unrelated ECs share a conserved fold suggests that these effectors have evolved from a conserved ancestral protein [58]. This scenario is consistent with the divergent evolution hypothesis. Here, rapid effector diversification causes the loss of amino acid similarity to the point that only the amino acids required for the overall structure are conserved [58]. In this study, I observed that some sequence-unrelated *V. inaequalis* ECs from the MAX-like and FOLD-like structural families had conserved structural cysteines. In these cases, I hypothesize that these families might be the result of divergent evolution. In contrast, *V. inaequalis* ECs from the LARS-like structural family had the overall conserved fold typical of LARS proteins, but lacked the previously reported conserved cysteines as well as the published LARS motif [59]. Therefore, in this case, I speculate that the LARS-like proteins of *V. inaequalis* could be the result of convergent evolution.

The research in this thesis, together with recent effectorome-level structural studies on the rice blast fungus *Magnaporthe oryzae*, the wilt fungus *Fusarium oxysporum* and other fungi [58-62] is starting to unravel the evolution of fungal effector proteins. However, these studies are still in their infancy and more sampling of species is required. A recent large-scale structural study by Seong & Krasileva et al. [62] explored the protein structures of the secretome from different fungi and reported that the MAX-like fold was almost exclusively found in *M. oryzae*. However, in this thesis, I reported an extreme expansion of this fold in *V. inaequalis*, highlighting the need for an increased sampling of species to understand the evolution of these proteins. Additionally, more sampling is needed to determine if some protein structures are overrepresented in fungi with specific lifestyles, such as those known to be non-pathogenic. Interestingly, the Seong & Krasileva

et al. [62] study reported that some effectors structural folds can be found in non-pathogenic fungal species [62]. However, this is not surprising, as it is currently known that effector proteins are used by all microbes independent of their lifestyle to establish and protect their niche [63]. Finally, another future interesting line of research could be to generate structural predictions of ECs from different subcuticular pathogens. Such an analysis could enable the identification of a core subcuticular effectorome that is not obvious at the amino acid level.

3.2.2. Exploring protein folds to understand effector functions

3.2.2.1. Effectors with a putative role in the manipulation of the host microbiome

In this study, I determined that the most common fold among *V. inaequalis* ECs was a killer protein 6 (KP6)-like fold, similar to that adopted by the antifungal KP6 protein of an *U. maydis* virus [64,65]. Notably, this fold is known or predicted to be adopted by the EC Zt-KP6-1 from the Septoria tritici blotch fungus *Zymoseptoria tritici* [66], two ECs from *F. fulva* [67], and a necrosis-inducing effector from the Cercospora leaf spot fungus *Cercospora beticola* [68]. In this thesis, I hypothesized that proteins with this fold might display toxic activities against microbes. Additionally, in this study, I reported for the first time that the KP6-like fold might be an additional conserved structural fold shared among fungal effectors. In line with this, a recent large-scale structural study showed that this fold was predicted to be adopted by a number of fungal ECs [60,62]. Surprisingly, the same study also reported that this fold was not predicted in the secreted proteins of non-phytopathogenic fungal species. The exclusive distribution of the KP6-like fold in plant-pathogenic species of fungi raises an interesting question: do these proteins solely function in microbial antagonism, or do they also have other roles? I believe that other functions are likely, as effectors with antimicrobial properties are expected to be shared among species with different lifestyles [63,69]. The above-mentioned fold distribution could suggest that these KP6-like

proteins also play a specialized role during the interaction with the plant, instead of manipulating microbial interactions in the environment. Nevertheless, increased sampling of species needs to be performed to develop any conclusions about the distribution of the fold. Additionally, future studies to experimentally validate and functionally characterize these proteins are needed. The starting point could be the expression of these ECs in a non-host system such as *Nicotiana benthamiana* to screen for those with cytotoxic activities, as reported for the KP6-like effector in *C. beticola* [68], and to perform *in vitro* antimicrobial assays using purified protein.

Additionally, I identified other ECs with crambin- or defensin-like structural folds, which are typically shared among proteins with antimicrobial activity [70]. Therefore, it is likely that a considerable proportion of the ECs from *V. inaequalis* are dedicated to antagonistic fungus–microbe interactions to ward off microbial competitors. A future line of research could focus on investigating the function of these ECs shortlisted for their putative antimicrobial role. However, it is important to note that many cysteine-rich effectors are likely to adopt toxin or defensin-like folds due to the stability that this fold provides in the hostile host environments [63]. Therefore, not all proteins with structural analogy to antimicrobial proteins will be associated with microbiota manipulation [63]. Arguably, a strategy to further prioritize ECs with putative antimicrobial activity for further study would be the study their gene expression profiles, as their expression might be distinct from effectors associated with the establishment of biotrophy [69].

After biotrophic host-colonization, *V. inaequalis* grows as a saprotroph in the leaf litter on the soil surface under apple trees, which is a hotspot for microbial diversity [71]. Once apple leaves decay and the plant immune defences dissipate, microbial competition is likely to increase as opportunistic saprophytic microbes emerge [63]. The colonization of leaf litter is crucial for *V. inaequalis* infection, as this stage is key to the production of sexual ascospores that act as primary inoculum for the following season. Therefore, it is expected that during late

infection, while transitioning from biotrophy to saprotrophy, *V. inaequalis* deploys a collection of effector proteins that manipulate the host microbiome. I suggest that ECs with late expression during infection should be prioritized for future studies for their putative antimicrobial activity. This is in line with the proposed hypothesis in Chapter 3, that cyclic ribosomally-synthesized and post-translationally modified peptides (RiPPs) called dikaritins might be associated with microbial competition, as genes encoding these peptides were observed to be mostly expressed during late infection.

3.2.2.2. Structurally conserved effectors: can we really infer function from structure?

The motivation behind the structural prediction of ECs is usually to shed light on their function. Indeed, in many cases, structural analogy to other proteins can provide key clues about their putative role during infection, as discussed in the section above. However, in this study, I reported that many ECs of *V. inaequalis* display a conserved fold which raises questions about the origin of such structural conservation. Recent studies have shown that effectors with conserved structural folds, such as members of the ToxA family, target different host proteins and perform different functions [72-75], suggesting that some protein folds may not have a conserved function and their protein structure simply provides a stable scaffold during plant–microbe interactions. Therefore, the prediction of effector tertiary structures does not always provide as much functional information as it might be expected. In these cases, this structural scaffold might acquire novel functions by changing surface properties or by developing loop features that can be altered to enable functional diversification [76]. In line with this hypothesis, in this study, I observed that many proteins with a conserved structural fold had a predicted disordered region. The flexibility of this disordered region could facilitate interactions with different host proteins [77]. Alternatively, as disordered regions evolve faster than non-disordered regions [78], these regions could facilitate the neofunctionalization of effector proteins. Therefore, to shed light on the

function of these structurally conserved effectors, more attention should be given to these intrinsically disordered regions.

Alternatively, some protein folds might be conserved as they facilitate interaction with specific host proteins. This is one of the hypotheses for the MAX-like effectors, as many MAX effectors in *M. oryzae* have been observed to translocate into cells where they are recognized by NLR R proteins with an integrated heavy metal-associated (HMA) domain [79-84]. Additionally, the host targets of some MAX effectors are HMA-containing proteins [85]. Therefore, it appears that MAX-like effectors are well suited for interaction with HMA domains [58,79,86,87]. However, recent research has shown that the conserved MAX effectors interact with HMA domains using different surfaces, suggesting that these effectors have independently evolved to bind HMA proteins [86]. Nevertheless, other MAX effectors interact with non-HMA proteins. For example, the AvrPiz-t MAX effector has been reported to interact with many host proteins (ligase and nucleoporin proteins) [88-91], while the MAX effector Avr-Pita has been found to interact with a rice cytochrome C oxidase [92]. Therefore, it appears that MAX effectors are not only well suited to interact with HMA proteins. This observation has led to the hypothesis that proteins with this fold share a conserved molecular mechanism that facilitates interaction with different host targets by a still unclear mechanism [86].

The discovery of MAX-like effectors in *V. inaequalis* reported in this thesis opens a new opportunity to investigate the evolution and functionality of this fold. Given the extensive differences between *V. inaequalis* and *M. oryzae*, regarding their host (dicot versus monocot) and lifestyle (subcuticular biotroph versus intracellular hemibiotroph), the study of the ViMAX-like ECs could give a wider perspective on the role of these effectors in the global context of plant–microbe interactions. A future line of research could be to identify the host targets of ViMAX-like ECs in apple. For that, a co-immunoprecipitation (co-IP) followed by mass spectrometry (MS)

from extracts of apple leaves infected with *V. inaequalis* expressing ViMAX-like effectors with a hemagglutinin (HA) tag could be performed. Later, structural modelling of MAX effectors with their host target could help elucidate the biophysical properties of the interaction. At a practical level, understanding the properties of the interaction between MAX effectors and HMA proteins, as well as other host targets, could help engineer an R protein that recognizes this conserved structural fold. The development of such an R protein could potentially confer plants with resistance against multiple unrelated plant pathogens.

3.2.3. Improving effector prediction pipelines

As discussed in Chapter 2, multiple bioinformatic approaches have been used to predict the effector catalogues of filamentous plant pathogens. In some cases, these approaches incorporate support from proteomic or transcriptomic experiments involving infected plant tissue. However, even when such analyses are performed, it is often difficult to ascertain what ECs might play an important role in promoting host-colonization. This is especially true for many ECs of fungal pathogens, which often lack conserved motifs or annotated functional domains that would otherwise give insights into their function. Thus, with these points in mind, it can be difficult to know which ECs to prioritise for further study.

In Chapter 3, I showed that transcriptomics combined with large-scale tertiary structure predictions can be used to help identify and prioritise ECs for further study. More specifically, at the start of this study, I predicted 1,369 proteins of *V. inaequalis* to be ECs. Of these, 686 ECs were found to be up-regulated during host infection, with ~200 of the 686 found to have structural similarity to Avrs from other plant-pathogenic fungi. These ~200 proteins now represent key candidate avirulence effectors of *V. inaequalis*. Notably, this list can be refined even more, by grouping ECs in families and selecting the most highly expressed member as the representative EC of the family. Based on this criterion, the number of ECs to initially screen for

a role in avirulence on apple could be as few as 12. Given my results, and how approachable large-scale structural predictions of proteins are becoming, I suggest that large-scale structural prediction should be integrated into all effector prediction pipelines.

Notably, AlphaFold2 has also opened the door to new, unexpected opportunities. A recent study tested if AlphaFold2 could predict a protein tertiary structure for spurious proteins that are the result of bioinformatic error. Importantly, this study by Monzon et al. [72] observed that, in most cases, AlphaFold2 failed to confidently predict a fold for these proteins [72]. Therefore, this algorithm can be used to inform if a protein is likely spurious or real (*bona fide*) [72]. Additionally, I suggest that structural searches in public databases could be used as a second layer of information to help determine if a protein is real or spurious. It is to be expected that if a protein has a good quality structural prediction by AlphaFold2 and shares structural similarities with proteins in the public database, it is a *bona fide* protein. Nevertheless, some proteins might display a novel fold. Therefore, this could only be used as an extra layer of information, not to discard gene predictions. This is very useful in the field of effector prediction as gene prediction in fungal genomes is in general very challenging. Additionally, prediction of *EC* genes poses even more challenges as these genes are usually in the vicinity of repetitive elements, usually lack obvious homology to other genes, and might display atypical codon usage, which hinder their prediction [93]. For these reasons, the majority of *in silico* gene prediction algorithms tend to discard these genes as spurious [93]. To avoid this problem, in this thesis I generated a manual annotation for *V. inaequalis* to include as many genes as possible, which increased the chances of generating a comprehensive effector catalogue. However, the immediate consequence of this pipeline was that many spurious genes were annotated in the genome. This is where integrating methods such as large-scale structural predictions with AlphaFold2 could become useful to discriminate between spurious genes and *EC* genes to help in the annotation of fungal effector catalogues.

3.2.4. Other future directions

This chapter has considerably extended our understanding of the effectors deployed by *V. inaequalis* during colonization of the subcuticular environment. However, this thesis is just a starting point toward understanding *V. inaequalis* effector biology and many questions remain unanswered. Firstly, the study presented here has focused on up-regulated *EC* genes during colonization of the subcuticular environment. To focus on up-regulated *EC* genes is a common strategy to prioritize *EC*s for study and it is especially suitable to identify genes that are associated with the establishment of biotrophy. However, at the same time, this is a limitation as some *EC* genes could be constitutively expressed. This indeed could be the case for putative antimicrobial *EC* genes that function through all the life stages of the fungus. Additionally, it is known that some genes with an important role during host-colonization are downregulated during infection [39,94]. Therefore, a study of the gene expression profiles of the non-upregulated EC genes could be performed in the future, to supplement the putative effector catalogue identified in this study.

Additionally, I suggest that the generation of a transcriptome covering the complete *V. inaequalis* lifecycle is essential to generate a more complete study of the biology of this pathogen. Such a transcriptome would be ideal to identify ECs with a putative role in manipulating the host microbiome. Ideally, this transcriptome could be generated from infected apple leaves in the field, instead of using detached apple leaves. Generating a transcriptome of *V. inaequalis* infecting the host in an orchard setting would better represent the natural conditions encountered by the pathogen, such as those related to microbial competition, inoculum pressure, and weather conditions. This would allow a better understanding of the biology of the fungus to be obtained, and would enable a more complete effector catalogue to be generated by identifying effectors specific for each lifecycle stage. Furthermore, it would be interesting to compare the transcriptome of *V. inaequalis* infecting an organic orchard and infecting a traditional orchard with fungicides.

Secondly, the strategies used by *V. inaequalis* to secrete and deliver effectors during host-colonization are still unknown. One hypothesis is that stromata could play a role in the delivery of effectors [3,50]. In line with this, localization of a ViAvrLm6-like EC and the Cin1 EC during host-colonization showed accumulation of these proteins in stromata [50,95]. Additionally, an ultrastructural study of *V. inaequalis* stromata, observed the presence of multivesicular bodies in this structure [96], suggesting a role for stromata in secreting molecules. Therefore, it is hypothesized that the stroma might be important for effector secretion, similar to haustoria developed by obligate biotrophic pathogens [37,97,98]. To test this hypothesis, an interesting follow-up experiment would be to perform a large-scale localization study of *V. inaequalis* ECs. For instance, *V. inaequalis* strains expressing some putative apoplastic and intracellular ECs fused to a fluorescent marker could be used to study the localization of these proteins during host-colonization by confocal laser scanning microscopy. This study could confirm the role of these infection structures in the secretion of effector proteins during host-colonization. Additionally, a laser microdissection study to generate an infection structure-specific transcriptome could shed light on the role of the stroma in effector delivery.

4. Chapter 4: Cell wall carbohydrate dynamics during the differentiation of infection structures by the apple scab fungus, *Venturia inaequalis*

4.1.1. Deciphering the cell wall: a promising target for antifungal control methods

As a starting point, this study characterized the cell wall carbohydrate composition of sporulating tubular hyphae developed by *V. inaequalis* in culture. These tubular hyphae resemble the hyphae developed by *V. inaequalis* on the surface of apple leaves, which are an important source of conidia for the spread of this pathogen in the orchard.

Studies on the hyphal cell wall of filamentous plant pathogens are scarce. To my knowledge, only a few studies have focused on the cell walls of plant-pathogenic fungi, including *F. oxysporum* [99] and the grey mold fungus *Botrytis cinerea* [100]. However, these studies only investigated the monosaccharide composition of cell walls, and only one study in the barley and rye scald fungus *Rhynchosporium secalis* investigated the glycosidic linkages of cell wall carbohydrates [101]. Therefore, this thesis adds to the overall knowledge of the cell wall composition in plant-pathogenic fungi.

Understanding the composition and biosynthesis of the cell wall in plant-pathogenic fungi can lead to the development of novel targeted fungicides. Another more sustainable control strategy is the use of fungal biocontrol agents (BCAs), such as some *Trichoderma* spp. [102]. The antagonistic potential of these BCAs has been associated with the secretion of cell wall-degrading enzymes (CWDEs) that break down the cell wall of fungal pathogens [103-105]. Therefore, increasing our knowledge of the cell walls of fungal pathogens can assist in the screening and identification of BCAs with CWDE catalogues specific to different plant-pathogenic fungi. Potentially, in the future, we could even engineer fungal BCAs in such a way that they produce tailored sets of CWDEs to target specific fungal plant pathogens.

4.1.2. Potential strategies to avoid MAMP-triggered immunity during colonization of the subcuticular host environment

The second part of the chapter reported studies of the subcuticular infection structures produced by *V. inaequalis* (i.e. runner hyphae and stromata), with a focus on cell wall composition and dynamics during host-colonization. Remarkably, the specialized infection structures produced by this fungus, or any other subcuticular plant-pathogenic fungus, had not been investigated in detail at the time this thesis was started. This study provided the first insights into how subcuticular plant-

pathogenic fungi differentiate and maintain infection structures during colonization of the hostile subcuticular environment of their host plants.

4.1.2.1. Transcriptional regulation of genes putatively associated with MAMP biosynthesis

First, in this chapter, I showed that many genes associated with the biosynthesis of cell wall-derived elicitors of plant defence, called microbe-associated molecular patterns (MAMPs), were down-regulated during host-colonization. Notably, the causal agent of maize anthracnose, *Colletotrichum graminicola*, has been reported to down-regulate key genes associated with β-1,6-glucan synthesis, with overexpression of these genes found to trigger a strong plant defence response [94]. Therefore, my study adds to the growing evidence that transcriptional regulation of genes associated with the biosynthesis of MAMPs might be one of the strategies used by plant-pathogenic fungi to avoid the elicitation of MAMP-triggered immunity. To confirm that the down-regulated genes are indeed encoding enzymes associated with MAMP biosynthesis, overexpression of these genes in *V. inaequalis* could be performed, in conjunction with apple infection assays, to investigate whether there is an impact on pathogen virulence and to monitor if plant defence responses are initiated.

Arguably, this transcriptional regulation is tightly controlled by *V. inaequalis* at different stages of infection structure morphogenesis. As infection by *V. inaequalis* is not synchronous, it would be challenging to obtain information about the dynamics of this transcriptional regulation. Ideally, *V. inaequalis* strains expressing the cell wall biosynthetic enzymes, fused to fluorescent reporters, under the control of native promoters, could be used to monitor the regulation of these genes at the transcriptional and translational levels during host-colonization using confocal laser scanning microscopy. Indeed, a similar assay in *C. graminiciola* showed weak localization of enzymes associated with β-glucan synthesis in biotrophic hyphae and strong production of these enzymes in necrotrophic hyphae [94]. Finally, the generation of an

infection structure-specific transcriptome by laser microdissection could also facilitate an understanding of the transcriptional regulation of these genes in the infection structures.

4.1.2.2. **V. inaequalis** *deacetylates chitin to chitosan on the surface of infection structures: what is the role of chitosan during infection?*

This study also revealed that *V. inaequalis* deacetylates chitin to chitosan on the surface of infection structures during host-colonization. Accumulation of chitosan on infection structures, such as invasive hyphae, has been observed in different plant pathogens [106,107]. This surface modification has been proposed to provide protection against cell wall degradation by plant chitinases and to prevent activation of MAMP-triggered immunity [107]. However, the biological importance of chitosan accumulation on the fungal cell wall during host-colonization has never been shown. A study of chitin deacetylases (CDAs) from *U. maydis* showed that deletion of *CDA4,* resulted in mutants depleted of chitosan on the biotrophic hyphae. These mutants without chitosan, did not display a change in virulence [106], even though an increased susceptibility to plant chitinases was observed [106]. Therefore, the lack of a virulence penalty observed by deleting *CDA4* suggests that the putative protective role of chitosan during host-colonization is redundant with other effectors secreted by this pathogen associated with downregulation of glycan-triggered immunity [106]. Additionally, deletion of other *CDA* combinations affected virulence but also generated morphogenesis defects; therefore, the contribution of chitosan during host-colonization was unclear [106]. Nevertheless, the study in *U. maydis* provided clear evidence for the requirement of chitosan in morphogenesis and cell wall integrity, as simultaneous deletion of all *CDA* genes was lethal [106]. Similarly, in *M. oryzae*, chitosan has been observed to be important for appressorial development and adherence to the host surface [108,109], suggesting additional roles for chitosan during host-colonization.

I hypothesize that chitosan in *V. inaequalis* might not only function as a 'stealth' molecule but might also play some role in morphogenesis. Remarkably, chitosan was not only observed around the periphery of infection structures, but it was also observed to accumulate between cells. Chitosan is a less rigid polymer than chitin [110]; therefore, this carbohydrate could be providing flexibility to the cell wall needed for morphogenesis. Additionally, this carbohydrate could also provide flexibility that enables the formation of these infection structures in the tight subcuticular environment. This thesis provides the first report of chitosan accumulation on the cell wall surface of infection structures produced by a subcuticular pathogen. Next, it would be interesting to investigate whether the accumulation of chitosan is conserved across fungi with this lifestyle.

Nevertheless, the relevance of chitosan accumulation on *V. inaequalis* cell wall during host-colonization remains to be assessed. In the future, reverse genetic studies could be performed to investigate the role of the different *CDAs* during host-colonization. Based on the expression profiles of the *CDA* genes, there are two obvious candidates, *CDA1* and *CDA6*, for further study. Certainly, the recent application of CRISPR-Cas9 technology to *V. inaequalis* (Chapter 5) will allow studying the role of chitosan by targeting these *CDAs*.

Additionally, in this study, I reported that one of the triggers for chitosan production during host-colonization is apple wax. However, apple wax is not the only trigger, as chitosan was also observed on the infection-like structures developed inside cellophane membranes (CMs), indicating that pressure could be another cue. Of note, the plant surface has been reported to be important in certain plant-pathogenic fungi for the induction of infection structure morphogenesis [111-113]. As mentioned above, in *M. oryzae*, chitosan has also been observed to be required for cell surface attachment and appressoria development on artificial hydrophobic surfaces [109]. Therefore, this study in *M. oryzae* hypothesized that chitosan was required for surface-sensing

Even more surprising, in *M. oryzae*, the addition of wax was enough to override the need for chitosan [109]. This observation highlights an intriguing link between wax, chitosan and appressorial development. The observation that wax is a trigger for chitosan production in *V. inaequalis* could be a starting point to elucidate some of the signalling pathways associated with the initial morphogenesis of infection structures by this fungus. For example, future studies could focus on investigating the differences in *V. inaequalis* gene expression in the presence and absence of apple wax.

4.1.2.3. Towards understanding the role of α-1,3-glucan in V. inaequalis

In this study, I reported the presence of α-1,3-glucan on tubular hyphae of *V. inaequalis* developed in culture. However, even though the α-1,3-glucan synthase gene *ViAGS2* was up-regulated *in planta*, this carbohydrate was not identified in the cell wall of the different cellular morphotypes developed during host-colonization. I suggest that the lack of α-1,3-glucan labelling could be due to problems with antibody affinity and penetrability inside apple tissue. Additionally, it is also possible that α-1,3-glucan forms part of a hyper-mobile water-soluble matrix as recently reported for *Aspergillus fumigatus* [114]. Arguably, such a water-soluble matrix would have been lost during sample preparation, as the antibody labelling protocol required multiple washing steps. As a future experiment, α-1,3-glucan localization could be investigated by generating a *V. inaequalis* strain expressing an α-1,3-glucan biosensor, which would allow live cell imaging studies to be performed. Such studies would ensure that the labelling limitations encountered above could be bypassed. As a potential biosensor, the α-1,3-glucan-binding domains DB1-CB6-DB2 from the α-1,3-glucanase of *Bacillus circulans* [115] could be fused to a fluorescent reporter such as green fluorescent protein (GFP).

As with chitosan, α-1,3-glucan has been proposed to function as a ‘stealth molecule’ that masks MAMPs from the plant pathogen cell wall that would otherwise activate the plant

immune system [116-118]. However, the studies proposing the role of α-1,3-glucan as a 'stealth molecule' display some clear weaknesses, and the function of this carbohydrate in virulence remains quite unclear [119]. A study in *M. oryzae* reported that deletion of an α-*1,3-glucan synthase* gene impacted virulence. This study also observed a small up-regulation of plant defence-related genes during infection with knock-out strains [116], which led to the conclusion that the loss of α-1,3-glucan elicited MAMP-triggered immunity. However, knock-out mutants also showed cell wall lysis before host penetration, indicating that they had some cell viability problems [116,119]. Additionally, the up-regulation of plant defence genes was minimal compared with a classical MAMP-triggered immune response [116,119]. Another study on the human pathogen *A. fumigatus* reported that *α-1,3-glucan synthase* knock-out strains trigger strong host immune responses in an animal system. However, this study also reported that loss of α-1,3-glucan causes a massive structural change in the cell wall, which leads to the exposure of MAMPs. This suggests that α-1,3-glucan could be more than just a 'stealth molecule' and that it might also play an important structural role in the cell wall [120]. Finally, a further study in *A. fumigatus* reported that α-1,3-glucan was not only part of the outer cell wall matrix, but that it also formed part of the core cell wall [121]. With these studies in mind, follow-up experiments that examine the location and dynamics of α-1,3-glucan in the cell wall of *V. inaequalis* are of paramount importance. These follow-up studies would shed light on the role that this carbohydrate plays in *V. inaequalis* and would provide insights into the general role of α-1,3-glucan in cell viability or evasion of plant defences during host-colonization.

5. Chapter 5: CRISPR-Cas9 gene editing and rapid detection of gene-edited mutants using high-resolution melting in the apple scab fungus, *Venturia inaequalis*

5.1.1. CRISPR-Cas9 opens the door to reverse genetic studies in *V. inaequalis*

One of the main objectives of this thesis was to develop a gene disruption protocol that will facilitate reverse genetic studies in *V. inaequalis*. At first, different homologous recombination-based methodologies were tested without success. The targeted gene deletion efficiency varies highly between fungi as it depends on two competing DNA repair mechanisms, homologous recombination and non-homologous end joining (NHEJ). Additionally, gene sequence, chromatin structure at the gene position, guanine/cytosine content of flanks, and other factors also affect targeted gene deletion efficiency [122]. In this thesis, attempts to perform gene deletions in *V. inaequalis* using homologous recombination were unsuccessful, suggesting that NHEJ is the dominant DNA repair mechanism in *V. inaequalis*. Multiple strategies have been developed to optimize homologous recombination-based gene deletions and screening over the years. One strategy is the use of fungal mutants defective in NHEJ; however, these mutants frequently show lower fitness and phenotypic defects that negatively influence downstream studies [122]. For this reason, this method was not tested in this thesis. Another strategy is the use of a split-marker system, which is based on the transformation of two fragments containing one flank (upstream and downstream of the gene of interest) and the partial resistant marker [123]. Therefore, deletion mutants only arise upon homologous recombination of the two fragments in the genome, facilitating the screening for knockouts. This strategy was used without success to attempt gene deletions in *V. inaequalis*, likely due to the low transformation efficiency in this fungus which made it difficult to successfully co-transform two plasmids.

Given the lack of success attempting gene deletions by homology-based methods, I attempted to generate a gene disruption using CRISPR-Cas9 technology. CRISPR Cas9 has been

used to generate gene disruptions in more than 40 species of filamentous fungi and oomycetes [124], including the Dothideomycete *L. maculans*, which is closely related to *V. inaequalis* [125]. The application of CRISPR-Cas9 technology to *V. inaequalis* was successful and led to the first published gene disruptions in *V. inaequalis*.

The protocol developed in this thesis only required the use of one autonomously replicating Golden Gate-compatible plasmid, which confers many advantages. One of the main benefits is the autonomously replicating nature of the plasmid, which leads to higher transformation efficiencies [126]. This is extremely advantageous to fungal species, such as *V. inaequalis*, with low transformation efficiency. Notably, this autonomously replicating plasmid has been successfully used for gene disruption in the forest pathogen *Dothistroma septosporum* [127], the apple pathogen *Neonectria ditissima* (unpublished, Liz M. Florez) and the fungal endophyte *Epichloë festucae* [128]. Additionally, in this chapter I show that, in most cases, the autonomous replicating plasmid is readily lost after the removal of the antibiotic selection. This represents many practical advantages, such as the development of footprint-less mutants. Furthermore, this allows the generation of multiple sequential gene disruptions, without the number of antibiotic markers available being a limitation. Therefore, sequential CRISPR-Cas9 deletions could be used to perform reverse genetic studies of expanded EC families in *Venturia* spp..

Finally, in this thesis, I developed a high-throughput screening method for CRISPR-Cas9 mutants that involves a high-resolution melting (HRM) analysis. This method is sensitive enough to detect single base pairs indels [129-131], which allows researchers to quickly screen for gene-edited mutants without the need to perform expensive sequencing. HRM has been used to screen gene-edited mutants in multiple systems, such as fish embryos [132], *Arabidopsis* [133] and rice plants [129]. However, to my knowledge, this is the first report of HRM being used for

the screening of CRISPR-Cas9 mutants in a fungal species. This technology is very cost-effective and, after the publication of this chapter, was used to successfully screen CRISPR-Cas9 mutants in the fungal pathogen *N. ditissima* (unpublished, Liz M. Florez).

5.1.2. There is room for improvement: future directions to optimize CRISPR-Cas9 gene editing in *V. inaequalis*

The *V. inaequalis* gene editing technology developed in this thesis is the most efficient described to date for this species. However, the gene disruption efficiency obtained was low compared with other fungal systems, where efficiency ranges from 10–100% [124]. The mutations observed in the *V. inaequalis* genome after CRISPR-Cas9 transformations were always small indels upstream of the PAM site, indicating that they were generated by NHEJ DNA repair. The low gene disruption efficiency observed could indicate that the NHEJ mechanism in *V. inaequalis* is highly efficient, which led to only a small number of indels after the double strand break generated by the Cas9 nuclease. Alternatively, the low efficiency could be the result of inefficient expression of the *Cas9* and small guide RNA (sgRNA). The first step towards optimizing this protocol would be to test expression levels of the *Cas9* gene after fungal transformation. The plasmid used here expresses *Cas9* under an *Aspergillus niger pyruvate kinase* gene promoter. A real-time quantitative PCR experiment could be performed to test the expression of the *Cas9* gene. On the occasion that the expression is low, a different promoter with a higher constitutive expression level could be used. Second, an alternative to increasing gene editing efficiencies could be to co-transform the CRISPR-Cas9 and sgRNA with a donor DNA, which has been observed to increase editing efficiencies in many fungal species [127,134]. The donor DNA consists of flanking regions to facilitate homologous integration, and a selection marker to improve the selection scheme for successful transformants. Even though the efficiency of homologous recombination appears to be low in *V. inaequalis*, these efficiency has been observed to increase in different filamentous fungi after a Cas9-mediated double strand break [124].

Finally, an exciting new avenue for improved functional studies in *V. inaequalis* could involve the development of a CRISPR-Cas9 protocol for simultaneous gene editing (multiplexing). In this way, genetic redundancy among EC family members, as well as the overall contribution of EC families to virulence, could be better assessed. Notably, CRISPR-Cas9 technology has been used to assess the functional redundancy of an EC family in *U. maydis* through simultaneous gene disruption [44]. To apply multiplexing in *V. inaequalis*, the CRISPR-Cas9 plasmid should be modified to integrate more cloning sites to express different sgRNAs under their own promoter [135]. Another alternative is to express multiple sgRNAs under one promoter, flanked by ribozyme sequences and a linker, which allows the cleavage and expression of the sgRNAs independently [136]. Intriguingly, a study in the fungal human pathogen *Blastomyces dermatitidis* reported that this single-promoter strategy led to higher transformation efficiencies than when using two independent promoters [136].

6. Final conclusion

Plant diseases threaten the increase in food production that is required to meet the food demands of a growing population. Additionally, climate change is increasing the number of plant disease outbreaks around the world [2]. To achieve food security, the development of novel control methods against plant diseases is of paramount importance [2]. Current control methods against scab are failing, with new fungicide-resistant [137,138] and cultivar resistance-breaking strains emerging constantly [139]. To optimize control methods, ensure their durability, and develop novel strategies, a deeper understanding of pathogen biology is required.

In this thesis (Chapter 3), I described the different stages of host-colonization, with a focus on the expression of *EC* genes. This chapter has considerably extended our understanding of *V. inaequalis* effector biology and has created many future lines of research to experimentally validate identified *EC* genes. Especially, in conjunction with tertiary structure predictions, I provided a list of EC proteins with a potential role in avirulence that should be studied further. Identification of novel avirulence effectors will facilitate screening of new scab *R* genes and ease the development of diagnostics techniques to identify *V. inaequalis* resistance-breaking strains in the field. This type of diagnostic technique is important to determine the frequency of resistance breaking strains among the populations, which helps to investigate the durability of apple cultivars carrying cognate *R* genes. Certainly, the use of single *R* genes has been observed to lead to the fast emergence of resistance-breaking strains. Therefore, assessing the durability of *R* genes, to identify the most durable *R* genes to stack in apple cultivars is seen as one avenue to obtaining durable resistance [139]. Furthermore, this study has added to the evidence that many effector proteins adopt common structural folds and provides some guidance to understanding their functions and evolution. In practical terms, identification of structurally conserved Avr effectors that putatively

interact directly with a cognate R protein could facilitate engineering of *R* genes to identify multiple Avr effectors.

This thesis (Chapter 4) also investigated, for the first time, the composition and dynamics of the *V. inaequalis* cell wall in culture and during host-colonization. By doing so, I increased our understanding of the strategies used by pathogens to avoid glycan-triggered immunity. The knowledge acquired from this chapter, specifically regarding major cell wall carbohydrates and biosynthetic enzymes, could potentially be used in future research involving the development of novel fungicides and BCAs efficient against scab. Finally, in Chapter 5, I describe the first gene disruption method in *V. inaequalis*. The inefficiency to achieve gene disruptions represented a bottleneck for further studies in this pathosystem. The technology described in this chapter will greatly facilitate future reverse genetics studies in this and other fungal species with low transformation efficiencies.

In conclusion, the knowledge acquired from this thesis not only furthered our understanding of *V. inaequalis* biology but can also be used to inform future control strategies against this pathogen and, potentially, other subcuticular pathogens.

7. References

1. Avery SV, Singleton I, Magan N, Goldman GH: **The fungal threat to global food security**. *Fungal Biology* 2019, **123**:555-557.
2. Ristaino JB, Anderson PK, Bebber DP, Brauman KA, Cunniffe NJ, Fedoroff NV, Finegold C, Garrett KA, Gilligan CA, Jones CM, et al.: **The persistent threat of emerging plant disease pandemics to global food security**. *Proceedings of the National Academy of Sciences* 2021, **118**:e2022239118.
3. Kucheryava N, Bowen JK, Sutherland PW, Conolly JJ, Mesarich CH, Rikkerink EH, Kemen E, Plummer KM, Hahn M, Templeton MD: **Two novel *Venturia inaequalis* genes induced upon morphogenetic differentiation during infection and *in vitro* growth on cellophane**. *Fungal Genetics and Biology* 2008, **45**:1329-1339.
4. Keitt GW, Leben C, Shay JR: ***Venturia inaequalis* (Cke.) Wint. IV. Further studies on the inheritance of pathogenicity**. *American Journal of Botany* 1948, **35**:334-336.
5. Nusbaum CJ, Keitt GW: **A cytological study of host-parasite relations of *Venturia inaequalis* on apple leaves**. *Journal of Agricultural Research* 1938, **56**:595-618.
6. Williams EB, Shay JR: **The relationship of genes for pathogenicity and certain other characters in *Venturia inaequalis* (CKe,) Wint**. *Genetics* 1957, **42**:704-711.
7. Fitzgerald AM, Mudge AM, Gleave AP, Plummer KM: ***Agrobacterium* and PEG-mediated transformation of the phytopathogen *Venturia inaequalis***. *Mycological Research* 2003, **107**:803-810.
8. Fitzgerald A, Van Kan JA, Plummer KM: **Simultaneous silencing of multiple genes in the apple scab fungus, *Venturia inaequalis*, by expression of RNA with chimeric inverted repeats**. *Fungal Genetics and Biology* 2004, **41**:963-971.
9. Bowen JK, Mesarich CH, Rees-George J, Cui W, Fitzgerald A, Win j, Plummer KM, Templeton MD: **Candidate effector gene identification in the ascomycete fungal phytopathogen *Venturia inaequalis* by expressed sequence tag analysis**. *Molecular Plant Pathology* 2009, **10**:431-448.
10. Deng CH, Plummer KM, Jones DAB, Mesarich CH, Shiller J, Taranto AP, Robinson AJ, Kastner P, Hall NE, Templeton MD, et al.: **Comparative analysis of the predicted secretomes of Rosaceae scab pathogens *Venturia inaequalis* and *V. pirina* reveals expanded effector families and putative determinants of host range**. *BMC Genomics* 2017, **18**:339.
11. Mesarich CH, Schmitz M, Tremouilhac P, McGillivray DJ, Templeton MD, Dingley AJ: **Structure, dynamics and domain organization of the repeat protein Cin1 from the apple scab fungus**. *Biochimica et Biophysica Acta* 2012, **1824**:1118-1128.
12. Rovenich H, Zuccaro A, Thomma BPHJ: **Convergent evolution of filamentous microbes towards evasion of glycan-triggered immunity**. *New Phytologist* 2016, **212**:896-901.
13. Schouten HJ, Brinkhuis J, Burgh AMvd, Schaart JG, Groenwold R, Broggini GAL, Gessler C: **Cloning and functional characterization of the *Rvi15* (*Vr2*) gene for apple scab resistance**. *Tree Genetics & Genomes* 2013, **10**:251-260.
14. de Jonge R, Peter van Esse H, Kombrink A, Shinya T, Desaki Y, Bours R, van der Krol S, Shibuya N, Joosten Matthieu HAJ, Thomma Bart PHJ: **Conserved fungal LysM effector Ecp6 Prevents chitin-triggered immunity in plants**. *Science* 2010, **329**:953-955.
15. Bolton MD, Van Esse HP, Vossen JH, De Jonge R, Stergiopoulos I, Stulemeijer IJE, Van Den Berg GCM, Borrás-Hidalgo O, Dekker HL, De Koster CG, et al.: **The novel *Cladosporium fulvum* lysin motif effector Ecp6 is a virulence factor with orthologues in other fungal species**. *Molecular Microbiology* 2008, **69**:119-136.

16. Bradshaw RE, Guo Y, Sim AD, Kabir MS, Chettri P, Ozturk IK, Hunziker L, Ganley RJ, Cox MP: **Genome-wide gene expression dynamics of the fungal pathogen *Dothistroma septosporum* throughout its infection cycle of the gymnosperm host *Pinus radiata***. *Molecular Plant Pathology* 2016, **17**:210-224.
17. Lanver D, Müller AN, Happel P, Schweizer G, Haas FB, Franitza M, Pellegrin C, Reissmann S, Altmüller J, Rensing SA, et al.: **The biotrophic development of *Ustilago maydis* studied by RNA-Seq analysis**. *The Plant Cell* 2018, **30**:300.
18. Gervais J, Plissonneau C, Linglin J, Meyer M, Labadie K, Cruaud C, Fudal I, Rouxel T, Balesdent M-H: **Different waves of effector genes with contrasted genomic location are expressed by *Leptosphaeria maculans* during cotyledon and stem colonization of oilseed rape**. *Molecular Plant Pathology* 2017, **18**:1113-1126.
19. Thakur K, Chawla V, Bhatti S, Swarnkar MK, Kaur J, Shankar R, Jha G: ***De novo* transcriptome sequencing and analysis for *Venturia inaequalis*, the devastating apple scab pathogen**. *PLoS ONE* 2013, **8**:e53937.
20. Skrzydeł J, Borowska-Wykręt D, Kwiatkowska D: **Structure, assembly and function of cuticle from mechanical perspective with special focus on perianth**. *International Journal of Molecular Sciences* 2021, **22**:4160.
21. Bowen JK, Mesarich CH, Bus VG, Beresford RM, Plummer KM, Templeton MD: ***Venturia inaequalis*: the causal agent of apple scab**. *Molecular Plant Pathology* 2011, **12**:105-122.
22. Balestrini R, Gómez-Ariza J, Klink VP, Bonfante P: **Application of laser microdissection to plant pathogenic and symbiotic interactions**. *Journal of Plant Interactions* 2009, **4**:81-92.
23. Honaas LA, Wafula EK, Yang Z, Der JP, Wickett NJ, Altman NS, Taylor CG, Yoder JI, Timko MP, Westwood JH, et al.: **Functional genomics of a generalist parasitic plant: laser microdissection of host-parasite interface reveals host-specific patterns of parasite gene expression**. *BMC Plant Biology* 2013, **13**:9.
24. Podgorny OV, Lazarev VN: **Laser microdissection: A promising tool for exploring microorganisms and their interactions with hosts**. *Journal of Microbiological Methods* 2017, **138**:82-92.
25. Tang W, Coughlan S, Crane E, Beatty M, Duvick J: **The application of laser microdissection to *in planta* gene expression profiling of the maize anthracnose stalk rot fungus *Colletotrichum graminicola***. *Molecular Plant-Microbe Interactions* 2006, **19**:1240-1250.
26. Hacquard S, Delaruelle C, Legué V, Tisserant E, Kohler A, Frey P, Martin F, Duplessis S: **Laser capture microdissection of uredinia formed by *Melampsora larici-populina* revealed a transcriptional switch between biotrophy and sporulation**. *Molecular Plant-Microbe Interactions* 2010, **23**:1275-1286.
27. Kameoka H, Maeda T, Okuma N, Kawaguchi M: **Structure-specific regulation of nutrient transport and metabolism in arbuscular mycorrhizal fungi**. *Plant and Cell Physiology* 2019, **60**:2272-2281.
28. Amselem J, Cuomo CA, van Kan JAL, Viaud M, Benito EP, Couloux A, Coutinho PM, de Vries RP, Dyer PS, Fillinger S, et al.: **Genomic analysis of the necrotrophic fungal pathogens *Sclerotinia sclerotiorum* and *Botrytis cinerea***. *PLoS Genetics* 2011, **7**:e1002230.
29. Bradley EL, Ökmen B, Doehlemann G, Henrissat B, Bradshaw RE, Mesarich CH: **Secreted glycoside hydrolase proteins as effectors and invasion patterns of plant-associated fungi and oomycetes**. *Frontiers in Plant Science* 2022, **13**.
30. Castruita-Domínguez JP, González-Hernández SE, Polaina J, Flores-Villavicencio LL, Alvarez-Vargas A, Flores-Martínez A, Ponce-Noyola P, Leal-Morales CA: **Analysis of a**

polygalacturonase gene of *Ustilago maydis* and characterization of the encoded enzyme. *Journal of Basic Microbiology* 2014, **54**:340-349.
31. Oeser B, Heidrich PM, Müller U, Tudzynski P, Tenberge KB: **Polygalacturonase is a pathogenicity factor in the *Claviceps purpurea*/rye interaction**. *Fungal Genetics and Biology* 2002, **36**:176-186.
32. Boutrot F, Zipfel C: **Function, discovery, and exploitation of plant pattern recognition receptors for broad-spectrum disease resistance**. *Annual Review of Phytopathology* 2017, **55**:257-286.
33. Ferrari S, Savatin DV, Sicilia F, Gramegna G, Cervone F, Lorenzo GD: **Oligogalacturonides: plant damage-associated molecular patterns and regulators of growth and development**. *Frontiers in Plant Science* 2013, **4**:49.
34. Federici L, Di Matteo A, Fernandez-Recio J, Tsernoglou D, Cervone F: **Polygalacturonase inhibiting proteins: players in plant innate immunity?** *Trends in Plant Science* 2006, **11**:65-70.
35. De Lorenzo G, Ferrari S: **Polygalacturonase-inhibiting proteins in defense against phytopathogenic fungi**. *Current Opinion in Plant Biology* 2002, **5**:295-299.
36. Rocafort M, Fudal I, Mesarich CH: **Apoplastic effector proteins of plant-associated fungi and oomycetes**. *Current Opinion in Plant Biology* 2020, **56**:9-19.
37. Lo Presti L, Lanver D, Schweizer G, Tanaka S, Liang L, Tollot M, Zuccaro A, Reissmann S, Kahmann R: **Fungal effectors and plant susceptibility**. *Annual Review of Plant Biology* 2015, **66**:513-545.
38. Wei W, Xu L, Peng H, Zhu W, Tanaka K, Cheng J, Sanguinet KA, Vandemark G, Chen W: **A fungal extracellular effector inactivates plant polygalacturonase-inhibiting protein**. *Nature Communications* 2022, **13**:2213.
39. Sánchez-Vallet A, Fouché S, Fudal I, Hartmann FE, Soyer JL, Tellier A, Croll D: **The genome biology of effector gene evolution in filamentous plant pathogens**. *Annual Review of Phytopathology* 2018, **56**:21-40.
40. Tan KC, Oliver RP: **Regulation of proteinaceous effector expression in phytopathogenic fungi**. *PLoS Pathogens* 2017, **13**:e1006241.
41. Prusky D, Alkan N, Mengiste T, Fluhr R: **Quiescent and necrotrophic lifestyle choice during postharvest disease development**. *Annual Review of Phytopathology* 2013, **51**:155-176.
42. Pedersen C, van Themaat EVL, McGuffin LJ, Abbott JC, Burgis TA, Barton G, Bindschedler LV, Lu X, Maekawa T, Weßling R, et al.: **Structure and evolution of barley powdery mildew effector candidates**. *BMC Genomics* 2012, **13**:694.
43. Wicker T, Oberhaensli S, Parlange F, Buchmann JP, Shatalina M, Roffler S, Ben-David R, Doležel J, Šimková H, Schulze-Lefert P, et al.: **The wheat powdery mildew genome shows the unique evolution of an obligate biotroph**. *Nature Genetics* 2013, **45**:1092-1096.
44. Schuster M, Schweizer G, Kahmann R: **Comparative analyses of secreted proteins in plant pathogenic smut fungi and related basidiomycetes**. *Fungal Genetics and Biology* 2018, **112**:21-30.
45. Menardo F, Praz CR, Wicker T, Keller B: **Rapid turnover of effectors in grass powdery mildew (*Blumeria graminis*)**. *BMC Evolutionary Biology* 2017, **17**:223.
46. Dutheil JY, Mannhaupt G, Schweizer G, C MKS, Münsterkötter M, Güldener U, Schirawski J, Kahmann R: **A tale of genome compartmentalization: the evolution of virulence clusters in smut fungi**. *Genome Biology Evolution* 2016, **8**:681-704.
47. Faino L, Seidl MF, Shi-Kunne X, Pauper M, van den Berg GC, Wittenberg AH, Thomma BP: **Transposons passively and actively contribute to evolution of the two-speed genome of a fungal pathogen**. *Genome Research* 2016, **26**:1091-1100.

48. Haas BJ, Kamoun S, Zody MC, Jiang RHY, Handsaker RE, Cano LM, Grabherr M, Kodira CD, Raffaele S, Torto-Alalibo T, et al.: **Genome sequence and analysis of the Irish potato famine pathogen *Phytophthora infestans***. *Nature* 2009, **461**:393-398.
49. Seidl MF, Thomma BP: **Sex or no sex: evolutionary adaptation occurs regardless**. *Bioessays* 2014, **36**:335-345.
50. Shiller J, Van de Wouw AP, Taranto AP, Bowen JK, Dubois D, Robinson A, Deng CH, Plummer KM: **A large family of *AvrLm6-like* genes in the apple and pear scab pathogens, *Venturia inaequalis* and *Venturia pirina***. *Frontiers in Plant Science* 2015, **6**.
51. Selker EU, Garrett PW: **DNA sequence duplications trigger gene inactivation in *Neurospora crassa***. *Proceedings of the National Academy of Sciences* 1988, **85**:6870-6874.
52. van Wyk S, Wingfield BD, De Vos L, van der Merwe NA, Steenkamp ET: **Genome-wide analyses of repeat-induced point mutations in the Ascomycota**. *Frontiers in Microbiology* 2021, **11**.
53. Fudal I, Ross S, Brun H, Besnard AL, Ermel M, Kuhn ML, Balesdent MH, Rouxel T: **Repeat-induced point mutation (RIP) as an alternative mechanism of evolution toward virulence in *Leptosphaeria maculans***. *Molecular Plant-Microbe Interactions* 2009, **22**:932-941.
54. Asai S, Furzer OJ, Cevik V, Kim DS, Ishaque N, Goritschnig S, Staskawicz BJ, Shirasu K, Jones JDG: **A downy mildew effector evades recognition by polymorphism of expression and subcellular localization**. *Nature Communications* 2018, **9**:5192.
55. Qutob D, Patrick Chapman B, Gijzen M: **Transgenerational gene silencing causes gain of virulence in a plant pathogen**. *Nature Communications* 2013, **4**:1349.
56. Illergård K, Ardell DH, Elofsson A: **Structure is three to ten times more conserved than sequence--a study of structural response in protein cores**. *Proteins* 2009, **77**:499-508.
57. Jumper J, Evans R, Pritzel A, Green T, Figurnov M, Ronneberger O, Tunyasuvunakool K, Bates R, Žídek A, Potapenko A, et al.: **Highly accurate protein structure prediction with AlphaFold**. *Nature* 2021, **596**:583-589.
58. de Guillen K, Ortiz-Vallejo D, Gracy J, Fournier E, Kroj T, Padilla A: **Structure analysis uncovers a highly diverse but structurally conserved effector family in phytopathogenic fungi**. *PLoS Pathogens* 2015, **11**:e1005228.
59. Lazar N, Mesarich CH, Petit-Houdenot Y, Talbi N, Li de la Sierra-Gallay I, Zélie E, Blondeau K, Gracy J, Ollivier B, Blaise F, et al.: **A new family of structurally conserved fungal effectors displays epistatic interactions with plant resistance proteins**. *PLoS Pathogens* 2022, **18**:e1010664.
60. Seong K, Krasileva KV: **Computational structural genomics unravels common folds and novel families in the secretome of fungal phytopathogen *Magnaporthe oryzae***. *Molecular Plant-Microbe Interactions* 2021:MPMI-03-21-0071-R.
61. Yu DS, Outram MA, Smith A, McCombe CL, Khambalkar PB, Rima SA, Sun X, Ma L, Ericsson DJ, Jones DA, et al.: **The structural repertoire of *Fusarium oxysporum* f. sp. *lycopersici* effectors revealed by experimental and computational studies**. *bioRxiv* 2021: 472499.
62. Seong K, Krasileva KV: **Comparative computational structural genomics highlights divergent evolution of fungal effectors**. *bioRxiv* 2022: 490317.
63. Snelders NC, Rovenich H, Thomma BPHJ: **Microbiota manipulation through the secretion of effector proteins is fundamental to the wealth of lifestyles in the fungal kingdom**. *FEMS Microbiology Reviews* 2022:fuac022.
64. Allen A, Chatt E, Smith TJ: **The atomic structure of the virally encoded antifungal protein, KP6**. *Journal of Molecular Biology* 2013, **425**:609-621.

65. Li N, Erman M, Pangborn W, Duax WL, Park C-M, Bruenn J, Ghosh D: **Structure of *Ustilago maydis* killer toxin KP6 α-subunit: A multimeric assembly with a central pore**. *The Journal of Biological Chemistry* 1999, **274**:20425-20431.
66. Padilla A, Hoh, F., De guillen, K.: **Zt-KP6-1: an effector from *Zymoseptoria tritici***. 2019.
67. Mesarich CH, Ökmen B, Rovenich H, Griffiths SA, Wang C, Karimi Jashni M, Mihajlovski A, Collemare J, Hunziker L, Deng CH, et al.: **Specific hypersensitive response-associated recognition of new apoplastic effectors from *Cladosporium fulvum* in wild tomato**. *Molecular Plant-Microbe Interactions* 2018, **31**:145-162.
68. Ebert MK, Rangel LI, Spanner RE, Taliadoros D, Wang X, Friesen TL, de Jonge R, Neubauer JD, Secor GA, Thomma BPHJ, et al.: **Identification and characterization of *Cercospora beticola* necrosis-inducing effector CbNip1**. *Molecular Plant Pathology* 2021, **22**:301-316.
69. Snelders NC, Kettles GJ, Rudd JJ, Thomma BPHJ: **Plant pathogen effector proteins as manipulators of host microbiomes?** *Molecular Plant Pathology* 2018, **19**:257-259.
70. Lee H-T, Lee C-C, Yang J-R, Lai JZC, Chang KY: **A large-scale structural classification of antimicrobial peptides**. *BioMed Research International* 2015, **2015**:475062.
71. Becher D, Bernhardt J, Fuchs S, Riedel K: **Metaproteomics to unravel major microbial players in leaf litter and soil environments: Challenges and perspectives**. *Proteomics* 2013, **13**:2895-2909.
72. Monzon V, Haft DH, Bateman A: **Folding the unfoldable: using AlphaFold to explore spurious proteins**. *Bioinformatics Advances* 2022, **2**:vbab043.
73. Sarma GN, Manning VA, Ciuffetti LM, Karplus PA: **Structure of Ptr ToxA: An RGD-containing host-selective toxin from *Pyrenophora tritici-repentis*** *The Plant Cell* 2005, **17**:3190-3202.
74. Di X, Cao L, Hughes RK, Tintor N, Banfield MJ, Takken FLW: **Structure-function analysis of the *Fusarium oxysporum* Avr2 effector allows uncoupling of its immune-suppressing activity from recognition**. *New Phytologist* 2017, **216**:897-914.
75. Wang C-IA, Gunčar G, Forwood JK, Teh T, Catanzariti A-M, Lawrence GJ, Loughlin FE, Mackay JP, Schirra HJ, Anderson PA, et al.: **Crystal structures of flax rust avirulence proteins AvrL567-A and -D reveal details of the structural basis for flax disease resistance specificity**. *The Plant Cell* 2007, **19**:2898-2912.
76. Outram MA, Figueroa M, Sperschneider J, Williams SJ, Dodds PN: **Seeing is believing: Exploiting advances in structural biology to understand and engineer plant immunity**. *Current Opinion in Plant Biology* 2022, **67**.
77. Marín M, Ott T: **Intrinsic disorder in plant proteins and phytopathogenic bacterial effectors**. *Chemical Reviews* 2014, **114**:6912-6932.
78. Brown CJ, Takayama S, Campen AM, Vise P, Marshall TW, Oldfield CJ, Williams CJ, Dunker AK: **Evolutionary rate heterogeneity in proteins with long disordered regions**. *Journal of Molecular Evolution* 2002, **55**:104-110.
79. Zhang X, He D, Zhao Y, Cheng X, Zhao W, Taylor IA, Yang J, Liu J, Peng YL: **A positive-charged patch and stabilized hydrophobic core are essential for avirulence function of AvrPib in the rice blast fungus**. *The Plant Journal* 2018, **96**:133-146.
80. Cesari S, Thilliez G, Ribot C, Chalvon V, Michel C, Jauneau A, Rivas S, Alaux L, Kanzaki H, Okuyama Y, et al.: **The rice resistance protein pair RGA4/RGA5 recognizes the *Magnaporthe oryzae* effectors AVR-Pia and AVR1-CO39 by direct binding**. *The Plant Cell* 2013, **25**:1463-1481.
81. Yoshida K, Saitoh H, Fujisawa S, Kanzaki H, Matsumura H, Yoshida K, Tosa Y, Chuma I, Takano Y, Win J, et al.: **Association genetics reveals three novel avirulence genes from the rice blast fungal pathogen *Magnaporthe oryzae*.** *The Plant Cell* 2009, **21**:1573-1591.

82. Ashikawa I, Hayashi N, Yamane H, Kanamori H, Wu J, Matsumoto T, Ono K, Yano M: **Two adjacent nucleotide-binding site–leucine-rich repeat class genes are required to confer *Pikm*-specific rice blast resistance**. *Genetics* 2008, **180**:2267.
83. Li W, Wang B, Wu J, Lu G, Hu Y, Zhang X, Zhang Z, Zhao Q, Feng Q, Zhang H, et al.: **The *Magnaporthe oryzae* avirulence gene *AvrPiz-t* encodes a predicted secreted protein that triggers the immunity in rice mediated by the blast resistance gene *Piz-t***. *Molecular Plant-Microbe Interactions* 2009, **22**:411-420.
84. Zhang S, Wang L, Wu W, He L, Yang X, Pan Q: **Function and evolution of *Magnaporthe oryzae* avirulence gene *AvrPib* responding to the rice blast resistance gene *Pib***. *Scientific Reports* 2015, **5**:11642.
85. Maidment JHR, Franceschetti M, Maqbool A, Saitoh H, Jantasuriyarat C, Kamoun S, Terauchi R, Banfield MJ: **Multiple variants of the fungal effector AVR-Pik bind the HMA domain of the rice protein OsHIPP19, providing a foundation to engineer plant defense**. *Journal of Biological Chemistry* 2021, **296**:100371.
86. Guo L, Cesari S, de Guillen K, Chalvon V, Mammri L, Ma M, Meusnier I, Bonnot F, Padilla A, Peng Y-L, et al.: **Specific recognition of two MAX effectors by integrated HMA domains in plant immune receptors involves distinct binding surfaces**. *Proceedings of the National Academy of Sciences* 2018, **115**:11637.
87. Mukhi N, Gorenkin D, Banfield MJ: **Exploring folds, evolution and host interactions: understanding effector structure/function in disease and immunity**. *New Phytologist* 2020, **227**:326-333.
88. Park C-H, Chen S, Shirsekar G, Zhou B, Khang CH, Songkumarn P, Afzal AJ, Ning Y, Wang R, Bellizzi M, et al.: **The *Magnaporthe oryzae* effector AvrPiz-t targets the RING E3 ubiquitin ligase APIP6 to suppress pathogen-associated molecular pattern-triggered immunity in rice**. *The Plant cell* 2012, **24**:4748-4762.
89. Park CH, Shirsekar G, Bellizzi M, Chen S, Songkumarn P, Xie X, Shi X, Ning Y, Zhou B, Suttiviriya P, et al.: **The E3 ligase APIP10 connects the effector AvrPiz-t to the NLR receptor Piz-t in rice**. *PLoS Pathogens* 2016, **12**:e1005529.
90. Tang M, Ning Y, Shu X, Dong B, Zhang H, Wu D, Wang H, Wang GL, Zhou B: **The Nup98 homolog APIP12 targeted by the effector AvrPiz-t is involved in rice basal resistance against *Magnaporthe oryzae***. *Rice* 2017, **10**:5.
91. Shi X, Long Y, He F, Zhang C, Wang R, Zhang T, Wu W, Hao Z, Wang Y, Wang G-L, et al.: **The fungal pathogen *Magnaporthe oryzae* suppresses innate immunity by modulating a host potassium channel**. *PLoS Pathogens* 2018, **14**:e1006878.
92. Han J, Wang X, Wang F, Zhao Z, Li G, Zhu X, Su J, Chen L: **The fungal effector Avr-Pita suppresses innate immunity by increasing COX activity in rice mitochondria**. *Rice* 2021, **14**:12.
93. Jones DAB, Bertazzoni S, Turo CJ, Syme RA, Hane JK: **Bioinformatic prediction of plant–pathogenicity effector proteins of fungi**. *Current Opinion in Microbiology* 2018, **46**:43-49.
94. Oliveira-Garcia E, Deising HB: **Attenuation of PAMP-triggered immunity in maize requires down-regulation of the key β-1,6-glucan synthesis genes *KRE5* and *KRE6* in biotrophic hyphae of *Colletotrichum graminicola***. *The Plant Journal* 2016, **87**:355-375.
95. Mesarich CH: **Investigating the structure & function of ViCin1, a novel repeat protein from the apple scab fungus *Venturia inaequalis*.** In *School of Biological Sciences*,. Edited by: The University of Auckland; 2011. vol PhD.
96. Dahmen H, Hobot JA: **Ultrastructural analysis of *Erysiphe graminis* haustoria and subcuticular stroma of *Venturia inaequalis* using cryosubstitution**. *Protoplasma* 1986, **131**:92-102.

97. O'Connell RJ, Panstruga R: **Tête à tête inside a plant cell: establishing compatibility between plants and biotrophic fungi and oomycetes**. *New Phytologist* 2006, **171**:699-718.
98. Mapuranga J, Zhang L, Zhang N, Yang W: **The haustorium: The root of biotrophic fungal pathogens**. *Frontiers in Plant Science* 2022, **13**:963705.
99. Schoffelmeer EAM, Klis FM, Sietsma JH, Cornelissen BJC: **The cell wall of *Fusarium oxysporum***. *Fungal Genetics and Biology* 1999, **27**:275-282.
100. Cantu D, Carl Greve L, Labavitch JM, Powell ALT: **Characterization of the cell wall of the ubiquitous plant pathogen *Botrytis cinerea***. *Mycological Research* 2009, **113**:1396-1403.
101. Pettolino F, Sasaki I, Turbic A, Wilson SM, Bacic A, Hrmova M, Fincher GB: **Hyphal cell walls from the plant pathogen *Rhynchosporium secalis* contain (1,3/1,6)-β-d-glucans, galacto- and rhamnomannans, (1,3;1,4)-β-d-glucans and chitin**. *The FEBS Journal* 2009, **276**:3698-3709.
102. Keswani C, Singh SP, Singh H: **A superstar in biocontrol enterprise: *Trichoderma* spp**. *Biotech Today* 2013, **3**:27-30.
103. Geraldine AM, Lopes FAC, Carvalho DDC, Barbosa ET, Rodrigues AR, Brandão RS, Ulhoa CJ, Lobo Junior M: **Cell wall-degrading enzymes and parasitism of sclerotia are key factors on field biocontrol of white mold by *Trichoderma* spp**. *Biological Control* 2013, **67**:308-316.
104. López-Mondéjar R, Ros M, Pascual JA: **Mycoparasitism-related genes expression of *Trichoderma harzianum* isolates to evaluate their efficacy as biological control agent**. *Biological Control* 2011, **56**:59-66.
105. Gruber S, Seidl-Seiboth V: **Self versus non-self: fungal cell wall degradation in *Trichoderma***. *Microbiology* 2012, **158**:26-34.
106. Rizzi Y S, Happel P, Lenz S, Urs M J, Bonin M, Cord-Landwehr S, Singh R, Moerschbacher B M, Kahmann R: **Chitosan and chitin deacetylase activity are necessary for development and virulence of *Ustilago maydis***. *mBio* 2021, **12**:e03419-03420.
107. El Gueddari NE, Rauchhaus U, Moerschbacher BM, Deising HB: **Developmentally regulated conversion of surface-exposed chitin to chitosan in cell walls of plant pathogenic fungi**. *New Phytologist* 2002, **156**:103-112.
108. Geoghegan IA, Sarah J. Gurr.: **Investigating chitin deacetylation and chitosan hydrolysis during vegetative growth in *Magnaporthe oryzae***. *Cellular Microbiology* 2017, **19**:e12743.
109. Geoghegan IA, Gurr SJ: **Chitosan mediates germling adhesion in *Magnaporthe oryzae* and is required for surface sensing and germling morphogenesis**. *PLoS Pathogens* 2016, **12**:e1005703-e1005703.
110. Doering TL: **How sweet it is! Cell wall biogenesis and polysaccharide capsule formation in *Cryptococcus neoformans***. *Annual Reviews in Microbiology* 2009, **63**:223-247.
111. Ziv C, Zhao Z, Gao YG, Xia Y: **Multifunctional roles of plant cuticle during plant-pathogen interactions**. *Frontiers in Plant Science* 2018, **9**.
112. Podila GK, Rogers LM, Kolattukudy PE: **Chemical signals from avocado surface wax trigger germination and appressorium formation in *Colletotrichum gloeosporioides***. *Plant Physiology* 1993, **103**:267-272.
113. Gilbert RD, Johnson AM, Dean RA: **Chemical signals responsible for appressorium formation in the rice blast fungus *Magnaporthe grisea***. *Physiological and Molecular Plant Pathology* 1996, **48**:335-346.

114. Chakraborty A, Fernando LD, Fang W, Dickwella Widanage MC, Wei P, Jin C, Fontaine T, Latgé J-P, Wang T: **A molecular vision of fungal cell wall organization by functional genomics and solid-state NMR**. *Nature Communications* 2021, **12**:6346.
115. Suyotha W, Yano S, Takagi K, Rattanakit-Chandet N, Tachiki T, Wakayama M: **Domain structure and function of α-1,3-glucanase from *Bacillus circulans* KA-304, an enzyme essential for degrading basidiomycete cell walls**. *Bioscience, Biotechnology, and Biochemistry* 2013, **77**:639-647.
116. Fujikawa T, Sakaguchi A, Nishizawa Y, Kouzai Y, Minami E, Yano S, Koga H, Meshi T, Nishimura M: **Surface α-1,3-glucan facilitates fungal stealth infection by interfering with innate immunity in plants**. *PLoS Pathogens* 2012, **8**:e1002882.
117. Fujikawa T, Kuga Y, Yano S, Yoshimi A, Tachiki T, Abe K, Nishimura M: **Dynamics of cell wall components of *Magnaporthe grisea* during infectious structure development**. *Molecular Microbiology* 2009, **73**:553-570.
118. Freytag S, Mendgen K: **Surface carbohydrates and cell wall structure of *in vitro*-induced uredospore infection structures of *Uromyces viciae-fabae* before and after treatment with enzymes and alkali**. *Protoplasma* 1991, **161**:94-103.
119. Oliveira Silva A-SL, Wirsel Stefan, Deising Holger: **Pathogenesis-related cell wall biogenesis with emphasis on the maize anthracnose fungus *Colletotrichum graminicola***. *Plants* 2022, **11**:849.
120. Beauvais A, Bozza S, Kniemeyer O, Formosa C, Balloy V, Henry C, Roberson RW, Dague E, Chignard M, Brakhage AA, et al.: **Deletion of the α-(1,3)-glucan synthase genes induces a restructuring of the conidial cell wall responsible for the avirulence of *Aspergillus fumigatus***. *PLoS Pathogens* 2013, **9**:e1003716.
121. Kang X, Kirui A, Muszyński A, Widanage MCD, Chen A, Azadi P, Wang P, Mentink-Vigier F, Wang T: **Molecular architecture of fungal cell walls revealed by solid-state NMR**. *Nature Communications* 2018, **9**:2747.
122. Frandsen RJ: **A guide to binary vectors and strategies for targeted genome modification in fungi using *Agrobacterium tumefaciens*-mediated transformation**. *Journal of Microbiology Methods* 2011, **87**:247-262.
123. Rahnama M, Forester N, Ariyawansa KGSU, Voisey CR, Johnson LJ, Johnson RD, Fleetwood DJ: **Efficient targeted mutagenesis in *Epichloë festucae* using a split marker system**. *Journal of Microbiological Methods* 2017, **134**:62-65.
124. Schuster M, Kahmann R: **CRISPR-Cas9 genome editing approaches in filamentous fungi and oomycetes**. *Fungal Genetics and Biology* 2019, **130**:43-53.
125. Idnurm A, Urquhart AS, Vummadi DR, Chang S, Van de Wouw AP, López-Ruiz FJ: **Spontaneous and CRISPR/Cas9-induced mutation of the osmosensor histidine kinase of the canola pathogen *Leptosphaeria maculans***. *Fungal Biology and Biotechnology* 2017, **4**:12-12.
126. Aleksenko A, Clutterbuck AJ: **Autonomous plasmid replication in *Aspergillus nidulans*: AMA1 and MATE Elements**. *Fungal Genetics and Biology* 1997, **21**:373-387.
127. McCarthy HM, Tarallo M, Mesarich CH, McDougal RL, Bradshaw RE: **Targeted gene mutations in the forest pathogen *Dothistroma septosporum* using CRISPR/Cas9**. *Plants* 2022, **11**:1016.
128. Miller TA, Hudson DA, Johnson RD, Singh JS, Mace WJ, Forester NT, Maclean PH, Voisey CR, Johnson LJ: **Dissection of the epoxyjanthitrem pathway in *Epichloë* sp. LpTG-3 strain AR37 by CRISPR gene editing**. *Frontiers in Fungal Biology* 2022, **3**: 944234.
129. Li R, Ba Y, Song Y, Cui J, Zhang X, Zhang D, Yuan Z, Yang L: **Rapid and sensitive screening and identification of CRISPR/Cas9 edited rice plants using quantitative**

real-time PCR coupled with high resolution melting analysis. *Food Control* 2020, **112**:107088.
130. Simko I: **High-resolution DNA melting analysis in plant research**. *Trends in Plant Science* 2016, **21**:528-537.
131. Wittwer CT: **High-resolution DNA melting analysis: advancements and limitations**. *Human Mutation* 2009, **30**:857-859.
132. Samarut É, Lissouba A, Drapeau P: **A simplified method for identifying early CRISPR-induced indels in zebrafish embryos using high resolution melting analysis**. *BMC Genomics* 2016, **17**:547.
133. Denbow CJ, Lapins S, Dietz N, Scherer R, Nimchuk ZL, Okumoto S: **Gateway-compatible CRISPR-Cas9 vectors and a rapid detection by high-resolution melting curve analysis**. *Frontiers in Plant Science* 2017, **8**:1171.
134. Foster AJ, Martin-Urdiroz M, Yan X, Wright HS, Soanes DM, Talbot NJ: **CRISPR-Cas9 ribonucleoprotein-mediated co-editing and counterselection in the rice blast fungus**. *Scientific Reports* 2018, **8**:14355.
135. Zhang Z, Mao Y, Ha S, Liu W, Botella JR, Zhu J-K: **A multiplex CRISPR/Cas9 platform for fast and efficient editing of multiple genes in *Arabidopsis***. *Plant Cell Reports* 2016, **35**:1519-1533.
136. Kujoth Gregory C, Sullivan Thomas D, Merkhofer R, Lee T-J, Wang H, Brandhorst T, Wüthrich M, Klein Bruce S: **CRISPR/Cas9-mediated gene disruption reveals the importance of zinc metabolism for fitness of the dimorphic fungal pathogen *Blastomyces dermatitidis***. *mBio* 2018, **9**:e00412-00418.
137. Polat Z, Bayraktar H: **Resistance of *Venturia inaequalis* to multiple fungicides in Turkish apple orchards**. *Journal of Phytopathology* 2021, **169**:360-368.
138. Cox KD: **Fungicide resistance in *Venturia inaequalis*, the causal agent of apple scab, in the United States**. In *Fungicide resistance in plant pathogens: principles and a guide to practical management*. Edited by Ishii H, Hollomon DW: Springer Japan; 2015:433-447.
139. Patocchi A, Wehrli A, Dubuis PH, Auwerkerken A, Leida C, Cipriani G, Passey T, Staples M, Didelot F, Philion V, et al.: **Ten years of VINQUEST: first insight for breeding new apple cultivars with durable apple scab resistance**. *Plant Disease* 2020, **104**:2074-2081.